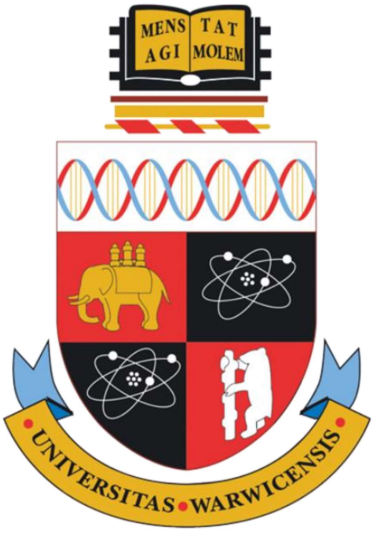

The role of solid particles in emulsion polymerization – synthesis and kinetic studies

by

Andrea Lotierzo

A thesis submitted in fulfilment of the requirements for the degree of

Doctor of Philosophy in Chemistry

Department of Chemistry

University of Warwick

May 2019

"Research is what I'm doing when
I don't know what I'm doing"

Wernher von Braun

Table of Contents

List of Figures

List of Tables

List of Schemes

Abbreviations & Symbols

A	Pre-exponential factor
A_h	Heat exchange surface area
a_0	Optimal area of the head group
ACVA	4-4′-Azobis(4-cyanovaleric acid)
AFM	Atomic force microscopy
AIBN	2,2′-Azobis(2-methylpropionitrile)
APS	Ammonium persulfate
ATRP	Atom transfer radical polymerization
BA	Butyl acrylate
BMA	Butyl methacrylate
CCT	Catalytic chain transfer
CCTP	Catalytic chain transfer polymerization
CHDF	Capillary hydrodynamic fractionation
CMC	Critical micelle concentration
$c_{p,i}$	Heat capacity at the temperature T of the i component
$C_{p,M}$	Monomer concentration of monomer within a latex particle
CRP	Controlled radical polymerization
Cryo-TEM	Cryogenic-transmission electron microscopy
C_T	Chain transfer coefficient
CTA	Chain transfer agent
C_T^{app}	Apparent chain-transfer coefficient
d	Particle diameter
D	Particle diameter measured *via* CHDF
DEGEEA	Di(ethylene glycol) ethyl ether acrylate
d_H	Hydrodynamic diameter
DLS	Dynamic light scattering
DLVO	Derjaguin, Landau, Verwey, Overbeek
$Đ_M$	Molecular weight dispersity
DMA	Dynamic mechanical analysis

DMF	Dimethyl formamide
DMSO	Dimethyl sulfoxide
DP	Degree of polymerization
DP_{target}	Targeted degree of polymerization
d_{SAXS}	Particle diameter measured *via* SAXS
DSC	Differential scanning calorimetry
d_{SEM}	Particle diameter measured *via* SEM
d_{th}	Theoretical diameter of a particle
E_a	Activation energy
E_k	Kinetic energy
F	Feeding flow rate
f	Ratio between silica and nanocomposite latex surface area
f_I	Capture efficiency
FRP	Free radical polymerization
GlyMA	Glycidyl methacrylate
GMA	Glycerol methacrylate
GO	Graphene oxide
HCl	Hydrochloric acid
HEMA	2-Hydroxyethyl methacrylate
HPLC	High performance liquid chromatography
HPMA	Hydroxypropyl methacrylate
HPMAm	2-Hydroxypropyl methacrylamide
HUFT	Hansen, Hugelstad, Fitch, Tsai
I	Ionic strength
j_{crit}	Critical chain length
k	Debye-Hückel parameter
K_a	Acid dissociation constant
k_b	Boltzmann constant
k_d	Initiator decomposition constant
K_{eq}	Equilibrium constant
k_p	Propagation rate coefficient
KPS	Potassium persulfate

k_t	Termination rate coefficient
k_{tr}	Chain transfer rate coefficient
l_C	Length of the lyophilic tail
LCST	Lower critical solution temperature
m	Mass
m_0	Monomer molar mass
MAA	Methacrylic acid
m_{Co}	Partitioning coefficient of cobalt catalysts between oil and water phase
M_i	Molar concentration of the *i* component
MMA	Methyl methacrylate
MMFT	Minimum film formation temperature
M_n	Number average molecular weight
mol_M	Initial moles of monomer
M_w	Weight average molecular weight
$\bar{n}$	Average number of radicals per particle
N	Nanogels
N_A	Avogadro number
NIPAM	N-Isopropylacrylamide
NMP	Nitroxide mediated radical polymerization
NMR	Nuclear magnetic resonance
N_{nano}	Number of nanogel particles
N_p	Number of particles
n_{patch}	Number of patches on a latex particle
n_r	Number of radicals produced
P	Packing parameter
PDEGMA	Poly(di(ethylene glycol) ethyl ether methacrylate)
PdI	Polydispersity index
PDMA	Poly(dimethylacrylamide)
PEGMEMA	Poly(ethylene glycol) methyl ether methacrylate
PISA	Polymerization induced self-assembly
PITSA	Polymerization induced thermal self-assembly
PS	Poly(styrene)

PTFE	Poly(tetrafluoroethylene)
q	Surface charge
Q_{acc}	Heat rate accumulated in the reactor
Q_J	Heat flow through the reactor wall
Q_{loss}	Heat loss
Q_r	Heat of reaction
Q_{st}	Heat rate due to stirring
r	Distance of any point in the double layer from the centre of a particle
RAFT	Reversible addition-fragmentation chain-transfer
RBF	Round bottom flask
RDRP	Reversible-deactivation radical polymerization
r_p	Particle radius
R_p	Rate of polymerization
R_s	Radius of a sphere
S	Surface area
SAXS	Small-angle X-ray scattering
SC	Solid content
SDS	Sodium dodecyl sulfate
SEC	Size exclusion chromatography
SEM	Scanning electron microscopy
SET-LRP	Single electron transfer living radical polymerization
Sld	Scattering length density
Sty	Styrene
T	Temperature
t	Time
$T_{avg,J}$	Average temperature in the reactor jacket
TEM	Transmission electron microscopy
t_{eq}	Time at which $N_{nano} = n_r$
TERP	Organotellurium-mediated living radical polymerization
T_g	Glass transition temperature
THF	Tetrahydrofuran
$T_{J,in}$	Temperature in the inlet of the reactor jacket

$T_{J,out}$	Temperature in the outlet of the reactor jacket
T_r	Reaction temperature
U	Global heat transfer coefficient
UCST	Upper critical solution temperature
v	Volume of the lyophobic chain
$\bar{v}$	Kinetic chain length
V_{H_2O}	Total volume of water
v_k	Velocity
$\hat{x}$	Grams of monomer converted to polymer
X	Monomer conversion
$X_{grav,f}$	Final conversion *via* gravimetry
X_i	Instantaneous monomer conversion
x_{sol}	Volume fraction of solvent in a micelle core
z_i	Charge of the *i* ion
α	Fraction of ionized acid groups
$\bar{\alpha}$	Acceleration parameter
β	Correction factor
ΔG	Change in Gibbs energy
ε	Specific permittivity of the solvent
ζ	Electrostatic potential at the surface of shear
θ_w	Three-point contact angle
ρ	Density
σ	Standard deviation
σ_{ow}	Monomer-water interfacial tension
ψ	Electrostatic potential
ψ_0	Surface electrostatic potential
Ω	Radial velocity

Acknowledgments

When I look back at the past few years, I see a number of people that helped me getting through what was one of the most rewarding and challenging experiences of my life. If you are in these pages you have been of incredible support and you have made the difference.

First and foremost, I'd like to thank my supervisor Stefan, who believed in my potential since day one, who trained me and taught me for endless hours. Thanks for always showing me a different idea from mine. If I am now writing this thesis is especially thanks to you.

Thanks to all my brits (and scots!). I left Italy not knowing that I would have found a new family in England. To the camping group, the biggest thank you. You have shown me the best parts of the English countryside, leaving all the problems behind to just relax and enjoy nature. Thank you for never let me navigate, apart from that one disastrous time. Thank you Sarah and Brooke, you welcomed me in your house 5 days after we met. I will never forget that. Thank you Ross, you have always been there all the times I thought I was going in the wrong direction. Thank you Sam, for teaching me all about English culture. You tried hard to teach me what an English pun is; sometimes I can make good ones now. Thank you Matt, if my English worsened in these years is only thanks to your intense slang classes. Thank you to all the great evenings spent together on the sofa. Thank you Mari, for bringing a bit of Italy into my life in Britain. Thank you for teaching me the small tricks in the kitchen and always sharing your delicious food with us. Thank you Josh, for always being cheerful, for teaching me how to fix bikes and always sharing your passions with others. Thank you Pat for all the great boardgame/movie nights. In general, thank you to all my housemates (you too Jonas!), for filling with laughter my homes.

Thanks to (the rest of) BonLab; Rob, Rob, Wai, Melody, Birsen, Yuanzhi, Sarah, Ryan, Jacob, Hayden, Sherry. I learned a great deal from you all.

Thank you to all my Italians, that were left behind but were always ready to welcome me back. Thank you Fede and Volto for the endless calls to support each other. You have been essential in these years. Thank you to all my friends and Family

for always making me feel at home when I visited. I could not have come this far without your support.

Finally, thank you Alessia, who more than anyone else had to suffer for my decision. You accepted it and never complained about the burden you had to carry. Who more than anyone was always ready to give support in the lows, cheer with me in the highs and gave advice in the doubt. You have been essential, a lighthouse, for these 4 years.

Declaration

This thesis is submitted to the University of Warwick in support of my application for the degree of Doctor of Philosophy. It has been composed by myself and has not been submitted in any previous application for any degree. The work presented (including data generated and data analysis) was carried out by the author except in the cases outlined below:

1. Cryogenic Transmission Electron Microscopy (Figures 2.3 and 2.4, Chapter 2; Figure 4.4, Chapter 4; Figure A4.1, Appendix A.4) was carried out by Dr. Saskia Bakker, University of Warwick.
2. Small Angle X-Ray Scattering (Figure 4.6, Chapter 4) was carried out by Dr. Steven Huband, University of Warwick.
3. Part of the image analysis using the software ImageJ (Figure 4.12, Chapter 4) and of Scanning Electron Microscopy (Figure 4.9, Chapter 4; Figure 5.4A, Chapter 5; Figures A4.4 and A4.7, Appendix A.4) were carried out by Dr. Brooke Longbottom, University of Cambridge.
4. Part of Scanning Electron Microscopy (Figure 5.4B-E, Chapter 5) was carried out by Dr. Shane Meaney, Monash University.

Parts of this thesis have been published by the author and are detailed in the publications list overleaf.

Signature: Date:

_____ _____

Publications List

- **A. Lotierzo**, B. W. Longbottom, W. H. Lee, S.A.F. Bon, *ACS Nano*, 2019, 13, 399-407 (Chapters 4 and 5)
- **A. Lotierzo**, R. M. Schofield and S. A. F. Bon, *ACS Macro Lett*., 2017, 6, 1438-1443 (Chapter 3)
- **A. Lotierzo** and S. A. F. Bon, S. A. F. *Polym. Chem*., 2017, 8, 5100-5111 (Chapter 2)

Other publications by the author:

- C. T. Desire, **A. Lotierzo**, R. D. Arrua, E. F. Hilder, S. A. F. Bon, *Green. Chem.*, 2018, 20, 2499-2511
- **A. Lotierzo**, V. Pifferi, S. Ardizzone, P. Pasqualin, G. Cappelletti, *Corrosion Science,* 2016, 110, 192-199

Abstract

Control of particle morphology and chemical functionality in polymer dispersions have been of growing interest in the scientific community for the past decades. The possibility of regulating asymmetry, in both shape and chemical composition, has been sought as a way of creating complex advanced materials. In these materials the mechanical and physico-chemical properties of different phases are combined, in a synergistic way, in an attempt of mimicking nature's behaviour.

This thesis particularly deals with nanocomposite materials: materials where at least one of the different phases has two or three dimensions of less than 100 nanometres. Among the plethora of synthetic pathways developed for the controlled synthesis of nanocomposite colloids, this work focuses on a process called Pickering emulsion polymerization; a seeded emulsion polymerization reaction where a polymer phase is formed *in-situ* in the presence of a stabilizing nano-sized colloid formed *ex-situ*. The product of the reaction typically is that of a polymeric particle surrounded by a dense shell of stabilizing agent. The main advantages are the ease of operation, absence of high shear homogenization steps and of molecular surfactants. The latter is of key importance for instance in coating applications where surfactant migration during and after film formation can be detrimental for the final film properties.

In this work, initially Pickering emulsion polymerization is thoroughly explored from a kinetic and mechanistic viewpoint using a model system consisting of SiO_2 nanoparticles and styrene or methyl methacrylate as monomers. These relatively well-known systems are used to draw more conclusive theories on the mechanism governing particle formation and specifically the mode of stabilizer adsorption at the polymer interface. Once assessed the main processes influencing the fate of the reaction, a first step towards the implementation of added complexity in the system is taken by moving towards polymeric block copolymer stabilizers, where the chemical composition can be tailored by changing the type of monomer used. Both dispersion and emulsion polymerization approaches are discussed, with a particular focus on the development of protocols which do not contain added coloration or malodorous compounds. This increases the complexity of the system as

the adopted chain-transfer agents require to operate in monomer starve fed conditions in order to allow control over chain-growth. This was found not to be compatible with dispersion polymerization, or polymerization induced self-assembly, reaction conditions. Nevertheless, a solution to the problem is proposed which yielded polymer self-assemblies of various morphologies.

Finally, nanometric polymeric stabilizers (*i.e.* crosslinked block copolymer micelles, or *nanogels*) produced by the more successful emulsion polymerization approaches are adopted in Pickering emulsion polymerization reactions as sole stabilizers. The controlled destabilization of the nanogels by pH adjustment and background electrolyte addition led to polymer colloids of Janus, patchy or armoured morphology. Such particles are characterized by a given number of surface protrusions, with the same chemical composition as the nanogels adopted in the protocol.

1

Introduction

1.1 Polymer colloids: a brief introduction

A colloid is a dispersion of fine particles, or a liquid, in a fluid medium. According to the IUPAC definition, colloidal systems are those with at least one of the dimensions between 1 nm and 1 μm.[1] When the dispersed phase is composed of a polymeric material, the term *polymer colloid* is adopted. This polymeric suspension, also historically called *latex*, is usually milky white or bluish translucent in appearance depending on the dimension of the dispersed particles. Polymer colloids find application in a number of fields, including the pharmaceutical,[2] adhesive[3] and coating[4] industries, the production of plastics, rubbers and foams,[5] in nanocomposite materials[6] and even as promising candidates in the next generation of solar cells[7] and batteries.[8]

Traditionally polymer colloids are synthetized by free radical polymerization (FRP), typically by emulsion polymerization. The development a number of controlled radical polymerization (CRP) and heterogeneous-type polymerization techniques brought to new pathways available for the synthesis of polymer dispersions. The next sections of the introduction of this thesis will focus on the description of some of these heterogeneous polymerization techniques and in particular of emulsion polymerization. This will be followed by the description of catalytic chain transfer polymerization (CCTP) and reversible addition fragmentation

chain transfer (RAFT) polymerization, which were applied to emulsion polymerization systems in the work described in this thesis.

1.2 Emulsion polymerization

Since its introduction on an industrial-scale plant in the mid-1930s, emulsion polymerization has become the most common radical polymerization process to form polymer dispersions, with millions of tons of synthetic polymer produced every year.[9] In its simplest form, a lyophobic monomer, a water soluble initiator, a stabilizing agent and a solvent are mixed together and heated to reaction temperature. Typically, water is used as dispersing medium and a sparingly water-soluble monomer is adopted. The stabilizing agent is historically a molecular surfactant. Other processes, defined as *soap free*, have also been developed where the stabilization is provided by the initiator residues only,[10] polymerizable amphiphiles,[11] comonomers[12] or solid particles[13] which are added to the base recipe in order to provide some form of electro-steric stabilization. Other ingredients such as buffers, salts or chain-transfer agents can also be added to the reaction pot to regulate the pH and ionic strength of the solution or the polymer average molecular weight. The name *emulsion polymerization* comes from the initial erroneous belief that the process consisted of the polymerization of monomer droplets. The latter is actually not the mechanism of emulsion polymerization as described by the classical qualitative description of this process by Harkins.[14]

1.2.1 Classical description

According to Harkins' theory, an emulsion polymerization process consists of three intervals. When monomer, surfactant, a water-soluble initiator (for instance a thermal initiator) and water are mixed together, the system is composed of surfactant micelles swollen in monomer and micrometric sized monomer droplets suspended in water. These droplets are partially stabilized by the presence of surfactant molecules adsorbed on their surface. Upon heating of the system to reaction temperature, radicals are produced in the water phase. At this point polymer particles are formed mostly within the micelles and in considerably lower extend in

the water phase and monomer droplets (Interval I). Interval I is characterized by an increase in the rate of polymerization (R_p), as a greater number of polymerization loci, or nanoreactors, are formed. In this regard, R_p in emulsion polymerization is described as the rate of a polymerization in bulk multiplied by the number of latex particles (N_p):[9]

$$R_p = \frac{N_p}{V_{H_2O}} \frac{k_p C_{p,M} \bar{n}}{N_A} \quad (1.1)$$

where k_p is the propagation rate coefficient of the monomer, $C_{p,M}$ is the concentration of the monomer within the latex particles, $\bar{n}$ is the average number of radicals per particle, V_{H_2O} is the volume of water and N_A is the Avogadro number.

The formed particles grow in size during Interval II. In Interval II the formed latex particles swollen with monomer polymerize at constant R_p as when monomer is consumed inside a particle, more monomer can diffuse from the monomer droplets to the water phase and then to the growing particles. Essentially, the droplets act as a reservoir of monomer. In this way, R_p is constant as all the parameters in Equation 1.1 are constant during this stage. When all the droplets are consumed, $C_{p,M}$ starts to decrease and the polymerization progressively slows down until it stops when the monomer is fully polymerized (Interval III). During this interval it is also possible to observe a decrease-increase-decrease behaviour in R_p. The sudden increase in R_p in interval III can be ascribed to the decrease in rate of termination within the particles, caused by a raise in internal viscosity. This phenomenon is called Trommsdorff or gel effect.[15] At the end of the reaction, if all the particles formed quickly and grew simultaneously, a reasonably monodispersed latex can be obtained.

In the initial theory by Harkins,[14] nucleation in the water phase (see homogenous nucleation) and of monomer droplets (see droplet nucleation) played little influence, although they already were identified as possible events. Depending on the reaction conditions these nucleation pathways can however be predominant, as it will be described in the next sections.

1.2.2 Homogeneous nucleation

The process described in Section 1.2.2 laid the foundations for a general better understanding of emulsion polymerization reactions. In actual fact, the original theory by Harkins still represents a simplification of a very complex system where particles can nucleate through a number of different mechanisms. This is complicated by the fact that, being a free radical polymerization reaction, the radicals can initiate, propagate, undergo transfer and terminate in the water phase and within the particles. In addition, these radicals can enter or exit a particle either directly or after having reacted with some monomer units. Despite the complexity of the system, theorical models are nowadays available to describe the different aspects of this polymerization mechanism.[16] Figure 1.1 presents schematically most of these aspects.

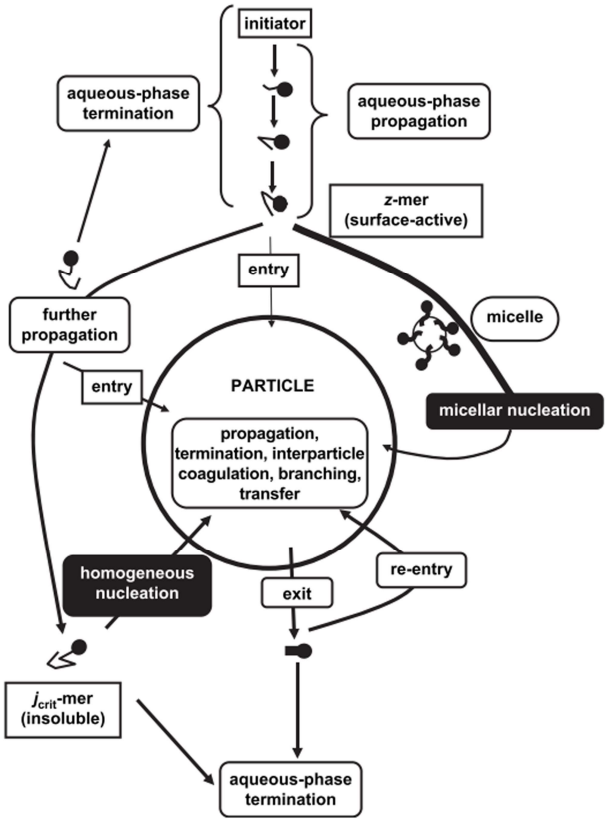

Figure 1.1 Schematic representation of the main events of an emulsion polymerization process. Reproduced with permission from ref. 16.

In emulsion polymerization, usually a sparingly water-soluble monomer is adopted. Upon initiator decomposition, the radicals can start reacting with the

monomer in the water phase forming an oligomeric radical. First a system with no surfactant or where the surfactant concentration is below the critical micelle concentration (CMC) will be described. In a system described in this way, particle formation follows a process called *homogeneous nucleation*, and it requires the monomer to be at least lightly soluble in water to take place.[17] Radicals in the water phase can propagate until the resulting oligomers reach a degree of polymerization, j_{crit}, at which they become insoluble and collapse forming new particles. The number of monomer units required for the oligomers to become insoluble varies depending on the monomer hydrophilicity.[18] This coil-to-globule transition excludes water and forms a primary particle that can be swollen with monomer and keep propagating.[16] Once they are formed, the primary particles can coagulate with one another to minimize their surface energy and increase surface charge density (provided by initiator residues). This model, was originally put forward by Fitch and Tsai,[19,20] then mathematically quantified by Hansen and Ugelstad;[21,22] HUFT (Hansen, Ugelstad, Fitch, Tsai) model.[16]

Once enough particles are formed, they will keep growing as described by Harkins' initial model.[14] During particle growth, as well as particle nucleation, radicals and oligoradicals can undergo a complex series of entry or exit events as shown in Figure 1.1. For a comprehensive description of these phenomena, the reader is directed to the extensive work performed, among the others, by Gilbert and co-workers.[16,18]

1.2.3 Heterogeneous nucleation

When nucleation is influenced by a hetero-phase, already phase-separated from solution, the process is called *heterogenous nucleation*. A simple example of a heterogenous nucleation mechanism is the process already described in Section 1.2.1; particles are formed by nucleation of micelles swollen in monomer. This process is called *micellar nucleation*. In this case, a radical propagates in the water phase until it forms a *z*-mer; a short oligomer, which is surface active but not insoluble, consisting of an initiator residue and z-monomer units.[16] As a result, a *z*-mer is shorter than an oligomer of degree of polymerization j_{crit}. This oligomer can enter or be captured by a micelle before reaching j_{crit}, which would result in the formation of a new particle.

As for j_{crit}, the number of monomer units required for the oligomer to become surface active varies depending on the monomer hydrophilicity.[18] Note that there is always competition between micellar and homogeneous nucleation. In fact, if the surface area of the micelles is not large enough to rapidly capture all the *z*-mers or radicals formed, then the oligomers will statistically have a higher chance of reaching j_{crit}.

Until now monomer droplets were considered as silent observers of the polymerization, with the main task of replenishing the consumed monomer in the particles. This is usually the case as the likelihood for a radical or *z*-mer to enter, and hence nucleate, a monomer droplet is very low. The likelihood of *droplet nucleation* is directly correlated with the difference in surface area between swollen micelles and monomer droplets. Typically, in an emulsion polymerization reaction 10^{17}-10^{18} micelles of 50-150 Å in diameter are present. In comparison, the bulk of the monomer is present in the form of 10^{9}-10^{11} monomer droplets of 1-10 μm in size.[9] In this sense, is more likely for a *z*-mer to bump into a micelle, entering it, with respect to a monomer droplet. Droplet nucleation starts to play an important role in particle formation when the average droplet size decreases, as this results in a larger number of droplets and greater surface area stabilized by surfactant molecules. In particular, if the monomer droplets are present in sizes of 100-500 nm, droplet nucleation becomes the predominant nucleation pathway.[23]

The presence of other (polymer) particles, referred to as *foreign particles* by Fitch,[20] can also influence nucleation in emulsion polymerization. The most common emulsion polymerization conducted in the presence of foreign particles is the so-called *seeded emulsion polymerization*, where polymer latex particles are used as heterogeneous nuclei. Usually, first a latex is synthetized *via* a batch emulsion polymerization process and then other monomer(s) are fed or batch added to the system to progress the polymerization. If the surface area of the seed latex is high enough, the number of particles in the seeded emulsion polymerization step equals the number of seed latex particles initially present. Other materials can also be used as foreign particles. For instance, emulsion polymerization was adopted to encapsulate metals,[24] metal oxides,[25] clays,[26] and pigments[27] within a layer of polymer. This is usually achieved by surface modification (covalent or *via* physical adsorption) of the inorganic phase prior to the polymerization, as for instance shown in recent work by Heuts et al. on the encapsulation of Gibbsite plates.[26,28] The

reasoning behind this is to increase the compatibility of these materials, for instance, in a polymer film. In order for the encapsulation process to be successful, the interfacial tension between polymer and inorganic phase must be low enough to favor good spreading of the polymer chains on its surface. An illustrative example is shown in Figure 1.2; the decrease in wettability between the polymerizing monomer and the solid particle leads to progressive phase separation of the polymer phase.[29] The extreme case is when the two phases interact very little, with consecutive total dewetting.

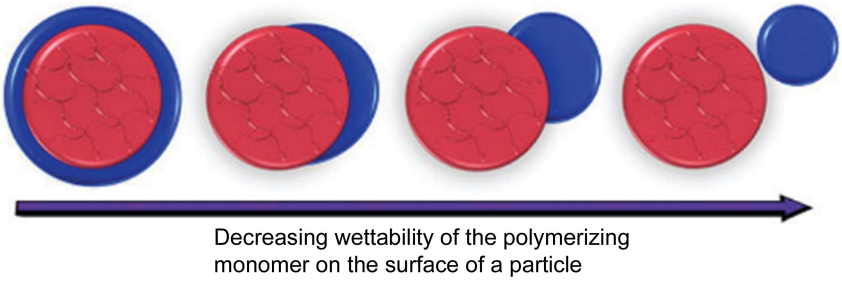

Figure 1.2 Schematic illustrating the effect of different wettability of a polymerizing monomer (blue) on a solid particle (red). The wettability governs the morphology obtained. Adapted with permission from ref. 29.

1.2.4 Other heterogeneous polymerization techniques

As previously explained, polymerizations can be carried out in other heterophase systems. In this section, miniemulsion and dispersion polymerization will be briefly described.

i) Miniemulsion polymerization

An emulsion characterized by oil droplets with diameters between 50 and 500 nm is defined as a miniemulsion.[9] Emulsions with such low droplet sizes are usually prepared by applying a great input of energy in the system, which increases the droplet surface area, and by readily stabilizing the newly formed surface area with surfactant molecules.[30] The high-force-dispersion devices commonly used for miniemulsion formations are ultrasound probes, for low volumes, and high-pressure homogenizers for larger volumes.[30] Depending on the process, a macroemulsion (d > 500 nm) is sometimes prepared first using a low-shear pre-emulsification step, which is then followed by the high-shear step, also called homogenization step.[31]

Generally speaking, a process where monomer miniemulsion droplets are polymerized is called *miniemulsion polymerization*. Miniemulsion polymerization is essentially an emulsion polymerization with the predominant action of droplet nucleation. In fact, as described in Section 1.2.3, when the average diameter of monomer droplets in emulsion polymerization drops to *ca.* < 500 nm, droplet nucleation starts to play an important role in the particle formation pathway. In this sense, miniemulsion polymerization systems are fairly similar to the emulsion counterparts. The main differences with emulsion polymerization are that both water and oil soluble initiators can be adopted, and that more hydrophobic monomers can be polymerized as monomer molecules do not need to diffuse across the continuous medium.[32] Instead, when monomers sparingly soluble in the continuous phase are adopted in a miniemulsion system, care must be taken against the destabilization of nanodroplets by Ostwald ripening.[33] As a result of a higher chemical potential of the monomer, or higher osmotic pressure, in small droplets with respect to larger ones, monomer molecules diffuse through the water phase from small to large droplets.[34] Therefore, small droplets progressively shirk while large droplets grow. This phenomenon is usually suppressed by addition of a *hydrophobe*; a low molecular weight, water insoluble (macro)molecule added to the droplets to counteract the droplet difference in osmotic pressure.[34]

As a comparison, when the reaction involves the polymerization of macroemulsion droplets, $1 < d < 100$ μm, then the process is rather called *suspension polymerization*.[35]

ii) Dispersion polymerization

An emulsion polymerization system where the monomer is soluble in the continuous phase, but the formed polymer is insoluble, is defined *dispersion polymerization*. Dispersion polymerization has gained considerable attention in the past decade and its nowadays one of the most popular ways of synthetizing polymer dispersions. Dispersion polymerization typically produces particles in the range of 1-15 μm.[9] However, more recent developments in the technique, see *polymerization-induced self-assembly* below, allow to produce particles in the range of 20-500 nm.[36]

Typically, dispersion polymerization systems start from a mixture of initiator, monomer, solvent and a stabilizing agent. The latter is usually a homopolymer, graft

copolymer or macromonomer that can provide some form of (electro-)steric colloidal stabilization.[9] For the purpose of this thesis, perhaps the most interesting systems are the ones in which the stabilizer is a lyophilic macro-chain transfer agent (CTA).[36] The reason for this is that during the chain-extension of the lyophilic macro-CTA in solution, a di-block copolymer consisting of a lyophilic first block and a lyophobic second block is formed. Therefore, the resulting di-block copolymer becomes progressively more surface active. This drives the self-assembly of these amphiphiles into supramolecular structures, depending on their packing parameters,[37] in a process that has been named *polymerization-induced self-assembly* or *PISA*. The interesting aspect of PISA is that during the reaction the volume ratio of the lyophilic and lyophobic blocks changes. As known from the previous literature, block copolymers can form supramolecular aggregates of various morphologies depending on the relative volume of the two blocks.[38–40] The fascinating aspect of PISA is hence that the block-copolymers formed can dynamically rearrange into various morphologies during the reaction.[41,42] Tailoring of the polymerization conditions has been shown to be able to produce pure phases of aggregates, reliably and in high concentrations.

1.3 Catalytic chain transfer polymerization

This section of the introduction will describe the principles behind catalytic chain transfer polymerization (CCTP) as a powerful tool for the production of α-hydrogen ω-unsaturated methacrylate macromonomers. These macromonomers are an interesting class of compounds as they can undergo reversible addition-fragmentation chain-transfer (RAFT) as it will be discussed in Section 1.4.

Catalytic chain-transfer to monomer in a radical polymerization was discovered in 1975 by Smirnov and Marchenko.[43] By addition of a cobalt porphyrin catalyst, the authors showed that they could control the molecular weight in a free radical polymerization of a methacrylate monomer. This led to considerable interest on this technique in the scientific community, with the development of a series of cobalt cobaloxime catalysts (**1**) with improved chain-transfer efficiencies (Scheme 1.1).[44,45] These catalysts are very sensitive to hydrolysis and oxidation, the latter both in solution and dry state. The issue was partially solved with the introduction of BF_2

bridges (**2**).[46] The catalysts of structure **2** are more resistant than **1**, although still sensitive towards acid hydrolysis or oxidation by desolved oxygen centered radicals (oxygen or peroxides), but they are safe to handle as a solid.[47,48] Different catalysts of structure **2** have been synthetized, with various R side chains. Perhaps the most commonly used cobalt cobaloxime in catalytic chain transfer polymerization is bis[(difluoroboryl) dimethylglyoximato] cobalt(II) also known as CoBF (Scheme 1.1, structure **2** for R = CH_3).

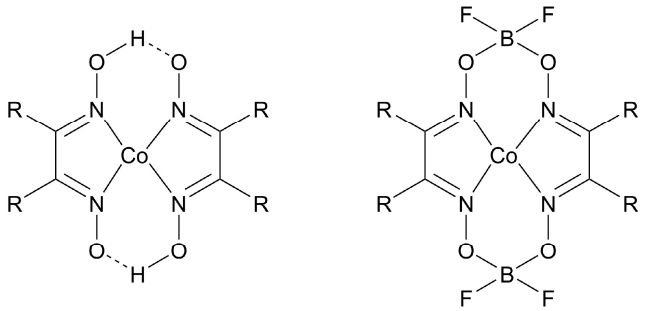

1 **2**

Scheme 1.1 Structures of common cobalt cobaloxime catalysts adopted in CCTP.

1.3.1 Features of CCTP

The main features of CCTP are the high chain-transfer coefficient (C_T) values and that the catalyst is not consumed during the reaction, leading to little metal contamination in the final product. In particular, $C_T \sim 4\times10^4$ using CoBF in the CCTP of methyl methacrylate in bulk.[49] Clearly, C_T greatly varies depending on the type of solvent adopted, the catalyst used and the monomer polymerized.[44,45] Another important aspect is whether the reaction is conducted in bulk, solution or emulsion conditions. Initially, only solution/bulk systems will be described, whereas catalytic chain-transfer in aqueous solution/emulsion polymerization will be treated in a separate section.

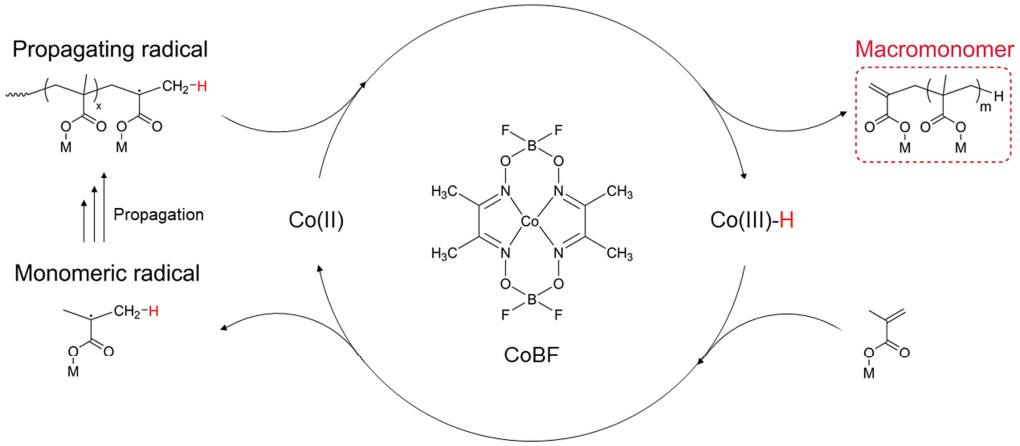

Scheme 1.2 Schematic of the mechanism of catalytic chain-transfer in the radical polymerization of a methacrylate monomer.

A cobaloxime mediated CCTP reaction proceeds *via* a two-step radical process with the Co(II) complex abstracting an H atom (red) from a propagating radical (Scheme 1.2).[43] This forms a Co(III) complex and a macromonomer chain. At this point, the catalyst is regenerated by H transfer to a monomer molecule, re-forming the Co(II) complex and a monomeric radical. As most of the polymer chains are initiated by the catalytic cycle, and not by an initiator residue, the polymer formed will mostly consist of α-hydrogen ω-unsaturated macromonomer chains.

Scheme 1.2 is a simplification of the process as it omits the presence of a possible reversible side reaction between Co(II) and a polymerizing radical, with the formation of a reversible Co-C bond.[50,51] This reaction was found to have no significant effect in methyl methacrylate polymerization but to greatly affect the polymerization of styrene and acrylic monomers.[52–54] Whereas in CCTP of methacrylates the molecular weight distribution is uniform with time, in the case of the one of styrene and acrylates it increases with time.[52] This "living" behavior was associated to the formation of a Co-C bond, which would be sterically suppressed by the presence of an α substituent in methacrylate monomers.[55] In this way the higher observed chain-transfer activity of a cobaloxime catalyst towards methacrylate monomers, or other monomers with a α-methyl substituent (e.g. α-methyl styrene[56] and methacrylonitrile[50]) is explained. Monomers without this substituent, such as acrylates, styrenes, acrylonitrile and vinyl acetate have instead shown much lower activity.[45,55,57,58]

An important aspect to consider when operating with cobalt cobaloximes is catalyst poisoning or degradation. Common solvents that do not severely compromise the catalyst activity, although they may somewhat affect it, for CCTP reactions are toluene, alcohols and acetonitrile.[49,52,59,60] Because of the sensitivity of the catalyst to hydrolysis, care must be taken when working in aqueous environment.

1.3.2 Catalytic chain transfer in aqueous environment

As previously mentioned, cobalt cobaloximes of structure **2** (Scheme 1.1), are sensitive towards oxidation by O_2[48] and peroxide[48,61,62] dissolved centered radicals as well as hydrolysis. In case of the rate of hydrolysis, a few measurements were made in an attempt to quantify the entity of the hydrolysis, however these were not made in a reactive systems (no radicals present).[44] The addition of 1.0% acetic acid in MMA bulk polymerization led to the deactivation of **1** (Scheme 1.1) at a rate of about 1.2% min^{-1} at 60°C.[63] In the presence of BF_2 bridges (**2**, R = CH_3), the decay at room temperature and pH = 1 was 0.6% min^{-1} in deaerated solutions.[47] The catalyst is however practically stable at room temperature, neutral pH and in absence of dissolved oxygen (**2**, R = Me, Ph).[47,48] No data is unfortunately available for the catalyst decomposition at reaction temperature (50-80°C), which is believed to be faster, especially in acidic environments.[64]

As a result of catalyst deactivation, generally the observed C_T in aqueous environments is lower than the one in apolar solvents or in bulk.[45] This problem was solved by Haddleton et al. which reported an extensive study on the synthesis of hydrophilic macromonomers in water/alcohol mixtures.[65] When batch adding the catalyst in aqueous CCTP reactions at acidic pH, free radical polymerization was observed. For this reason, the approach already proven successful for CCT emulsion polymerization was adopted;[64,66] the reactions were performed under semi-batch conditions, with a mixture of catalyst and monomer progressively fed in the reaction medium. It is clear that because of catalyst deactivation the observed C_T was much lower than what normally observed; $C_T \sim 1000$.

Apart from aqueous solution polymerization conditions, catalytic chain transfer (CCT) has also been applied to emulsion systems for the production of polymer colloids. The first studies of CCT in emulsion appeared in the mid/late 1990s

and have continued for 10/15 years with contributions from Moad et al.,[66,67] Haddleton,[64,68] Meuldijk, Van Herk and Heuts.[69–72] The product of the reaction consists of latex particles made of macromonomer chains. Lately, the technique is been gaining renewed interest with new investigations on the application of CCT in emulsion for the synthesis of multiblock copolymer latexes,[73,74] crosslinked-block copolymer micelles (Chapter 4)[75] and emulsion polymerization surfmers.[76]

In order for these reactions to be successful, peroxide initiators are avoided, it is operated in absence of oxygen and in semi-batch conditions.[45] Furthermore, additional complications arise when operating in emulsion medium. The first important aspect to consider is the partitioning of both monomer and catalyst between the organic and aqueous phase. In particular, the partitioning of the catalyst between monomer and aqueous phase was defined:[45]

$$m_{Co} = \frac{[Co]_{disp}}{[Co]_{aq}} \tag{1.2}$$

where $[Co]_{disp}$ and $[Co]_{aq}$ are the concentrations of cobalt catalyst respectively in the dispersed (*i.e.* monomer droplets, polymer particles and/or micelles) and aqueous phases.

Low values of m_{Co} will imply that a substantial amount of the catalyst is in the water phase, leading to overall lower catalytical activity within the particles.[69] m_{Co} is naturally highly depended on the R substituent of **2** (Scheme 1.1); for the system MMA/water, m_{Co} = 0.31-0.72, 19-60 and ∞ respectively for R = CH_3, Et and Ph.[45]

A second crucial aspect to ensure good catalytical activity is the movement of the catalyst inside the polymerizing particles. When forming high glass transition temperature (T_g) polymers, if the particle reaches a glassy state during the polymerization, the viscosity inside the particle rises and the catalyst movement in the particle becomes severely restricted.[64,68,77–79] A solution to circumvent this problem is either copolymerizing in the presence of a low T_g monomer,[78] or adding a pre-shot of monomer/catalyst mixture.[68,77,79]

1.4 Reversible addition-fragmentation chain-transfer

Control of macromolecular chain architecture in polymer science was initiated by the discovery of anionic living polymerization by Szwarc.[80,81] The elimination of transfer and termination reactions, along with a faster initiation rate compared with the rate of propagation implicated that at any time in the reaction: 1) the number average molecular weight of the polymer chains could be predicted as the ratio of reacted monomer and initiator used and 2) that all the chains were polymerizing at the same rate.[82,83] The same molecular weight control was later also achieved in radical polymerization by developing a series of reversible-deactivation radical polymerization (RDRP) techniques.[84–87] Contrarily to anionic polymerization, radical polymerization is characterized by slow initiation and complete termination of growing polymer chains.[88] Two different approaches were adopted to allow control over molecular chain architecture in this case. The first focused on fast initiation of all the growing polymer chains and minimization of termination events by using intermittingly active propagating species: the radicals are rapidly trapped in a deactivated state and can alternate between being active and inactive (Scheme 1.3A).[85] Some of the most common RDRP techniques are based on this approach, such as nitroxide mediated radical polymerization (NMP),[89,90] atom transfer radical polymerization (ATRP)[85,91] and the same catalytic chain transfer polymerization (CCTP) discussed in Section 1.3.[43–45]

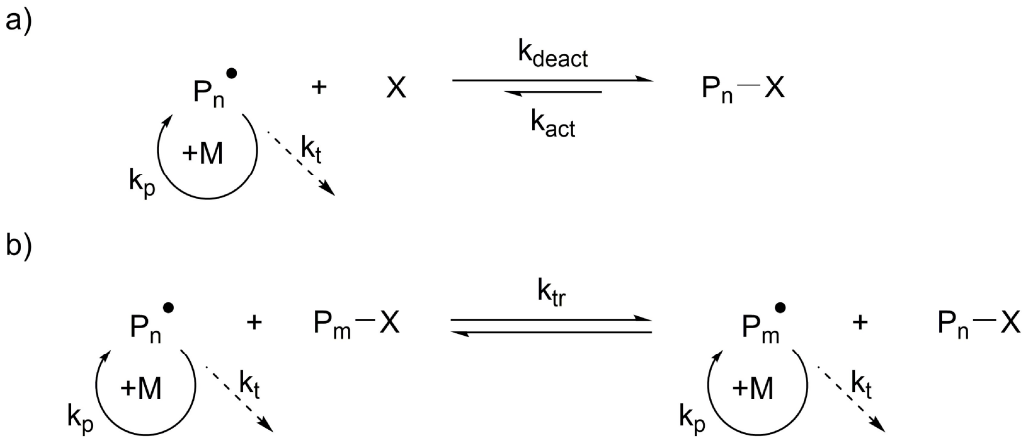

Scheme 1.3 Reversible-deactivation radical polymerization by a) reversible termination and b) degenerative chain transfer.

The second approach makes use of intermittingly active propagating species too but it focuses on a thermodynamically neutral transfer reaction: the radicals cycle between an active and inactive state *via* a degenerative chain-transfer process (Scheme 1.3B).[85] The commonly known reversible addition-fragmentation chain-transfer (RAFT) is based on this principle.[85,87,92]

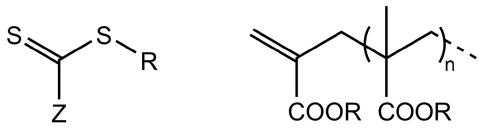

3 **4**

Scheme 1.4 Common classes of RAFT agents.

Nowadays the RAFT reactions most commonly adopted are based on thiocarbonylthio functionalities (**3**), which are exchanged between growing polymer chains (Scheme 1.4). A RAFT polymerization essentially can be seen as the insertion of monomer repeating units between the S-R bond of **3**, forming a macro-RAFT agent; a polymeric unit ending with a RAFT agent functionality.[87] The effectiveness of a RAFT agent depends on the selection of the Z and R groups of **3**. The general rule is that R• should be a better homolytic leaving group than a propagating radical P_n•, or R• should be a more stable radical than P_n• (Scheme 1.5).[85] However, care must be taken as too stable R• will not be able to reinitiate polymerization.[92]

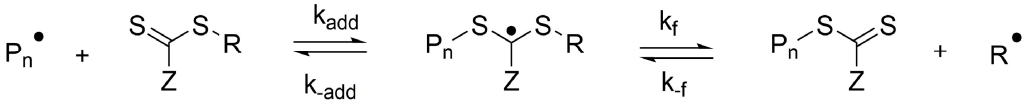

Scheme 1.5 Initialization/pre-equilibrium in a RAFT process.

RAFT polymerization using organo-sulfur chain-transfer agents (**3)** was developed on the back on the discovery by Moad et al. that ω-unsaturated methacrylate-based macromonomers, prepared by CCTP, could undergo the degenerative RAFT mechanism (Scheme 1.4, **4**).[66,67] **4** is essentially a macro-RAFT agent consisting of a methacrylate backbone and a vinyl functional end group. Despite being less active chain-transfer agents,[93,94] the advantage of the use of

macromonomer chemistry over sulfur-based RAFT agents is clearly the absence of added coloration and malodorous compounds.

RAFT using methacrylate macromonomers proceeds in an analogue way to what already described for thiocarbonylthio RAFT agents; monomer units are inserted between the α and β carbon atoms with respect to the vinyl bond. In particular, once an intermediate **A** between a propagating radical and a macromonomer is formed, this can fragment backward (k_{-add}), leading the initial reagents, or forward (k_f) to allow propagation of the macromonomer, now of structure **B** (Scheme 1.6).[45,66,67] The end product, when a methacrylate monomer is adopted in the reaction, is a di-block copolymer which bears a final unsaturated vinyl group with side group R from the initial macromonomer. Instead, when the same reaction is conducted in the presence of acrylates or styrene, graft copolymers are formed.[45,66,67]

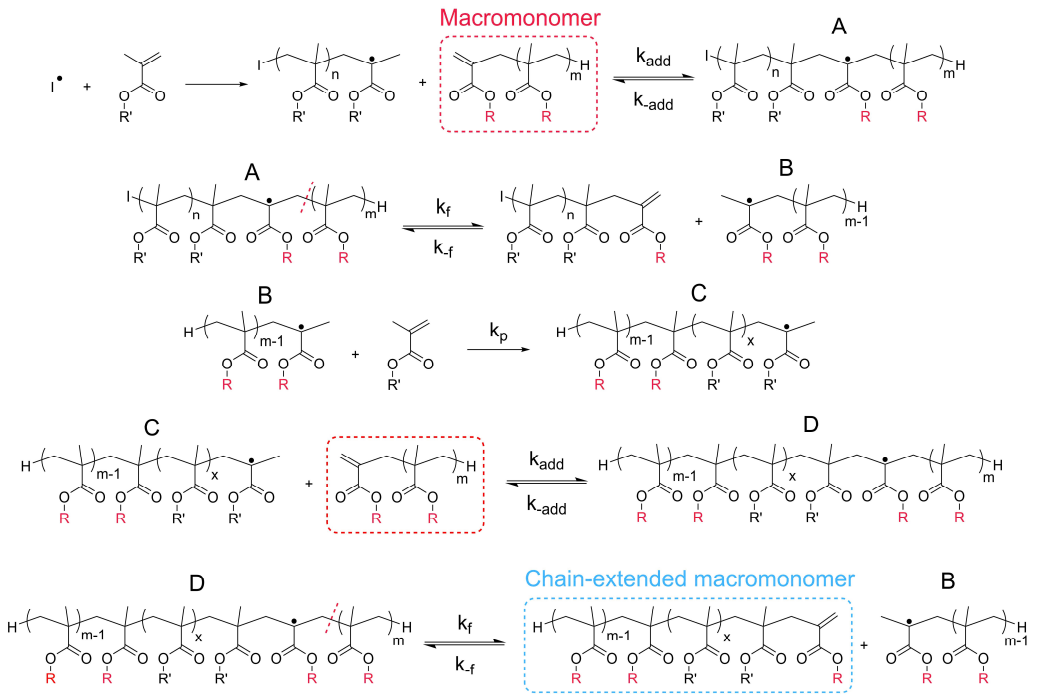

Scheme 1.6 RAFT polymerization adopting a ω-unsaturated methacrylate macromonomer. I is an initiator residue.

In a truly degenerative process, the equilibrium constant (K_{eq}) between reagents and products shown in Scheme 1.3B (and in first two lines of Scheme 1.6) is equal to 1.[85] In reality, K_{eq} may have different values for oligomers of different lengths

or among chains with different R side groups.[93,94] In addition, contrarily to the reaction mediated by organo-sulfur RAFT-agents, in RAFT systems where methacrylate macromonomers are adopted the transfer rate coefficients (k_{tr}) are much smaller than the propagation rates (k_p).[85] Therefore, the chain transfer coefficient, $C_T = k_{tr}/k_p$, has much lower values than for instance a dithioester or thiocarbonylthio RAFT agent; $C_T \sim 0.21$ for a ω-unsaturated methacrylate macromonomer (DP ≈ 24) in the bulk polymerization of methyl methacrylate,[94] whereas typically C_T = 10-100 for organo-sulfur RAFT agents.[87] This leads to polymers with higher dispersities ($Đ_M$) when using methacrylate macromonomers. Polymers with $Đ_M$ as low as 1.2 can still be obtained when operating in monomer starved-fed polymerization conditions, especially in emulsion polymerization systems (see Section 1.3.2).[67,73]

1.5 Thesis outline

This thesis deals with the synthesis of nanocomposite polymer colloidal suspensions where the sole stabilizing agent is a nanometric inorganic or polymeric material. In the case of polymeric stabilizers, two different synthetic pathways will be explored focusing on the absence of malodorous sulfur compounds in the protocol.

After the brief theoretical background presented in this chapter, **Chapter 2** contains a thorough description of a process called *Pickering emulsion polymerization* for the synthesis of polymer particles surrounded by a dense shell of nanometric colloids. In particular SiO_2 nanospheres were adopted as a model system. The adsorption of the stabilizer to the polymer interface, the reaction kinetics and particle formation are investigated in order to have an in-depth understanding of all the parameters governing the reaction. The Pickering-type agent was found to play a prime role in the particle formation stage of the process. Different strategies to enhance the interaction between stabilizing and stabilized phase are also discussed.

Chapter 3 deals with the application of α-hydrogen ω-unsaturated methacrylate-based macromonomers, made by catalytic chain-transfer, to dispersion polymerization for the synthesis of polymeric nanoparticles of different morphologies. All the difficulties regarding the adoption of these macro-chain transfer agents to dispersion polymerization, or *polymerization induced self-assembly*,

are listed and explored from a kinetic viewpoint. Reaction conditions are reported to obtain polymeric particles to be used as stabilizing agents for the process described in Chapter 2. The solutions found still consist of a long and complicated series of reactions, which limit the applicability of the technique.

Chapter 4 is divided in two parts. First, a novel and alternative synthetic pathway to obtain polymer micelles suspensions is described. This overcomes the inherent limitations of methacrylate macromonomers by operating in starved seeded emulsion polymerization conditions. In the second part these polymeric micelles, which are previously bundled together *via* a crosslinking step, are used as stabilizers in an emulsion polymerization reaction similarly to what described in the first experimental chapter. These particles act as seeds for further polymerization to proceed. However, given their crosslinked nature, the newly formed polymer phase-separates on the side of the particle upon growth. The adopted crosslinked polymer micelles, also called *nanogels* in this work, are methacrylic acid-functionalized. Tailoring of the reaction conditions by pH regulation, with consecutive adjustment of the stabilizer surface charge density, is shown to lead to the controlled formation of Janus and patchy particles with a varying number of nanogel patches present on the latex surface.

Similarly, in **Chapter 5** controlled destabilization of the nanogels, coupled to an emulsion polymerization reaction, is explored *via* background electrolyte addition. Even in this case the different morphologies of the latexes obtained at increasing [NaCl] are analysed. Of particular interest are the structures formed at high ionic strength in the dispersing medium which are characterized by micrometric sized latexes covered by a dense shell of nanogels. Kinetic studies are presented in order to establish the mechanism of particle formation. At the end of the chapter, some preliminary film formation studies are shown for the fabrication of coherent polymeric films characterized by an intricate substructure of nanogels.

References

(1) *Colloidal* in *IUPAC Compendium of Chemical Terminology*, IUPAC, Research Triagle Park, NC

(2) C. Pichot, T. Delair and A. Elaïssari, in *Polymeric Dispersions: Principles and Applications*, Springer Netherlands, Dordrecht, 1995, pp. 515–539

(3) R. Jovanović and M. A. Dubé, *J. Macromol. Sci. Part C Polym. Rev.*, 2004, **44**, 1–51

(4) S. Jiang, A. Van Dyk, A. Maurice, J. Bohling, D. Fasano and S. Brownell, *Chem. Soc. Rev.*, 2017, **46**, 3792–3807

(5) A. K. Van Der Vegt, *From polymers to plastics*, VSSD, Delft, 2006

(6) T. Wang and J. L. Keddie, *Adv. Colloid Interface Sci.*, 2009, **147–148**, 319–332

(7) M. Chen, M. Z. Mokhtar, E. Whittaker, Q. Lian, B. Hamilton, P. O'Brien, M. Zhu, Z. Cui, S. A. Haque and B. R. Saunders, *Nanoscale*, 2017, **9**, 10126–10137

(8) A. Snezhko, I. S. Aranson, N. Becker, T. Proslier, A. Demortière and M. V. Sapozhnikov, *Nat. Commun.*, 2014, **5**, 1–7

(9) P. A. Lovell and M. S. El-Aasser, *Emulsion Polymerization and Emulsion Polymers*, J. Wiley, 1997

(10) J. W. Goodwin, J. Hearn, C. C. Ho and R. H. Ottewill, *Br. Polym. J.*, 1973, **5**, 347–362

(11) H. A. S. Schoonbrood and J. M. Asua, *Macromolecules*, 1997, **30**, 6034–6041

(12) D. Arunbabu, Z. Sanga, K. M. Seenimeera and T. Jana, *Polym. Int.*, 2009, **58**, 88–96

(13) P. J. Colver, C. A. L. Colard and S. A. F. Bon, *J. Am. Chem. Soc.*, 2008, **130**, 16850–16851

(14) W. D. Harkins, *J. Am. Chem. Soc.*, 1947, **69**, 1428–1444

(15) T. J. Tulig and M. Tirrell, *Macromolecules*, 1982, **15**, 459–463

(16) S. C. Thickett and R. G. Gilbert, *Polymer (Guildf).*, 2007, **48**, 6965–6991

(17) W. J. Priest, *J. Phys. Chem.*, 2005, **56**, 1077–1082

(18) R. G. Gilbert, *Emulsion polymerization, a mechanistic approach.*, Academic Press Inc., San Diego, 1995

(19) R. M. Fitch, *Br. Polym. J.*, 1973, **5**, 467–483

(20) R. M. Fitch, *Polymer Colloids: A Comprehensive introduction*, Academic Press, London, 1997

(21) J. Ugelstad and F. K. Hansen, *Rubber Chem. Technol.*, 1976, **49**, 536–609

(22) F. K. Hansen and J. Ugelstad, *J. Polym. Sci. Polym. Chem. Ed.*, 1978, **16**, 1953–1979

(23) F. J. Schork, Y. Luo, W. Smulders, J. P. Russum, A. Butté and K. Fontenot, in *Advances in Polymer Science*, 2005, vol. 175, pp. 129–255

(24) L. Scarabelli, M. Schumacher, D. Jimenez de Aberasturi, J.-P. Merkl, M. Henriksen-Lacey, T. Milagres de Oliveira, M. Janschel, C. Schmidtke, S. Bals, H. Weller and L. M. Liz-Marzán, *Adv. Funct. Mater.*, 2019, **29**, 1809071–1809081

(25) X. Cheng, M. Chen, S. Zhou and L. Wu, *J. Polym. Sci. Part A Polym. Chem.*, 2006, **44**, 3807–3816

(26) O. P. Loiko, A. B. Spoelstra, A. M. Van Herk, J. Meuldijk and J. P. A. Heuts, *Polym. Chem.*, 2017, **8**, 2909–2912

(27) D. Nguyen, H. S. Zondanos, J. M. Farrugia, A. K. Serelis, C. H. Such and B. S. Hawkett, *Langmuir*, 2008, **24**, 2140–2150

(28) O. P. Loiko, A. B. Spoelstra, A. M. Van Herk, J. Meuldijk and J. P. A. Heuts, *RSC Adv.*, 2016, **6**, 80748–80755

(29) B. T. T. Pham, C. H. Such and B. S. Hawkett, *Polym. Chem.*, 2015, **6**, 426–435

(30) K. Landfester, *Annu. Rev. Mater. Res.*, 2006, **36**, 231–279

(31) K. Landfester, in *Topics in Current Chemistry*, 2003, vol. 227, pp. 75–123

(32) T. G. T. Jansen, J. Meuldijk, P. A. Lovell and A. M. van Herk, *J. Polym. Sci. Part A Polym. Chem.*, 2016, **54**, 2731–2745

(33) K. Landfester, *Macromol. Rapid Commun.*, 2001, **22**, 896–936

(34) J. M. Asua, *Prog. Polym. Sci.*, 2002, **27**, 1283–1346

(35) B. Brooks, *Chem. Eng. Technol.*, 2010, **33**, 1737–1744

(36) S. L. Canning, G. N. Smith and S. P. Armes, *Macromolecules*, 2016, **49**, 1985–2001

(37) J. N. Israelachvili, *Intermolecular and Surface Forces*, Academic Press., London, 2nd. Ed., 1991

(38) Y. Mai and A. Eisenberg, *Chem. Soc. Rev.*, 2012, **41**, 5969

(39) D. E. Discher and A. Eisenberg, *Science (80-.).*, 2002, **297**, 967–973

(40) K. E. B. Doncom, L. D. Blackman, D. B. Wright, M. I. Gibson and R. K. O'Reilly, *Chem. Soc. Rev.*, 2017, **46**, 4119–4134

(41) A. Blanazs, J. Madsen, G. Battaglia, A. J. Ryan and S. P. Armes, *J. Am. Chem. Soc.*, 2011, **133**, 16581–16587

(42) L. P. D. Ratcliffe, B. E. McKenzie, G. M. D. Le Bouëdec, C. N. Williams, S. L. Brown and S. P. Armes, *Macromolecules*, 2015, **48**, 8594–8607

(43) A. Gridnev, *J. Polym. Sci. Part A Polym. Chem.*, 2000, **38**, 1753–1766

(44) A. A. Gridnev and S. D. Ittel, *Chem. Rev.*, 2001, **101**, 3611–3659

(45) J. P. A. Heuts and N. M. B. Smeets, *Polym. Chem.*, 2011, **2**, 2407–2407

(46) A. Bakac, M. E. Brynildson and J. H. Espenson, *Inorg. Chem.*, 1986, **25**, 4108–4114

(47) A. Marchaj, A. Bakac and J. H. Espenson, *Inorg. Chem.*, 1992, **31**, 4860–4863

(48) A. Bakac and J. H. Espenson, *J. Am. Chem. Soc.*, 1984, **106**, 5197–5202

(49) D. M. Haddleton, D. R. Maloney, K. G. Suddaby, A. V. G. Muir and S. N. Richards, *Macromol. Symp.*, 1996, **111**, 37–46

(50) D. A. Morrison, T. P. Davis, J. P. A. Heuts, B. Messerle and A. A. Gridnev, *J. Polym. Sci. Part A Polym. Chem.*, 2006, **44**, 6171–6189

(51) G. E. Roberts, J. P. A. Heuts and T. P. Davis, *Macromolecules*, 2000, **33**, 7765–7768

(52) J. P. A. Heuts, D. J. Forster, T. P. Davis, B. Yamada, H. Yamazoe and M. Azukizawa, *Macromolecules*, 1999, **32**, 2511–2519

(53) B. B. Wayland, L. Basickes, S. Mukerjee, M. Wei and M. Fryd, *Macromolecules*, 1997, **30**, 8109–8112

(54) B. B. Wayland, G. Poszmik, S. L. Mukerjee and M. Fryd, *J. Am. Chem. Soc.*, 1994, **116**, 7943–7944

(55) S. C. J. Pierik, PhD Thesis, Eindhoven University of Technology, 2002

(56) A. A. Gridnev, *J. Polym. Sci. Part A Polym. Chem.*, 2002, **40**, 1366–1376

(57) G. E. Roberts, J. P. A. Heuts and T. P. Davis, *J. Polym. Sci. Part A Polym. Chem.*, 2003, **41**, 752–765

(58) G. E. Roberts, C. Barner-Kowollik, T. P. Davis and J. P. A. Heuts, *Macromolecules*, 2003, **36**, 1054–1062

(59) K. A. McEwan, S. Slavin, E. Tunnah and D. M. Haddleton, *Polym. Chem.*, 2013, **4**, 2608–2614

(60) J. D. Biasutti, G. Evan Roberts, F. P. Lucien and J. P. A. Heuts, *Eur. Polym. J.*, 2003, **39**, 429–435

(61) A. A. Gridnev, *Polym. J.*, 2005, **24**, 613–623

(62) D. Kukulj, T. P. Davis and R. G. Gilbert, *Macromolecules*, 1997, **30**, 7661–7666

(63) D. Chao, S. Itsuno and K. Ito, *Polym. J.*, 1991, **23**, 1045–1052

(64) K. G. Suddaby, D. M. Haddleton, J. J. Hastings, S. N. Richards and J. P. O'Donnell, *Macromolecules*, 1996, **29**, 8083–8091

(65) D. M. Haddleton, E. Depaquis, E. J. Kelly, D. Kukulj, S. R. Morsley, S. A. F. Bon, M. D. Eason and A. G. Steward, *Polym. Sci. Part A Polym. Chem.*, 2001, **39**, 2378–2384

(66) J. Krstina, C. L. Moad, G. Moad, E. Rizzardo, C. T. Berge and M. Fryd, *Macromol. Symp.*, 1996, **111**, 13–23

(67) J. Krstina, G. Moad, E. Rizzardo, C. L. Winzor, C. T. Berge and M. Fryd, *Macromolecules*, 1995, **28**, 5381–5385

(68) D. M. Haddleton, D. R. Morsley, J. P. O'Donnell and S. N. Richards, *J. Polym. Sci. Part A Polym. Chem.*, 1999, **37**, 3549–3557

(69) N. M. B. Smeets, T. G. T. Jansen, T. J. J. Sciarone, J. P. A. Heuts, J. Meuldijk and A. M. Van Herk, *J. Polym. Sci. Part A Polym. Chem.*, 2010, **48**, 1038–1048

(70) N. M. B. Smeets, U. S. Meda, J. P. A. Heuts, J. T. F. Keurentjes, A. M. van Herk and J. Meuldijk, *Macromol. Symp.*, 2007, **259**, 406–415

(71) N. M. B. Smeets, J. P. A. Heuts, J. Meuldijk, M. F. Cunningham and A. M. van Herk, *Macromolecules*, 2009, **42**, 7332–7341

(72) N. M. B. Smeets, J. P. A. Heuts, J. Meuldijk, M. F. Cunningham and A. M. van Herk, *Macromolecules*, 2009, **42**, 6422–6428

(73) N. G. Engelis, A. Anastasaki, G. Nurumbetov, N. P. Truong, V. Nikolaou, A. Shegiwal, M. R. Whittaker, T. P. Davis and D. M. Haddleton, *Nat. Chem.*, 2017, **9**, 171–178

(74) G. Nurumbetov, N. Engelis, J. Godfrey, R. Hand, A. Anastasaki, A. Simula, V. Nikolaou and D. M. Haddleton, *Polym. Chem.*, 2017, **8**, 1084–1094

(75) A. Lotierzo, B. W. Longbottom, W. H. Lee and S. A. F. Bon, *ACS Nano*, 2019, **13**, 399–407

(76) I. Schreur-Piet and J. P. A. Heuts, *Polym. Chem.*, 2017, **8**, 6654–6664

(77) S. A. F. Bon, D. R. Morsley, J. Waterson, D. M. Haddleton, M. R. Lees and T. Horne, *Macromol. Symp.*, 2001, **165**, 29–42

(78) D. Kukulj, T. P. Davis, K. G. Suddaby, D. M. Haddleton and R. G. Gilbert, *J. Polym. Sci. Part A Polym. Chem.*, 2000, **35**, 859–878

(79) D. R. Morsley, PhD Thesis, University of Warwick, 1999

(80) M. Szwarc, *Nature*, 1956, **178**, 1168–1169

(81) M. Szwarc, M. Levy and R. Milkovich, *J. Am. Chem. Soc.*, 1956, **78**, 2656–2657

(82) D. Baskaran and A. H. E. Muller, *Prog. Polym. Sci.*, 2007, **32**, 173–219

(83) *Living polymerization* in *IUPAC Compendium of Chemical Terminology*, IUPAC, Research Triagle Park, NC

(84) G. Gody, T. Maschmeyer, P. B. Zetterlund and S. Perrier, *Nat. Commun.*, 2013, **4**, 2505

(85) W. A. Braunecker and K. Matyjaszewski, *Prog. Polym. Sci.*, 2007, **32**, 93–146

(86) A. D. Jenkins, R. G. Jones and G. Moad, *Pure Appl. Chem.*, 2009, **82**, 483–491

(87) D. J. Keddie, *Chem. Soc. Rev.*, 2014, **43**, 496–505

(88) G. Moad and D. H. Solomon, *The chemistry of free radical polymerization*, Elsevier Science Inc., Oxford, UK, 2nd editio., 1995

(89) J. Nicolas, Y. Guillaneuf, C. Lefay, D. Bertin, D. Gigmes and B. Charleux, *Prog. Polym. Sci.*, 2013, **38**, 63–235

(90) P. B. Zetterlund, S. C. Thickett, S. Perrier, E. Bourgeat-Lami and M. Lansalot, *Chem. Rev.*, 2015, **115**, 9745–9800

(91) K. Matyjaszewski, *Macromolecules*, 2012, **45**, 4015–4039

(92) S. Perrier, *Macromolecules*, 2017, **50**, 7433–7447

(93) L. Hutson, J. Krstina, C. L. Moad, G. Moad, G. R. Morrow, A. Postma, E. Rizzardo and S. H. Thang, *Macromolecules*, 2004, **37**, 4441–4452

(94) C. L. Moad, G. Moad, E. Rizzardo and S. H. Thang, *Macromolecules*, 1996, **29**, 7717–7726

2

Pickering emulsion polymerization: a kinetic investigation

Pickering emulsion polymerization offers a versatile way of synthetizing hybrid core-shell latexes where a polymer latex is surrounded by an armour of nanoparticles. A clear understanding of the polymerization process is however missing, especially regarding the mechanism of particle formation. This limits the application of the technique for the fabrication of more complex colloids, where, for instance, entirely different stabilizers are used. In this regard, the Pickering emulsion polymerization of methyl methacrylate (MMA) in the presence of nano-sized colloidal silica (Ludox TM-40) is thoroughly analysed. Mechanistic insight is provided by analysing the adsorption of the stabilizer to monomer droplets or swollen latexes, and the polymerization in presence of different amount of stabilizing agent. It was found that the adhesion of the Pickering nanoparticles to the latex surface was not spontaneous. This supported the theory of a coagulative nucleation mechanism based on the heterocoagulation of a growing oligoradical with the Pickering stabilizer. Polymerization kinetics followed by reaction calorimetry showed an increase in rate of polymerization for higher SiO_2 loadings. The conclusions drawn in this chapter are case specific, but the physico-chemical phenomena described are of relevance for systems where different reactions conditions are adopted (Chapters 4 and 5).

2.1 Introduction

Waterborne nanocomposite polymer dispersions in which individual particles are composed of a mixture of a polymeric and an inorganic phase, such as a metal oxide, are an interesting class of materials. The main advantages are the use of water as continuous phase, with clear environmental benefits, and the dual nature of these particles. In this way the physical and mechanical properties of inorganic materials can be combined with the processability and flexibility of polymers. Cases have been reported where the inorganic component was incorporated into dried polymer films to add magnetic response,[1–3] enhance UV absorbance/scattering,[4] or to improve thermal and flame retardant,[5–7] mechanical[5,7–10] or tack adhesion properties.[11] Often, as it is the case in the last example, a synergy in performance is found, hereby outperforming analogous blends of the inorganic and organic components.

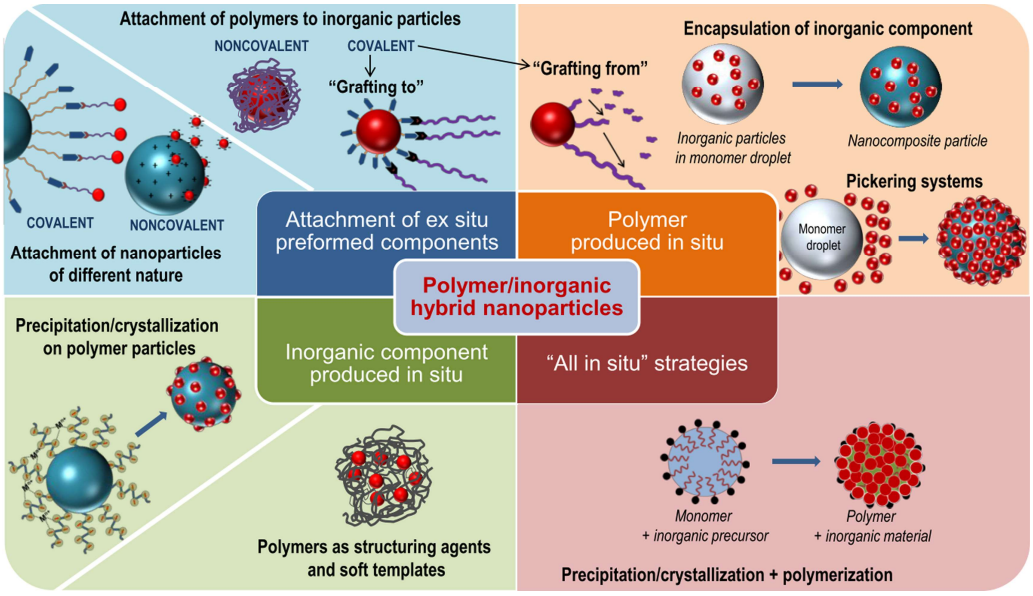

Figure 2.1 Synthetic strategies for the formation of hybrid inorganic/polymer particles. Reproduced with permission from ref. 12.

The approaches adopted for the waterborne synthesis of nanocomposite polymer latexes generally differ in whether the polymerization and/or the synthesis of the inorganic component is conducted *in situ* or *ex situ* (Figure 2.1).[12,13] One morphology type of hybrid particles are armoured polymer colloids in which a

polymeric core is surrounded with an inorganic layer (Figure 2.2). A synthetic strategy towards the fabrication of these particles is Pickering stabilization, a phenomenon whereby particles adhere to a soft deformable interface of, for example, an emulsion droplet.[14–16] The use of such particles as Pickering stabilizers in heterogeneous polymerization processes was first described by Rohm and Trommsdorff in 1934-35.[17] In their work, the authors used talc, barium sulphate, kaolin clay and aluminium oxide in the suspension polymerization of a variety of monomers. Since then Pickering-type heterophase polymerizations have been developed further and now include mini-emulsion,[18–20] dispersion[21,22] and emulsion polymerization processes,[23–29] using a variety of monomers and with a range of fillers, such as silica, laponite clay, magnetite, titanium dioxide, graphene oxide.[30] The two main drivers for the development of heterogeneous Pickering polymerization processes are the already mentioned combination of properties of different materials and that no molecular surfactants are required. The latter offers a big advantage to the paint industry as surfactant migration often deteriorates the performance of coatings.[31,32]

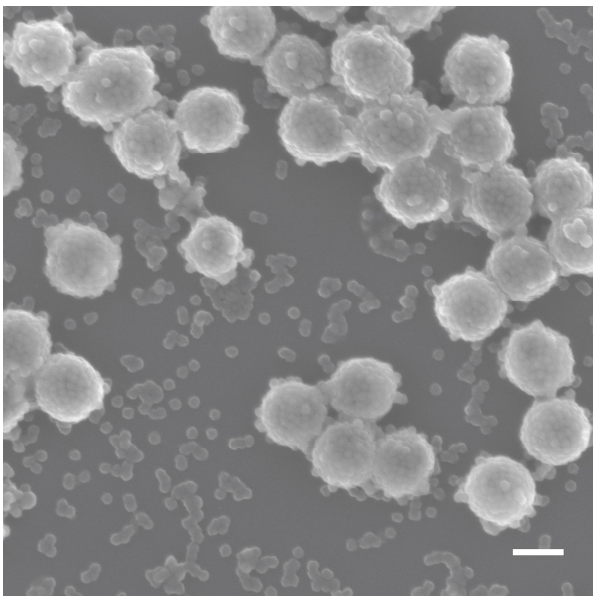

Figure 2.2 SEM image of PMMA-SiO_2 nanocomposite armoured latex particles obtained *via* Pickering emulsion polymerization. Scale bar: 200 nm.

Amongst the different Pickering-type heterogenous polymerization processes, Pickering emulsion polymerization represents an attractive synthetic route

to fabricate hybrid armoured particles of sub-micron size. The name *Pickering emulsion polymerization* derivates from the similarity of this reaction to a standard emulsion polymerization: monomer, water and initiator are mixed with a stabilizer and the latex particles are formed *in situ*, covered by the stabilizing agents. Traditionally, such stabilizers are (macro)molecular amphiphiles, whereas in this process nanosized colloids are adopted. The word *Pickering* is here used given the similarity with Pickering stabilization.[17]

Pickering emulsion polymerization in the literature is often erroneously associated to the polymerization of monomer droplets stabilized by solid particles. The latter should rather be called Pickering suspension polymerization, or if the armoured droplets are small, Pickering mini-emulsion polymerization. This if the standard nomenclature used for (macro)molecular surfactants is adopted. Instead, in Pickering emulsion polymerization, the stabilizer is wrapped onto the surface of the latex particles *in situ*, during their formation. This process presents advantages over the Pickering mini-emulsion strategy as the high-shear emulsification step is omitted. In fact, the preparation of the mini-emulsion is not trivial to scale up, one reason being the abrasive nature of hard nanoparticle suspensions under high shear emulsification conditions.

In the past 10 years Pickering emulsion polymerization has been widely investigated. Hybrid latexes of a wealth of different polymeric compositions have been designed, which included an outer layer of silica spheres,[23,24,27] iron oxide particles,[3] clay disks,[25,29,33] graphene oxide sheets,[28] cerium dioxide spheres[4] or cellulose nanocrystals.[34] In order to obtain these intricate morphologies, in Pickering emulsion polymerization good affinity is required between the two phases. Different strategies have been adopted to enhance the compatibility of the two components, for instance making use of electrostatic attraction,[23] operating at a pH where the inorganic sols are only lightly charged,[24] adding background electrolytes to screen the surface charge[28] or making use of specific interactions between (co)-monomers and the inorganic materials.[27,35] If this prerequisite is met, the nucleated particles are surrounded by Pickering stabilizers from the first stages of the polymerization and they appear fully covered while they grow.[23,24] One other key aspect of this process is that, similarly to (macro)molecular surfactants, larger stabilizer amounts lead to a greater number of particle formed.[25,26] As a result, latexes with tailored sized are

synthetized. Some outstanding questions are however still present on the mechanism of this process, in particular regarding the formation of the hybrid particles and the mechanism of adsorption of the stabilizer at the polymer surface. A clearer understanding on the formation of these colloids is of key importance when designing new materials, with more complex particle morphologies, using entirely different stabilizing agents or where different fillers are incorporated. On this point, overall the previous literature agrees that latex particles form and the stabilizers can spontaneously adsorb at the newly generated bare surface area, increasing the colloidal stability of the system.[23,24,27,36] In addition, it has been suggested that a heterocoagulation process between growing oligomers in the water phase and the inorganic component is in act.[23,24,27,28,33] Clarity is missing regarding which one is the predominant mechanistic pathway or rather if one of the two could be incorrect depending on the system in exam. A second important aspect, which is more of academic relevance, is how the kinetics of Pickering emulsion polymerization compares to standard emulsion polymerization reactions. As explained, if the reaction conditions allow so, typically charged colloids surround the latex particles at every stage of the polymerization. Previous studies on the radical entry coefficient in poly(acrylic acid) electrosterically stabilized latexes showed that longer carboxylic acid hairs on the latex surface significantly reduced the number of radicals per particle, $\bar{n}$, when a persulfate initiator is adopted.[37,38] This suggested that similarly a charged particle at the latex interface would have the same effect.[27] An in-depth kinetic investigation related to Pickering emulsion polymerization was missing until very recently when Sheibat-Othman et al. showed that $\bar{n}$ was independent of the inorganic layer in clay stabilized styrene emulsion polymerizations.[39] As a result the polymerization kinetics could be simulated with already existing polymerization models, independent of the inorganic layer.

In order to address these points, a series of experiments were designed using methyl methacrylate (MMA) as monomer and silica nanoparticles as stabilizers. A small study using styrene is also shown for discussion purposes. Systems containing silica are of particular relevance as the addition of (modified) silica nanoparticles as a separate additive to coating formulations was shown to improve dirt pick-up,[40] optical properties[41] and scratch resistance of the films.[42] The discussion of the chapter will be divided in three sections. First, the adsorption of the inorganic particles onto

MMA monomer droplets and latex particles is discussed. In this section, the interaction between growing oligoradicals in the water phase and the Pickering stabiliser is discussed using styrene as a reference hydrophobic monomer. Second, kinetic data on the Pickering emulsion polymerization of methyl methacrylate in presence of the silica nanosol is presented. Finally, in the last section some further considerations on particle formation are made. It is straightforward that the conclusions drawn for this system are case specific, although the physico-chemical phenomena described can be extended to processes using different reaction conditions (*e.g.* stabilizer, pH, monomer).

2.2 Results and discussion

2.2.1 Adsorption of the stabilizer on monomer droplets & soft latex particles

The interactions between the inorganic and organic components in Pickering emulsion polymerization were explored using a model system consisting of a water-based silica sol and methyl methacrylate (MMA), or styrene, as monomer. In order to investigate the particle formation step of this process, it was decided to first understand whether the silica nanospheres can spontaneously adhere to the monomer droplet/water interface as well as the poly(methyl methacrylate)/water interface. Answering the latter is of key importance as during stage two of a conventional emulsion polymerization process (Harkins classical model)[43] polymer latex particles swollen with monomer are the *loci* where the polymerization takes place.[44] This experiment is hence designed to indicate if the latex particles form and silica adsorbs at their surface as new surface area to stabilize is available or a different mechanism is operating. To address this point, the discussion will here be presented in this sequence:

1. Adhesion to microsized monomer droplets
2. Adhesion to nanozised monomer droplets
3. Adhesion to nanosized soft latex particles fully swollen with monomer

In a characteristic Pickering emulsion polymerization experiment, a water-based sol of colloidal silica was adjusted to acidic pH (3.5-5.5) and added to a 1 L reactor along with the monomer, in this study methyl methacrylate. Lowering the pH

has been shown to be essential to increase the affinity between the organic and inorganic phases for this system.[24] Next, the components are stirred together using an impeller or anchor blade at 200-300 rpm. Through continuous agitation, a coarse dispersion of micrometric size droplets in water is formed. The colloidal particles at this stage can be suspended in water and/or be adsorbed at the monomer-water droplet interface. It has previously been suggested that the stabilizer is adsorbed on monomer droplets in the case of the Pickering emulsion polymerization of styrene using nano-sized silica particles as Pickering stabilizer and in the presence of poly(ethylene glycol) mono methyl ether methacrylate as comonomer.[27] The same was claimed for the system of styrene in the presence of Laponite clay,[36] and the copolymerization of MMA and *n*-butyl acrylate in the presence of glycerol-functionalized silica and a cationic initiator.[23] On the contrary, this could not be necessarily the case for the methyl methacrylate-nanosilica system discussed in this chapter. In exploratory experiments there seemed to be no difference in the stability of the coarse emulsion generated when stirring together water and methyl methacrylate in the absence or presence of silica. In both cases, the monomer droplets phase-separated and coalesced within minutes. This is however not strong proof of either silica adsorption or not. An energy-based analysis of the system can explain these observations. In a first approximation, only surface energy will be taken into account. When discussing Pickering stabilization, one of the most commonly reported equations is the energy necessary to remove a solid particle from a flat liquid-liquid interface, in this case oil-water (Equation 2.1):

$$\Delta G = \pi r_p^{\,2} \sigma_{ow} (1 \pm |\cos \theta_w|)^2 \tag{2.1}$$

where r_p is the particle radius, σ_{ow} is the monomer-water interfacial tension, θ_w is the three-point contact angle. ΔG is ≥ 0 as energy needs to be applied to remove the stabilizer from the interface.

The choice of either + or – sign in Equation 2.1 depends on if the particle is moved from the interface to either of the phases. For instance, a – sign will be used if a hydrophobic colloid is moved from the interface to the oil phase, a + sign if it is moved to the water phase. Usually, for an effective Pickering stabilizer $\Delta G >> k_b T$ (thermal energy), implying that these particles are irreversibly adsorbed at the interface. In the case of 25 nm silica nanoparticles, σ_{ow} = 12.0 mN/m and 25°C, ΔG to

move the particles to the water phase ranges 0.4 - 1600×k_bT when θ_w goes from 10° to 90° (Section A.1 in the Appendix). In comparison ΔG for a molecular surfactant is *ca.* 5×k_bT.[45] Next, these silica nanoparticles are assumed to be adsorbed on a 100 μm droplet, assuming no energy difference generated from curvature effects (*i.e.* Laplace pressure).[46] The kinetic energy (E_k) of this droplet was then calculated (Section A.1). In crude approximation, for the droplet to be fully stabilized by the solid nanoparticles, the energy to displace these particles (ΔG) must be considerably higher of its kinetic energy. This if full energy dissipation is assumed in result of a collision of this droplet with any interface, for example the upper air-water interface or another droplet. E_k was found to be of the same magnitude and even higher than ΔG, with values 18 – 7.7×10^4×ΔG for θ_w varying from 10° to 90° (Section A.1). This implies that even if the silica was adsorbed on micrometric monomer droplets, it could easily be displaced from the interface upon monomer droplet shirking or collision. When considering smaller droplets, for instance of 100 nm in diameter, ΔG can be in the same order of magnitude or exceed E_k, inferring that, depending on the contact angle, the silica particles may be tightly bound to the monomer droplets.

In the previous paragraph silica was assumed to move freely between water and the interface. In actual facts, the presence of a curved interphase,[46] or electrostatic and van der Waals interactions (as explained by the DLVO theory)[47] play an additional, significant role. This can result in an energy barrier against adsorption, which becomes not spontaneous even when thermodynamically favourable.[48,49] To investigate whether or not silica nanoparticles spontaneously adhere to 100-300 nm droplets of MMA, 3 mini-emulsions of 10 wt% MMA (containing 8 wt% hexadecane to suppress Ostwald ripening)[50] were prepared in water. This was done by applying a great input of energy to the system through ultrasound. The first two mini-emulsions were prepared in the presence (A) and absence (B) of silica nanoparticles. In the third (C) system, the nano-silica was added after sonication. Next, the mini-emulsions were stored for 21 days at room temperature, after which the image in Figure 2.3 was taken. Note that these mini-emulsions were not polymerized.

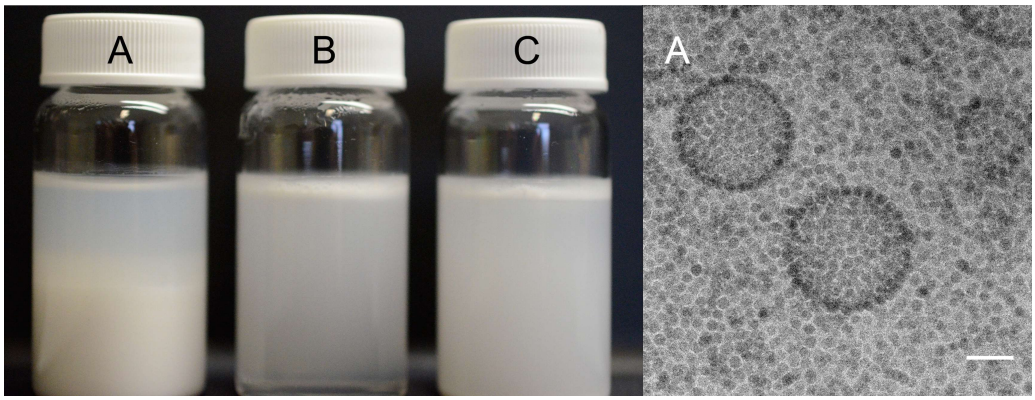

Figure 2.3 (Left) Three mini-emulsions of MMA in water (8 wt% hexadecane with respect to MMA) prepared through emulsification by ultrasound. Emulsion (A) was emulsified in the presence of nanosized silica and the other two (B and C) in the absence of silica. In the case of emulsion (C), the stabilizer was added afterwards. (Right) Cryo-TEM image of emulsion (A). Scale bar: 100 nm.

After preparation of mini-emulsions (B) and (C), a number of large monomer droplets emerged rapidly at the top of the vials through coalescence and creaming. After ageing, these two emulsions showed a clear layer of monomer at the air/water interface (Figure 2.3), indicating that substantial coalescence of the monomer droplets had occurred. The remaining opacity is logical as the distance travelled through buoyancy of small MMA droplets (< 300 nm in diameter) is < 5.4 mm after 21 days at 20°C.[51] Emulsion (C) was more opaque than (B), probably due to the presence of the silica nanoparticles. On the contrary, the first mini-emulsion (A) contained no layer of monomer at the air/water interface. Instead, the mini-emulsion seemed to have partially sedimented. For this to happen, the monomer droplets need to have a density greater than water, which can easily be demonstrated mathematically to be the case for small MMA droplets roughly < 350 nm armoured with a layer of silica nanoparticles. The presence of silica nanoparticles on the surface of the MMA droplets from mini-emulsion (A) was confirmed by cryo-TEM analysis (Figure 2.3, right). Strikingly, no settling of mini-emulsion (C) was observed, indicating that spontaneous adhesion of silica nanoparticles to droplets of MMA does not occur. This indicates that even if the adsorption is thermodynamically favourable, and the electrosteric stabilization of the inorganic particles is sufficient, it appears that there is a barrier against spontaneous adsorption. This could be the result of the electrostatic repulsion between a negative SiO_2 nanoparticle approaching the MMA-

water interface and the negatively charged surface of a monomer droplet.[52] In fact, it has been previously shown that the presence of the double layer provides an electrostatic barrier and can retard or prevent the adsorption of particles at soft interfaces.[48,49] The intensity of this barrier can be surprisingly higher than the hydrodynamic forces pushing the particle towards the droplet.[53,54] As a result, even in the presence of weak forces, external work must be often applied *via* high shear or sonication in order to observe adsorption of particles at a reasonable rate,[54,55] which would confirm the observed results.

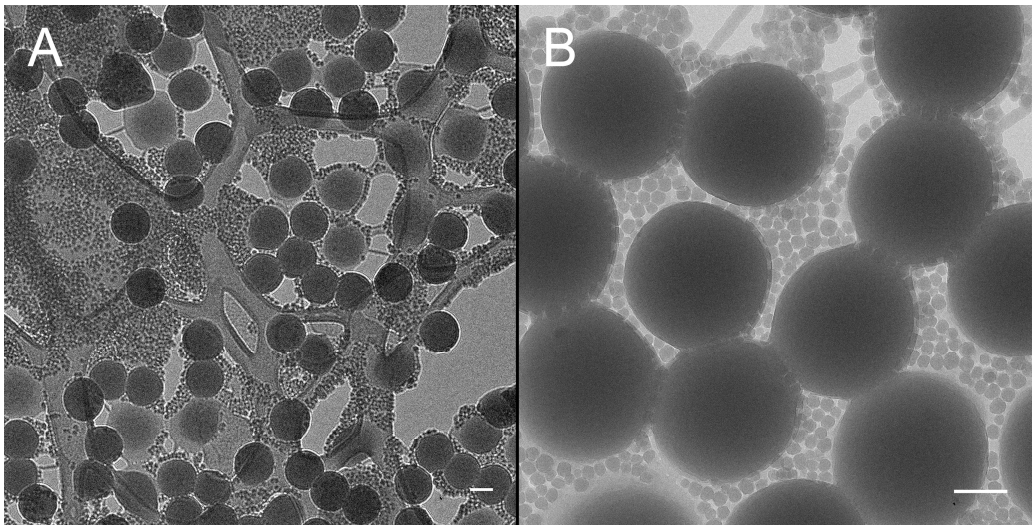

Figure 2.4 Cryo-TEM pictures of soap-free monomer-swollen PMMA latex particles (average diameter ~ 180 nm) in the presence of Ludox TM-40 at pH 4.5. Scale bars: a) 400 nm and b) 100 nm.

The last model system to test is the adsorption of silica to the surface of a swollen latex particle, which as explained in actual fact can be seen as a monomer droplet containing polymer chains.[44] This experiment aims at emulating stage two of emulsion polymerization, where polymer latex particles swollen with monomer are present.[43] When a mixture of a soap-free dialyzed PMMA latex fully swollen with MMA and nanosilica at acidic pH was analysed *via* Cryo-TEM and SEM, no silica was adsorbed on the latex surface (Figure 2.4 and A2.1A). Interestingly, when the same system was exposed to sonication, only latex particles covered in silica were found (Figure A2.1B). Both these two results reinforced the hypothesis of an energy barrier against adsorption, which in case of swollen particles is enhanced due to additional

surface charge (*i.e.* initiator fragments)[56] and likely due to loss of entropy as polymer chains have less conformational freedom when a particle is at the interface.

The results presented until now clearly show that the adhesion of silica nanoparticles does not occur spontaneously, at least when operating in absence of additional attractive forces (*e.g.* Coulombic attraction). The reason for silica adsorption to the latex particles must then be the result of the polymerization process itself. Previously, Colver et al. suggested that, for the MMA polymerization in the presence of SiO_2 nanospheres, spontaneous adsorption of the stabilizer to the newly formed PMMA surface was the reason for the formation of hybrid armoured particles.[24] However, in their study they also hinted that in the early stages of the polymerization a growing oligoradical in the water phase could heterocoagulate onto a silica nanoparticle, hence influencing the number of particles nucleated. In this way silica would behave as a "foreign particle" as described by Fitch (see Section 1.2.3),[57] providing that there is favourable interaction between the two components. This *heterogeneous* nucleation mechanism is a variation of the well-known *homogenous* nucleation mechanism (HUFT-theory): growing oligoradicals in the water phase separate from solution after having reached the critical chain length (j_{crit}) at which they become insoluble in the continuous phase and precipitate as primary particles.[57] The primary particles can subsequently assemble into larger coalesced clusters, hereby minimizing their free energy by decreasing the overall surface area. Instead, when seed particles are present, growing oligomers can heterocoagulate onto seed particles. Clearly, when the seeds are crosslinked or solid, as in the present case, after heterocoagulation the forming polymer phase-separates on the particle surface, rending it amphiphilic and hence surface active. Here it is hypothesised that these Janus-like primary structures can rearrange and cluster forming a small latex particle surrounded by silica spheres. This is supported by the previous observation that the nucleated particles appear to be fully surrounded by Pickering stabilizers from the first stages of the polymerization.[23,24] Once a sufficient number of "clusters" is formed, newly formed amphiphilic stabilizers will statistically have a higher chance of adsorbing at the cluster surface instead of forming new particles, hence explaining how the latexes stay fully covered during their growth. Figure 2.5 shows a schematic of the proposed mechanistic pathway.

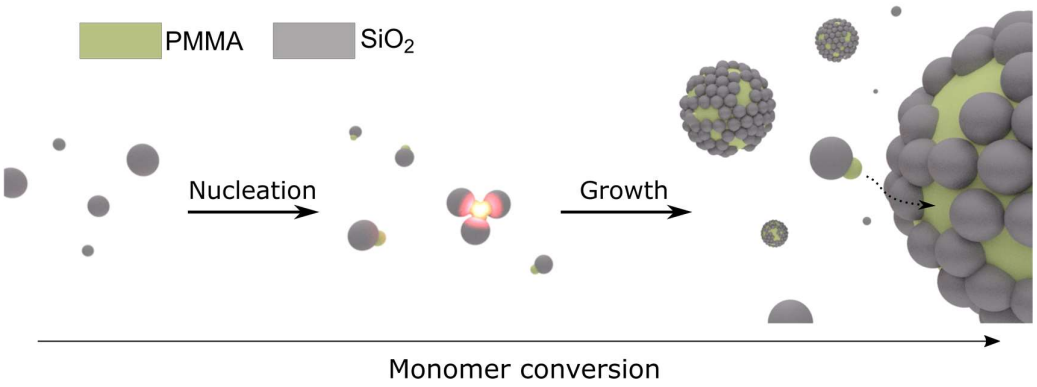

Figure 2.5 Schematic illustrating the proposed mechanism for Pickering emulsion polymerization of methyl methacrylate (MMA) using nanosilica as stabilizer and an anionic initiator.

A similar mechanism was also theorized for other Pickering emulsion polymerization systems. Sheibat-Othman and Bourgeat-Lami reported the synthesis of polystyrene/SiO_2 and poly(styrene-*co*-methyl methacrylate)/SiO_2 nanocomposites formed in the presence of poly(ethylene glycol) methyl ether methacrylate (PEGMEMA).[27] In their work they reported that the particle formation was a combination of heterocoagulation of an oligomer on SiO_2 particles and spontaneous adsorption of SiO_2 onto coagulated primary particles. The latter event is more likely to happen for this system given the presence of PEGMEMA comonomers which can be directly adsorbed on the SiO_2 surface,[58,59] in a way already rendering it partially amphiphilic. Thickett et al. reported the use of graphene oxide in *ab initio* emulsion polymerization, agreeing on a coagulative mechanism involving oligoradicals and graphene oxide sheets.[28] The same was also reported for the synthesis of clay-armored poly(vinylidene chloride-*co*-methyl acrylate) latexes by Lansalot, Bourgeat-Lami et al.[33] A final interesting example is the reported copolymerization of methyl methacrylate and *n*-butyl acrylate using glycerol functionalized silica and 2,2'-azobis(2-methylpropionamidine) as initiator by Armes et al.[23] In their work they explained that the formation of the armoured structures went through a Janus-like intermediate derived by surface polymerization of the cationic initiator adsorbed on the silica surface.

A simple way to prove the validity of this mechanism is designing a system with tailored wettability of the oligomeric radicals. In this way it can be expected that the efficiency of the adsorption can be varied by changing the hydrophilic-hydrophobic balance of the polymer phase. To illustrate this concept, a series of batch emulsion polymerization experiments were designed using styrene as a monomer. As expected, being more hydrophobic than MMA, there is no strong interaction between silica and poly(styrene) (PS) and only bare latex particles were observed (Figure 2.6A). Next, small amounts (up to 3.0 wt%) of hydrophilic comonomers were added to the emulsion polymerization in order to tailor the hydrophilicity of the polymer phase (Table 2.1).

Table 2.1 Comonomers used in the SiO_2-stabilized styrene emulsion polymerizations.

Comonomer	wt%*	Coverage
Methacrylic acid (MAA)	1.0	None
	3.0	None
Di(ethylene glycol) ethyl ether acrylate (DEGEEA)	1.0	Partial
	3.0	Full
MAA/DEGEEA 1/1 w/w	1.0	None
Acrylamide	3.0	None
2-hydroxyethyl methacrylate (HEMA)	3.0	None
Hydroxypropyl methacrylate (HPMA)	3.0	None

Note: Reactions conducted at pH 5.5, 62°C. Ammonium persulfate (APS) was used as initiator; APS/Styrene: 0.14 wt%; solid content (based on monomer only) = 12.7 wt%; silica-to-monomer weight ratio (SiO_2/M) = 1.00 w/w.

The only comonomer that improved SiO_2 adsorption onto the PS surface was di(ethylene glycol) ethyl ether acrylate (DEGEEA). Interestingly, it was also found that the increase in DEGEEA concentration from 1.0 wt% to 3.0 wt% led to higher surface coverage (Figure 2.6B and 2.6C). A good explanation is the strong attractive interaction between the pendant ethylene oxide units and the silica surface,[58,59] as also showed by previous work from Sheibat-Othman and Bourgeat-Lami.[27] This is also combined with low water solubility of DEGEEA at reaction temperature 62-63°C (the cloud point in water is close to room temperature),[60] which would likely result in favoured adsorption on SiO_2. Contrarily, hydroxypropyl methacrylate (HPMA), 2-

hydroxyethyl methacrylate (HEMA) and acrylamide were not effective. The poor results may originate from the large difference in water solubility with respect to styrene, leading to a significant proportion of the comonomer homopolymerizing in the water phase. Methacrylic acid (MAA) is also rather hydrophilic but can promote interaction with silica through H-bonding.[35] However, under reaction conditions, pH ≈ 5, the carboxylic acid groups are partially dissociated and the charge repulsion between the negatively charged carboxylic groups and the silica surface seemed to be the predominant effect; only a very small proportion of the stabilizer was found adsorbed at the PS surface (Figure 2.6D). Even when a mixture of 0.5 wt% of DEGEEA and 0.5 wt% of MAA were adopted, the two effects cancelled out and bare particles were obtained.

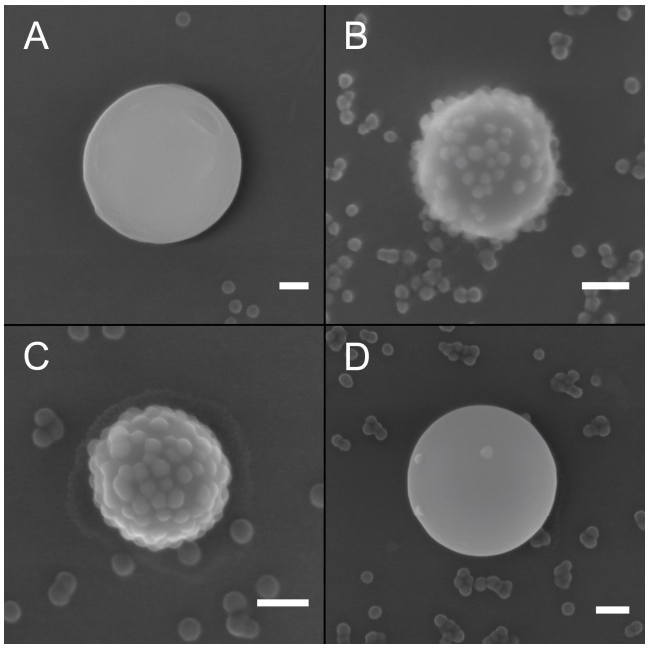

Figure 2.6 SEM images of the latex particles resulting from the Pickering emulsion polymerization of styrene a) in the absence of comonomer, in the presence of b) 1.0 wt% (with respect to styrene) and c) 3.0 wt% of di(ethylene glycol) ethyl ether acrylate or d) 1.0 wt% of MAA. Scale bars: 100 nm. For additional pictures see Figure A2.2.

The mechanism theorized for this reaction can also explain the difference in silica surface packing density observed between the polystyrene-SiO_2 (Figure 2.6) and the PMMA-SiO_2 hybrid latexes (Figure 2.2 and 2.7A). The reason could be the quick consumption of the more hydrophilic comonomer in the early stages of the reaction

in the styrene polymerizations. This would initially lead to a given amount of silica nanoparticles adsorbed at the surface, that would then remain constant during particle growth. Instead, in the case of MMA growing oligoradicals capable of interact with SiO_2 would be formed in the water phase as long as monomer molecules are present in the water phase (until stage III of emulsion polymerization). Once enough latex particles are nucleated, SiO_2-polymer Janus precursors would be captured by existing particles, increasing the density of adsorbed stabilizer.

Contrarily to what discussed for monomer droplets, once the armoured particles are formed, the stabilizer is strongly looked on its surface. PMMA-SiO_2 nanocomposite latexes extremely diluted in water did not show any desorption of the stabilizer, even after 6 months. No desorption was also observed when sodium dodecyl sulfate was added to the PMMA-SiO_2 armoured latex and ultrasounds (frequency 37%) were applied for 5 min. Moreover, dynamic partitioning across particles is also prohibited; mixing an armoured PMMA-SiO_2 nanocomposite latex with a soap-free PMMA latex and stirring the suspension overnight showed no silica redistribution, confirming what elegantly shown in similar experiments conducted by Armes et al.[61,62]

In conclusion to this section, a heterocoagulation event between a growing oligoradical and a silica nanoparticle was hypothesized being the main pathway for armoured particle formation. Such mechanism is also indirectly confirmed by studies on the self-assembly of growing soft-hard Janus polymer particles into clusters which resemble what obtained in Pickering emulsion polymerization.[63–65] The only difference is that in Pickering emulsion polymerization the Janus precursor is made locally and it exists only for a short time. If this mechanism was valid it would also imply that at any reaction time, there can never been more silica particles adhered to the surface than the total number of radicals that underwent "entry" in a silica particle. This if exit events are excluded. For instance, when considering a reaction initiated by 0.117 g of APS, in 671.00 g of water and at 62°C (k_d = 7.1 × 10^{-6} s^{-1}),[66] after 10 min of reaction time 1.1 × 10^{18} radicals are produced when a capture efficiency, f_1, of 0.5 is used to account for the fraction of radicals actually undergoing entry (for more details on the calculations see Equation 4.3 in Chapter 4).[67] In a typical experiment, for instance SiO_2/M = 1.5 w/w (Table 2.2), at this reaction time *ca.* 4.4×10^{16} nanocomposite latex particles (Table 2.3) which have an average

hydrodynamic diameter of 100 nm (Figure 2.8A) have been formed. This would result in 7.6×10^{17} silica nanoparticles adhered to the surface of the latex (packing parameter P = 0.909).[18] The comparison of this value with the number of radicals generated is striking and reinforces the proposed mechanism. Note that in these calculations the hydrodynamic diameter was used instead of the real particle size. The use of the latter leads to overall fewer silica nanoparticles adsorbed at the latex, still validating the hypothesis made.

2.2.2 Rate of polymerization

In the first section of this chapter it is concluded that the most likely pathway for silica adhesion is the Pickering emulsion polymerization process itself, with waterborne oligomeric propagating radicals acting as mediators. As a result, the presence of the silica nanospheres is expected to have a strong influence on the polymerization kinetics and in particular the rate of polymerization. To investigate this, a series of batch emulsion polymerizations of MMA in the presence of varying amounts of SiO_2 nanoparticles were run. MMA was chosen because with this monomer, armoured latex particles can be formed without the need of an auxiliary comonomer.[26] The polymerizations were performed at different silica-to-monomer weight ratios (SiO_2/M). The water-to-monomer ratio and initiator concentration were kept constant (Table 2.2).

Table 2.2 Pickering emulsion polymerizations of methyl methacrylate conducted in the presence of varying SiO_2-to-monomer weight ratios (SiO_2/M).

SiO_2/M w/w	m_{water} / g	m_{silica} /[a] g	d_H / nm	PdI / -
2.00	428.8	429.8	460	0.105
1.50	493.2	322.3	382	0.071
1.00	557.7	214.9	349	0.076
0.75	589.9	161.2	356	0.088
0.50	622.2	107.6	1033	0.253
0.10	673.7	21.5	2281	0.882
0.00	686.6	0.0	845	0.269

Note: Reactions conducted at pH 3.5, 62°C. APS/MMA: 0.14 wt%; solid content (based on monomer only) = 12.7 wt%.

[a] Mass of SiO_2 dispersion in water (*ca.* 40 wt% of silica).

The SiO_2/M ratio was varied from 0.10 to 2.00 w/w and a polymerization without SiO_2 was also performed as a reference. The theoretical final solid content in the absence of stabilizer was 12.5 wt%, based on full conversion of MMA. At this solid content and in the absence of any stabilizer, the system lost colloidal stability in the final stage of the emulsion polymerization, monomer conversion (X) > 0.8, and coagulated. SEM analysis of a sample taken at the end of the reaction showed that secondary nucleation occurred which may be the result of the observed coagulation (Figure 2.7C).

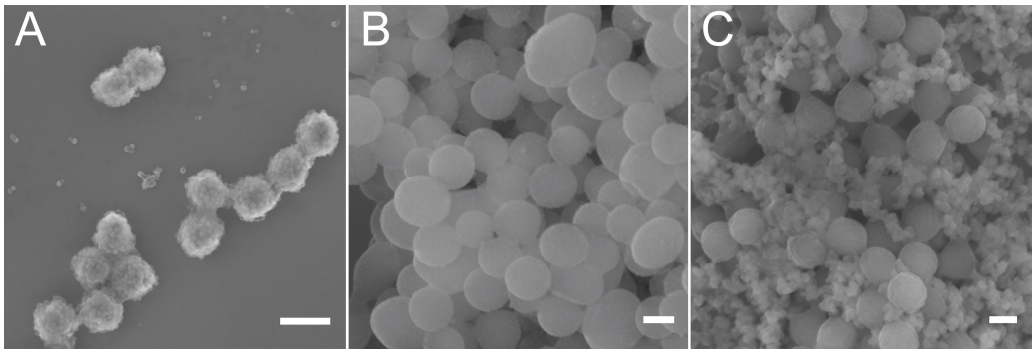

Figure 2.7 SEM pictures of latex nanoparticles formed in the case of a) SiO_2/M=1.50 w/w, b) SiO_2/M = 0.10 w/w, c) SiO_2/M = 0.00 w/w. Scale bars: 300 nm.

In all the experiments in the presence of nano-sized silica, armoured core-shell particles were formed (illustrative examples are provided with Figures 2.7A and 2.7B). Fully stable latexes were obtained for SiO_2/M = 0.75 w/w or higher. Instead, polymerizations conducted at lower silica concentrations resulted in coagulation or microcoagulation of the system. For instance, at SiO_2/M = 0.10 w/w full coagulation arose at approximately 40% monomer conversion, with the formation of clusters of 2 or more fused particles (Figure 2.7B). In the case of SiO_2/M = 0.50 w/w, micro-coagulation was observed, characterized by flocks of clustered particles (Figure A2.3).

The particle size distribution was followed throughout the Pickering emulsion polymerization process (Figure 2.8 for kinetics; Table 2.2 for final values). From this it is evident that the addition of the Pickering stabilizer resulted in a marked reduction of the average particle size, and thus production of a greater number of latex particles. For $SiO_2 \geq 0.75$ w/w, similar particles sizes were observed,

phasing out the effect of the stabilizer on the final latex size. When looking at the particle size dispersity (*PdI*) (Figure 2.8B) two things are worth mentioning. First, the increase in dispersity, which is sometimes observed at higher monomer conversion, is directly associated with coagulation. For example, at $SiO_2/M = 0.10$ w/w the onset of coagulation starts already at $X = 0.15$. Second, there is an initial drop of dispersity as a function of monomer conversion, which appears to extend to greater values of X when more silica is used. This is likely the result of the interference of the scattering signal from the silica nanoparticles. The more the silica is consumed in the reaction, the more the influence is negligible. One final remark is that at the highest SiO_2/M ratio, particles about 100 nm larger than the ones with lower SiO_2 loadings, $0.75 \leq SiO_2/M \leq 1.50$ w/w, were obtained. The viscosity increased noticeably during the reaction due to the high targeted solid content of 37.5 wt%. The reaction did not coagulate but the *PdI* was higher and around 0.10-0.15, likely as a result of prolonged nucleation. Therefore, it appears that there is a window for the amounts of Pickering stabilizer that can be used, below and above which coagulation or broadly dispersed latexes are obtained.

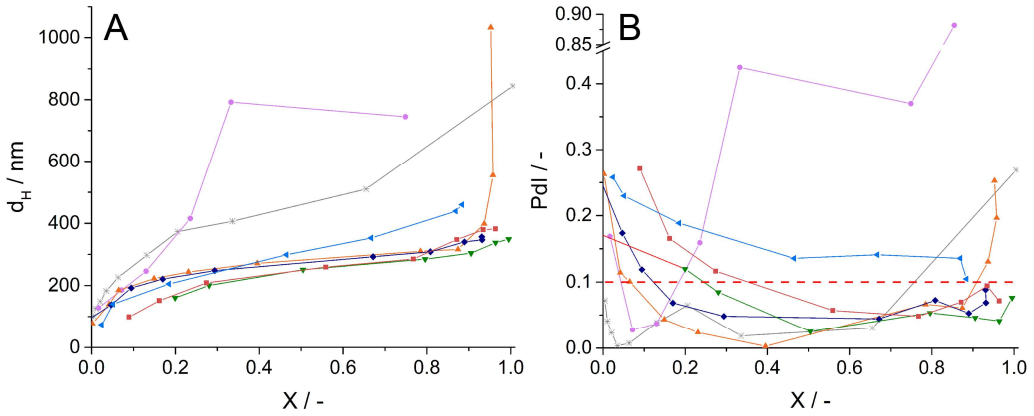

Figure 2.8 Pickering emulsion polymerization of MMA in the presence of different silica/monomer ratios (SiO_2/M). a) Variation of the hydrodynamic diameter (d_H) and b) and the particle dispersity (*PdI*) with X. SiO_2/M = 0.00 (grey), 0.10 (pink), 0.50 (orange), 0.75 (dark blue), 1.00 (green), 1.50 (red), 2.00 (light blue) w/w. The red dotted line represents the *PdI* value below which the latexes were considered of low dispersity.

The kinetics of these emulsion polymerizations were followed online by reaction calorimetry (see Section 2.4.3) using a home-made calorimetry reactor

(Figure A2.4). This allowed to indirectly measure the instantaneous heat of reaction Q_r as a function of the polymerization time. A sample curve displaying Q_r from before initiator injection until the end of the polymerization is showed in Figure 2.9, whereas Figure 2.10A contains the data of all the polymerizations at different SiO_2/M ratios.

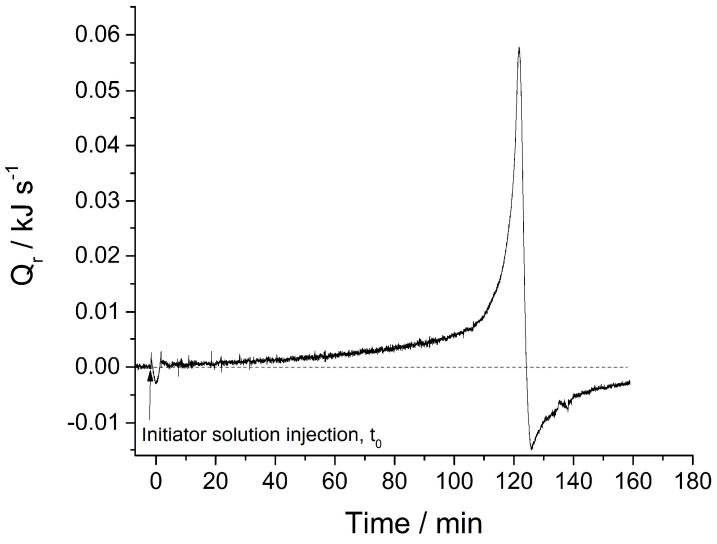

Figure 2.9 Variation of the heat of reaction (Q_r) for the emulsion polymerization of methyl methacrylate (MMA) conducted in absence of silica.

All the curves in Figures 2.9 and 2.10 present a region of steady polymerization followed by a sudden steep increase in Q_r attributed to the occurrence of the gel effect, or Trommsdorff-Norrish effect.[68] The gel effect results from a raise in the reaction rate caused by a drop in the rates of diffusion. The occurrence of this phenomenon in the free radical polymerization of MMA is known to take place at about 20-30% of monomer conversion,[69] as supported by the data collected. The auto-acceleration proceeds until high monomer conversion, *ca.* $X > 0.8$, when the combination of the increase in viscosity of the system, the reduction in the monomer concentration and intraparticle diffusion eventually slow the overall polymerization down. It can be noticed that with the given system and the used calibrations a full monitoring of the polymerization through the whole reaction time was tedious (Figure 2.10B). The drastic drop in temperature after the occurrence of the gel effect is such that the calculated Q_r values after this point are negative even though the reaction has not reached full conversion yet (Figure 2.9). For the purpose of the discussion, only stages of the polymerization up to 80% conversion will be analysed,

for which the calculated values for monomer conversion (see Equation 2.8 in the experimental section) are in excellent agreement with independent gravimetric data (Figure 2.10B).

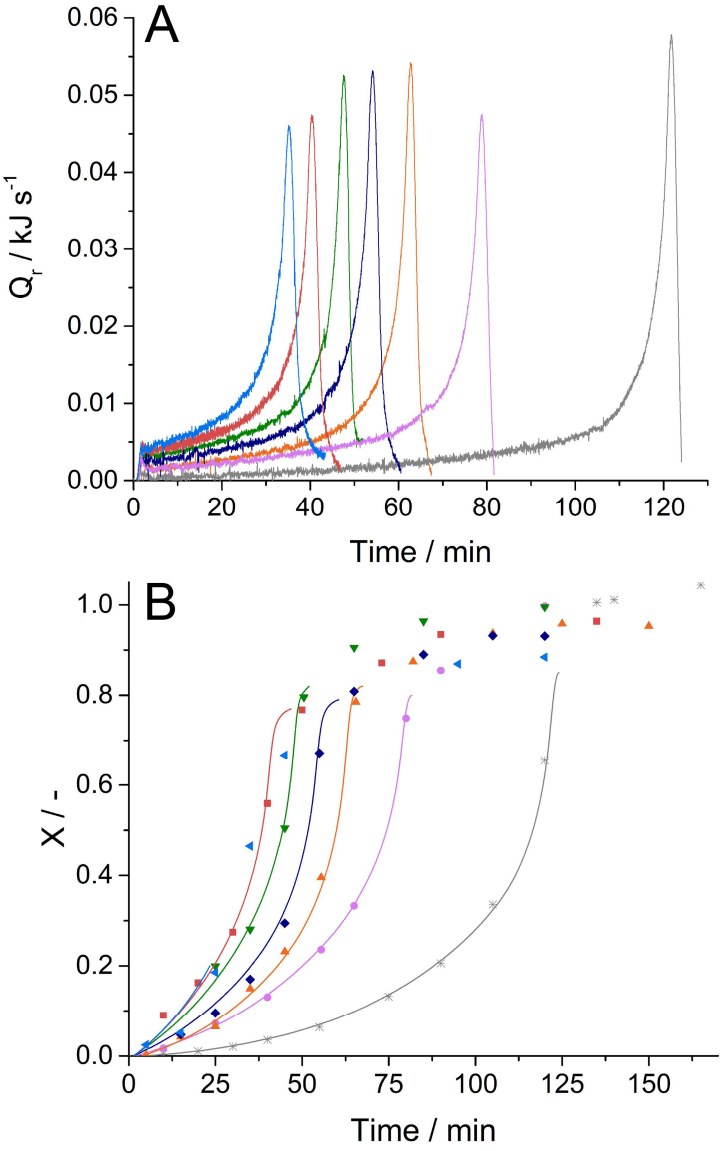

Figure 2.10 a) Variation of the heat of reaction (Q_r) for the Pickering emulsion polymerization of methyl methacrylate (MMA) in the presence of different initial nanosilica/MMA weight ratios (SiO_2/M); b) Estimated monomer conversion from calorimetry data (lines) compared to conversion measured from gravimetry samples withdrawn during the reaction (points). SiO_2/M = 0.00 (grey), 0.10 (pink), 0.50 (orange), 0.75 (dark blue), 1.00 (green), 1.50 (red), 2.00 (light blue) w/w.

An initial look at the reaction heat and monomer conversion data shows that addition of a small amount of silica to the system (SiO_2/M = 0.10 w/w) already led to a considerable shortening of the time required to reach the glassy state (peak in Figure 2.10A) and high monomer conversion, with respect to the reference system in absence of any stabilizer. Further additions of silica progressively played a smaller role in reducing the overall polymerization time until its influence became almost negligible. This is logical as once the silica surface area is large enough to rapidly capture all the oligomers formed, further additions will not lead to additional increase of the rate of reaction. Similar results were reported by Teixeira et al.[25] and by Sheibat-Othman, Bourgeat-Lami et al.[29,70] using Laponite clay in the polymerization of styrene/*n*-butyl acrylate and styrene, respectively. When taking a closer look at the data in Figure 2.10, higher rates of polymerization (R_p) are observed at low to intermediate monomer conversion when increasing amounts of silica are used. R_p can be calculated from conversion data using Equation 2.2:

(2.2) $$R_p = \frac{dX}{dt}\frac{mol_M}{V_{H_2O}}$$

where mol_M is the initial moles of monomer and V_{H_2O} is the total volume of water.

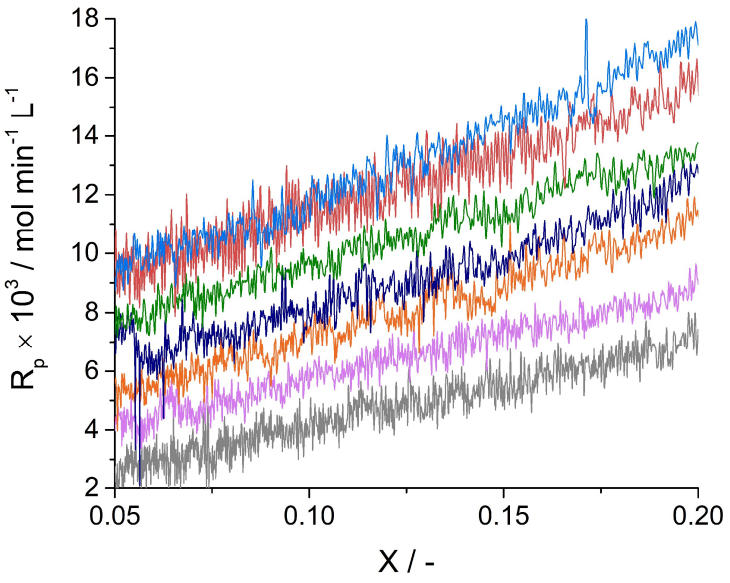

Figure 2.11 Variation in the polymerization rate (R_p) until 20% conversion for the Pickering emulsion polymerization of MMA in the presence of nanosilica. SiO_2/M = 0.00 (grey), 0.10 (pink), 0.50 (orange), 0.75 (dark blue), 1.00 (green), 1.50 (red), 2.00

(light blue) w/w. A broader look at the reaction rates until between 0% and 80% conversion can be found in the Appendix (Figure A2.5a).

R_p calculated in this way is displayed in Figure 2.11. The rate is reported for X between 5% and 20%, as for X > 20% the influence of the Trommsdorff-Norrish effect greatly affects the reaction kinetics (Figure A2.5A). Instead, for X < 5% the signal-to-noise due to the initiator injection is high, especially for the fastest experiments (Figure 2.9). In addition, at very low conversions new particles are still nucleating, resulting in an additional increase in R_p. Roughly, R_p increased with a factor of 4 moving from the polymerization in absence of stabilizer to the one with the highest amount. The origin of these observations can be explained by a number of factors. As explained in Chapter 1, in emulsion polymerization R_p equals the rate of a polymerization in bulk multiplied by the number of latex particles (N_p):

$$R_p = \frac{N_p}{V_{H_2O}} \frac{k_p C_{p,M} \bar{n}}{N_A} \tag{2.3}$$

where k_p is the propagation rate coefficient of the monomer, $C_{p,M}$ is the concentration of the monomer within the latex particles, $\bar{n}$ is the average number of radicals per particle and N_A is the Avogadro number.

k_p in Equation 2.3 was approximately constant for X = 0.05 to 0.20 and for all the reactions performed at different SiO_2/M loadings (Table A2.1). In fact, the increase in temperature between 5% and 20% conversion was 0.6-1.0°C, leading in variations of k_p of only 1.35-2.35%, with similar values across all the runs, hence not explaining the observed trend. $C_{p,M}$ is here reasonably assumed to be constant in all the different reactions at conversions 5-20%; $C_{p,M}$ = 6.6 $\pm$ 0.1 M for PMMA latexes fully swollen in MMA.[67] It is known from previous literature that the concentration of monomer within a polymer latex increases with particle size rapidly until 40-60 nm in diameter and then more slowly to reach an equilibrium value.[71] Even in case of small differences between the samples, it is expected that latexes at lower SiO_2/M will have a higher $C_{p,M}$ at the same value of X,[71] which is opposite of what observed. This means that the reason for the observed 4-fold increase in R_p at different SiO_2/M is related to $\bar{n}$ and, hence, the number of particles, N_p, confirming what previously observed from DLS analysis of the latexes (Table 2.2 and Figure 2.8).

A second observation is that R_p increased linearly with X for $0.05 \leq X \leq 0.20$ for all the reactions but the one conducted at the highest [SiO_2], where the increase did not follow a perfect straight fit (Figure 2.11 and Figure A2.5b). This is arguably the effect of the absence of a steady-state in polymerization rate in stage II of methyl methacrylate emulsion polymerization as observed by Gilbert et al.[67] As explained later in the text, the absence of a steady state is linked with the linear increase of $\bar{n}$ with conversion in stage II. $C_{p,M}$ is also expected to increase within the 5-20% conversion range, however as discussed this trend is usually not linear.[71] Finally, it is not excluded that N_p may still change in this lower conversion range. In this regard, an extra effort was made in analysing the complex nucleation events in Pickering emulsion polymerization in the last section of the Results and Discussion section. However, it is unlikely for N_p to increase linearly with conversion once enough particles have already been nucleated and hence a considerable amount of SiO_2 has been consumed. An exception could be the reaction with SiO_2/M = 2.00 w/w with a possible combination of prolonged nucleation and linear increase in $\bar{n}$ with conversion.

Table 2.3 Number of nucleated particles (N_p) determined *via* SEM analysis.

SiO_2/M	d_{SEM} /[a] nm	σ /[b] nm	N_p / -
2.00	153	18	4.01×10^{16}
1.50	148	12	4.43×10^{16}
1.00	170	14	2.93×10^{16}
0.75	211	9	1.53×10^{16}
0.50	198	12	1.85×10^{16}
0.10	462	88	1.46×10^{15}
0.00	416	15	2.00×10^{15}

[a] Diameter of the poly(methyl methacrylate) phase only, roughly determined by SEM images on an average of *ca.* 100 particles.
[b] Standard deviation of d_{SEM}.

Knowing R_p, $\bar{n}$ can be calculated by rearranging Equation 2.3. In order to do this, N_p is needed. Usually, relatively accurate values for N_p are obtained from SEM/TEM images by measuring the number-based average particle diameter. In this work, this is complicated by the presence of a shell of SiO_2 nanospheres on the latex surface, with additional spheres that can be dried or be adsorbed on top of the shell. In this way, measuring the diameter of the polymer only phase is not trivial and only

rough indicative values can be obtained. An indicative number-based size of the polymer phase only of the latexes was indicatively measured from SEM images and from this N_p was calculated (Table 2.3). It is clear that (micro)coagulation greatly affected the measured N_p for SiO_2/M = 0.00, 0.10 and 0.50. Overall, N_p calculated in this way confirmed what was previously observed; the addition of SiO_2 led to a considerable increase in N_p, which resulted in a surge in the rate of polymerization (Figure 2.11). The obtained values for $\bar{n}$ for the Pickering emulsion polymerization of MMA in the presence of nanosilica are presented in Figure 2.12 for 0.50 ≤ SiO_2/M ≤ 2.00 w/w.

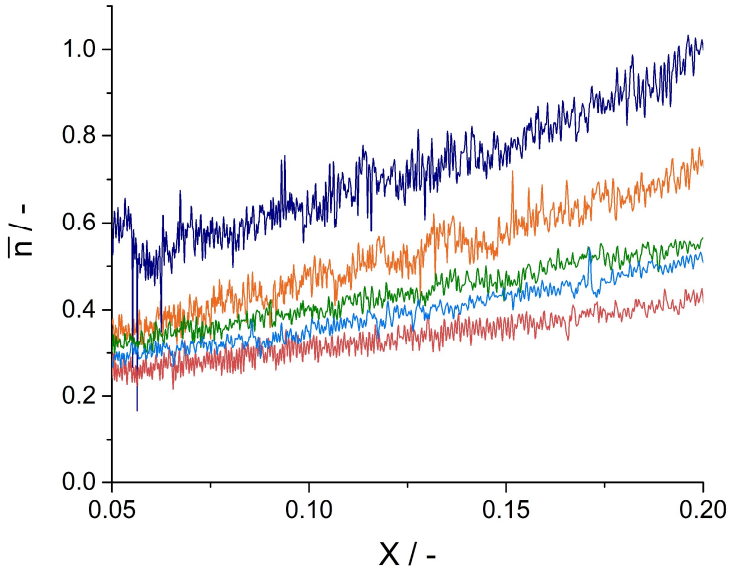

Figure 2.12 Variation in the average number of radicals per particle ($\bar{n}$) between 5% and 20% conversion for the Pickering emulsion polymerization of MMA in the presence of nanosilica. SiO_2/M = 0.50 (orange), 0.75 (dark blue), 1.00 (green), 1.50 (red), 2.00 (light blue) w/w.

All the reactions in absence of coagulation showed $\bar{n}$ values between 0.25 and 1.00 for 0.05 < X < 0.20 and experienced a linear increase with conversion. As previously explained, this is in agreement with the behaviour observed in conventional surfactant stabilized emulsion polymerizations of MMA.[67] Gilbert et al. argued that this trend could be quantified with Equation 2.4 and according to an acceleration parameter, $\bar{\alpha}$:

$$\bar{n} = \bar{n}_0 + \bar{n}_1 \hat{x} \tag{2.4}$$

(2.5) $$\bar{\alpha} = \frac{\bar{n}_1}{\bar{n}_0}$$

where $\bar{n}_0$ is the initial average number of the radicals, $\bar{n}_1$ is the rate (or slope) at which $\bar{n}$ increases with respect to the grams of monomer converted to polymer, $\hat{x}$. Note that in the work of Gilbert, seeded systems were investigated and $\bar{\alpha}$ was made dimensionless by multiplication with the grams of polymer already present in the reactor from the seed addition.

Table 2.4 Acceleration parameter ($\bar{\alpha}$) between 5 and 20% conversion for the reactions performed at different SiO2/M weight ratios.

SiO_2/M	$\bar{n}_1$ / g^{-1}	$\bar{n}_0$ / -	$\bar{\alpha}$ / g^{-1}
2.00	0.018	0.204	0.087
1.50	0.013	0.198	0.066
1.00	0.018	0.242	0.075
0.75	0.035	0.349	0.099
0.50	0.029	0.215	0.136
0.10	0.295	2.210	0.133
0.00	0.209	0.682	0.307

The origin of this acceleration according to the authors can be attributed to a decrease in the pseudo first order rate of termination, resulted from the increase in swollen latex size in the second stage of the emulsion polymerization.[67] $\bar{\alpha}$ was calculated by replotting the $\bar{n}$ data with respect to $\hat{x}$ (Figure A2.6) and ranged between 0.066 and 0.136 in the SiO_2 stabilized emulsion polymerizations (Table 2.4). When in the work by Gilbert et al.[67] $\bar{\alpha}$ was calculated according to Equation 2.5, in the experiments with a similar radical flux, $\bar{\alpha}$ ~ 0.28 (Table 2.4). Unfortunately, direct comparison between the two systems is complicated by the different reaction conditions adopted: in the work from Gilbert et al. a seeded system, using KPS at 50°C was adopted, compared to the *ab initio* experiments of this chapter, using APS at 62°C and conducted in the presence of inorganic colloids. As a result, it is not straightforward to argue similarities or dissimilarities in the two systems. However, here it is believed that the reason for the a higher $\bar{n}_1$ value on the experiments from Gilbert et al. was the lower polymerization temperature of their experiments. This would greatly influence the viscosity within the particles[72] and, therefore, would cause a further drop in the termination rate.[68] For the rest, overall both systems obey

pseudo bulk kinetics[38] and $\bar{n}_0$ is within the same range when reactions with similar N_p and radical flux are compared. Hence, it can be concluded that kinetically the two systems are not that different and share the same features. This is surprising as latexes with a hairy layer of poly(acrylic acid) showed 10 times less radicals per particles in the same reaction conditions of latexes stabilized by conventional surfactants (KPS as initiator).[38] Confirmation of the kinetic similarity between conventional stabilization and stabilization by means of solid particles comes from more recent work by Sheibat-Othman et al.[39] Their work on the styrene emulsion polymerization stabilized by inorganic clay platelets showed complete parallelism between processes conducted in presence and absence of clay. The similarities were to the point that the clay was found to play no influence on $\bar{n}$. $\bar{n}$ decreased for experiments involving a larger clay concentration only as a result of a lower size of the particles formed, hence higher N_p, and not because of the presence of a layer of clay on the particle surface. As a result, the polymerization kinetics could be simulated and fitted with conventional emulsion polymerization theorical models.

2.2.3 Final considerations

In the last part of this chapter a few more comments regarding particle nucleation will be made. In conventional soap-free emulsion polymerization particle nucleation stops when growing oligoradicals are captured exclusively by existing latex particles.[66] This happens when the total surface area of the latex particles is large enough to prevent further aqueous phase propagation, which leads to the formation of new primary particles. Instead, in Pickering emulsion polymerization a growing oligomer can "enter" a silica nanoparticle, sticking to it under the conditions of favourable wetting. As a result, the nucleation process is strongly influenced by the presence of silica nanoparticles suspended in the water phase; more SiO_2 leads to more nanocomposite latexes formed. In this regard, one interesting observation is that at the end of Pickering emulsion polymerizations of methyl methacrylate, when using SiO_2 nanospheres, there is a portion of the stabilizer left in the water phase at the end of the reaction (See Figure 2.2 as a qualitative example).[26] Depending on the entity of such excess, there will be competition for an oligomer in the water phase between entering an existing latex or entering a silica nanosphere suspended in water, leading to the formation of new primary particles. In the latter case, depending

on the number of Janus-like SiO_2 precursors formed, nucleation *via* clustering of primary particles may occur across the whole length of the reaction, leading to highly dispersed latexes. However, this is in contrast with the observation that relatively low dispersity latexes are obtained, when operating at the correct stabilizer-to-polymer ratio. To investigate this, the parameter *f* is introduced as the ratio between the silica and nanocomposite latex surface area (Equation 2.6):

$$f = \frac{m_{SiO_2,0}\rho_p\left(d_H\beta - 2d_{SiO_2}\right)^3}{m_{M,0}X\rho_{SiO_2}d_{SiO_2}{d_H}^2\beta^2} - \frac{4P\left(d_H\beta - 2d_{SiO_2}\right)^2}{{d_H}^2\beta^2} \quad (2.6)$$

where $m_{SiO_2,0}$ is the initial mass of silica, ρ_{SiO_2} is its density, d_{SiO_2} is the average silica diameter according to TEM measurements, *P* is a packing parameter for the SiO_2 nanospheres adsorbed at the latex surface and β is a correction factor to account for use of the hydrodynamic diameters instead of the actual nanocomposite latex sizes.

This parameter essentially describes the likelihood for a growing oligoradical to bump into a silica nanoparticle with respect to a nanocomposite particle. Note that Equation 2.6 takes into account the decrease in silica concentration in the water phase due to the adsorption of the stabilizer onto the latex particles (See Appendix A.2 for the derivation of Equation 2.6).[26] The packing parameter *P* in Equation 2.6 was previously found to be equal to 0.909 for the assembly of 206 SiO_2 nanoparticles on a 162 nm latex sphere.[18] Despite it has already been observed that different silica loadings led to different packing of the stabilizer on the latex surface, for simplicity of the discussion *P* was considered constant across all the samples. In the case of the correction factor, β, it was observed that the SiO_2 nanoparticles used, of 24 ± 3 nm in diameter according to previous TEM measurements, had d_H of *ca*. 35 nm.[26] Assuming that the surface of the nanocomposite latexes is SiO_2-like, this gives a correction factor β = 0.69, which is approximately what found by comparing the latex diameters *via* SEM and DLS analysis.

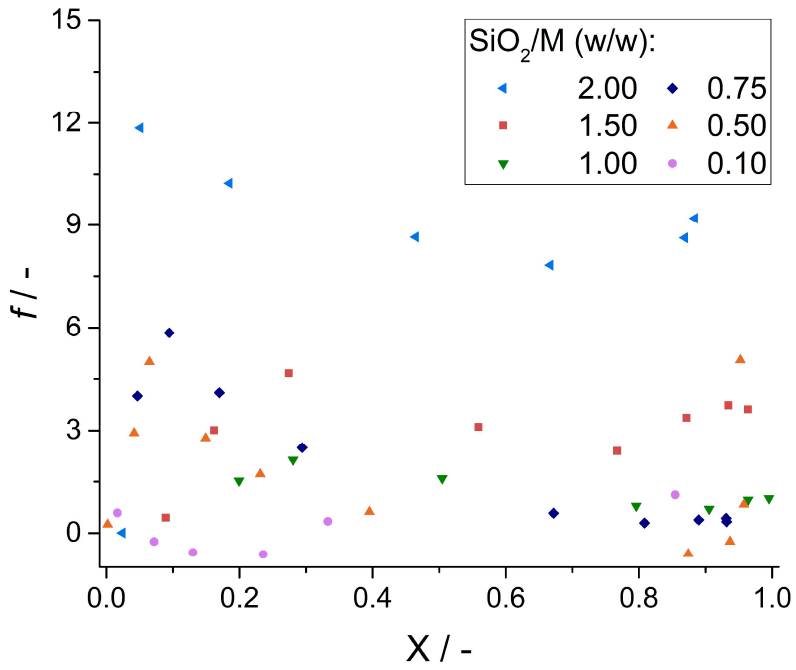

Figure 2.13 Variation of the ratio *f* (silica/nanocomposite particles surface area) as a function of monomer conversion (*X*) for the Pickering emulsion polymerization of MMA and nanosilica.

The variation of *f* with monomer conversion for the different Pickering emulsion polymerizations tested is shown in Figure 2.13. Overall, the data presented inferred a somewhat long nucleation period as for a growing oligomer in water it appeared that was more likely, *i.e.* $f > 1$, to bump into a silica particle than a latex particle until high monomer conversion. At the beginning of the reaction high values of *f* were expected as a growing polymer chain will preferentially enter a silica nanoparticle. This would lead to the rapid formation of armoured latexes, with a consecutive drop in the value of *f*. In actual facts, in Figure 2.13 *f* occasionally appeared to first increase and then drop with conversion. This was just an artefact as *ca.* 70-100 nm clusters were quickly formed at very low conversion (Figure 2.8), leading to an overestimation of the calculated number of particles formed. Approaching higher monomer conversions, *f* reached a steady value, which increased for higher SiO_2 loadings. In particular, $f \sim 1$ for $0.75 \leq SiO_2/M \leq 1.00$ w/w at $X \geq 0.8$, suggesting that it was still quite likely for an oligomer to heterocoagulate on the surface of a silica particle. Instead, for the two highest SiO_2 concentrations, *f* reached an equilibrium value of 3-10. In this way the rather high value of dispersity

for SiO_2/M = 2.00 w/w would be explained as prolonged nucleation (Table 2.2). Finally, the negative values of *f* observed for the two reactions that (micro)-coagulated, 0.10 ≤ SiO_2/M ≤ 0.50 w/w, were the direct result of the onset of particle aggregation, as also observed by DLS (Figure 2.8).

Further considerations need to be made in light of these results. First, in Equation 2.6 the latexes are considered to be unswollen in monomer. This would result in an increase in the latexes surface area up to 80%, if $C_{p,M}$ = 6.6 M,[67] with a consecutive considerable decrease in *f*. Second, only a monolayer of silica is assumed to be adsorbed at the nanocomposite latex particle surface. From Figure 2.2 and 2.7 it appears that more silica spheres can adsorb on top of the armoured latexes, after heterocoagulation with an oligomer. In this way, a SiO_2 Janus-like unstable precursor could adsorb at the surface of a nanocomposite latex before clustering to form a new particle with other primary particles. The counter argument is here that the observed multi-layered adsorption could just be the result of drying effects during SEM sample preparation. However, multi-layer adsorption on armoured latexes was recently shown by Sheibat-Othman et al. for the styrene Pickering emulsion polymerization in presence of clay platelets.[29] One clear difference between the two systems is the possibility for clay disks to stack on one another by van der Waals interactions. Lastly, the data presented does not take into account that in actual facts, the production of oligomers is strongly suppressed after *ca.* 30% conversion, as the monomer is mostly inside the latex particles. This would explain why an excess of stabilizer is present in the water phase at the end of an MMA Pickering emulsion polymerization. On the contrary, when vinyl acetate is used, because of its much higher water solubility (0.15 and 0.50 M respectively for MMA and vinyl acetate in water at 50°C),[66] almost no excess is observed in water after polymerization.[26]

In conclusion, the true *f* values can significantly vary from those reported in Figure 2.13. Lower values would imply that the tendency of nucleating a second crop of particles is suppressed and the final *PdI* is low. This would be in agreement with the experimental observations of this chapter. Nonetheless, Equation 2.6 is able to explain qualitatively the results obtained, shedding further light on the optimal SiO_2/M ratio to use to avoid an excessively long nucleation, with consequent large excess of stabilizer left unreacted in water.

2.3 Conclusion and outlook

This chapter investigated various aspects of silica-stabilized Pickering emulsion polymerizations, in an attempt to come to a better understanding of the overall mechanism of this process. Methyl methacrylate and styrene were used as model hydrophilic and hydrophobic monomers. Along with an extensive series of comments and explanations regarding this polymerization, perhaps two observations stand out. The first is that the silica nanoparticles do not spontaneously adhere to soft latex particles, in absence of attractive forces. This has interesting implications in designing more complex, multi-layered colloids. For example, under these experimental conditions it appears that it is not possible to wrap a swollen seed latex in silica nanospheres and polymerize the monomer to achieve the same core-shell morphology, as in the *ab initio* equivalent. The latter described approach could have been a simple solution to carefully control particle nucleation and achieve an overall higher solid content, which is necessary to form cohesive polymer films. The second outstanding observation is that not great difference was observed kinetically between standard and Pickering emulsion polymerization of methyl methacrylate. Comparison of the data obtained in this work and from previous literature revealed similar kinetic features such as the number of radical per particles, linear increase of $\bar{n}$ in stage II and onset of Trommsdorff effect, with both systems obeying pseudo bulk kinetics. This was surprising as an increased barrier for entry was expected due to the presence of an inorganic shell of particles on the latex surface. Such observation was confirmed and more thoroughly investigated in recent work by Sheibat-Othman et al.[39] In their work the authors observed no difference in $\bar{n}$ for styrene polymerizations conducted in the presence or absence of clay disks as stabilizers. The main implication of these observations is the possibility of simulating these reactions using already existing models which omit the presence of an inorganic shell on the latex surface.

From the results presented in this chapter it is clear that one of the key aspects of Pickering emulsion polymerization is the interaction between the stabilizing agent and the organic phase. As explained in the first section of the chapter, this can be enhanced in a multitude of ways. Herein, the colloidal suspension of the stabilizer was made *unstable*, by decreasing its surface charge, in order to form more *stable* supra-structures. The same concept, applied to Pickering emulsion polymerizations

using a different kind of stabilizer, is re-proposed in Chapters 4 and 5 for the production of polymer latexes of different morphologies using polymeric stabilizers. This introductory set of experiments provided a more thorough understanding of the aspects of this polymerization type and enabled the development of the processes described in the later sections of the thesis.

2.4 Experimental

2.4.1 Materials

Methyl methacrylate (MMA) and styrene (purities ≥ 98%) were purchased from Sigma Aldrich and filtered through basic aluminium oxide to remove the inhibitor. Methacrylic acid (≥ 98%), acrylamide (≥ 98%), hydroxypropyl methacrylate (mixture of isomers, 97%), di(ethylene glycol) ethyl ether acrylate (90% aq.), 2-hydroxyethyl methacrylate (97%), ammonium persulfate (APS) (98%), hexadecane (≥ 99%), colloidal nano silica Ludox TM-40 (d ≈ 25 nm, aq. 40 wt%), were purchased from Sigma Aldrich and used as received. Hydrochloric acid (HCl, aq. 37 wt%) was supplied by Fisher Scientific.

2.4.2 Equipment & methods

All the emulsion polymerizations were carried out in a home-made calorimetry reactor (Figure A2.4) consisting of a 1 L vacuum jacketed vessel (Radleys Ltd.) equipped with a PFTE three blade impeller (Cowie Ltd.) and three high precision Pt100 temperature probes (Omega Engineering inc. and Radleys Ltd.). The three probes measured the temperature of the circulating fluid (silicon oil, kinematic viscosity at 20°C = 10.8 mm^2/s, Julabo GmbH) in the inlet/outlet of the reactor jacket and inside the reactor. These probes were connected to a temperature logger that recorded and displayed the temperatures every second. Extra insulating material (nitrile rubber, thickness 13 mm, RS Components Ltd.) was present around the reactor main body and on the lid. The reactor was run in isoperibolic mode; the temperature of the jacket ($T_{avg,J}$) was kept constant and the reactor temperature (T_r) followed the reaction profile. The silicon oil flux was high and around 11 L min^{-1} in a

way to minimize the temperature difference between the inlet ($T_{J,in}$) and outlet ($T_{J,out}$) of the jacket.

A Branson 450 W digital sonifier was used to make oil-in-water mini-emulsions. pH measurements were taken on a pH benchtop meter A211 (Thermo Scientific Orion). Average particle sizes and distributions were measured by dynamic light scattering (DLS) using a Malvern Zetasizer Nano. Scanning electron microscopy (SEM) and cryogenic transmission electron microscopy (cryo-TEM) analyses were performed on a Zeiss Supra 55-VP FEGSEM and a Jeol 2200FS TEM, respectively.

2.4.3 Calorimetric data analysis

The energy balance equation for a batch calorimetry reactor is given by:[73]

$$Q_{acc} = Q_{st} + Q_r - Q_J - Q_{loss} \tag{2.7}$$

where Q_{acc} is the heat rate accumulated in the reactor, Q_{st} represents the heating due to stirring (here assumed to be zero),[74] Q_r is the heat rate of reaction, Q_J is the heat flow through the reactor wall due to the energy exchange between the reaction medium and the circulating fluid, Q_{loss} is the energy dissipated by the system. Note that all heats are expressed as power, in J s^{-1}.

Q_{acc} and Q_J can be calculated from the following expressions:

$$Q_{acc} = \frac{dT_r}{dt}\left(\sum c_{p,i} m_i\right) \tag{2.8}$$

$$Q_J = UA_h(T_r - T_{avg,J}) \tag{2.9}$$

where $c_{p,i}$ is the heat capacity at the temperature T of the i component, m_i is its mass, U is the global heat transfer coefficient, A_h is the reactor wall surface area of contact between the reaction mixture and the circulating fluid.

Knowing Q_r, the instantaneous monomer conversion (X) can then be estimated:

$$X = \frac{\int_0^{t_i} dQ_r}{\int_0^{t_f} dQ_r} X_{grav,f} \tag{2.10}$$

where $X_{grav,f}$ is the final conversion obtained by gravimetry. This term is added to correct for the actual final conversion of the reaction, otherwise the integrated ratio always equals 1.[75]

Just as a commercial reactor calorimeter, such as the RC1 (Mettler Toledo), UA_h was calculated before and after every reaction and this two-points calibration was used to account for its variation during the reaction.[75,76] Instead of using an electrical heater like in the RC1 reactor, UA_h was measured from temperature ramps before and after the polymerization.[74] As reported in the literature, UA_h can be estimated by plotting $\ln((T_J-T_0)/(T_J-T_{r,i}))$ vs. time during a heating ramp.[77] UA_h can be then obtained from the slope of the resulting straight line:

$$Slope = \frac{UA_h}{\sum c_{p,i} m_i} \tag{2.11}$$

UA_h was found to vary from 3.70 ± 0.06 J K^{-1} s^{-1} before the polymerization to 2.61 ± 0.24 J K^{-1} s^{-1} after the reaction (Table 2.5). The feasibility of this method along with the accuracy of the calculated values were checked with an electrical heater using a procedure explained elsewhere.[78] A value of 4.5 ± 0.10 J K^{-1} s^{-1} was found using just deionized water. The approach adopted here allows to calculate UA_h in reaction conditions and takes into account the volume contraction due to polymerization and solvent evaporation. Q_{loss} was determined by imposing Q_r to be 0 before the initiator injection (Figure 2.9). In this way, Q_{loss} was found to be 2.76 ± 0.25 J s^{-1} (Table 2.5).

Table 2.5 Values of UA_h before, $(UA_h)_i$, and after, $(UA_h)_f$, polymerization and heat loss, Q_{loss}.

SiO_2/M	$(UA_h)_i$ / J K^{-1} s^{-1}	$(UA_h)_f$ / J K^{-1} s^{-1}	Q_{loss} / J s^{-1}
2.00	3.80	2.45	2.90
1.50	3.74	2.25	2.60
1.00	3.71	2.38	3.00
0.75	3.70	2.82	3.00
0.50	3.70	2.73	2.30
0.10	3.60	2.80	2.80
0.00	3.67	2.84	2.70

2.4.4 Typical Pickering emulsion polymerization protocol

86.0 g of silica nanoparticles (214.9 g of Ludox TM-40, aq. 40 wt%) were diluted in 557.7 g of water and the pH of the sol was adjusted to 3.5 using conc. HCl (aq.). The dispersion was poured into the reactor, the reactor was sealed and the void volume was purged with nitrogen gas for 10 minutes. The reaction mixture was further purged for 35 minutes under stirring at 225 rpm. The monomer (MMA, 85.8 g) was separately purged for 15 minutes and injected into the system. The reactor was heated to 62°C (circulator set to 63°C) for 2 hours to reach steady state conditions (with respect to temperature). 3.0 ml of purged deionised water were heated to 75°C and added to a purged sealed vial containing APS (0.117 g). The resulted solution was then immediately injected into the reactor to start the polymerization.

Samples (typically 1 g) were withdrawn throughout the polymerization to check monomer conversion *via* gravimetry.

2.4.5 Miniemulsions preparation

For the preparation of miniemulsion A, 36.0 g of Ludox TM-40 were diluted with 144.0 g of deionized water in a glass jar and the pH of the suspension was adjusted to 3.5 using concentrated HCl (aq.). 16.5 g of MMA were added to the suspension along with 1.3 g of hexadecane to suppress Oswald ripening (8.0 wt% with respect to MMA).[50] The suspension was sonicated under vigorous stirring at 70% amplitude for 3 minutes with 30 sec wait every 30 sec. The jar was immersed in an ice bath during the sonication to prevent temperature rise.

References

(1) N. Yanase, H. Noguchi, H. Asakura and T. Suzuta, *J. Appl. Polym. Sci.*, 1993, **50**, 765–776

(2) Z. Xu, A. Xia, C. Wang, W. Yang and S. Fu, *Mater. Chem. Phys.*, 2007, **103**, 494–499

(3) K. Li, P. Y. Dugas, M. Lansalot and E. Bourgeat-Lami, *Macromolecules*, 2016, **49**, 7609–7624

(4) J. L. Keddie, E. Bourgeat-Lami, F. Dalmas, K. L. Elidottir, S. J. Hinder, I. Martín-Fabiani, M. Lansalot, M. L. Koh and I. Jurewicz, *ACS Appl. Nano Mater.*, 2018, **1**, 3956–3968

(5) X. Zhou, H. Shao and H. Liu, *Colloid Polym. Sci.*, 2013, **291**, 1181–1190

(6) T. Kashiwagi, A. B. Morgan, J. M. Antonucci, M. R. VanLandingham, R. H. Harris, W. H. Awad and J. R. Shields, *J. Appl. Polym. Sci.*, 2003, **89**, 2072–2078

(7) T.-H. Hsieh, J.-K. Huang, K.-S. Ho, X. Bi, T.-H. Ho, S.-S. Yang and Y.-C. Chang, *J. Polym. Sci. Part B Polym. Phys.*, 2008, **46**, 1214–1225

(8) M. Al-Qadhi, N. Merah and Z. M. Gasem, *J. Mater. Sci.*, 2013, **48**, 3798–3804

(9) Y. Kim and J. L. White, *J. Appl. Polym. Sci.*, 2003, **90**, 1581–1588

(10) R. Ollier, E. Rodriguez and V. Alvarez, *Compos. Part A Appl. Sci. Manuf.*, 2013, **48**, 137–143

(11) T. Wang, P. J. Colver, S. A. F. Bon and J. L. Keddie, *Soft Matter*, 2009, **5**, 3842–3849

(12) M. A. Hood, M. Mari and R. Muñoz-Espí, *Materials (Basel).*, 2014, **7**, 4057–4087

(13) E. Bourgeat-Lami, *J. Nanosci. Nanotechnol.*, 2002, **2**, 1–24

(14) P. Finkle, H. D. Draper and J. H. Hildebrand, *J. Am. Chem. Soc.*, 1923, **45**, 2780–2788

(15) S. U. Pickering, *J. Chem. Soc., Trans.*, 1907, **91**, 2001–2021

(16) W. Ramsden, *Proc. R. Soc. London*, 1904, **72**, 156–164

(17) US 2171765 A, 1939

(18) S. Fortuna, C. A. L. Colard, A. Troisi and S. A. F. Bon, *Langmuir*, 2009, **25**, 12399–12403

(19) S. A. F. Bon and P. J. Colver, *Langmuir*, 2007, **23**, 8316–8322

(20) S. Cauvin, P. J. Colver and S. A. F. Bon, *Macromolecules*, 2005, **38**, 7887–7889

(21) M. J. Percy, V. Michailidou, S. P. Armes, C. Perruchot, J. F. Watts and S. J. Greaves, *Langmuir*, 2003, **19**, 2072–2079

(22) M. Gill, J. Mykytiuk, S. P. Armes, J. L. Edwards, T. Yeates, P. J. Moreland and C. Mollett, *J. Chem. Soc., Chem. Commun.*, 1992, **0**, 108–109

(23) L. A. Fielding, J. Tonnar and S. P. Armes, *Langmuir*, 2011, **27**, 11129–11144

(24) P. J. Colver, C. A. L. Colard and S. A. F. Bon, *J. Am. Chem. Soc.*, 2008, **130**, 16850–16851

(25) R. F. A. Teixeira, H. S. McKenzie, A. A. Boyd and S. A. F. Bon, *Macromolecules*, 2011, **44**, 7415–7422

(26) C. A. L. Colard, R. F. A. Teixeira and S. A. F. Bon, *Langmuir*, 2010, **26**, 7915–7921

(27) N. Sheibat-Othman and E. Bourgeat-Lami, *Langmuir*, 2009, **25**, 10121–10133

(28) S. C. Thickett and P. B. Zetterlund, *ACS Macro Lett.*, 2013, **2**, 630–634

(29) B. Brunier, N. Sheibat-Othman, Y. Chevalier and E. Bourgeat-Lami, *Langmuir*, 2016, **32**, 112–124

(30) A. Schrade, K. Landfester and U. Ziener, *Chem. Soc. Rev.*, 2013, **42**, 6823–6839

(31) D. Scalarone, M. Lazzari, V. Castelvetro and O. Chiantore, *Chem. Mater.*, 2007, **19**, 6107–6113

(32) S. Jiang, A. Van Dyk, A. Maurice, J. Bohling, D. Fasano and S. Brownell, *Chem. Soc. Rev.*, 2017, **46**, 3792–3807

(33) L. Delafresnaye, P.-Y. Dugas, P.-E. Dufils, I. Chaduc, J. Vinas, M. Lansalot and E. Bourgeat-Lami, *Polym. Chem.*, 2017, **8**, 6217–6232

(34) E. Limousin, N. Ballard and J. M. Asua, *Polym. Chem.*, 2019, **10**, 1823–1831

(35) M. J. Percy, J. I. Amalvy, D. P. Randall, S. P. Armes, S. J. Greaves and J. F. Watts, *Langmuir*, 2004, **20**, 2184–2190

(36) N. Sheibat-Othman, A. M. Cenacchi-Pereira, A. M. Dos Santos and E. Bourgeat-Lami, *J. Polym. Sci. Part A Polym. Chem.*, 2011, **49**, 4771–4784

(37) S. C. Thickett and R. G. Gilbert, *Macromolecules*, 2006, **39**, 6495–6504

(38) S. C. Thickett and R. G. Gilbert, *Polymer (Guildf).*, 2007, **48**, 6965–6991

(39) B. Brunier, N. Sheibat-Othman, Y. Chevalier and É. Bourgeat-Lami, *AIChE J.*, 2018, **64**, 2612–2624

(40) EP2408864, 2012

(41) J. Moghal, S. Reid, L. Hagerty, M. Gardener and G. Wakefield, *Thin Solid Films*, 2013, **534**, 541–545

(42) F. Bauer, R. Flyunt, K. Czihal, M. R. Buchmeiser, H. Langguth and R. Mehnert, *Macromol. Mater. Eng.*, 2006, **291**, 493–498

(43) W. D. Harkins, *J. Am. Chem. Soc.*, 1947, **69**, 1428–1444

(44) P. A. Lovell and M. S. El-Aasser, *Emulsion Polymerization and Emulsion Polymers*, J. Wiley, 1997

(45) D. J. French, A. T. Brown, A. B. Schofield, J. Fowler, P. Taylor and P. S. Clegg, *Sci. Rep.*, 2016, **6**, 31401

(46) J. P. Bum, D. Lee and E. M. Furst, in *Pickering-Stabilized Emulsions and Colloids*, eds. T. Ngai and S. A. F. Bon, Royal Society of Chemistry, Cambirdge, 2015

(47) P. C. Hiemenz and R. Rajagopalan, *Principles of Colloid and Surface Chemistry*, Taylor and Francis Group, 1997

(48) S. Kutuzov, J. He, R. Tangirala, T. Emrick, T. P. Russell and A. Böker, *Phys. Chem. Chem. Phys.*, 2007, **9**, 6351

(49) A. M. Rahmani, A. Wang, V. N. Manoharan and C. E. Colosqui, *Soft Matter*, 2016, **12**, 6365–6372

(50) J. M. Asua, *Prog. Polym. Sci.*, 2002, **27**, 1283–1346

(51) G. G. Stokes, *Trans. Cambridge Philos. Soc.*, 1851, **9**, 8–106

(52) H. Wang, V. Singh and S. H. Behrens, *J. Phys. Chem. Lett.*, 2012, **3**, 2986–2990

(53) S. Tcholakova, N. D. Denkov and A. Lips, *Phys. Chem. Chem. Phys.*, 2008, **10**, 1608–1627

(54) A. Stocco, E. Rio, B. P. Binks and D. Langevin, *Soft Matter*, 2011, **7**, 1260

(55) K. Du, E. Glogowski, T. Emrick, T. P. Russell and A. D. Dinsmore, *Langmuir*, 2010, **26**, 12518–12522

(56) K. H. Van Streun, W. J. Belt, P. Piet and A. L. German, *Eur. Polym. J.*, 1991, **27**, 931–938

(57) R. M. Fitch, *Polymer Colloids: A Comprehensive introduction*, Academic Press, London, 1997

(58) P. Aranda and E. Ruiz-Hitzky, *Chem. Mater.*, 1992, **4**, 1395–1403

(59) N. Derkaoui, S. Said, Y. Grohens, R. Olier and M. Privat, *Langmuir*, 2007, **23**, 6631–6637

(60) C. R. Becer, S. Hahn, M. W. M. Fijten, H. M. L. Thijs, R. Hoogenboom and U. S. Schubert, *J. Polym. Sci. Part A Polym. Chem.*, 2008, **46**, 7138–7147

(61) J. a Balmer, O. O. Mykhaylyk, J. P. a Fairclough, A. J. Ryan, S. P. Armes, M. W. Murray, K. a Murray and N. S. J. Williams, *J. Am. Chem. Soc.*, 2010, **132**, 2166–2168

(62) J. A. Balmer, E. C. Le Cunff and S. P. Armes, *Langmuir*, 2010, **26**, 13662–13671

(63) J. Yuan, W. Zhao, M. Pan and L. Zhu, *Macromol. Rapid Commun.*, 2016, **37**, 1282–1287

(64) T. S. Skelhon, Y. Chen and S. A. F. Bon, *Soft Matter*, 2014, **10**, 7730–7735

(65) D. J. Kraft, W. S. Vlug, C. M. Van Kats, A. Van Blaaderen, A. Imhof and W. K. Kegel, *J. Am. Chem. Soc.*, 2009, **131**, 1182–1186

(66) R. G. Gilbert, *Emulsion polymerization, a mechanistic approach.*, Academic Press Inc., San Diego, 1995

(67) M. J. Ballard, D. H. Napper and R. G. Gilbert, *J. Polym. Sci. Polym. Chem. Ed.*, 1984, **22**, 3225–3253

(68) E. Trommsdorff, H. Kohle and P. Langally, *Makromol. Chem.*, 1948, **1**, 169

(69) S. T. Balke and A. E. Hamielec, *J. Appl. Polym. Sci.*, 1973, **17**, 905–949

(70) B. Brunier, N. Sheibat-Othman, M. Chniguir, Y. Chevalier and E. Bourgeat-Lami, *Langmuir*, 2016, **32**, 6046–6057

(71) K. Tauer, H. Kaspar and M. Antonietti, *Colloid Polym. Sci.*, 2000, **278**, 814–820

(72) R. S. Porter and J. F. Johnson, *J. Polym. Sci. Part C Polym. Symp.*, 2007, **15**, 373–380

(73) M. Esposito, C. Sayer, R. A. F. Machado and P. H. H. Araújo, *Macromol. Symp.*, 2008, **271**, 38–47

(74) E. Bourgeat-Lami, N. Sheibat-Othman and A. M. Dos Santos, in *Polymer Nanocomposites by Emulsion and Suspension Polymerization*, Royal Society of Chemistry, Cambridge, 2011, pp. 269–311

(75) L. V. De La Rosa, E. D. Sudol, M. S. El-Aasser and A. Klein, *J. Polym. Sci. Part A Polym. Chem.*, 1996, **34**, 461–473

(76) S. BenAmor, D. Colombié and T. McKenna, *Ind. Eng. Chem. Res.*, 2002, **41**, 4233–4241

(77) F. X. McConville, *The Pilot Plant Real Book*, FXM Engineering and Design, 1st ed., 2002

(78) I. S. De Buruaga, A. Echevarría, P. D. Armitage, J. C. De la Cal, J. R. Leiza and J. M. Asua, *AIChE J.*, 1997, **43**, 1069–1081

3

"Sulfur-free" polymer self-assemblies *via* dispersion polymerization

This chapter contains selected studies on the applicability of methacrylate-based ω-end macromonomers in dispersion polymerization. This process, also named polymerization induced self-assembly (PISA), is an attractive synthetic route to produce self-assembled colloidal nano-structures of various morphologies. The use of methacrylate macromonomers as reversible addition-fragmentation chain-transfer (RAFT) agents in heterogeneous polymerizations is however not trivial, because of their inherent low chain-transfer activity. This will be demonstrated studying the well-known 2-hydroxypropyl methacrylate (HPMA) aqueous chain-extension of poly(glycerol methacrylate) (PGMA) macro-RAFT agents. In this work it is demonstrated that two obstacles need to be overcome when using ω-end methacrylate macromonomers; the lower chain-transfer coefficient relative to the more common sulfur-based RAFT-agents and uncontrolled nucleation events. (Semi)-batch dispersion polymerizations of HPMA in presence of PGMA macromonomers showed limited control over chain-growth and polymer self-assembly. These issues were tackled by starting the polymerization with an amphiphilic thermo-responsive diblock copolymer, already "phase-separated" from solution. In this way, polymer colloids of various morphologies were obtained, without the need of sulfur-based RAFT agents.

3.1 Introduction

Control of macromolecular chain architecture using radical polymerizations has gone through a renaissance as a result of the development of "reversible-deactivation radical polymerization" (RDRP).[1–3] Accessible routes towards the synthesis of amphiphilic polymers have catalyzed scientific studies into the self-assembly behavior of such polymers in liquids. Control over the dynamics of the self-assembly process and the resulting morphologies of the polymeric colloidal objects have been of considerable interest.[4–6] Polymerization induced self-assembly (PISA) is an emerging area that couples control of chain-growth, and thus molecular architecture, with dynamic self-assembly of the produced macromolecules into colloidal structures. [7–14] Along with conventional emulsion polymerization, in the past 20 years since its development, PISA has become a popular synthetic approach to make polymeric dispersions. PISA is a heterogeneous polymerization technique, typically performed under dispersion or emulsion polymerization conditions. When performed in dispersion polymerization conditions, typically a lyophilic polymer dissolved in a solvent is chain-extended with a monomer which is also lyophilic, but the polymer is not. Hence, during the chain-extension the second block gradually becomes insoluble. This drives the assembly of the block copolymer chains into colloidal objects, which can be seen as a particle nucleation event.

One of the key aspects of PISA is that the polymer chains can dynamically rearrange into different colloidal morphologies (*e.g.* spheres, worms and vesicles) throughout the polymerization.[12,13] The reason for this is that amphiphilic molecules (Figure 3.1), and hence macromolecules such as block copolymers, form different self-assembled superstructures in solution. The favored dynamic superstructure can be predicted using the packing parameter (P) (Equation 3.1):[15]

$$P = \frac{v}{a_0 l_C} \tag{3.1}$$

where v is the volume of the lyophobic chain, a_0 is the optimal area of the head group and l_C is the length of the lyophilic tail.

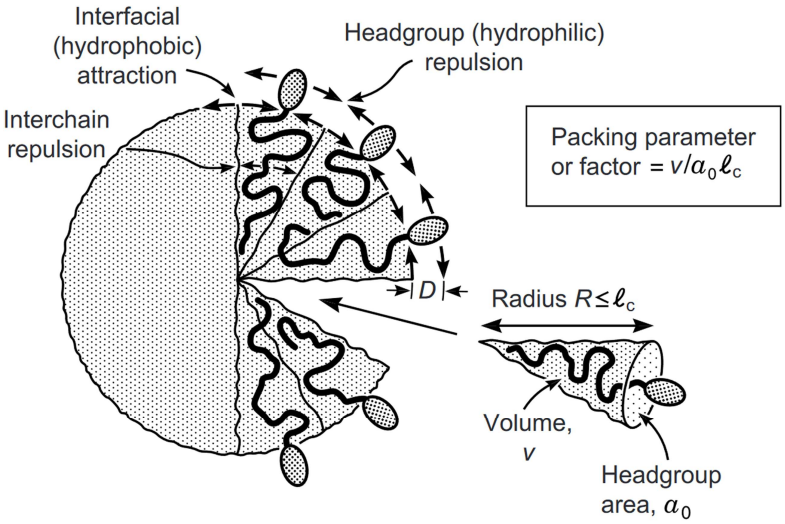

Figure 3.1 Schematic of an amphiphile forming a self-assembled aggregate in solution. v is the lyophobic chain volume, l_c is the lyophilic chain length and a_0 is the headgroup area. v, l_c and a_0 set limits on how the chains can pack together in the form of a packing parameter $P = v/l_c a_0$. Reproduced with permission from ref. 15.

The calculated value of P for the molecular building block, in its conformational arrangement being part of a particular suprastructure, should agree with the value of P for the suprastructure itself. As stated by Israelachvili, the following ranges of the packing parameter favor the formation of certain aggregate morphologies: $P \leq 1/3$ for spherical micelles, $1/3 < P < 1/2$ for non-spherical ellipsoidal micelles, $P \approx 1/2$ for cylindrical or rod-like micelles, $1/2 < P < 1$ for various interconnected structures, $P \approx 1$ for bilayer and lamellar vesicles and $P > 1$ for a family of "inverted" structures.[15] It is straightforward that the same holds for diblock copolymers, with a variety of structures reported. One of the most outstanding examples was showed by Eisenberg et al. with the formation of 8 different morphologies from amphiphilic poly(styrene)-*block*-poly(acrylic acid) copolymers in water (Figure 3.2).[4] In relation to PISA reactions, the most commonly observed structures are spherical micelles, rod-like micelles or worms and vesicles.[11,16]

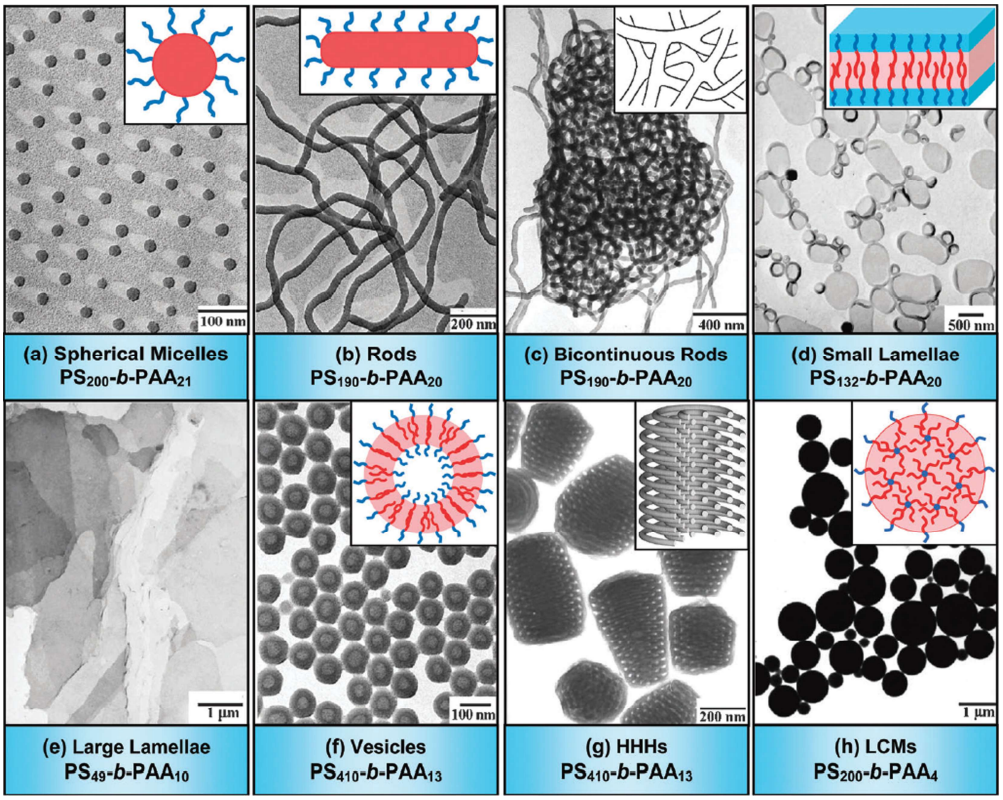

Figure 3.2 Transmission electron microscopy (TEM) micrographs of the different morphologies formed from amphiphilic poly(styrene)-*block*-poly(acrylic acid) (PS_x-*b*-PAA_y) copolymers. Inset: corresponding schematic diagrams. HHHs: hexagonally packed hollow loops. LCMs: large compound micelles, in which inverse micelles consist of a PAA core surrounded by PS coronal chains. Reproduced with permission from ref. 4.

More complex PISA reactions are those where the dynamic rearrangement of polymer chains, due to the change in the relative block volume between lyophobic and lyophilic segments of the chain, are coupled with a temperature-induced phase transition.[17] This is the case for examples of PISA using thermo-responsive polymers which exhibit lower (or upper) critical solution temperature (LCST, or UCST) behavior.[18–26] This allows for temperature-induced morphological transitions, decoupled from the polymerization process. A few examples are here analyzed. Sumerlin, Haddleton et al. reported the polymerization-induced thermal self-assembly (PITSA) of N-isopropylacrylamide from a lyophilic reversible addition-fragmentation chain-transfer (RAFT) agent in water, above the LCST of poly(N-isopropylacrylamide) (PNIPAM).[25] The diblock copolymers formed self-assembled structures after reaching a chain length at which the PNIPAM was insoluble. Self-

assembly was hence induced by both temperature and polymerization. In order to be able to characterize the colloidal structures formed at room temperature, the particles were crosslinked at reaction temperature the end of the polymerization. As a result, the final observed structures were indicative of the morphology formed during the reaction. An interesting approach, not strictly related to PISA, was reported by Monteiro et al. in the RAFT emulsion polymerization of styrene using a low molecular weight PNIPAM RAFT agent and a poly(NIPAM-*b*-dimethylacrylamide) (PNIPAM-*b*-PDMA) block copolymer.[21,22] In water, above the LCST of PNIPAM, swollen micelles were formed, stabilized by the PDMA block, and containing the PNIPAM portion of the copolymer, along with the RAFT agent. In essence, particle nucleation, or *self-assembly*, was skipped and the micelles were used to carry out the chain extension with styrene. In follow up work, the same research group adopted a PNIPAM macro-RAFT agent in styrene emulsion polymerization, above the PNIPAM LCST.[19] When cooling the system after polymerization, the PNIPAM block underwent a lyophobic-lyophilic transition, with a change in the packing parameter *P*, which drove a reorganization of the polymer chains. This was however possible only if the chains were in a fluid state. Upon cooling of the system, different morphologies could be obtained provided that the poly(styrene) core was kept fluid by either presence of large proportions of unreacted monomer or toluene addition. The difference with the approach from Haddleton, Sumerlin et al.[25] is that in the latter case the structures observed were not or may not be indicative of the system at reaction temperature. The same concept was adopted by Quinn, Davis et al. in the use of thermo-responsive poly(di(ethylene glycol) ethyl ether methacrylate)-*co*-N-(2-hydroxypropyl methacrylamide) (PDEGMA-*co*-PHPMAm) macro-RAFT agents in a styrene emulsion polymerization, conducted above the PDEGMA LCST.[20] After the reaction, toluene was added as a plasticizer for the poly(styrene) core and as a way to vary the hydrophobic block volume *v*. As a function of the amount of toluene added, spherical, rod-like, vesicle and lamellar structures were observed.

In all the examples above, organo-sulfur RAFT agents were adopted. PISA using this class of RAFT agents has been developed in a variety of different solvents and a wealth of monomers.[9,11,16,27–30] Other RDRP methods have also been applied to PISA in order to overcome the inherent limitations of RAFT polymerizations that use organo-sulfur compounds (*i.e.* yellow color and malodorous odor). These methods

include nitroxide-mediated radical polymerization (NMP),[12,26,31] atom transfer radical polymerization (ATRP),[32,33] single electron transfer living radical polymerization (SET-LRP)[34] and organotellurium-mediated living radical polymerization (TERP).[35] However, additional drawbacks may be introduced by the use of these alternative RDRP techniques. For instance, the NMP and TERP examples reported above suffered from low monomer conversion (~50-80%)[12,26,31,35] and in ATRP metal contaminants are introduced, [Cu] = 0.15-3.30 mg/ml in the examples given.[32,33]

In this chapter the use of a different form of RDRP applied to PISA will be explored. As explained in Section 1.4 of the introductory chapter of this thesis, RAFT polymerization using sulfur-based chemistry was developed on the back of the discovery that α-hydrogen ω-unsaturated methacrylate-based macromonomers (Scheme 3.1) could undergo the degenerative RAFT mechanism.[36,37]

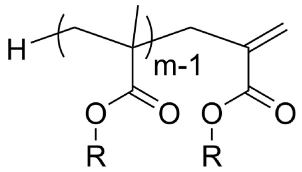

Scheme 3.1 General structure of an α-hydrogen ω-unsaturated methacrylate macromonomer of average degree of polymerization, $DP = m$.

This work conducted by Moad and coworkers demonstrated that "living" radical polymerizations using these macromonomers as RAFT agents was possible, facilitated by monomer starved-fed emulsion polymerization conditions (see Scheme 1.6 for the RAFT mechanism).[37] In this work, the slow feed of monomer was the key to achieve control of chain growth, obtaining polymers of dispersity ($Đ_M$) as low as 1.2. Recently, Haddleton et al. pushed this concept forward and showed that multi-block methacrylic copolymer latexes could be made using similar seeded starved emulsion polymerization conditions.[38] The strength of this form of controlled radical polymerization is the ease of operation and the little catalyst contamination, [Co] < 0.1 ppm in this work, along with the absence of added coloration or malodorous compounds. These features make the described macromonomers desirable candidates to be used as macro-RAFT agents in PISA. In parallel to the development of the work presented in this chapter, Zetterlund et al. independently attempted to carry out PISA in dispersion polymerization conditions by replacing the conventional

organo-sulfur RAFT agents with macromonomers similar to the ones described above.[39] The approach followed by Zetterlund et al. was however the one of a standard batch PISA process. In their work, methyl α-(bromomethyl)acrylate was used as chain-transfer agent for the synthesis of a lyophilic poly(ethylene glycol) methyl ether methacrylate macro-RAFT agent. The latter was subsequently used in the dispersion polymerization reaction of benzyl methacrylate. Despite resulting in limited conversion, lack in control of chain-growth and limited control over the morphologies formed, their work indicated a potential pathway to PISA by this *sulfur-free* RAFT process, with the observation of both spherical and rod-like colloids.

In this chapter, general mechanistic insight and understanding of the reaction conditions necessary to attain control of the PISA process using methacrylate-based macromonomers as RAFT agents is provided. This will be done by exploring the chain-extension of poly(glycerol methacrylate) (PGMA) and thermo-responsive poly(glycerol methacrylate)-*block*-poly(poly(ethylene glycol) methyl ether methacrylate) (PGMA-PPEGMEMA) macromonomers in water with hydroxypropyl methacrylate (HPMA). It is anticipated that in order to achieve control of chain-growth and of the morphologies obtained, nucleation needs to be decoupled from the polymerization process and, as already shown by previous literature,[36–38] seeded starved-fed conditions are required.

3.2 Results and discussion

The aqueous dispersion polymerization, or polymerization induced self-assembly, of PGMA-PHPMA is a well know process, mainly investigated by Armes et al.[11,13,40–42] In this previous work, a 2-cyano-2-propyl dithiobenzoate RAFT agent was adopted for the synthesis of the PGMA macro-RAFT agent. Being such a well-studied and characterized system, the same reaction was taken as a model system for the present investigation to study the applicability of methacrylate macromonomers as macro chain-transfer agents (CTA) in PISA reactions. In this way, results substantially different during the dispersion polymerization reaction can be attributed to the different CTA adopted in this work. The full synthetic pathway adopted in this chapter is shown in Scheme 3.2.

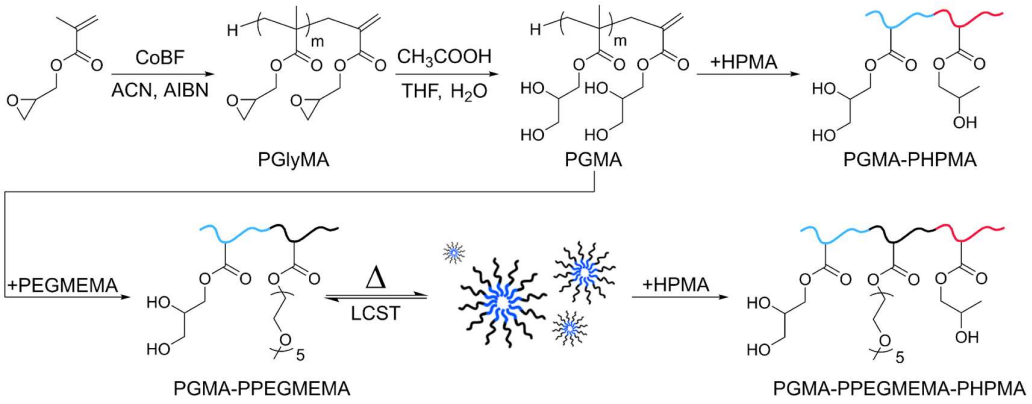

Scheme 3.2 Synthetic pathway for the synthesis of poly(glycerol methacrylate) (PGMA) and poly(glycerol methacrylate)-*block*-poly(poly(ethylene glycol) methyl ether methacrylate) (PGMA-PPEGMEMA) macromonomers and their subsequent chain-extension with HPMA in aqueous PISA.

3.2.1 Poly(glycerol methacrylate) macromonomer synthesis

Water soluble poly(glycerol methacrylate) (PGMA) macromonomers were obtained from the hydrolysis of glycidyl methacrylate macromonomers (PGlyMA) synthetized by means of catalytic chain-transfer polymerization (CCTP). As explained in Chapter 1, CCTP is based on the use of certain Co(II) complexes as efficient chain-transfer agents in the polymerization of methacrylates.[36,43,44] The advantages are the high chain-transfer coefficient (C_T) (~4×10^4 using bis[(difluoroboryl) dimethylglyoximato]cobalt(II) (CoBF) for the CCTP of methyl methacrylate in bulk)[45] and that the catalyst is not consumed during the reaction, leading to little metal contamination in the final product. Haddleton et al. reported the synthesis of semi-batch CCTP of glycerol methacrylate in water/methanol 66/33 v/v mixture using CoBF as a catalyst.[46] High monomer conversions were observed (≥ 92.0%), with an apparent chain-transfer coefficient (C_T^{app}) of 958. C_T is often defined as apparent, or observed, for instance in case of catalyst partitioning in heterogeneous systems[47,48] or catalyst poisoning/deactivation.[45,47,49,50] The semi-batch addition of monomer and catalyst was found to be necessary to prevent the catalyst deactivation, or hydrolysis, especially in aqueous acidic environments. The same research group also reported the synthesis of poly(glycidyl methacylate) macromonomers by solution CCTP in acetonitrile, with a C_T^{app} of *ca.* 6.4×10^3.[51] For the present investigation, it was decided to be more "catalyst efficient" and the latter approach

was followed. Different amounts of catalyst, CoBF, were adopted in the batch solution polymerization of glycidyl methacrylate at 50 wt% monomer in acetonitrile, at 70°C for 2h, in order to fabricate macromonomers with varied number average degree of polymerization (*DP*) (Table 3.1). The polymers were recovered after solvent evaporation and after being washed with an excess of a pentane:methanol 5:1 v:v mixture. Macromonomers with dispersity ($Đ_M$) of about 2.0 were obtained for [CoBF]/[GMA] < 4.61×10^{-6}, which were somewhat higher of what previously reported ($Đ_M$ ~ 1.76/1.86).[51] However, in the previous literature a monomer concentration of 33 wt% was used instead, and the reaction was left to react for 24h, explaining the difference in results observed. Note that a dispersity of 2 is expected for transfer dominated molecular weight distributions.[52]

Table 3.1 Poly(glycidyl methacrylate) (PGlyMA) macromonomer synthetized *via* catalytic chain transfer polymerization (CCTP) using CoBF as a catalyst.

Sample[a]	[CoBF]/[GlyMA] ×10^6 / -	M_n /[b] g/mol	M_w /[b] g/mol	$Đ_M$ / -	*DP* /[c] -
1	0.29	28400	57600	2.03	200 (-)
2	1.15	8800	17700	2.02	62 (50)
3	1.70	5200	10900	2.08	37 (32)
4	2.30	4400	8800	2.01	31 (27)
5	4.61	1900	4500	2.39	13 (13)
6	4.86	1100	3600	3.15	8 (11)
7	9.47	500	1800	3.76	3 (7)

Note: Reactions conducted at 50 wt% in acetonitrile, at 70°C for 2h; AIBN/GlyMA: 0.7 mol%.
[a] Sample numbers in **bold** were used in chain-extension experiments (solution and dispersion polymerizations). Samples were washed with an excess amount of pentane:methanol 5:1 v:v prior to size exclusion chromatography (SEC) analysis, with the exception of the samples which numbers are in *italic*. The latter were injected after solvent evaporation (acetonitrile).
[b] Molecular weights relative to poly(methyl methacrylate) narrow standards and reported to the closest hundred.
[c] Calculated from M_w (SEC) for the Mayo plot, as recommended by Heuts et al.[43] Numbers in brackets were calculated by ^{1}H-NMR as shown in Figure 3.4.

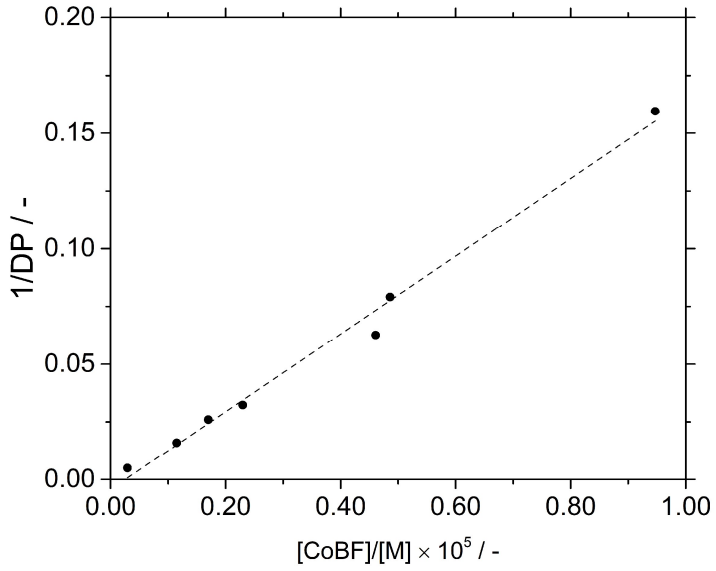

Figure 3.3 Mayo plot for the CCTP of glycidyl methacrylate in acetonitrile. The dotted line is a linear regression of the data; $R^2 = 0.988$.

Analysis of the variation of the *DP* with increasing [CoBF] *via* the so-called Mayo plot[53] showed a C_T^{app} of 16.8×10^3 (Figure 3.3). The *DP* to be used for this plot was calculated as suggested by Heuts et al.; $DP = M_w/(2\times m_0)$, where m_0 is the monomer molar mass.[43] The 2 in the equation results from the theoretical dispersity of the molecular weight distribution for a transfer dominated system which is equal to 2.[52] The reason for this is the more reliable measure of M_w than M_n by SEC, especially when analysing low-molar mass polymers.[43] In comparison, a C_T^{app} value of 15.0×10^3 was obtained when the Mayo plot was plotted from the ^{1}H-NMR calculated *DP*. The synthetized PGlyMA macromonomers were then hydrolysed to obtain the desired poly(glycerol methacrylate) (PGMA) macromonomers; PGlyMA was desolved in a THF/acetic acid 2:3 v:v mixture at 80°C, to which water was drop added to form an oil-in-water emulsion. After 7h the solvents were evaporated and the polymer was washed with an excess of diethyl ether. The efficiency of the epoxide ring hydrolysis was checked with ^{1}H-NMR by observing the disappearance of the two peaks at 2.67 and 2.81 ppm attributed to the O-CH_2- epoxide protons (Figure 3.4B) and the simultaneous appearance of the protons b′,c′,d′ (3.30-4.20 ppm) and e′,f′ (4.30-5.40 ppm) (Figure 3.4A). It is worth mentioning that in the given reaction conditions, a mixture of the 2,3-dihydroxy and 1,3-dihydroxy substituted units are obtained, with a predominance of the 2-3 substitution (*ca.* 77%).[54]

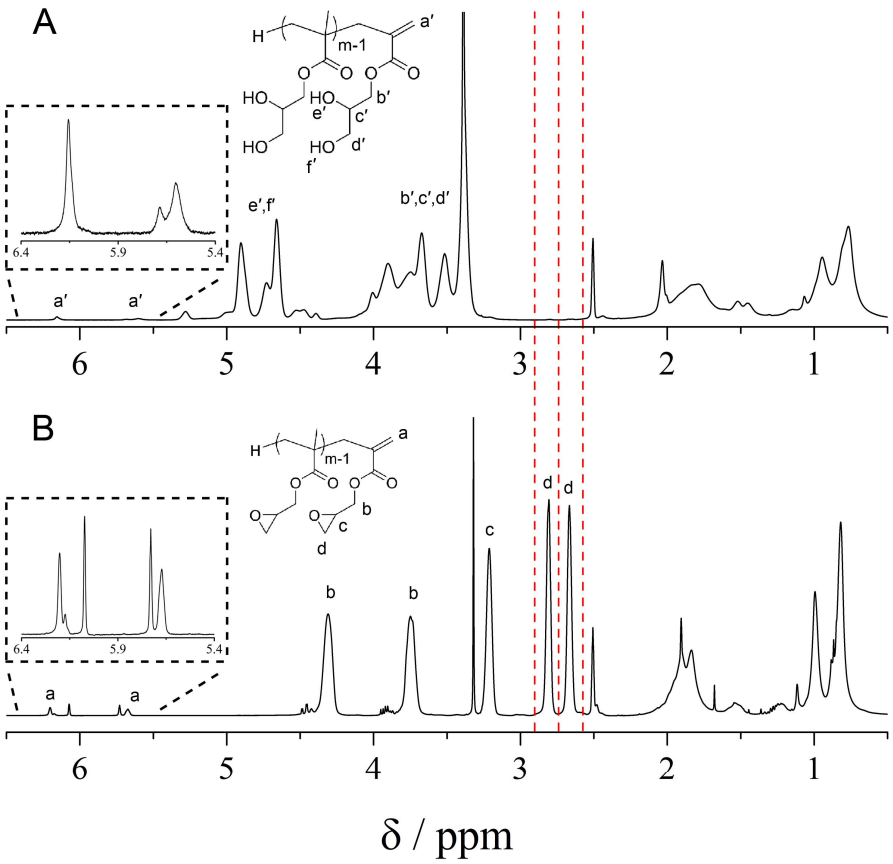

Figure 3.4 ^{1}H-NMR spectra (d^{6}-DMSO) of (A) poly(glycerol methacrylate) macromonomer (PGMA) and (B) poly(glycidyl methacrylate) macromonomer (PGlyMA), highlighting the disappearance of the epoxide protons after the ring opening reaction (Sample 3, Table 3.1). *DP* calculated as *b*/*a* in spectrum B.

3.2.2 Polymerization induced self-assembly

Initially, a $PGMA_{50}$ macromonomer (Sample 2, Table 3.1) was used as water-soluble macro-RAFT agent and chain-extended with HPMA in batch aqueous dispersion polymerization (Scheme 3.2; Run 1, Table 3.2). As previously mentioned, PGMA-PHPMA block copolymers have been widely studied in aqueous dispersion PISA using benzodithioate transfer agents, showing effective chain-extension and access to higher order morphologies. [11,13,40–42] As explained in the introductory section of this thesis (Section 1.2.4), because PHPMA is lyophobic, during chain-growth the resulting diblock copolymer becomes surface active and phase-separates forming in a self-assembled structure. However, when using methacrylate macromonomers based-CTAs, polymerizations using similar reaction conditions resulted in low

monomer conversion, no observable chain-extension (Figure 3.5) and a lot of coagulation along with the formation of a milky white suspension.

Table 3.2 Experimental conditions for the chain-extension of PGMA and PGMA-PPEGMEMA macromonomers with HPMA in aqueous PISA.

Run	DP_{PGMA}	$DP_{PPEGMEMA}$	F /[a] h^{-1}	Initiator	T / °C	DP_{target}[b]
1	50	/	Batch	Batch	70	96
2[d]	50	/	25	Batch	70	150
3[d]	27	/	15.3	Batch	70	91
4[e]	32	/	9.3	Fed[c]	80	100
5[f]	32	10	9.3	Fed[c]	80	125

Note: In runs 1-3 and 4-5 the initiators were respectively ACVA and KPS. Initiator/HPMA; 0.6-1.1 mol%.

[a] Feed rate = $mol_{HPMA} \times mol_{macromonomer}^{-1} \times h^{-1}$. See Table 3.4 for feed rates in $ml \times h^{-1}$.

[b] Targeted DP of HPMA block.

[c] 10% of initiator pre-shot, the rest was fed.

[d,e,f] Monomer and initiator feeding time was 6, 8, 10 h respectively.

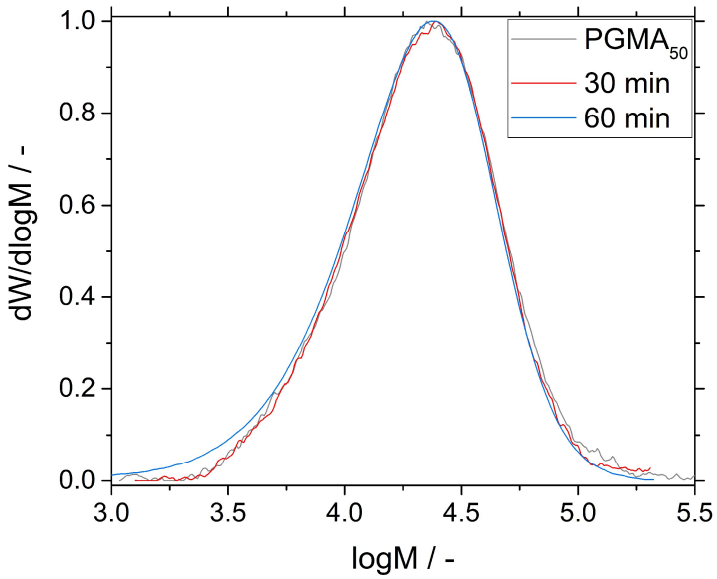

Figure 3.5 Molecular weight distribution during the HPMA batch chain-extension of a $PGMA_{50}$ macromonomer (Run 1) in aqueous dispersion polymerization.

This result is to be expected given the much lower reported chain-transfer coefficient (C_T) of methacrylate macromonomers in comparison to the widely adopted dithioesters or trithiocarbonates macro-RAFT agents; typically C_T is at least

10 for well controlled RAFT processes, with the most active RAFT agents having C_T > 100.[55] Instead, C_T for a ω-unsaturated methacrylate macromonomer (DP ≈ 24) was estimated to be ~ 0.21 for the bulk polymerization of methyl methacrylate.[56] The in comparison low C_T values for methacrylate-based macromonomers represent the downfall of their application in a batch PISA process. In fact, when using sulfur-based RAFT agents higher monomer concentrations are normally tolerated. To illustrate the point, for the present discussion the kinetic chain length, $\bar{\nu}$, will be invoked as an indicative measure for control of chain growth (Equation 3.2):[57]

$$\bar{\nu} = \frac{k_p[M][P\bullet]}{2k_t[P\bullet]^2 + k_{tr}[MM][P\bullet]} \quad (3.2)$$

where k_p, k_t and k_{tr} are respectively the propagation, termination and transfer rate coefficients, [M], [MM] and [P•] are respectively the monomer, macromonomer and radical concentrations. For this work only transfer to macromonomer events will be taken into account.

Equation 3.2 can be simplified for transfer dominated systems (Equation 3.3):

$$\bar{\nu} \approx \frac{k_p[M]}{k_{tr}[MM]} \approx \frac{1}{C_T}\frac{[M]}{[MM]} \quad (3.3)$$

$\bar{\nu}$ is to be interpreted as an instantaneous average number average degree for polymerization; once the RAFT agent is in an active state, $\bar{\nu}$ indicates how many repeating units are added to the growing polymer chain before another transfer event brings the RAFT agent back to a dormant state. For ideal living conditions $\bar{\nu}$ should then have a value ≤ 1, this to allow for control of monomer sequence. It is clear that high monomer concentrations are allowed in PISA using sulfur-based RAFT agents as a result of much higher C_T values.

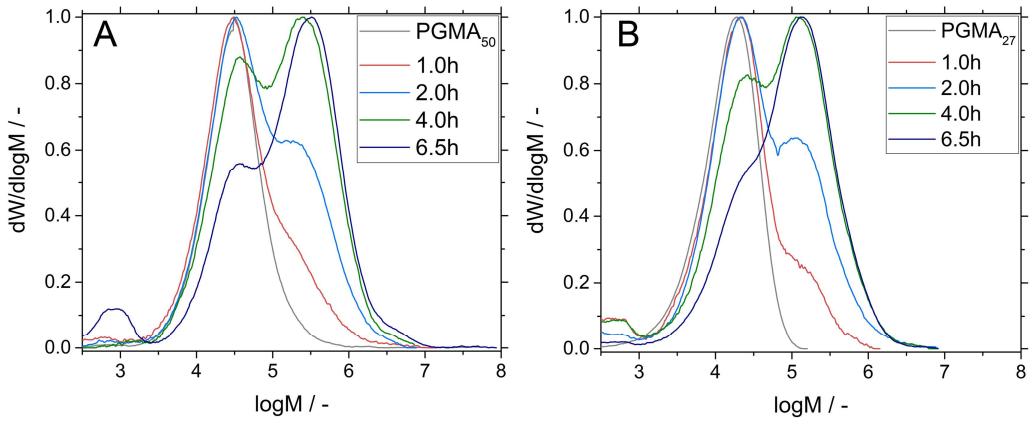

Figure 3.6 Molecular weight distribution during the HPMA chain-extension of a) $PGMA_{50}$ (Sample 2, Table 3.1) and b) $PGMA_{27}$ (Sample 4, Table 3.1) macromonomers in aqueous dispersion polymerization (Runs 2 and 3, respectively).

For this reason, the HPMA chain-extension was re-attempted by feeding the monomer at a slow rate (F = 25.0 h^{-1}) over 6 hours, meeting the required condition of having low overall monomer concentration (Run 2, Table 3.2). The flow rates (F) are reported as moles of HPMA monomer per hour, normalized by the moles of CTA present in the reaction (see Table 3.4 for ml×h^{-1} data). Hence, F is equal to the number of monomer units that should be added to the macromonomer chain-end per hour, assuming complete monomer conversion. Figure 3.6A shows the molecular weight distributions at different stages of the polymerization, whereas details on the molecular weight, conversion data and $Đ_M$ can be found in the Appendix (Table A3.1). Unexpectedly, the molecular weight of the forming diblock copolymer did not grow linearly with conversion. A "jump" in molecular weight was rather observed, which did not appear to increase significantly over the reaction timescale. This means that $\bar{\nu}$ must be considerably > 1. An indicative estimate of the extent of $\bar{\nu}$ in the polymerization conditions can be obtained from the molecular weight distributions by SEC. This is done by ignoring the different solubility, and hence exclusion, behavior of the PGMA-PHMA block copolymers and PMMA (SEC column calibrant). Under these assumptions, $\bar{\nu} \approx 2000$, hence inferring to a standard free radical polymerization process (with arguably still limited termination). Strikingly, the "jump" in molecular weight was similar to what was previously shown by Zetterlund et al. in recent similar work on the applicability of methacrylate macromonomers in PISA.[39] In their work, batch conditions were adopted, in the same way as in Run 1,

resulting in high v_k and hence favoring high monomer insertions at the macromonomer ω-end. In this case, similar results were obtained even by applying semi-batch conditions.

In order to minimize this effect, the experiment was then repeated using a macromonomer with lower *DP*, $PGMA_{27}$ (Sample 4, Table 3.1), in an attempt to increase [MM] in Equation 3.3, and lowering the feeding rate to 15.3 h^{-1} (Run 3, Table 3.1). Again, analogous results were obtained, suggesting limited control on chain-growth (Figure 3.6B and Table A3.2). It is interesting to note that the extent of the molecular weight "jump" was decreased, with $\bar{v} \approx 750$.

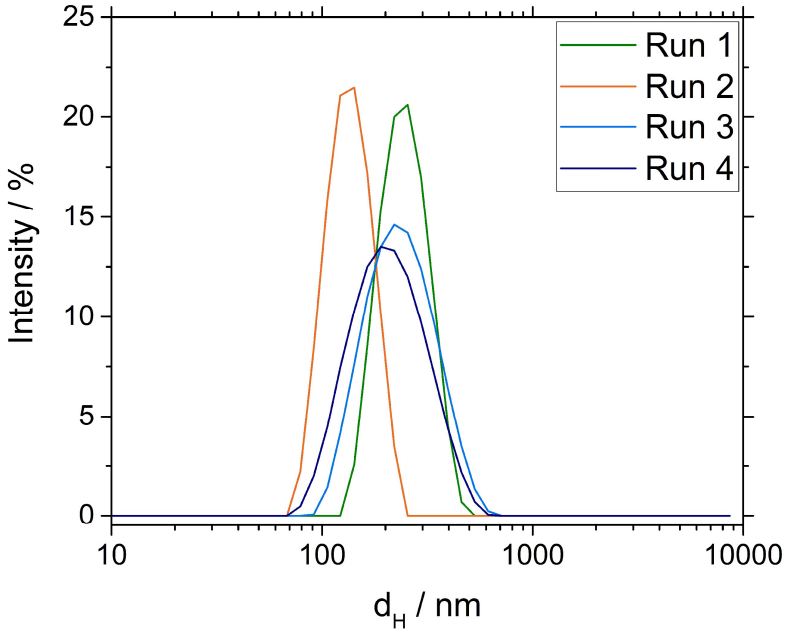

Figure 3.7 Intensity-based size distribution of Run 1 (Green), Run 2 (Orange), Run 3 (Light Blue), Run 4 (Dark Blue) at 30 min reaction time, as shown by dynamic light scattering (DLS) measurements.

Dynamic light scattering (DLS) measurements showed that in all the batch and semi-batch dispersion polymerization experiments large colloidal objects ($d_H \approx$ 140-250 nm) were formed at the reaction time of 30 minutes (Figure 3.7). This was similarly observed by Zetterlund et al. in their experiments where large spherical and rod-like particles were formed at monomer conversions as little as 2-4%.[39] In both investigations, this indicated a conventional particle nucleation process, more similar to what observed in emulsion polymerization (see Section 1.2), as a direct result of

loss of control in chain-growth. To illustrate this point, in the case of Run 2, if all the HPMA fed in the reaction had reacted with the macromonomer in equal proportion, $PGMA_{50}HPMA_3$ polymers would have been formed after 30 min. The formation of large particles from $PGMA_{50}HPMA_3$ at this concentration is in contrast to what reported in case of the HPMA extension of sulfur-based $PGMA_{47}$ macro-RAFT agents in aqueous PISA.[40] In the latter, micellar nucleation occurred with the formation of $PGMA_{47}PHPMA_{90}$ polymers in correspondence with the observation of 20 nm colloidal objects, as shown by DLS.

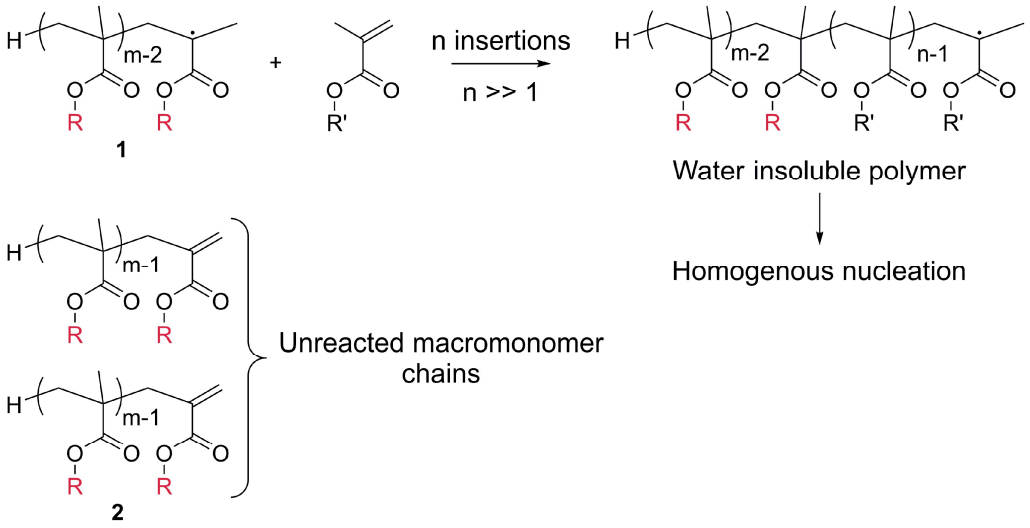

Scheme 3.3 Schematic illustrating the origin of the molecular weight bimodality along with the formation of homogenously nucleated particles. Once a macromonomer, of $DP = m$ and of general structure **2,** is in the active state (structure **1)**, n monomer insertions (with $n >> 1$) at the macromonomer chain-end cause the resulting block copolymer to become insoluble. The resulting macromonomer can collapse forming a new particle, as described by the theory of homogenous nucleation in emulsion polymerization.[58] Most of the polymer chains **2** have not reacted yet, leading to a bimodal molecular weight distribution.

The DLS and SEC data essentially suggested that the chain-extension was not living; multiple insertions of HPMA occurred at the macro-CTA ω-end after every macromonomer activation and not all the polymer chains reacted at the same time, hence inferring a standard FRP process with limited termination. A plausible explanation for this behavior is the following. Every time a radical-activated macromonomer species is formed (structure **1**, Scheme 3.3), the extent of the addition of HPMA is such that the resulting di-block copolymer becomes first surface active

and then insoluble. This results in the formation of new particles. Once this happens, HPMA from the water phase will diffuse and swell these particles, increasing the monomer concentration locally at point of polymerization. The observed high values for the kinetic chain length and thus loss of control of chain growth are hence explained. Note that this experimentally will be amplified in case of inhibition/retardation phenomena at the start of the polymerization process, for example due to presence of inhibitors. This also explains the bimodality of the molar mass distributions as the macromonomer has a low reactivity toward chain-transfer events, as evident from the low value of C_T. As a result, in these experimental conditions the timescales of full monomer conversion and complete macromonomer incorporation are out of sync.

It is worth mentioning that favored partitioning of monomer within the particles does not typically feature a dispersion polymerization process as the dispersing medium is a good solvent for the monomer[59] (however it is observed in HPMA dispersion polymerizations).[40] In dispersion polymerization, the reaction proceeds both within the nucleated particles and in solution and the rate of polymerization is the sum of these two events.[60,61] In this sense the temperature at which the polymerization is carried out is crucial as it determines the monomer and polymer solubility in the solvent (commonly affected for hydroxy functionalized methacrylates),[62–64] as well as the radical production. In case of observed favored partitioning, the process is clearly more similar to a starved seeded emulsion polymerization of a relative water-soluble monomer. Nevertheless, for simplicity the process will still be called dispersion polymerization in this chapter. Despite the adopted nomenclature, this preferential partitioning has important implications on the polymerization itself, especially when using methacrylate macromonomers. Typical PISA reactions adopt organo-sulfur macro-RAFT agents of narrow $Đ_M$. During the reaction, the lyophilic macro-CTA is chain-extended in solution until it becomes surface active and self-assembles. Given the low dispersity of these systems, the chains typically all grow at the same rate and, hence, self-assemble at the same moment when they reach the required packing parameter P to form a given structure. The difference with the system discussed in this chapter is that when larger dispersity macromonomers are adopted ($Đ_M$ ~ 2.0), low molecular weight chains (present in greater concentration) become surface active way earlier than longer chains. This

when assuming equal growth of all the chains. Shorter chain will consequently assemble first, swell with more monomer and hence have a greater probability to grow even further. This will further accentuate the molecular weight bimodality observed in Run 2 and 3.

Further optimization of the reaction conditions could minimize the monomer accumulation in the system. This was done by reducing the feed rate of monomer further (Run 4, same reaction conditions as Run 5). Additionally, the reaction temperature was raised to 80°C as transfer events have a higher activation energy than propagation and they are favored at higher temperatures.[2] The combination of lower feed rate and higher temperature indeed showed some improvements (Figure 3.8, Table A3.3). Nevertheless, a "jump" of molecular weight was still visible so that large colloidal objects ($d \approx 290$ nm) at the beginning of the reaction were still formed (Figures 3.7 and 3.9).

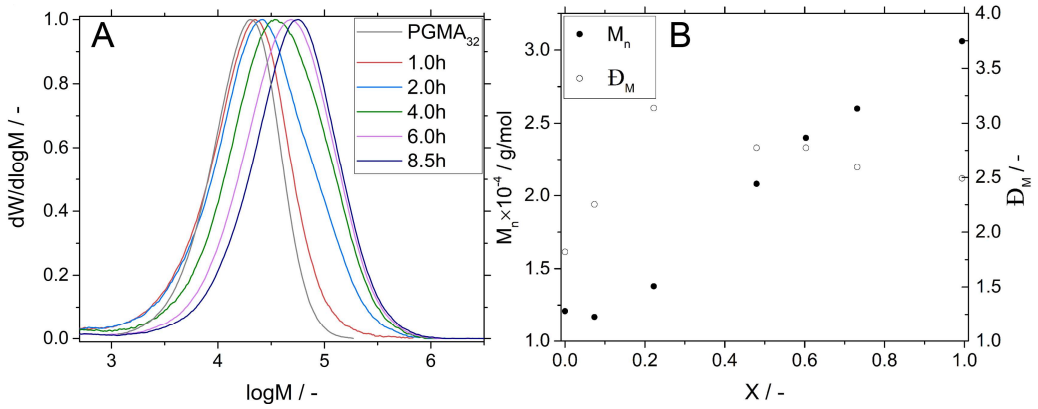

Figure 3.8 A) Molecular weight distribution during the HPMA semi-batch chain-extension of a $PGMA_{32}$ macromonomer (Sample 3, Table 3.1) in aqueous dispersion polymerization (Run 4). B) (•) Variation of M_n and (○) $Đ_M$ with X in Run 4.

The results from these experiments show that there is a fine balance in experimental conditions needed to alleviate the effects of the local monomer concentration influenced by monomer feed rate and partitioning events. The system is further complicated by an especially tedious control on particle nucleation. This essentially infers that PISA with control of propagation starting from a solution of the studied class of methacrylate-based macromonomers may not be possible.

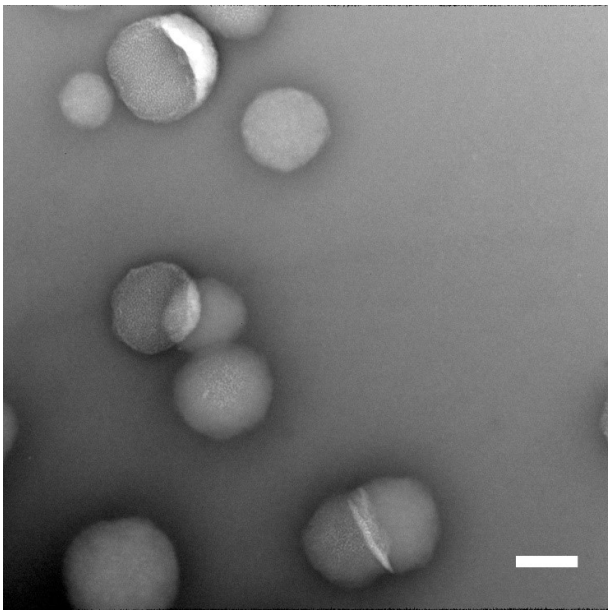

Figure 3.9 Negative stain TEM picture of a sample taken at 30 min reaction time in Run 4. Scale bar: 200 nm.

One possible solution to circumvent this problem is skipping this uncontrolled particle nucleation event and to operate under seeded starved dispersion polymerization conditions. Thermo-responsive $PGMA_{32}PPEGMEMA_{10}$ macromonomers were prepared by chain-extension of a $PGMA_{32}$ macromonomer with a second hydrophilic monomer, PEGMEMA 300, which exhibits a lower critical solution temperature (LCST) behavior in water.[65] The chain-extension was conducted under semi-batch aqueous solution polymerization conditions at 60°C by feeding the monomer over 200 minutes. The polymer was purified by dialysis against water. After chain-extension an upward shift in the molecular weight distribution was observed *via* SEC (Scheme 3.2, Figure 3.10). Next, the aq. $PGMA_{32}PPEGMEMA_{10}$ solution was heated to 80°C, above the polymer LCST (Figure A3.1). This essentially allowed to control particle nucleation by means of an LCST-type phase transition decoupled from polymerization. In fact, heating the system to 80°C resulted in the formation of a colloidal dispersion, which was used as a seed, to which HPMA was fed to chain-extend (Run 5). Essentially the reaction was operated under starved seeded dispersion polymerization conditions similar to those reported by Moad et al.[36] and more recently by Haddleton et al.[38] In this work though, a water soluble monomer was adopted and colloidal particles which were the result of the self-

assembly of the thermo-responsive macromonomers were used instead of latex particles made of macromonomer chains.

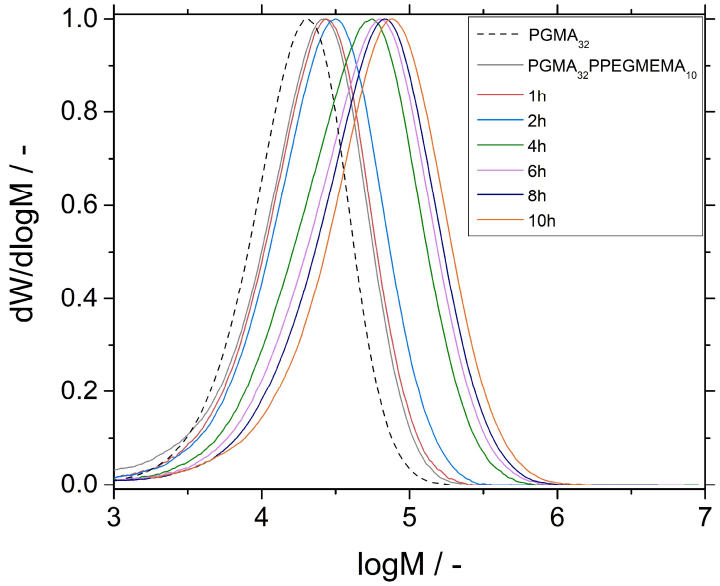

Figure 3.10 Molecular weight distribution during the HPMA chain-extension of $PGMA_{32}PPEGMEMA_{10}$ (Run 5).

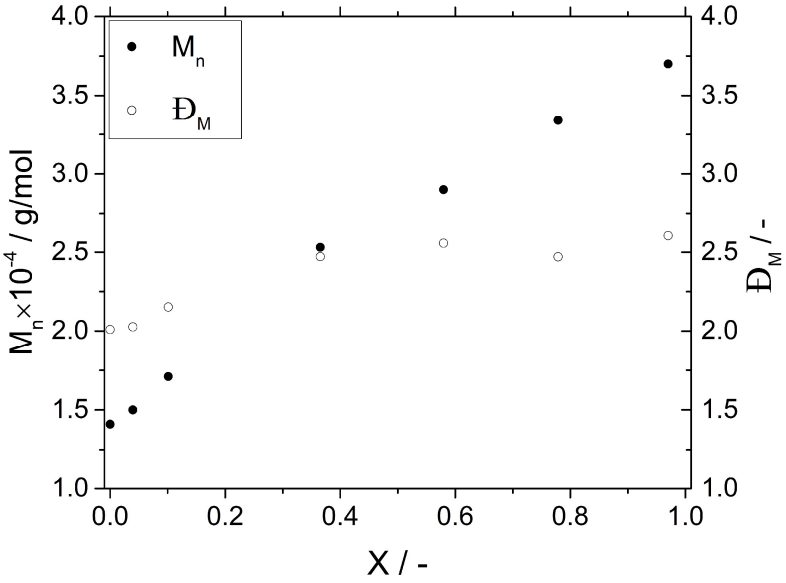

Figure 3.11 (•) Variation of M_n and (○) $Đ_M$ with X during the HPMA chain-extension of $PGMA_{32}PPEGMEMA_{10}$ in water (Run 5).

Table 3.3 Evolution of molecular weight and dispersity during the semi-batch HPMA chain-extension of a $PGMA_{32}PPEGMEMA_{10}$ macromonomer in aqueous dispersion polymerization (Run 5).

Time / h	$M_w \times 10^{-4}$ / g/mol	$M_n \times 10^{-4}$ / g/mol	$M_p \times 10^{-4}$ / g/mol	$Đ_M$ / -	X_i[a] / -	X[b] / -	DP_{HPMA}[c] / -
0	2.84	1.41	2.61	2.01	0.00	0.00	0
1	3.04	1.50	2.70	2.02	0.39	0.04	5
2	3.68	1.71	3.19	2.13	0.51	0.10	13
4	6.25	2.53	5.64	2.47	0.91	0.37	46
6	7.42	2.90	6.49	2.47	0.97	0.58	73
8	8.26	3.35	7.02	2.58	0.97	0.78	97
10	9.64	3.70	7.71	2.61	0.97	0.97	121

[a] Instantaneous monomer conversion (X_i). DMF was used as internal standard.
[b] Cumulative monomer conversion (X).
[c] DP of the HPMA block in $PGMA_{32}PPEGMEMA_{10}PHPMA_z$; Estimated from X_i, assuming only CTA chain-extension.

Indeed, the chain-extension in the presence of $PGMA_{32}PPEGMEMA_{10}$ pre-assembled colloidal objects resulted in an upward shift in the molecular weight distributions during the reaction, with control of chain-growth as function of monomer conversion (Figures 3.10 and 3.11). The apparent acceleration observed between 2 and 4 hours was the result of monomer accumulation in the system as observed from the values of instantaneous conversion (X_i) (Table 3.3). The success of the chain-extension despite the initial monomer accumulation confirmed the robustness of the protocol. Although, an increase in dispersity ($Đ_M$) from about 2 to around 2.5 was still observed, which explains the non-perfect linearity of M_n with X (Figure 3.11), and can be attributed to the initial partial monomer accumulation in the system. Runs 4 and 5 are however inherently different. In fact, in the latter, DLS measurements indicated the formation of narrowly dispersed 40 nm particles after 2h (Figure 3.12), in contrast to what observed in the (semi-)batch dispersion polymerization experiments (Figure 3.7). In Run 5, these objects grew in size up to 6 h, after which the dispersity broadened and larger colloidal structures appeared (Figure 3.12).

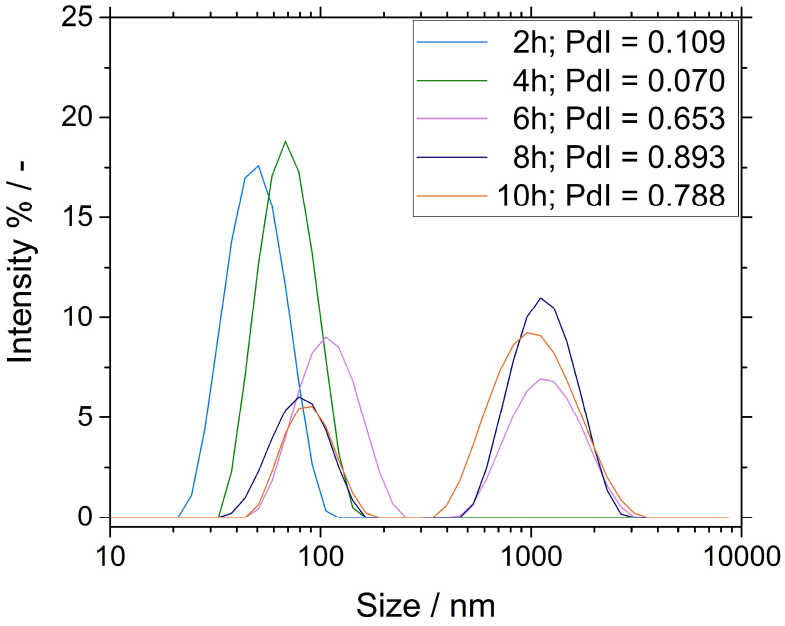

Figure 3.12 Evolution of the intensity-based size distribution and polydispersity index (*PdI*) of $PGMA_{32}$-$PPEGMEMA_{10}$ during the chain-extension with HPMA (Run 5) as shown by DLS measurements.

Negative stain transmission electron microscopy (TEM) analysis showed that indeed spherical objects were formed after 2h (Figure 3.13A). This morphology dynamically changed into branched worm-like structures as observed after 8 h (Figure 3.13C). The overall viscosity of the system markedly increased at this stage, as usually observed when polymer worms are formed.[16] Finally, after 10 h (with a noticeable drop in viscosity of the dispersion) the system rearranged again away from worm-like structures into larger spherical aggregates (Figure 3.13D). To date it is still not clear whether these objects, or the ones formed in the early stages of the previous reactions (for instance Figure 3.9 for Run 4), have a full or hollow core (*i.e.* vesicles).

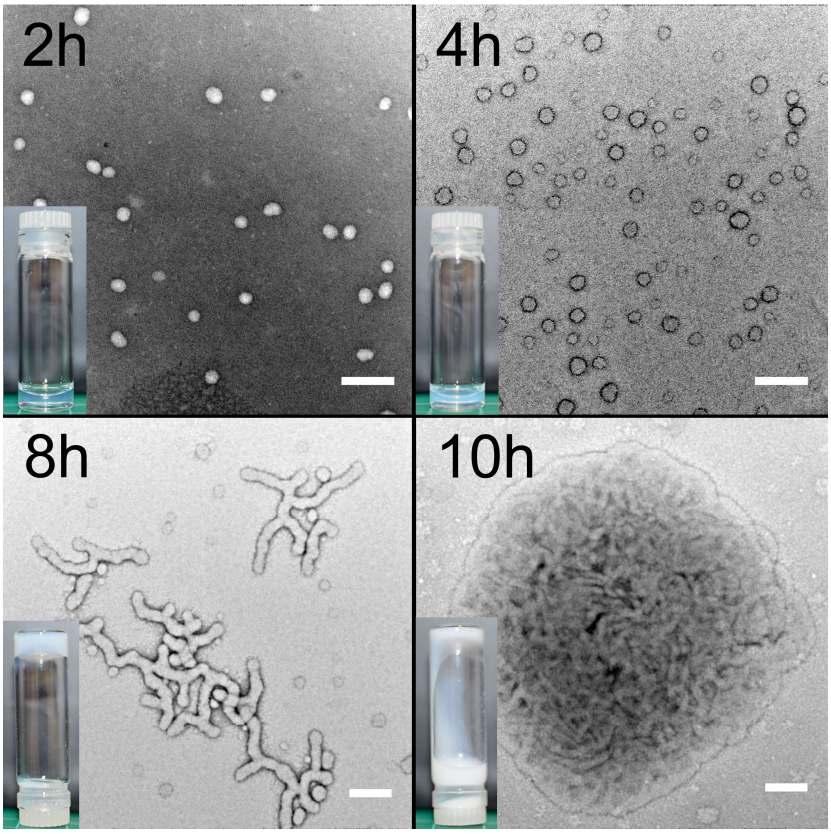

Figure 3.13 Negative stain TEM pictures of samples taken at 2h, 4h, 8h and 10h during the HPMA chain-extension of a $PGMA_{32}PPEGMEMA_{10}$ macromonomer in water (Run 5); scale bars: 200 nm. Inset: pictures of the sample appearance before 50-fold dilution for TEM analysis.

It is also important to point out that the final morphologies observed in Figure 3.13 are likely to be not indicative of the structures formed in the reaction mixture at 80°C, as the PPEGMEMA block undergoes a hydrophobic-hydrophilic transition at T < 70°C (Figure A3.1). This approach is similar to other research by Monteiro et al. where thermo-responsive polymers were applied to PISA and where only the self-assembled structures obtained at room temperature were analyzed.[19] In this work and in previous research, upon cooling to room temperature the system will rearrange into the most thermodynamically stable structure, provided that the system is in a fluid state and not kinetically trapped. This is also the case for the copolymers adopted in this chapter despite the relatively high glass transition temperature (T_g) of 2-(hydroxypropyl methacrylate) of *ca.* 76°C.[66]. In fact, according to previous research the volume fraction of water in the PHPMA block (hydrophobic

block), x_{sol}, was 0.16, 0.88 and 0.87 respectively for vesicles, worms and spherical micelles composed of $PGMA_{54}PHPMA_{140}$ at 0°C.[42] Whilst data for x_{sol} is not available for these copolymers at 80°C, the high values at 0°C, especially for spheres and worms, are indicative of a high degree of hydration of the PHPMA block which would act as a plasticizer for the hydrophobic block.

As a final observation, the colloidal morphologies appear to be less defined than the ones formed in PISA mediated by organo-sulfur RAFT agents. Although this is likely to be related to the higher dispersity of the block copolymers made in this work, *i.e.* $Đ_M > 2$, the influence of dispersity in polymer self-assembly is not always predictable. For instance, Lynd et al. observed that entirely different morphologies could be obtained by solely changing the dispersity of poly(ethylene-*co*-propylene)-*block*-poly(lactide) copolymers.[67] Similarly, Mahanthappa et al. synthetized poly(ethylene oxide-*block*-1,4-butadiene-*block*-ethylene oxide) copolymers of molar masses that should have theoretically assembled in vesicles (according to *P*, Equation 3.1).[68] The high dispersity of the butadiene block, *i.e.* $Đ_M = 1.75$, however resulted in the formation of a mixture of spheres, worms and vesicles. In contrast, Eisenberg at al. showed that poly(styrene-*block*-acrylic acid) copolymers assembled in narrower-sized vesicles when the molecular weight dispersity was higher.[69,70] Finally, Sawamoto et al. observed that ill-defined, *i.e.* $Đ_M = 2.3\text{-}2.4$, statistical copolymers of PEGMEMA and dodecyl methacrylate could assemble in narrow-dispersity ($Đ_M$ = 1.2-1.3) particles.[71] The take-home message from these previous studies is that dispersity does play a key role in influencing polymer self-assembly, although the final result is not straightforward. In this regard, the reader is directed to a recent thorough review by Gibson, O'Reilly et al.[72]

3.3 Conclusion and outlook

In this chapter the application of methacrylate macromonomers in dispersion polymerization, or polymerization induced self-assembly, was investigated. The results presented show that PISA is practically not successful starting from a macromonomer solution. In standard PISA reactions, *i.e.* when effective macro-CTAs are adopted, particle nucleation, or micellar formation, is observed when the growing diblock copolymer becomes surface active and self-assembles to decrease the total

system free energy. When using ω-end unsaturated methacrylate macromonomers, one must face with the dramatically lower C_T. Successful chain-extension in these instances was only observed when particle nucleation, and the associated monomer partitioning, was skipped. The discussed approach deals with the use of a thermo-responsive macromonomer, able to generate a colloidal dispersion at reaction temperature. This *seed* was used as reaction *loci* for the PISA process to take place. In this way monomer fed to the reaction mixture was compartmentalized across the different seed particles and the overall local monomer concentration was kept low. As a result, both control of chain-growth and dynamic transformation of the block copolymer colloidal structures were achieved.

One could argue that the proposed solution is in fact *not* a PISA process anymore. This in the sense that the self-assembly is not *induced* by polymerization, but rather by temperature. In this sense the correct definition could be a seeded dispersion polymerization followed by a Temperature-Directed Morphology Transformation[18] or Temperature-Directed Self-Assembly,[23,24] both definitions originally found in the work from Monteiro et al. Whilst the proposed solution does not represent a standard PISA process, it definitely describes a step *towards* the development of polymer dispersions of intricate particle morphology, with the advantage that conventional organo-sulfur based RAFT agents can be omitted. Furthermore, added advantages of the use of methacrylate macromonomers with respect to NMP, ATRP or TERP mediated PISA reactions (see Introduction of this chapter) are that high monomer conversion can be achieved and that the metal contamination in the final product is negligible; [Co] < 0.1 ppm in this work.

The research presented in this chapter highlights three major drawbacks to the use of methacrylate macromonomers to PISA reactions. These are the higher size dispersity of the colloids produced, the applicability to methacrylate monomers only and, more importantly, the low values of the chain-transfer coefficient, C_T. Especially the last point adds further complication to an otherwise relatively simple synthetic process. From an industrial viewpoint, or more generally when thinking about using such colloids for specific applications, the proposed solution can be of limited relevance. For this reason, in Chapter 4 we present a new, simpler process for making methacrylate macromonomer-based self-assembled objects, *i.e.* block copolymer micelles, by only using industrially friendly emulsion polymerization reactions.

3.4 Experimental

3.4.1 Materials

Glycidyl methacrylate (GlyMA) (97%), poly(ethylene glycol) methyl ether methacrylate (PEGMEMA, average molecular weight 300), hydroxypropyl methacrylate (HPMA) (97%, mixture of isomers) were purchased from Sigma Aldrich and filtered through activated neutral aluminium oxide to remove the inhibitors. 2,2'-azobis(2-methylpropionitrile) (AIBN) was purchased from Sigma Aldrich and recrystallized from methanol. Potassium persulfate (KPS) (99%), 4-4'-azobis(4-cyanovaleric acid) (ACVA) (98%), d_6-DMSO, glacial acetic acid, acetonitrile (HPLC grade), tetrahydrofuran (THF), pentane, methanol, diethyl ether, anhydrous dimethyl formamide (DMF) were purchased from Sigma Aldrich and used as received. Bis[(difluoroboryl) dimethylglyoximato]cobalt(II) (CoBF) was synthetized according to the literature.[73]

3.4.2 Equipment & methods

^{1}H-NMR spectra were recorded on a Bruker HD-400 spectrometer using d_6-DMSO and anhydrous DMF respectively as solvent and internal standard. Average particle sizes and distributions were measured by dynamic light scattering (DLS) on a Malvern Zetasizer Nano. Molecular weights were measured by size exclusion chromatography (SEC) on an Agilent PL-SEC 50 equipped with UV and RI detectors and two Polargel M Columns operating at 60°C. DMF + 0.1 wt% LiBr was used as eluent for the SEC analysis and the system was calibrated using narrow molecular weight poly(methyl methacrylate) (PMMA) standards. The SEC samples were prepared at 2-3 mg/ml and were filtrated through a 0.2 µm PTFE filter before injection. Dialysis was performed using semipermeable cellulose tubing (3.5 kDa molecular weight cutoff). Transmission electron microscopy (TEM) analysis was performed on a Jeol 2011 TEM fitted with a Gatan Ultrascan 1000 camera. Samples were diluted 50-fold and one drop was casted on a carbon coated, glow-discharged TEM copped grid. After 2 min the drop was blotted off with filter paper and the grid was negatively stained by four successive casts of one drop of 2% uranyl acetate aqueous solution. Every drop was left on the grid for one min before being blotted off with filter paper. UV-Vis spectra were recorded on an Agilent technologies Cary

60 UV-Vis equipped with a Quantum Northwest TC 1 temperature controller and a 1 cm path length quartz cuvette was used for the analysis. For every temperature, the sample was allowed to equilibrate for 5 min before each measurement was recorded (transmittance mode, λ = 700 nm).

3.4.3 Poly(glycidyl methacrylate) (PGlyMA) macromonomer synthesis

In a typical catalytic chain transfer polymerization (CCTP) experiment CoBF (3.5 mg) and GlyMA (15.0 ml) were purged with nitrogen in separated sealed vials equipped with magnetic bars for 1h. After this time, 10.0 ml of GlyMA were added to the vial containing CoBF using a degassed syringe. This mixture was stirred vigorously until complete dissolution of the catalyst. Meanwhile, GlyMA (25.0 ml, 188.2 mmol), acetonitrile (25.0 ml), AIBN (0.21 g, 1.3 mmol) were added to a 250 ml RBF and purged with nitrogen under stirring for 30 min. Different amounts of the catalyst solution were added to the reaction mixture using a degassed syringe. The polymerization was carried out for 2h at 70°C, after which the reaction was quenched by simultaneous cool down and introduction of oxygen. Finally, acetonitrile was evaporated and the polymer was purified by 3x washing in an excess amount of pentane:methanol 5:1 v:v.

The final number average degree of polymerization (*DP*) was estimated *via* ^{1}H-NMR from the ratio between the integrals of the -OCH_2- (b) and the vinyl (a) peaks (Figure 3.4B).

3.4.4 Ring opening of the PGlyMA macromonomer

The $PGlyMA_{XX}$ macromonomer (7.0 g) was dissolved in 120 ml mixture of THF and glacial acidic acid (2:3 v:v) and added to a three-neck 500 mL RBF equipped with a condenser, a dropping funnel and a magnetic stirring bar. After complete dissolution of the polymer, the reactor was immersed in an oil bath set at 80°C and water (150 mL) was added gradually in 5 min time. A white emulsion was formed during the addition of water. The reaction was carried out at 80°C for 7 hours and resulted in a transparent solution. Next, the solvents were evaporated and the polymer was washed twice with an excess of diethyl ether. Deionized water was at

this point added to make a 10 wt% solution. This polymer was finally dialyzed against water when it was used in the HPMA chain-extensions (Runs 1-4).

3.4.5 Chain-extension of poly(glycerol methacrylate) (PGMA) macromonomers with HPMA

In a typical HPMA chain-extension (Run 4), poly(glycerol methacrylate) macromonomer ($PGMA_{32}$) (1.161 g), H_2O (16.253 g), DMF (0.051 g) were added to a 50 ml RBF equipped with a magnetic stirring bar. Next, the reaction mixture was purged with N_2 for 30 min and the RBF was submerged in an oil bath (set to 80°C). After 5 minutes, a pre-shot of aqueous KPS solution (0.1 ml, 5.3 mg/ml) was added to the system. HPMA (3.220 g), and the remaining KPS solution (0.9 ml) were fed over 8 h. Note that both the KPS solution and HPMA had also been previously purged with N_2 for 30 min. The reaction was allowed to react for another 30 min after all the monomer and initiator were injected. After this time, the reaction was quenched by simultaneously purging with air and cooling. Table 3.4 reports the details on the amounts of reagents used in all the HPMA chain-extensions using PGMA and PGMA-PPEGMEMA polymers, as well as the initiator and monomer feed rates.

Table 3.4 Amounts of reagents used and feed rates for all the HPMA chain-extensions (Runs 1-5).

Run	Polymer / mmol	H_2O / g	DMF / mmol	Initiator		HPMA	
				mmol	Feed rate / ml×h^{-1}	mmol	Feed rate / ml×h^{-1}
1[a]	0.166	17.670	2.074	0.013	Batch	15.88	Batch
2[a]	0.125	19.043	0.279	0.012	Batch	20.80	0.483
3[a]	0.231	19.005	0.573	0.023	Batch	21.10	0.475
4[b]	0.226	17.189	0.702	0.023	0.113	22.68	0.395
5[c]	0.196	17.306	0.743	0.019	0.113	24.55	0.342

[a] ACVA was used as initiator (2 eq. NaOH also added to the reaction), targeted solid content (SC) = *ca.* 17.5 %, 70°C.

[b,c] SC respectively *ca.* 20.5 and 22.7 %. KPS was used as initiator, T = 80°C, 90% of initiator solution fed into the system, 10% added as pre-shot before starting feeding (1.0 ml total solution).

3.4.6 Chain-extension of the poly(glycerol methacrylate) (PGMA) macromonomer with poly(ethylene glycol) methyl ether methacrylate (PEGMEMA)

Poly(glycerol methacrylate) macromonomer ($PGMA_{32}$) (6.145 g, 1.276 mmol), KPS (44.6 mg, 0.191 mmol), H_2O (12 g), DMF (125.6 mg, 1.718 mmol) were added to a 25 ml RBF equipped with a magnetic stirring bar. Next, the reaction mixture was purged with N_2 for 30 min and the RBF was submerged in an oil bath (set to 60°C). After 5 minutes, PEGMEMA 300 (4.953 g, 15.310 mmol), which had been previously purged with N_2 for 30 min was fed over 200 min (1.312 ml/h). The reaction was allowed to react for another 40 min after all the monomer was injected. The reaction was then quenched by simultaneous purge of air and cool down of the reaction system. The final product was finally dialyzed against deionized water in order to remove any residual monomer and salts. Theoretical targeted *DP* = 12. Final conversion (estimated by ^{1}H-NMR) ≈ 80%.

References

(1) G. Gody, T. Maschmeyer, P. B. Zetterlund and S. Perrier, *Nat. Commun.*, 2013, **4**, 2505

(2) W. A. Braunecker and K. Matyjaszewski, *Prog. Polym. Sci.*, 2007, **32**, 93–146

(3) A. D. Jenkins, R. G. Jones and G. Moad, *Pure Appl. Chem.*, 2009, **82**, 483–491

(4) Y. Mai and A. Eisenberg, *Chem. Soc. Rev.*, 2012, **41**, 5969

(5) D. E. Discher and A. Eisenberg, *Science (80-.).*, 2002, **297**, 967–973

(6) G. Srinivas, D. E. Discher and M. L. Klein, *Nat. Mater.*, 2004, **3**, 638–644

(7) G. Delaittre, J. Nicolas, C. Lefay, M. Save and B. Charleux, *Chem. Commun.*, 2005, **1**, 614–616

(8) C. J. Ferguson, R. J. Hughes, D. Nguyen, B. T. T. Pham, R. G. Gilbert, A. K. Serelis, C. H. Such and B. S. Hawkett, *Macromolecules*, 2005, **38**, 2191–2204

(9) S. Boissé, J. Rieger, K. Belal, A. Di-Cicco, P. Beaunier, M.-H. Li and B. Charleux, *Chem. Commun.*, 2010, **46**, 1950–1952

(10) N. J. Warren, O. O. Mykhaylyk, D. Mahmood, A. J. Ryan and S. P. Armes, *J. Am. Chem. Soc.*, 2014, **136**, 1023–1033

(11) S. L. Canning, G. N. Smith and S. P. Armes, *Macromolecules*, 2016, **49**, 1985–2001

(12) E. Groison, S. Brusseau, F. D'Agosto, S. Magnet, R. Inoubli, L. Couvreur and B. Charleux, *ACS Macro Lett.*, 2012, **1**, 47–51

(13) A. Blanazs, A. J. Ryan and S. P. Armes, *Macromolecules*, 2012, **45**, 5099–5107

(14) B. Charleux, G. Delaittre, J. Rieger and F. D'Agosto, *Macromolecules*, 2012, **45**, 6753–6765

(15) J. N. Israelachvili, *Intermolecular and Surface Forces*, Academic Press., London, 2nd. Ed., 1991

(16) L. P. D. Ratcliffe, B. E. McKenzie, G. M. D. Le Bouëdec, C. N. Williams, S. L. Brown and S. P. Armes, *Macromolecules*, 2015, **48**, 8594–8607

(17) Q. Zhang, C. Weber, U. S. Schubert and R. Hoogenboom, *Mater. Horizons*, 2017, **4**, 109–116

(18) Z. Jia, V. A. Bobrin, N. P. Truong, M. Gillard and M. J. Monteiro, *J. Am. Chem. Soc.*, 2014, **136**, 5824–5827

(19) S. Kessel, C. N. Urbani and M. J. Monteiro, *Angew. Chemie - Int. Ed.*, 2011, **50**, 8082–8085

(20) N. P. Truong, M. R. Whittaker, A. Anastasaki, D. M. Haddleton, J. F. Quinn and T. P. Davis, *Polym. Chem.*, 2016, **7**, 430–440

(21) C. N. Urbani and M. J. Monteiro, *Macromolecules*, 2009, **42**, 3884–3886

(22) K. O. Sebakhy, S. Kessel and M. J. Monteiro, *Macromolecules*, 2010, **43**, 9598–9600

(23) V. A. Bobrin and M. J. Monteiro, *J. Am. Chem. Soc.*, 2015, **137**, 15652–15655

(24) V. A. Bobrin, S.-P. R. Chen, Z. Jia and M. J. Monteiro, *ACS Macro Lett.*, 2017, **6**, 1047–1051

(25) C. A. Figg, A. Simula, K. A. Gebre, B. S. Tucker, D. M. Haddleton and B. S. Sumerlin, *Chem. Sci.*, 2015, **6**, 1230–1236

(26) X. G. Qiao, P. Y. Dugas, B. Charleux, M. Lansalot and E. Bourgeat-Lami, *Polym. Chem.*, 2017, **8**, 4014–4029

(27) L. A. Fielding, J. A. Lane, M. J. Derry, O. O. Mykhaylyk and S. P. Armes, *J. Am. Chem. Soc.*, 2014, **136**, 5790–5798

(28) M. J. Derry, O. O. Mykhaylyk and S. P. Armes, *Angew. Chemie Int. Ed.*, 2017, **129**, 1772–1776

(29) S. Dong, W. Zhao, F. P. Lucien, S. Perrier and P. B. Zetterlund, *Polym. Chem.*, 2015, **6**, 2249–2254

(30) S. Y. Khor, N. P. Truong, J. F. Quinn, M. R. Whittaker and T. P. Davis, *ACS Macro Lett.*, 2017, **6**, 1013–1019

(31) X. G. Qiao, M. Lansalot, E. Bourgeat-Lami and B. Charleux, *Macromolecules*, 2013, **46**, 4285–4295

(32) S. Sugihara, S. P. Armes and A. L. Lewis, *Angew. Chemie - Int. Ed.*, 2010, **49**, 3500–3503

(33) K. H. Kim, J. Kim and W. H. Jo, *Polymer (Guildf).*, 2005, **46**, 2836–2840

(34) V. Kapishon, R. A. Whitney, P. Champagne, M. F. Cunningham and R. J. Neufeld, *Biomacromolecules*, 2015, **16**, 2040–2048

(35) Y. Kitayama, K. Kishida, H. Minami and M. Okubo, *J. Polym. Sci. Part A Polym. Chem.*, 2012, **50**, 1991–1996

(36) J. Krstina, C. L. Moad, G. Moad, E. Rizzardo, C. T. Berge and M. Fryd, *Macromol. Symp.*, 1996, **111**, 13–23

(37) J. Krstina, G. Moad, E. Rizzardo, C. L. Winzor, C. T. Berge and M. Fryd, *Macromolecules*, 1995, **28**, 5381–5385

(38) N. G. Engelis, A. Anastasaki, G. Nurumbetov, N. P. Truong, V. Nikolaou, A. Shegiwal, M. R. Whittaker, T. P. Davis and D. M. Haddleton, *Nat. Chem.*, 2017, **9**, 171–178

(39) D. Zhou, R. P. Kuchel and P. B. Zetterlund, *Polym. Chem.*, 2017, **8**, 4177–4181

(40) A. Blanazs, J. Madsen, G. Battaglia, A. J. Ryan and S. P. Armes, *J. Am. Chem. Soc.*, 2011, **133**, 16581–16587

(41) N. J. Warren and S. P. Armes, *J. Am. Chem. Soc.*, 2014, **136**, 10174–10185

(42) C. J. Mable, M. J. Derry, K. L. Thompson, L. A. Fielding, O. O. Mykhaylyk and S. P. Armes, *Macromolecules*, 2017, **50**, 4465–4473

(43) J. P. A. Heuts and N. M. B. Smeets, *Polym. Chem.*, 2011, **2**, 2407–2423

(44) A. A. Gridnev and S. D. Ittel, *Chem. Rev.*, 2001, **101**, 3611–3659

(45) D. M. Haddleton, D. R. Maloney, K. G. Suddaby, A. V. G. Muir and S. N. Richards, *Macromol. Symp.*, 1996, **111**, 37–46

(46) D. M. Haddleton, E. Depaquis, E. J. Kelly, D. Kukulj, S. R. Morsley, S. A. F. Bon, M. D. Eason and A. G. Steward, *Polym. Sci. Part A Polym. Chem.*, 2001, **39**, 2378–2384

(47) D. Kukulj, T. P. Davis, K. G. Suddaby, D. M. Haddleton and R. G. Gilbert, *J. Polym. Sci. Part A Polym. Chem.*, 2000, **35**, 859–878

(48) N. M. B. Smeets, J. P. A. Heuts, J. Meuldijk and A. M. van Herk, *J. Polym. Sci. Part A Polym. Chem.*, 2008, **46**, 5839–5849

(49) G. E. Roberts, J. P. A. Heuts and T. P. Davis, *J. Polym. Sci. Part A Polym. Chem.*, 2003, **41**, 752–765

(50) S. A. F. Bon, D. R. Morsley, J. Waterson, D. M. Haddleton, M. R. Lees and T. Horne, *Macromol. Symp.*, 2001, **165**, 29–42

(51) K. A. McEwan, S. Slavin, E. Tunnah and D. M. Haddleton, *Polym. Chem.*, 2013, **4**, 2608–2614

(52) P. C. Hiemenz and T. P. Lodge, *Polymer Chemistry*, Taylor and Francis Group, 2nd ed., 2007

(53) R. A. Gregg and F. R. Mayo, *Discuss. Faraday Soc.*, 1947, **2**, 328–337

(54) S. E. Shaw, T. Russo, D. H. Solomon and G. G. Qiao, *Polymer (Guildf).*, 2006, **47**, 8247–8252

(55) D. J. Keddie, *Chem. Soc. Rev.*, 2014, **43**, 496–505

(56) C. L. Moad, G. Moad, E. Rizzardo and S. H. Thang, *Macromolecules*, 1996, **29**, 7717–7726

(57) S. A. F. Bon, PhD Thesis, Eindhoven University of Technology, 1998

(58) R. M. Fitch, *Br. Polym. J.*, 1973, **5**, 467–483

(59) S. Kawaguchi and K. Ito, in *Advances in Polymer Science*, 2005, vol. 175, pp. 299–328

(60) S. F. Ahmed and G. W. Poehlein, *Ind. Eng. Chem. Res.*, 1997, **36**, 2605–2615

(61) S. F. Ahmed and G. W. Poehlein, *Ind. Eng. Chem. Res.*, 1997, **36**, 2597–2604

(62) T. Sentoukas and S. Pispas, *J. Polym. Sci. Part A Polym. Chem.*, 2018, **56**, 1962–1977

(63) Z. Cao, W. Liu, G. Ye, X. Zhao, X. Lin, P. Gao and K. Yao, *Macromol. Chem. Phys.*,

2006, **207**, 2329–2335

(64) E. H. Leduc and S. J. Holt, *J. Cell Biol.*, 1965, **26**, 137–155

(65) Y. Kotsuchibashi, M. Ebara, T. Aoyagi and R. Narain, *Polymers (Basel).*, 2016, **8**, 380

(66) J.-F. Pei, C.-Z. Cai, Y.-M. Zhu and B. Yan, *Macromol. Theory Simulations*, 2013, **22**, 52–60

(67) N. A. Lynd and M. A. Hillmyer, *Macromolecules*, 2005, **38**, 8803–8810

(68) A. L. Schmitt, M. H. Repollet-Pedrosa and M. K. Mahanthappa, *ACS Macro Lett.*, 2012, **1**, 300–304

(69) O. Terreau, C. Bartels and A. Eisenberg, *Langmuir*, 2004, **20**, 637–645

(70) O. Terreau, L. Luo and A. Eisenberg, *Langmuir*, 2003, **19**, 5601–5607

(71) Y. Hirai, T. Terashima, M. Takenaka and M. Sawamoto, *Macromolecules*, 2016, **49**, 5084–5091

(72) K. E. B. Doncom, L. D. Blackman, D. B. Wright, M. I. Gibson and R. K. O'Reilly, *Chem. Soc. Rev.*, 2017, **46**, 4119–4134

(73) A. Bakac, M. E. Brynildson and J. H. Espenson, *Inorg. Chem.*, 1986, **25**, 4108–4114

4

Polymeric nanogels as stabilizers in emulsion polymerization

Crosslinked block copolymer micelles, here called *nanogels*, are synthetized and used as colloidal stabilisers in emulsion polymerization. The macromolecular building blocks of the nanogels were synthesized using a combination of catalytic chain transfer (CCT) emulsion polymerization and reversible addition-fragmentation chain-transfer (RAFT) of methacrylate monomers. The nanogels were adopted in standard styrene emulsion polymerizations as either aqueous dispersion or dry powder form, allowing to control the final latex particle size and its dispersity. Hence, they acted in the same way as a molecular surfactant, with the added advantage that they cannot migrate upon drying of the colloidal suspension. Tailoring of the polymerization conditions, such as by adjusting the suspension pH before polymerization, led to anisotropic Janus and patchy colloids, where a latex particle was decorated by a number of patches on its surface. The synthetic pathway is such that the nanogels can be designed to carry a desired *functionality*. As a result of their crosslinked nature, such functionality will be (over)expressed in the regions of the latex where the patches are present. Overall, these nanogel stabilized emulsion polymerizations have the potential to become a new attractive way of fabricating functional polymer colloids of various morphologies.

4.1 Introduction

The last two decades have seen a surge in efforts to synthesize anisotropic colloidal particles;[1,2] particles with asymmetry in shape and/or chemical composition. Great interest has been shown towards the design and hierarchical assembly of these anisotropic objects, in an attempt to mimic biological precision. A wide variety of shapes in colloidal particles have been reported including cubes,[3] cylinders,[4] ellipsoids,[5] disks,[6] and more exotic varieties such as tetrapods,[7] matchsticks,[8,9] and even "octopus ocellatus" particles.[10]

Anisotropic colloids with "broken" symmetry are promising candidates as next-generation building-blocks for advanced functional supracolloidal materials.[11] The prerequisites for an ideal next-generation material are a desired geometric uniformity of its building-blocks and the presence of *functional sites* as a way to depict directionality and render the desired packing parameter necessary to assemble into a thermodynamically pre-defined supracolloidal structure.[12] The architectural nature of the anisotropic particle is critical to tune the assembly process and these colloids are designed keeping in mind the second reorganization, or *self-assembly*, step. The concept of "patchy" particles is often used in this field - particles which have functional sites with a distinct physicochemical characteristic on their surface. The simplest subclass of patchy colloids consists of particles having one patch, or protrusion, which are commonly referred to as Janus particles.

Elegant examples of tailored self-assembly in supracolloidal structures using these types of colloids are present in the literature. For instance, Glotzer and coworkers showed *in silico* that colloidal crystals with diamond symmetry, of importance for band gap materials, could be formed using model hard spheres with attractive patches.[13] Sacanna and coworkers reported the assembly of "lock" and "key" colloids which mimic the site specificity of enzymes and receptors to direct supracolloidal assembly.[14,15] Kumacheva *et al.* designed cetyltrimethylammonium bromide-coated gold nanorods with polystyrene molecules grafted to both ends that could self-assemble in rings, chains, side-to-side bundles and nanospheres in selective solvents.[16] Granick *et al.* reported that spherical polymer microspheres, made hydrophobic on one hemisphere, could self-assemble in helical-like suprastructures by increasing the ionic strength of the dispersing medium.[17] Instead,

when two opposite sides of the microspheres were modified, making "two-sided" Janus particles, the colloidal crystallization into Kagome lattices was observed.[18] Müller, Gröschel *et al.* investigated the use of triblock terpolymers that could form soft patchy particles as building blocks for hierarchical assembly.[19] The formation of supracolloidal polymer chains, spherical clusters and mixed structures laterally decorated by smaller Janus particles was observed.

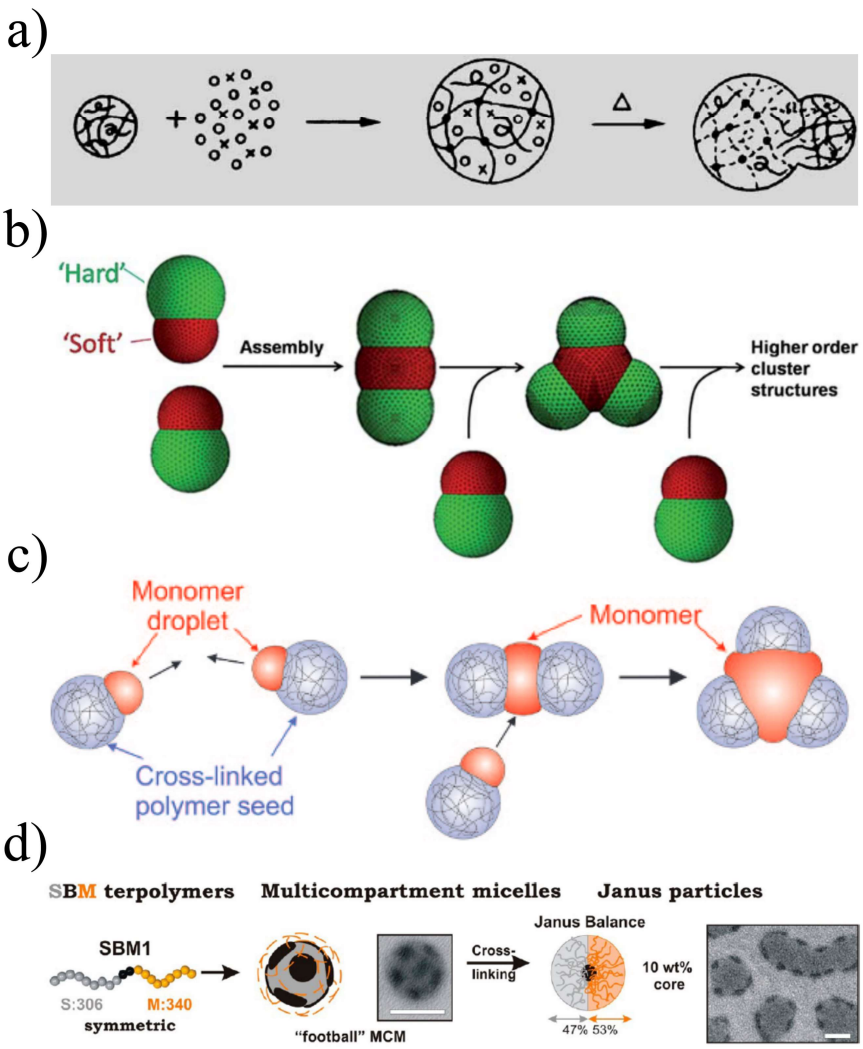

Figure 4.1 Approaches to synthesize polymeric Janus and patchy particles *via* a) swelling of crosslinked polymer seeds followed by polymerization[20] and self-assembly of b) hard-soft Janus particles,[21] c) colloids bearing liquid protrusions,[22] d) terpolymers into multicompartment micelles.[23] Pictures are adapted with permission from ref. 20-23.

In recent years, we have witnessed a revolution in the number of approaches to fabricate Janus and patchy particles.[24–26] When narrowing down to the field of polymer science, a number of approaches stand out. Perhaps the simplest approach to synthetize a polymeric Janus particle is swelling of a crosslinked polymer seed with a second monomer, followed by polymerization (Figure 4.1A).[20] Given the crosslinked nature of the seed particle, the second polymer will start growing inside the seed, essentially forming an interpenetrated polymer network, and will then phase-separate on one side of its surface. Similarly, Janus particles can be made by surface nucleation from a crosslinked polymeric seed.[27] Patchy particles can be formed from Janus building-blocks *via* clustering of colloidal objects through collision of either hard-soft Janus particles (Figure 4.1B)[21] or particles with liquid protrusions (Figure 4.1C).[22] A different synthetic pathway is designing block-copolymers that can self-assemble in multicompartment micelles in a selected solvent (Figure 4.1D).[23] Other approaches include: assembly of colloidal clusters by using confined solid[28] or droplet templated geometries;[29,30] heterocoagulation of oppositely charged colloids,[31] or using depletion interaction;[14] microfluidic strategies including polymerization using droplets;[32] lithography,[33] microcontact printing[34] and roll-to-roll printing;[34,35] physical deposition after immobilization;[36] surface modification of Pickering stabilizers.[37,38] Whereas a plethora of synthetic methods is available, a continuous challenge is always to be able to make these materials in scalable amounts using straightforward reproducible synthetic protocols.[26,39] This is especially true when seeking industrial applicability.

This chapter reports details of a new robust approach to produce patchy and Janus polymer particles, consisting of a standard polymer spherical latex decorated by a number of functional patches on its surface. This is done by modification of a conventional industrially-applicable emulsion polymerization process; the patchy particles are made *in-situ* when the latexes are synthetized in presence of a suspension of patches. The patches are introduced in the form of crosslinked block copolymer micelles, here defined as *nanogels*, of 15-30 nm in diameter. When conventional emulsifiers, such as (macro)molecular surfactants, are used in emulsion polymerization, they spread over the entire surface of the latex particle to minimize interfacial tension. In this way spherical particles are obtained. Instead, in this work the macromolecular surfactants, here with carboxylic acid functionality, were pre-

bundled into nanogels to avoid spreading and hereby introducing distinct functional sites in the latexes. Tailoring of the reaction conditions allowed to produce Janus particles, patchy latexes with appreciable control of the surface density of the patches and armoured morphologies consisting of a shell of densely packed nanogels surrounding a polymeric core. In particular, the formation of armoured particles is discussed in Chapter 5.

4.2 Results and discussion

The discussion of this chapter will be divided in three parts. First the synthesis of polymeric nanogels *via* catalytic chain transfer emulsion polymerization and reversible addition-fragmentation chain-transfer (RAFT) will be presented. This will be followed by the application of these nanogels as sole stabilizers in standard emulsion polymerization reactions for the production of Janus and patchy colloids. Finally some kinetic considerations will be made on selected experiments.

4.2.1 Synthesis of polymeric nanogels

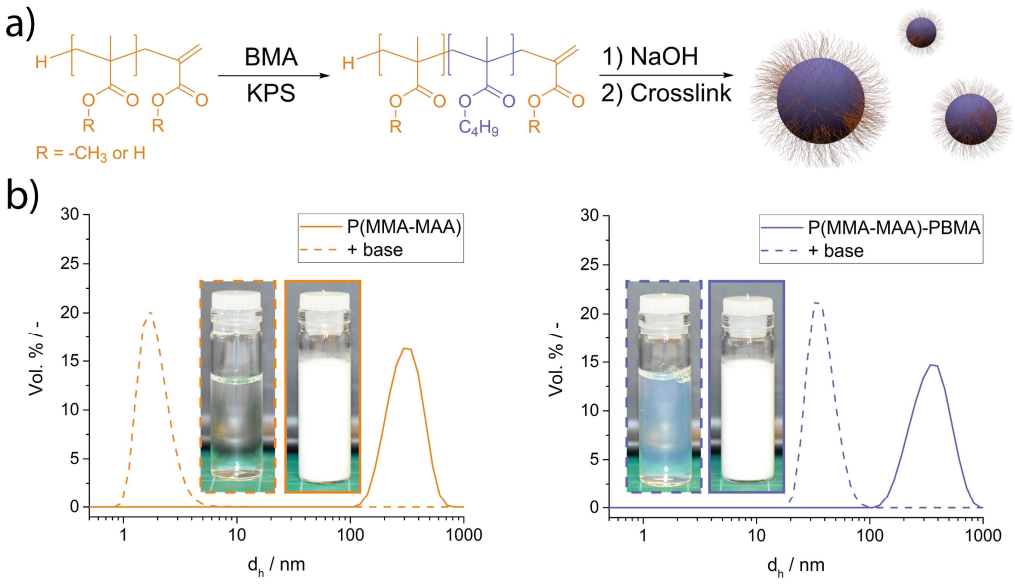

Figure 4.2 a) Synthesis of crosslinked poly(methyl methacrylate-methacrylic acid)-*block*-poly(*n*-butyl methacrylate) P(MMA-MAA)-PBMA copolymer nanogels. b) Size distribution *via* dynamic light scattering (DLS) and visual appearance before and after addition of base to the polymer latexes.

The nanogels adopted in this work were made by core-crosslinking of ω-end unsaturated poly(methyl methacrylate-methacrylic acid)-*block*-poly(*n*-butyl methacrylate) P(MMA-MAA)-PBMA copolymer micelles synthetized *via* sulfur-free RAFT.[40–43] Figure 4.2A shows a schematic of the synthetic approach used.

Initially, cobalt-mediated catalytic chain transfer polymerization (CCTP)[44,45] using a mixture of methyl-methacrylate (MMA) and methacrylic acid (MAA) (1.8:1.0 molar ratio) was carried out as a semi-batch emulsion polymerization process.[40,41] The reactions were carried out at *ca.* 16 wt%, using ACVA as initiator. The polymer latexes made in this way consist predominantly of ω-end unsaturated poly(methyl methacrylate-*co*-methacrylic acid) P(MMA-MAA) macromonomers (Figure 4.2A, orange structure). Either bis[(difluoroboryl) dimethylglyoximato] cobalt(II) (CoBF) or bis[(difluoroboryl) diethylglyoximato] cobalt(II) (Et-CoBF) were used as catalysts for CCTP reactions (Figure 4.3).[44,45] When using Et-CoBF, similar results in terms of molecular weight distributions and dispersity were obtained with catalyst concentrations 4 times lower with respect to CoBF. This is the result of the much higher reported monomer/water partitioning coefficient for Et-CoBF with respect to CoBF (see Section 1.3.2).[44,45]

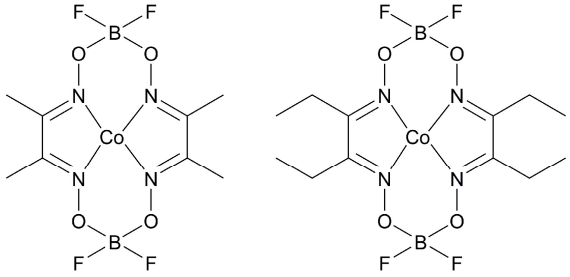

Figure 4.3 Structures of the cobalt catalysts adopted in the synthesis of methacrylate macromonomers: bis[(difluoroboryl) dimethylglyoximato] cobalt(II) (CoBF) and bis[(difluoroboryl) diethylglyoximato] cobalt(II) (Et-CoBF).

A semi-batch addition of catalyst and monomers was necessary to contrast the catalyst deactivation in acidic aqueous environment.[46] In this work 20.0 vol% of the monomers/catalyst mixture was injected as a pre-shot in the system whilst the remaining 80.0 vol% was fed over 24 min as reported by Haddleton et al.[43,47] The reason for the initial pre-addition of monomer is to do with the partitioning of the

catalyst within the newly formed particles in the early stages of the polymerization. Once a particle is formed, excess monomer swells these particles, lowering their T_g, and hence allowing free movement of the catalyst.[47–49] The P(MMA-MAA) macromonomer latexes were designed in a way that the addition of a base would result in the total dissolution of the latex into polymer chains.[47] Indeed, upon addition of 1.05 eq. of NaOH or NH_3 with respect to MAA, the polymer dispersion became transparent and the formation of solvated polymer chains was observed by DLS (Figure 4.2B, orange).

The macromonomers synthesized in this way are an interesting class of compounds as they can operate as macro-RAFT agents in the synthesis of methacrylate block copolymers, with the added advantage that they do not contain sulfur.[40,41,50] These macro-RAFT agents were chain-extended with *n*-butyl methacrylate (BMA) using an analogous semi-batch emulsion polymerization protocol as originally reported by Moad et al.[40,41] and Haddleton et al.[43] In this step both BMA and the initiator (potassium persulfate, KPS) were fed to the polymer dispersion to chain-extend. Upon addition of base, these diblock copolymer latex particles disassembled to form an aqueous dispersion of copolymer micelles (Figure 4.2 and A4.1). Note that the synthesis of such copolymer micelles could not be achieved in a controlled fashion by chain-extension of a lyophilic polymer *via* dispersion polymerization, or polymerization-induced self-assembly (PISA), as explained in Chapter 3.[42] In contrast, the synthetic approach presented in this chapter allows to produce with ease large amounts of block copolymer micelles in a one-pot, three-step procedure. It is clear that this synthetic pathway could be a simpler solution for the synthesis of spherical micelles, rod-like micelles and vesicles *via* seeded dispersion or (seeded) emulsion polymerization, without the need of organo-sulfur RAFT agents.

The formed block-copolymer micelles were finally covalently core crosslinked by feeding trimethylolpropane trimethacrylate and KPS to the diblock copolymer micelle dispersion over 5h at 85°C. The system was then allowed to react overnight to yield the nanogels (Figure 4.4). To validate that the polymer chains were indeed bundled into nanogels, DLS analysis were carried out in MeOH before and after crosslinking (Figure 4.5A). When the crosslink step was not carried out, only solvated polymer chains were observed in DLS measurements.

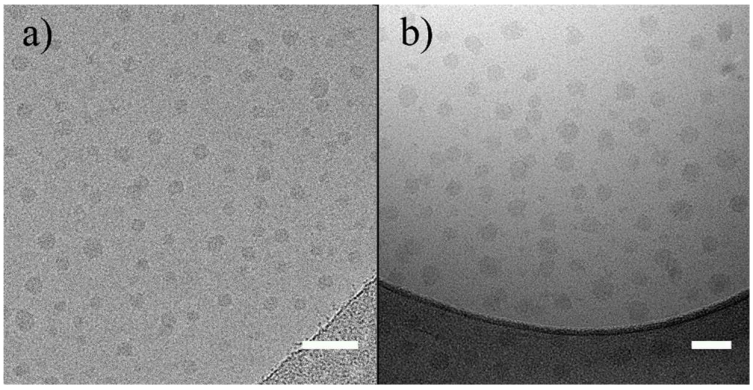

Figure 4.4 Cryo-TEM images of the nanogels N1 (A) and N2 (B) obtained through crosslinking with trimethylolpropane trimethacrylate. Scale bars: 50 nm.

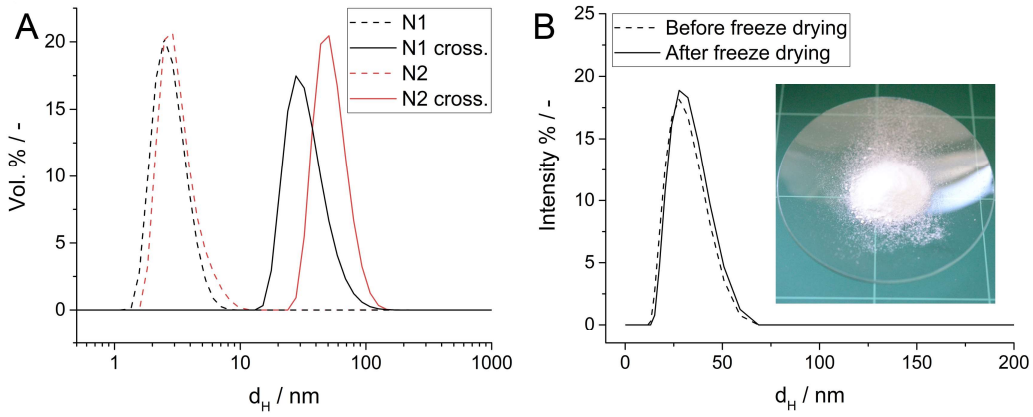

Figure 4.5 A) Hydrodynamic diameter (d_H) of N1 and N2 before and after crosslinking in MeOH. B) Size distribution by dynamic light scattering of N1 nanogels before freeze drying and after being freeze dried and redispersed in water. Inset: the freeze-dried powder can be used instead of the colloidal suspension in the emulsion polymerization.

Two different nanogels were synthetized for this work, N1 and N2 (Table 4.1). The number average degree of polymerization (*DP*) of the corona hydrophilic block was 17 and 53 respectively, as measured by ^{1}H-NMR spectroscopy (see Figure 4.16). The BMA core hydrophobic block was 10 in both cases. Upon crosslinking, one feature of the nanogels is that they contain two types of carbon-carbon double bonds, reactive towards further polymerization. These are a combination of the ω-end macromonomer vinyl groups and pendant vinyl groups from the trifunctional crosslinker. Their presence was confirmed by ^{1}H-NMR (Figure A4.2). It is still under

investigation whether this is a required or additional feature in the application presented in this chapter. Interestingly, the nanogels can be stored and used as freeze-dried powder and can easily be re-dispersed in water (Figure 4.5B).

Table 4.1 Nanogels adopted in this work.

	SEC[a]			SAXS[b]	DLS[c]	
	M_w / kg mol^{-1}	M_n / kg mol^{-1}	$Đ_M$ / -	d_{SAXS} / nm	d_H / nm	PdI / -
N1	5.6	3.5	1.6	18	30	0.14
N2	11.8	9.0	1.3	23	56	0.04

[a] Size exclusion chromatography (SEC) on the P(MMA-MAA)-PBMA unimers prior to crosslinking; eluent: DMF + 5 mM NH_4BF_4, calibration: PMMA narrow standards. $Đ_M$ = polymer dispersity.
[b] Small-angle X-ray scattering (SAXS) data (Figure 4.6, Table A4.1); measured at 10.0 mg/ml, pH 6.0.
[c] Measured at 5.0 mg/ml, pH = 8.5.

The hydrodynamic diameter of the synthetized nanogels was 30 and 56 nm respectively for N1 and N2 at pH 8.5 (Table 4.1). A measure of the actual nanogel size was provided by small-angle X-ray scattering (SAXS) on 1.0 wt% nanogel suspensions in water at pH 6.0 (Figure 4.6). Both a spherical and a core-shell sphere form factor were tested for the fitting of the scattering patterns. For a mathematical description of the models the reader is directed to the related literature,[51] whereas the parameters used for the fittings are found in Table A4.1. As expected, both could be fitted with a spherical form factor, with N1 having a profile more similar to a simple sphere and N2 slightly more similar to a core-shell sphere. The diameter from these measurements (d_{SAXS}) were 18 and 23 nm respectively for N1 and N2.

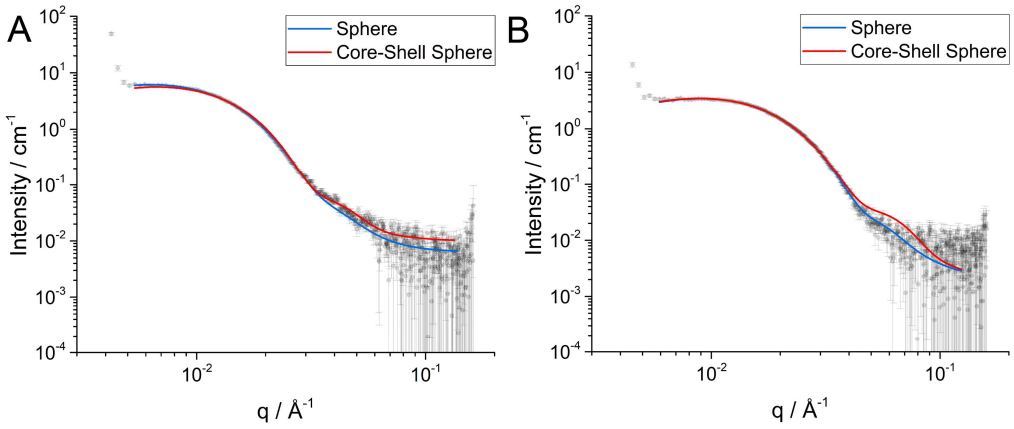

Figure 4.6 SAXS patterns of a 1.0 wt% suspension of N2 (A) and N1 (B) nanogels in deionized water.

4.2.2 Nanogels as stabilizers in emulsion polymerization

The synthesized P(MMA-MAA)-*block*-PBMA crosslinked micelles were tested as stabilizers in standard soap-free batch emulsion polymerizations of styrene (Tables A4.2 and A4.3 for experimental details). The reactions were carried out overnight in deionized water at 75°C, using KPS as initiator (KPS/styrene = 0.07-0.15 wt%). Initially, the pH of the suspension was adjusted to 8.8 before polymerization. When the reaction was carried out in absence of nanogels, a polystyrene latex of relatively narrow particle size distribution was obtained (d_H = 292 nm, Figure 4.7).

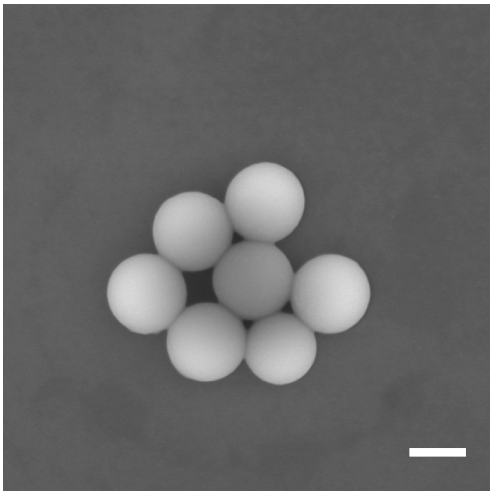

Figure 4.7 SEM image of narrow dispersity spherical latex particles produced by soap-free emulsion polymerization of styrene in absence of nanogels as stabilizers (Run 29, Table A4.3). The pH was adjusted to 8.1 and a 1:1 w:w $NaHCO_3$:KPS ratio

was used to buffer the drop in pH resulted by the KPS decomposition.[52] Scale bar = 200 nm.

Next, nanogels were added to the reaction medium before polymerization in varying ratios from 0.1 to 40.0 wt% wrt monomer, defined as weight of nanogels divided by weight of styrene × 100 (N/Sty). In the same way as conventional surfactants, the addition of both N1 and N2 nanogels had a pronounced effect on the average particle diameter and its distribution as shown by DLS measurements on the final latexes (Figure 4.8). In particular, the initial addition of small amounts of nanogels resulted in a marked reduction in particle diameter, with a broadening of the particle size distribution for further additions.

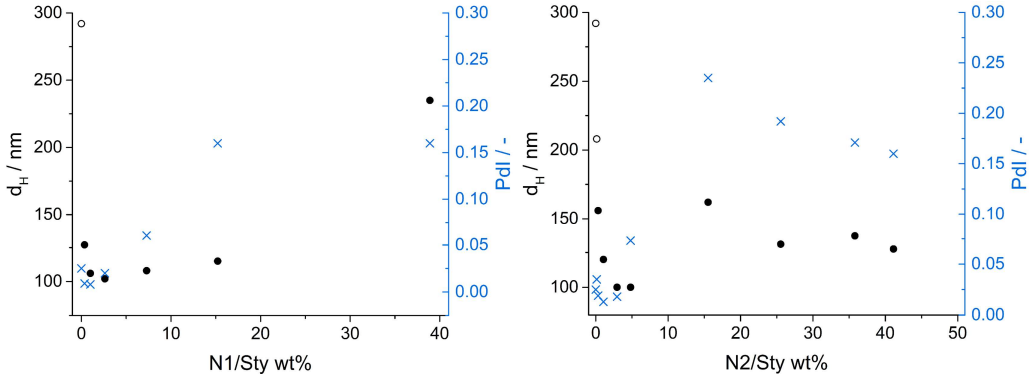

Figure 4.8 Hydrodynamic diameter (d_H) and polydispersity index (PdI) of the final latexes obtained *via* emulsion polymerization of styrene at pH 8.8, carried out in the presence of various amounts of N1 (left) and N2 (right), expressed as a weight ratio with respect to styrene. Empty circles: reactions run in the presence of a buffering agent, sodium hydrogen carbonate ($NaHCO_3$), to counteract the pH drop from the KPS decomposition.[52] The initial pH in the reaction in absence of nanogels was 8.1.

The strong dependence of d_H with nanogel concentration suggested that their presence had a major effect on the latex particle formation step in the emulsion polymerization process. As explained in Section 1.2, in a soap-free emulsion polymerization the nucleation of latex particles takes place in the water phase following the so-called homogenous nucleation mechanism (HUFT-theory); the monomer dissolved in the continuous phase polymerizes until it reaches a degree of polymerization, j_{crit}, at which the waterborne oligomer collapses forming a primary particle.[53] In the present case, growing oligomers in the water phase can be captured

by the nanogels instead,[53] before j_{crit} is reached, hereby affecting particle nucleation. In a way, they can act as micelles in surfactant-stabilized emulsion polymerizations.

This phenomenon resembles the influence on the nucleation of latex particles and their stabilization by inorganic sols of various morphologies (spheres,[54,55] disks,[56,57] sheets[58]), cellulose nanocrystals[59] and organic Janus particles[60,61] in seeded emulsion polymerizations. This effect was also observed in Chapter 2 when discussing the nano-SiO_2 stabilized emulsion polymerizations.[62] As described and shown in Chapter 2, when using inorganic nanoparticles, the morphology of the resulting latex generally is that of a polymer particle with an outer armour of relatively close packed nanoparticles (see Figure 2.2).

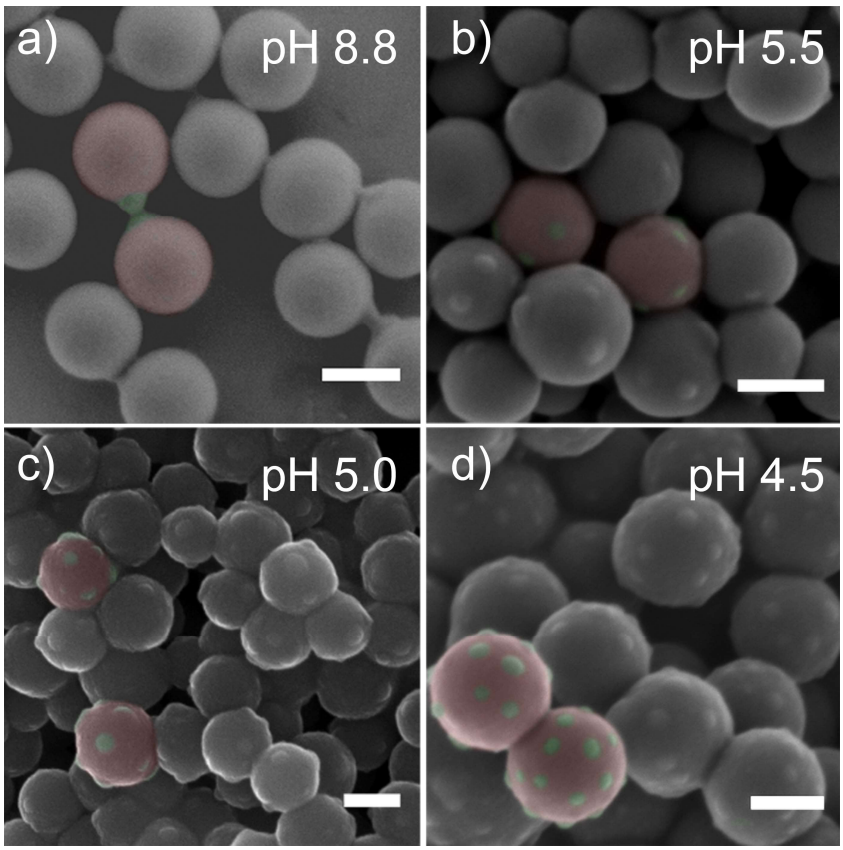

Figure 4.9 False coloured SEM images of emulsion polymerizations using N1 at 2.8 wt% wrt monomer in which the pH was adjusted to 8.8 (A), 5.5 (B), 5.0 (C) and 4.5 (D) prior to polymerization. Scale bars: 100 nm.

Instead, electron microscopy analysis of the polymer latexes made in presence of relatively small amounts of nanogels (< 3.0 wt% wrt to monomer) revealed

polystyrene particles with no more than one nanogel lobe on the surface (Figures 4.9A and A4.3). It is straightforward that statistically the nanogel will be in the upper or lower (hidden) part of the latex when imaging these particles. This is especially true when the volume difference between the two phases is large; the volume of the nanogel:poly(styrene) *ca.* 1:100 in Run 4 (Table A4.2). Indeed 51% of the latexes had a visible patch on the surface in this sample and, as explained, no particle was observed to carry more than one nanogel. Therefore, this emulsion polymerization method provides versatile access to polymer Janus particles, characterized by a single nanogel protrusion. In order for the phase-separation to take place, it is important that the micelles are crosslinked. Emulsion polymerizations where non-crosslinked polymer micelles were used instead, resulted in spherical latex particles without distinct patches (Figure A4.4). In this reaction the amphiphilic block-copolymer chains can spread across the latex surface in the same way as a conventional molecular surfactant. Instead, when these micelles are crosslinked beforehand, they provide access to a material where the nanogel phase is phase-separated in one area only, to minimize the system free energy.[20] For this initial investigation, the nanogels were conveniently synthetized with carboxylic acid functionality. It is evident that the chemical specificity of the patch can be tuned in the synthesis of the nanogels, therefore providing a convenient route towards the fabrication of Janus polymer particles with a single *functional* patch.

It can be expected that an increase in nanogel concentration would result in particles bearing multiple patches. This was indeed the case. However, the average particle diameter, number of lobes, and particle size distribution became erratic (Figures 4.8 and A4.5). Additionally, these samples seemed to result in a broad mixture of particles bearing from 1 to multiple lobes, with a likely large proportion of unreacted nanogels.

In Chapter 2 it was discussed that when operating with inorganic charged particles in Pickering emulsion polymerization processes, the affinity between polymer phase and the stabilizer can be enhanced by adding background electrolytes[58] or by pH adjustment.[55,63] In a way it is operated in conditions for which the stabilizer is close to instability. The same concept was used for studies on the ordering of charged silica nanoparticles onto mini-emulsion droplets.[64] It should indeed be possible to synthetize latexes bearing multiple nanogel patches, without

loss of control of the latex particle size distribution, by following the same approach. By varying the emulsion polymerization conditions with a focus on the electrostatic features of the nanogels, regulation of the number of patches *per* particle, and hence control of patch density was achieved. Both pH adjustment and background electrolyte addition were tested. In this chapter only the data regarding the pH regulation will be discussed, whereas Chapter 5 will present data regarding the addition of salt. Figure 4.8 shows that by adjusting the pH of the nanogel suspension to different starting values, polystyrene latexes carrying a varied number of nanogels were obtained.

As anticipated, this behaviour is linked to the electrostatic interactions of the nanogels. The previous set of emulsion polymerizations were conducted at pH 8.8. At this pH the nanogels are colloidally stable due to the presence of deprotonated carboxylic acid groups in their corona. An indicative measure for the relative number of anionic charges present in a nanogel particle is the fraction of ionized carboxylic acid groups, α. Its value is linked directly to pH in the form of a modified version of the Henderson–Hasselbalch equation (Equation 4.1):[65,66]

(4.1) $$pK_a = pH + n \log \frac{1-\alpha}{\alpha}$$

n is a constant; $n = 1$ for a monoacid and $n > 1$ for a polyacid.[65,66] In the latter, the pK_a increases as a function of α.[67] The values of the dissociation constant are not known for the P(MMA-MAA)-*block*-PBMA copolymers used in this chapter. For the purpose of the discussion, indicative values for poly(acrylic acid)-*co*-poly(*n*-butyl methacrylate) and poly(methacrylic acid) respectively from Winnik et al.[67] and Katchalsky et al.[66] will be used. At pH 8.8, α approaches a value of 1.0. In this case, at high anionic charge density and potency in electrostatic stabilization, it is plausible that Janus particles are formed upon radical entry into a nanogel "seed" particle, which is swollen with styrene monomer (Figure 4.10). As the polymerization proceeds, a polystyrene lobe phase-separates from the crosslinked nanogel core, forming a small anisotropic colloid. The charged nanogel warrants colloidal stability of the Janus particle upon further growth of the poly(styrene) lobe. In a way, the proposed mechanism is similar to what shown for the synthesis of polymer Janus particles from swelling of crosslinked latexes with a second monomer and then followed by polymerization (Figure 4.1A).[20] The results presented in this chapter

suggest that the swelling stage may not be necessary, even when adopting rather hydrophobic monomers such as styrene.

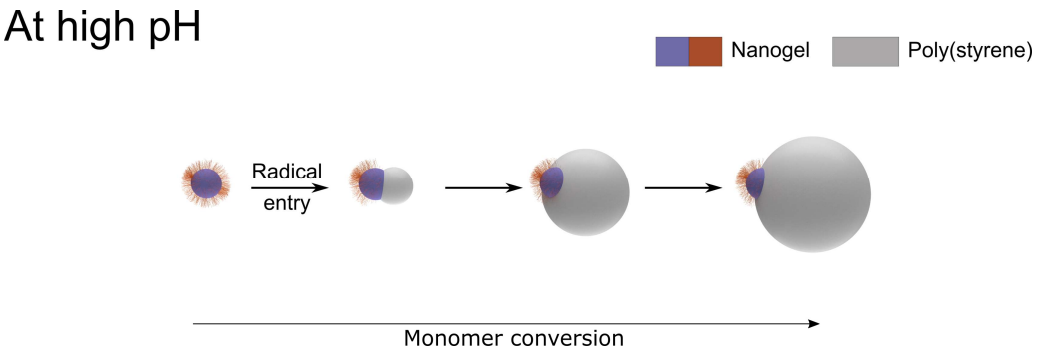

Figure 4.10 Proposed mechanism for the formation of Janus particles in the emulsion polymerization of styrene carried out in presence of nanogel particles at high pH.

When decreasing the pH of the nanogel dispersions in water, the loss of surface charge due to the protonation of the carboxylic acid groups, that is the decrease in α, results in a gradual loss of colloidal stability. This behaviour was confirmed when monitoring the average nanogel hydrodynamic diameter (d_H) and ζ-potential *vs.* pH by DLS (Figure 4.11).

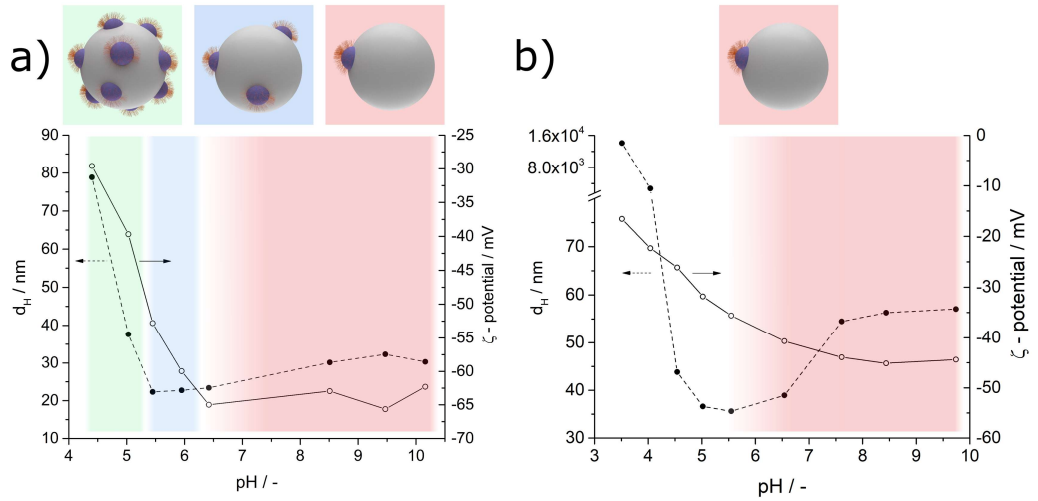

Figure 4.11 Hydrodynamic diameter (d_H) and ζ-potential variation for a) N1 and b) N2 as a function of pH. As the double layer is compressed, different particle morphologies can be obtained in the styrene emulsion polymerization.

Initially, d_H decreased as a result of a lower charge density down to *ca.* pH 5.5. At even lower pH, an increase in size and dispersity was observed due to a loss in electrostatic colloidal stability which induced particle clustering. In particular, when N1 was used and the pH was set to 5.5 ($\alpha \approx 0.16$-0.22),[66,67] low dispersity patchy particles were formed (Figure 4.9B). In this reaction, instead of just one, a few nanogel lobes could be seen on the polystyrene surface. When the pH was further decreased to 5.0 ($\alpha \approx 0.12$) and 4.5 ($\alpha \approx 0.08$),[66,67] an increasing number of patches on the surface was achieved and, as to be expected, overall larger particles were obtained (Figures 4.9C-D). Note that in the case of the reaction run at pH 4.5 some coagulum was formed. This is logical as this reaction operates well below the pK_a of the carboxylic acid groups,[67] placing the nanogels at the edge of their colloidal stability. Under these acidic conditions the nanogels can likely operate as conventional Pickering stabilizers and adhere to soft interfaces. In other words, they can adsorb to the interface of monomer droplets, prior to polymerization. Indeed, small amounts of polymerized monomer droplets with a patchy layer of nanogel particles were observed at pH 4.5 (Figure A4.7).

To investigate these observations (Figures 4.9A-D) in greater detail we carried out in depth image analysis of the SEM data (Figure 4.12). This to not only get a more accurate view on the size distribution of the Janus and patchy particles, but also to statistically quantify the patch density of particles formed at the different values of pH. ImageJ was used to manually measure particle size and area, and nanogel area on a particle by particle basis in order to assign the number of patches to the poly(styrene) surface area. The observed number of patches in the SEM images was multiplied by 2 to give n_{patch} to account for patches on the hidden side of the latexes.

By regulating the pH in emulsion polymerizations, from 8.8 down to 4.5 using N1 nanogels, the particle size of the patchy latexes increased as the pH was lowered; average diameters of 79 ± 5, 118 ± 9, 134 ± 9, 165 ± 14 nm respectively for pH 8.8, 5.5, 5.0 and 4.5 (Figure 4.12A). The surface area fraction (surface coverage) of patches on the PS surface increased from 3.0 to 16.6% (Figure 4.12B) and the number of patches could be varied from 1 to roughly 18 per latex particle (Figure 4.12C).

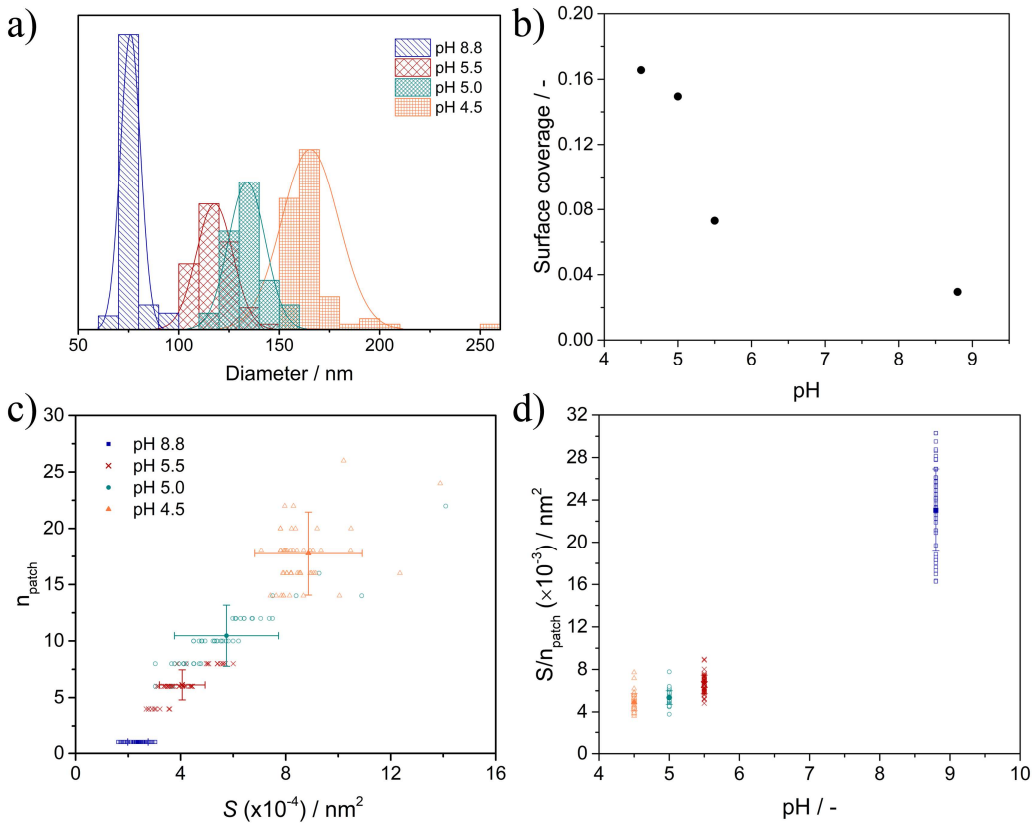

Figure 4.12 Image analysis of SEM data of latexes made at different pH using N1 nanogels. a) Latex particle diameters showing a normal distribution. b) Fraction of the latex surface area covered by nanogels (surface coverage) for the emulsion polymerization of styrene conducted at different pH. c) Number of patches (n_{patch}) on the poly(styrene) surface *vs.* total latex surface area (S). d) Surface area *per* patch as a function of pH used in the emulsion polymerization. Population averages (filled symbols) are shown for c) and d) with their relative standard deviations.

As explained, the role of the nanogels in the formation of patchy particles is to provide electrostatic stability. Whereas at pH 8.8, α approaches a value of 1.0, at pH 5.5, 5.0 and 4.5 α was measured to be *ca.* 0.22-0.16, 0.12 and 0.08 respectively for poly(methacrylic acid).[66,67] This is in agreement to what shown in Figure 4.11; at pH lower than 6.5 (α ~ 0.5)[66] the ζ-potential starts decreasing rapidly with pH. In essence more nanogel patches are required to maintain colloidal stability. This also explains the increase in particle diameter upon decrease in pH, as the number of polymerization *loci* is suppressed when multiple nanogels are present on the same latex particle. Similarly to what suggested for the reactions at high pH, the formation of these patchy particles is likely a combination of coagulative assembly of growing

Janus particles early on in the polymerization process and pre-assembly of nanogels prior to polymerization (Figure 4.13). At the beginning of the polymerization, initial multi-patch clusters can be formed by either nanogel clustering, as suggested by Figure 4.11, or assembly of not fully stabilized small anisotropic particles. The latter mechanism is suggested by previous literature on the self-assembly of hard-soft Janus colloids into bigger clusters as described in the introductory section of the chapter (Figures 4.1B-C).[21,22,68] Once these clusters are formed, new anisotropic particles or nanogels can adsorb at the polystyrene bare surface as the particle grows, in a way to increase colloid stability.

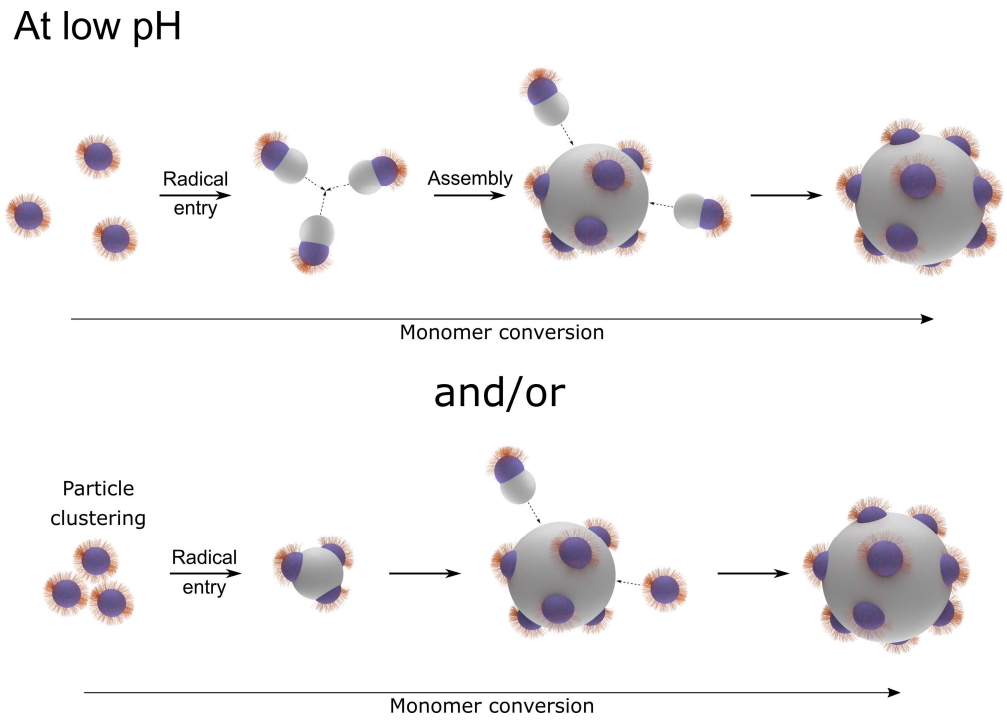

Figure 4.13 Proposed mechanism for the formation of patchy particles in the emulsion polymerization of styrene carried out in presence of nanogel particles at low pH.

An interesting comparison of this system can be made with charged colloidal particles at soft liquid-liquid interfaces. Previous studies on the two-dimensional ordering of these colloids adsorbed on a soft interface showed no dependence in spatial arrangement on pH[69] or salt concentration.[70] In particular, in previous work by Schmitt, Ravaine et al. while investigating the adsorption of poly(N-isopropylacrylamide)-poly(acrylic acid) microgels at the air-water interface, no

difference in spacing between the microgels was found at pH 6.0 and 3.0.[69] A comparison with these systems is reasonable as up to high monomer conversion (~ 70/80%) the latex particle core is in a soft state.[71] A measure of the spacing of the nanogels on the poly(styrene) surface is the surface area per patch (S/n_{patch}), calculated as the ratio of the latex surface area divided by the number of patches present. When S/n_{patch} is plotted as a function of pH (Figure 4.12D), a clear correlation between the spacing of the nanogels on the surface of the polystyrene and what in essence is the degree of ionization of the nanogels is observed. However, the difference is larger when moving from pH 8.8 to 5.5 but phases out upon further pH decrease, confirming what previously observed in the literature.[69] Unfortunately no data was presented for pH > 6.0 in the work by Schmitt, Ravaine et al., so a direct comparison in this range of pH was not possible.

The experiments where the pH was adjusted to values < 5.5 were not always straightforward, especially when the nanogels N2 were adopted. As explained before, at pH lower than 5.5 the system coagulated (Figure A4.6B) as a result of a low overall stability of N2 at more acidic pH (Figure 4.11B). An attempt to circumvent the occasional coagulation issues in acidic conditions was to decrease the pH *in-situ* during particle formation. The idea was to allow the particles to start growing as small soft peanut-shaped particles that could then self-assemble in a supracolloidal patchy structure when colloidal stability is lost (*i.e.* when pH ~ 5.0). This can be conveniently achieved by increasing the radical flux, or in other words, by adding more initiator to the system while operating at the same temperature. In fact, the decomposition of persulfates in water is known to release hydrogen sulphate ions and to be acid catalysed.[52] In absence of $NaHCO_3$ as buffer and at very low nanogel concentrations, for example 0.11 wt% wrt monomer in Runs 14 and 26 (Tables A4.2 and A4.3), the composition of KPS resulted in pH drop *in-situ* to *ca.* 3.4 during the reaction. As a result, what appeared being near monodisperse patchy particles of bigger sizes could also be targeted at much lower nanogel concentrations than when the pH was lowered before starting the polymerization (Figure 4.14). However, further mathematical analysis of the system, presented in the following section of the discussion, were in contrast with this initial observation.

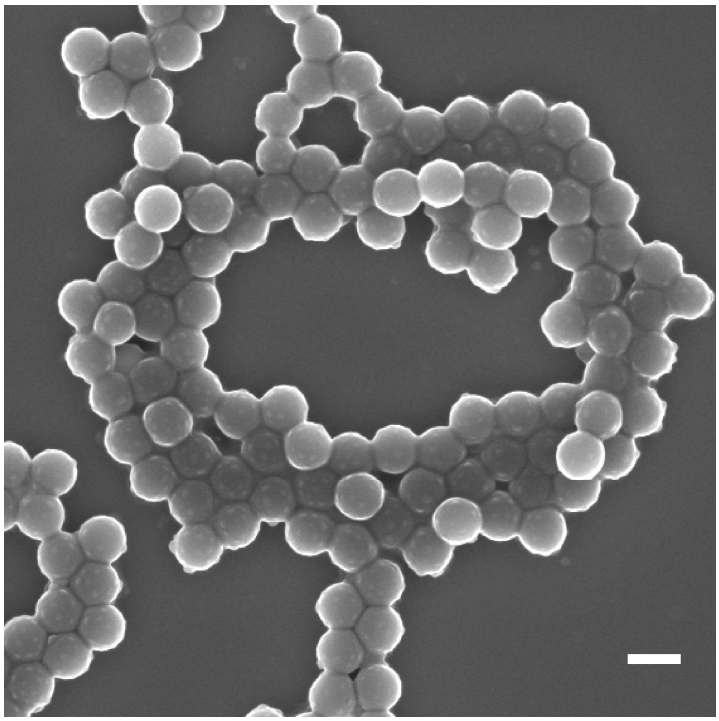

Figure 4.14 SEM picture of the emulsion polymerization of styrene conducted at N2/Sty 0.11 wt% and 0.15 mg/ml of KPS (Run 26). Scale bar = 200 nm.

4.2.3 Final considerations

After the observations presented in the previous section, it was decided to analyse the system more carefully from a kinetic viewpoint. Initially it was decided to further analyse the final size of the latexes produced. The reason behind this is that the emulsion polymerization in the presence of nanogels as stabilizers at high pH was described to be the growth of a polystyrene lobe off a nanogel seed particle (Figure 4.10). Hence, theoretically the number of latex particles, N_p, should be equal to the number of seeds particles added to the reactor, N_{nano}. N_{nano} was calculated from Equation 4.2:

(4.2) $$N_{nano} = \frac{g_{nano} 6}{\rho_{nano} \pi d_{SAXS}^{\ 3}}$$

where g_{nano} is the mass of nanogels added, ρ_{nano} is their density (assumed to be 1.1 g/cm^3) and d_{SAXS} is the nanogels diameter determined by SAXS measurements (Table 4.1).

It is clear that the calculation of N_{nano} is very sensitive to the values of diameter and density chosen. N_p was measured using a formula analogue to Equation 4.2, where the size of the poly(styrene) lobe only of the latex particles measured by SEM, d_{SEM}, was used instead. Table 4.2 shows the values of N_{nano} and N_p for both N1 and N2 at N/Sty < 3.00 wt%, along with their ratio N_{nano}/N_p.

Table 4.2 Comparison between i) initial number of nanogels and number of formed latex particles, ii) observed (d_{SEM}) and theoretical (d_{th}) size of the poly(styrene) latexes, assuming equal growth from all the nanogels.

Nanogel	N/Sty wt% / -	pH / -	d_{SEM} / nm	d_{th} / nm	N_{nano}/N_p / -
/	/	8.1	273	/	0.00
N1	0.36	8.8	109	116	0.76
N1	1.01	8.8	85	82	1.01
N1	2.85	8.8	79	59	2.10
N1	2.85	5.5	118	/	7.57
N1	2.85	5.0	134	/	11.09
N1	2.85	4.5	165	/	20.70
N1[a]	0.12	8.8	160	/	0.80
N2	0.13	8.8	181	226	0.60
N2	0.32	8.8	145	169	0.75
N2	1.05	8.8	107	113	1.00
N2	2.93	8.8	85	81	1.40
N2[a]	0.11	8.8	175	/	0.46

[a] Reactions where the pH during the reaction dropped *in situ* to *ca.* 3.4 (Run 14 and 26).

Table 4.2 shows that at pH 8.8 for N/Sty < 3.00 wt%, that is approximately the minimum of the curve of d_H over N/Sty (Figure 4.7), indeed the ratio N_{nano}/N_p is close to unity in most cases. This not only provides extra confirmation of the proposed mechanism as depicted in Figure 4.10, but also indicates the ideal N/Sty wt% ratio for Janus particle formation. In particular, comparison of d_{SEM} with the theoretical size of the poly(styrene) phase, assuming equal distribution of styrene across all the nanogels, d_{th}, shows that when $N_{nano}/N_p > 1$ then $d_{SEM} > d_{th}$, whereas if $N_{nano}/N_p < 1$ then $d_{SEM} < d_{th}$, as expected. Hence, these results infer that when $N_{nano}/N_p > 1$, for the reactions conducted at pH 8.8, a portion of nanogels could be left unreacted as only Janus particles are observed at the end of the reaction. The same data is displayed for clarity in Figure 4.15, where to the left of the dotted line, which is $N_p/N_{nano} = 1$, there

is secondary nucleation of new latex particles which will not have a nanogel on their surface. Instead, to the right of the dotted line uncomplete nucleation is expected to occur. The same cannot be argued for the reactions carried out at lower pH, as in these cases N_{nano}/N_p can be higher both as a result of incomplete nanogel nucleation and because more nanogels are adsorbed on the polystyrene surface. Interestingly, for these reactions at lower pH the values of N_{nano}/N_p are close to what experimentally observed by SEM image analysis (Figure A4.8).

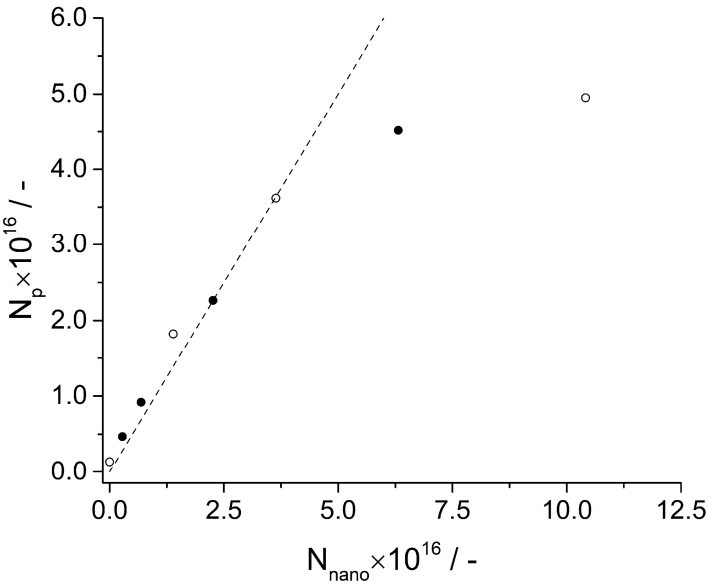

Figure 4.15 Variation of the number of latexes formed (N_p) with the number of nanogels (N_{nano}) introduced in emulsion polymerizations carried out at pH 8.8, for N/sty < 3.00 wt% wrt monomer. N1 = empty symbols, N2 = filled symbols. The dotted line is $N_p/N_{nano} = 1$.

The fact that a portion of the nanogels could have been left unreacted in the system could be explained in terms of slow nucleation of the nanogels or, in other words, low radical flux. Generally speaking, a seed latex, such as a nanogel particle, is nucleated upon radical entry.[72] For these seeded emulsion polymerizations to be successful, nucleation needs to be fast enough to allow all the seeds to grow at a similar rate. The opposite scenario is that a portion of the seeds is nucleated and start to grow before the rest. This would increase its capacity of swelling more monomer and would result in a higher chance of being reinitiated given the larger surface area. As a first approximation, in order to get an estimate of the frequency of radical entry, the number of radicals produced in the reaction was compared to the number of

nanogels present in the reaction system. In a standard thermally-initiated free-radical polymerization, the radical production is obtained in terms of initiator decomposition from Equation 4.3.

(4.3) $$n_r = 2N_A f_I V_{H_2O}[I_0](1-e^{-k_d t})$$

where V_{H_2O} is the volume of water, N_A is the Avogadro number, f_I is the capture efficiency, $[I_0]$ is the initiator initial concentration, k_d is the initiator decomposition rate coefficient and t is the time in seconds.

The capture efficiency f_I is essentially the fraction of formed radicals that enters the particles either directly or after reacting with monomer in the water phase. f_I for persulfate initiated styrene emulsion polymerization stabilized by anionic surfactants was calculated at the $[I_0]$ of this system to be *ca.* 0.12 and 0.15, respectively for N1 and N2.[72] k_d for a persulfate initiator at reaction temperature can be calculated from the Arrhenius equation (Equation 4.4):

(4.4) $$k_d = Ae^{-\frac{E_a}{RT}}$$

where $A = 8\times10^{15}$ s^{-1} and E_a = 135 kJ/mol for persulfate decomposition.[73] k_d is in s^{-1}.

Next, a comparison was made between n_r and the number of nanogels particles present, N_{nano}, for reactions at N/Sty < 3.00 wt% wrt monomer. In particular, the results will be shown for the reactions performed at pH 8.8, although it is straightforward that the same holds for reactions carried out at different pH. Equation 4.3 was used to calculate the number of radicals produced at a certain reaction time, t_{eq}, at which $n_r \geq N_{nano}$ (Table 4.3).

Table 4.3 Timescales of equal number of radicals produced and nanogels present in the polymerizations at high pH and for N/Sty < 3.00 wt%.

Nanogel	N/Sty wt% / -	$N_{nano} \times 10^{-16}$ / -	t_{eq} / s
N1[a]	0.12	0.45	10
N1	0.36	1.39	57
N1	1.01	3.64	159
N1	2.85	10.41	420
N2[a]	0.11	0.24	5
N2	0.13	0.28	6
N2	0.32	0.69	14
N2	1.05	2.26	43
N2	2.93	6.31	120

[a] Reactions where the pH during the reaction dropped *in situ* to *ca.* 3.4 (Run 14 and 26).

t_{eq} is an interesting parameter as it gives an idea of the frequency of radical entry in a particle. For simplicity, in this discussion f_I was kept constant for different amounts of nanogels added. In actual fact, f_I is correlated to N_{nano},[72] hence at lower [N_{nano}], higher t_{eq} are expected than those reported in Table 4.3. The calculated values of t_{eq} interestingly show that, especially for N1, the adopted initiator flux was insufficient for every particle to react at an equal rate. This may not only result in broadening of the particle size distribution, even though generally rather monomodal Janus particles are produced, but can indeed result in fractions of unreacted or partially reacted nanogels. As explained previously, in the case of prolonged nucleation events, the first batch of nucleated nanogels will start growing and as a result will have a higher chance of being reinitiated given the larger surface area. This would also explain why at high [N_{nano}] the observed size of the Janus particles was larger than the theoretical one (Table 4.2), as the monomer spread over a limited number of nanogel.

Even though the calculated values of t_{eq} are indicative of a particularly slow nucleation process, the absolute values are clearly overestimated. In actual facts, radical exit can happen across the whole polymerization and hence the same radical can initiate multiple particles,[72] leading to a drop in t_{eq}.

One final comment is related to the latexes produced in conditions of low nanogel concentration and with the pH dropping *in-situ* during the reaction (Run 14 and 26). Taking as example Run 26 (Table A4.3 and Figure 4.14), N_{nano}/N_p = 0.46 (Table 4.2), inferring that actually there is only about half nanogel available per particle. This striking result is in direct contrast with what showed in Figure 4.14. The first possible explanation for the observed "patchiness" of these latexes is actually the result of the carbon sputtering process carried out before SEM analysis. The reaction was however repeated 3 times and the same outcome was observed. The second, is related to the crosslinking step of the nanogels. Taking a step back, it is known from the literature that complete core-crosslinking of unimers in arm-first nanogels can require a large excess of crosslinker with respect to unimers and long polymerization times.[74,75] For instance, Davis, Boyer et al. reported that for a series of arm-first star polymers a crosslinker-to-unimer ratio of 8:1 led to the highest incorporation, ~ 90%, of arms in most cases.[76] The ratio when considering the double functionality of the crosslinker was 16:1. In the experimental conditions adopted in this work, this ratio was 1.7-2.5 (or 5.1-7.5 considering the triple functionality of the crosslinker adopted). Additionally, in the experiments from David, Boyer et al. the crosslinker was polymerized with a monofunctional monomer, whereas in this chapter pure crosslinker was adopted. This, along with the very low water solubility of the crosslinker adopted in this work, may have led to lower crosslinking density than originally predicted. Going back to the emulsion polymerizations, this is likely to be not a problem at low radical flux as in the reaction the higher molecular weight polymers formed can hold the nanogel together. However, at much higher radical flux, for instance Run 14 and 26 (*i.e.* low *in-situ* pH reactions), the much lower molecular weight poly(styrene) may result in a spreading of nanogel fractals (of a few crosslinked unimers) on the latex surface. This, in a way, would still result in latexes with functional patches on their surface. A more in-depth analysis of the crosslinking step of the synthetized nanogels will be able to identify whether this is the reason behind the observed patchiness in these reaction conditions.

4.3 Conclusion and outlook

In this chapter the synthesis of polymeric nanogels and their application as stabilizers in emulsion polymerization was explored. Typically, emulsion polymers are stabilized by molecular or macromolecular surfactants. In Chapter 2 it was showed that stable latexes can also be synthetized using inorganic colloids. Here the same is demonstrated with crosslinked block copolymer micelles, or nanogels. One clear advantage over the use of inorganic colloids is the range of latex morphologies accessible with this new methodology (Janus, patchy and armoured). At the same time, it was showed that the electro-steric stabilization provided is such that no additional amphiphile is needed to warrant colloidal stability. One could say that these nanogels serve as reactive surfactants or *surfmers*, as they still contain double bonds reactive towards further polymerization. From a different viewpoint, they can be seen as Pickering stabilizers, in the same way as the SiO_2 nano-spheres in Chapter 2, as they adhere to the polymer soft interphase during particle formation. In both cases, this technology has the potential to solve the problem of surfactant migration in dried films, which often deteriorates the final film performance.[39,77]

In this work the nanogels were produced by covalent crosslinking of block copolymer micelles, the polymer chains of which were synthetized through a combination of catalytic chain-transfer emulsion polymerization and reversible addition fragmentation chain-transfer (RAFT) of methacrylate monomers. It is obvious that the nanogels can be made *via* different controlled radical polymerization techniques, the closest analogue being conventional sulphur-based RAFT, or even free-radical polymerization. A logical extension would be to incorporate chemical functional groups into the nanogels. The ease customization of polymer materials with respect to the inorganic counter parts represents a second great advantage. Without drastic changes in the synthetic protocol, methacrylate monomers carrying poly(ethylene glycol), urea, amino, epoxide, sulfate, vinyl, hydroxy, hydrolysable inorganic precursors (*i.e.* 3-(trimethoxysilyl) propyl groups), metal-complexing aceto-acetoxy groups[78] can give specific *function* to the resulting patchy and Janus particles. In particular, the last two examples could open towards hybrid organic/inorganic patchy particles where the mechanical and catalytic properties of the inorganic components are combined with the film-forming properties and ease of processability of polymeric materials.

One of the biggest limitations of this synthetic protocol is the dispersity of both patch density and size. The is especially true when comparing these colloids to the ones made by microfluidic or lithography strategies. In these examples however the size of the particles ranges in the order of tens of μm in diameter.[32–34] With the current technology, template-based techniques are not applicable in the order of 50-300 nm. In this size range the proposed approach shows its full potential as based on the convenient, straightforward and industrially scalable protocols of emulsion polymerization.

4.4 Experimental

4.4.1 Materials

Methyl methacrylate (MMA) (99%), *n*-butyl methacrylate (BMA) (99%) and styrene (≥ 99%) were purchased from Sigma Aldrich and filtered through activated basic aluminium oxide prior to use to remove the inhibitors. Potassium persulfate (KPS) (99%), 4-4'-azobis(4-cyanovaleric acid) (ACVA) (98%), methacrylic acid (MAA) (99%), trimethylolpropane trimethacrylate (technical grade), trimethylolpropane triacrylate (technical grade), trimethylolpropane ethoxylated triacrylate avg. M_w 428 g/mol (technical grade), sodium dodecyl sulphate (SDS) (≥ 98.5%), sodium hydrogen carbonate ($NaHCO_3$) (≥ 99.7 %), sodium hydroxide (NaOH) (≥ 97%), D_2O (99.9 atom %D) and d_6-DMSO (99.9 atom %D) were purchased from Sigma Aldrich and used as received. Bis[(difluoroboryl) dimethylglyoximato] cobalt(II) (CoBF) and bis[(difluoroboryl) diethylglyoximato] cobalt(II) (Et-CoBF) were synthetized according to the literature.[79,80]

4.4.2 Equipment & methods

^{1}H-NMR spectra were recorded on freeze-dried polymers on either a Bruker HD-300 or a Bruker HD-400 spectrometer using d_6-DMSO as solvent. The spectra were recorded at 10 wt% polymer in deuterated solvent. Average particle sizes and distributions were measured by dynamic light scattering (DLS) on a Malvern Zetasizer Nano ZS or a Malvern Zetasizer Ultra operating at 25°C and at a detection angle of 173°. ζ-Potential measurements were carried out on the Malvern Zetasizer

Ultra at 0.5 wt% in deionized water using disposable folded cuvettes (Malvern). Molecular weights and dispersity values were measured by size exclusion chromatography (SEC) on an Agilent 390-MDS equipped with a Polar Gel Guard and two Polar Gel mixed-D columns operating at 60°C. DMF with 5mM NH_4BF_4 was used as eluent for the SEC analysis and the system was calibrated using narrow molecular weight poly(methyl methacrylate) standards. The SEC samples were prepared at 1-2 mg/ml and were filtrated through a 0.2 µm hydrophilic PTFE filter before injection. Dialysis was performed using semipermeable cellulose tubing (3.5 kDa molecular weight cutoff). Cryogenic Transmission electron microscopy (cryo-TEM) analyses were performed on a Jeol 2200FS TEM. Scanning electron microscopy (SEM) images were collected on a ZEISS Gemini SEM. Samples were diluted in deionized water and casted on a silicon wafer fragment, which had been adhered to an aluminium stab using conductive copper tape. The samples prepared in this way were carbon coated before imaging. Image analysis of SEM data was performed using ImageJ. Size data was obtained by measuring the Feret diameter. Nanogel and latexes surface area were measured by drawing ellipses and measuring the pixel areas. Patches were manually counted and multiplied x2 to account for the hidden surface of the bottom half of the particles.

Small-angle X-ray scattering (SAXS) measurements were made using a Xenocs Xeuss 2.0 equipped with a micro-focus Cu K_α source collimated with Scatterless slits. The scattering was measured using a Pilatus 300k detector with a pixel size of 0.172 µm x 0.172 µm. The distance between the detector and the sample was calibrated using silver behenate ($AgC_{22}H_{43}O_2$), giving a value of 2.480(5) m. The magnitude of the scattering vector (q) is given by $q = 4\pi \sin\theta/\lambda$, where 2θ is the angle between the incident and scattered X-rays and λ is the wavelength of the incident X-rays. This gave a q range for the detector of 0.005 $Å^{-1}$ and 0.16 $Å^{-1}$. A radial integration of the 2D scattering profile was performed using FOXTROT software[81] and the resulting data corrected for the absorption, sample thickness and background. Finally, the scattering intensity was then rescaled to absolute intensity using glassy carbon as a standard.[82] The samples were prepared at 10 mg/ml in water and loaded in 1.0 mm glass capillaries. SAXS pattern were collected at 25°C for 60 min. Patterns were analyzed using the software SasView[83] and the data fitted using a sphere[51] or core-shell sphere form factor[51] with the addition of a hayter_msa structure factor[84,85]

to take into account the coulombic repulsion between charged particles. The scattering length densities (sld) were calculated using SasView.

4.4.3 Synthesis of polymer nanogels

The synthesis of the polymeric nanogels was performed in a 250 ml glass reactor equipped with a PTFE coated anchor overhead stirrer and a PTFE coated temperature probe. Two sets of reactions conditions are reported for the synthesis of smaller (N1) or bigger (N2) nanogels (Table 4.4). All the reagents added to the reactors are intended to be purged with nitrogen for at least 30 min prior to addition, even when not specified.

Table 4.4 Number (M_n), weight (M_w) average molecular weights and polymer dispersity ($Đ_M$) as measured by size exclusion chromatography (SEC).

		M_n /kg mol^{-1}	M_w /kg mol^{-1}	$Đ_M$	DP [a]
N1	Step 1	2.9	4.3	1.5	17
	Step 2	3.5	5.6	1.6	10
N2	Step 1a	6.7	9.7	1.4	24
	Step 1b	8.6	11.3	1.3	29
	Step 2	9.0	11.8	1.3	10

[a] *DP* is here the number average degree of polymerization of the specific synthetic step.

The *DP* of the polymers was determined on the first block, P(MMA-MAA), step 1 or step 1a, *via* ^{1}H-NMR (Figure 4.16) using Equation 4.5:

$$DP = \frac{2}{5}\frac{\int(b)-1}{\int(a)}+1 \quad (4.5)$$

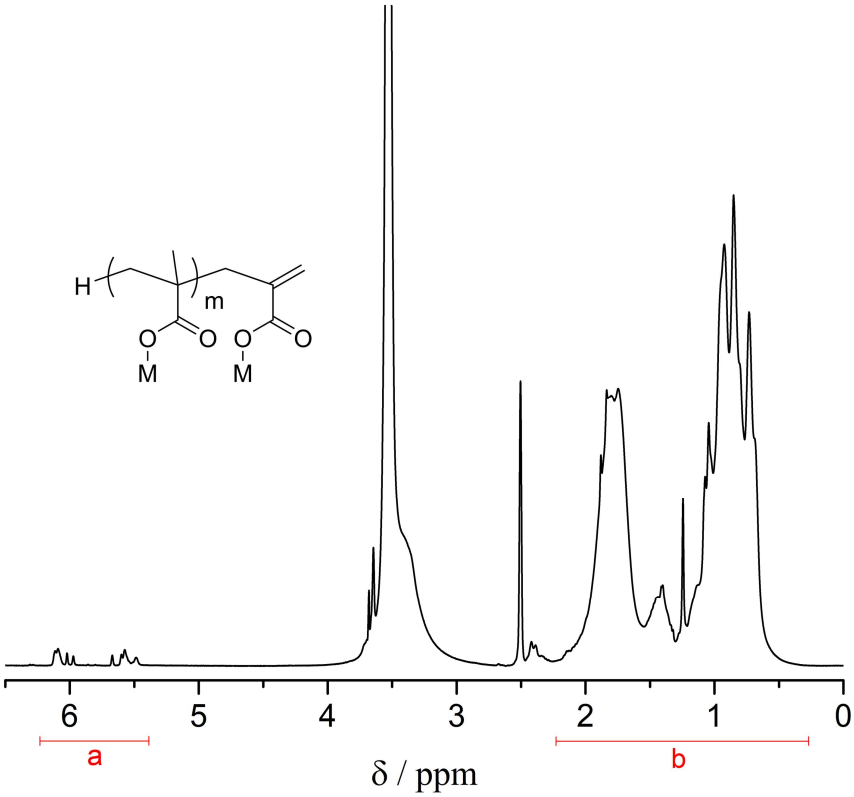

Figure 4.16 ^{1}H-NMR (d^{6}-DMSO) spectrum after step 1a during the synthesis of N2. *a* and *b* are the integrals used to calculate the *DP* = m + 1.

Step 1: Synthesis of a macromonomer latex *via* catalytic chain-transfer polymerization (CCTP) in a semi-batch emulsion polymerization process

The protocol adopted for the synthesis of macromonomer latexes *via* catalytic chain-transfer polymerization represents a modified version of what previously reported by Moad *et al.*[40] and Haddleton *et al.*[43] In a typical emulsion polymerization experiment CoBF (8.2 mg) and a MAA:MMA 30:70 v:v mixture (25.0 ml) were purged with nitrogen in separated sealed vials equipped with magnetic bars for 1h. After this time, 22.0 ml of the monomer mixture were added to the vial containing CoBF using a degassed syringe. This mixture was stirred vigorously until complete dissolution of the catalyst; mild ultrasound treatment was used to favour dissolution in this step. Meanwhile, SDS (0.3 g), H_2O (130.0 g), ACVA (0.5 g) were added to a 250 ml reactor and purged with nitrogen for 1 h under vigorous stirring at 300 rpm. Note that ACVA it is not soluble at this stage. After this, the reaction mixture was heated up to 72°C, which rendered ACVA soluble in water. The reaction was started with the addition

of 20% by volume of the monomer mixture (the rest was fed at 0.666 ml/min over 24 min, total volume added to the reactor = 20.0 ml) and it was carried out for 1h at 72°C. Next, the system was heated to 82°C and the reaction was left to reach full conversion for one extra hour.

For the synthesis of N2, 5.5 mg of CoBF were adopted (Step 1a). After the 2h reaction time, more water (60.0 g) was added to the system. The macromonomer was chain-extended by feeding more monomer mixture (MAA:MMA 30:70 v:v, 16.0 g, 15.4 ml) and aqueous KPS solution (5.6 mg/ml, 16.0 g) over 3h at 85°C (Step 1b). The reaction mixture was left for extra 30 min after this time to reach full conversion.

Step 2: Chain-extension with *n*-butyl methacrylate (BMA) *via* reversible addition-fragmentation chain transfer (RAFT)

For the synthesis of N1, 120.0 g of latex were diluted with 38.0 g of water. The reaction was conducted at 85°C while BMA (14.1 ml) and aqueous KPS solution (12.6 ml, 5.6 mg/ml) were fed over 2 h. After feeding, the reaction was allowed to proceed for extra 30 min. For the synthesis of N2, H_2O (23.0 g), latex (120.0 g), BMA (5.6 ml), aq. KPS (5.0 ml, 5.6 mg/ml) were used instead. In both cases a theoretical BMA DP of 10 was targeted.

Step 3: Latex Solubilization and polymer micelle crosslinking

For the synthesis of N1 nanogels, 133.1 g of BMA chain-extended latex were diluted with 40.0 ml water and 37.3 g of NaOH (1.0 M, *aq.*) were injected into the system. NaOH was added to a 1.05:1.00 molar ratio wrt MAA. The system was left to equilibrate at 85°C for 30 min and during this time it turned from milky white to translucent blue. Next, trimethylolpropane trimethacrylate was added to the system (5.9 ml) and aqueous KPS solution (12.6 ml, 5.6 mg/ml) was fed over 5 h. The system was then allowed to fully react overnight. During this stage limited precipitation occurred, which was removed by filtration using hydrophilic PTFE 0.45 μm filters. Final solid content: 11.7 wt%. When synthetizing N2 nanogels, water (22.0 ml), NaOH (1.0 M *aq.*, 51.3 ml), trimehylolpropane trimethacrylate (5.6 ml), aqueous KPS solution (6.0 ml, 5.6 mg/ml) were used instead. Final solid content: 11.4 wt%.

The crosslinking step was also carried out using trimethylolpropane triacrylate or trimethylolpropane ethoxylated triacrylate (avg. M_w = 428 g/mol) obtaining similar preliminary results. In this manuscript only the data and experiments involving the trimethacrylate will be shown for simplicity.

For imaging purposes, the nanogels may need to be dialyzed to remove the large amount of salt present. Note that this is not required for the following emulsion polymerization reactions to be successful. Alternatively, a volatile organic base, ammonia (NH_3), can be adopted. This can then be easily evaporated after the crosslinking step. Even in this case, NH_3 was added to a 1.05:1.00 molar ratio wrt MAA.

4.4.4 Emulsion polymerization using nanogels as stabilizers

The emulsion polymerizations were carried out in either a 250 ml reactor apparatus as described above, or a sealed 250 ml round bottom flask equipped with an oval stirrer bar. Little difference was found when repeating the same reactions with the two set-ups.

In a typical emulsion polymerization experiment (Run 15, Table A4.3), an aqueous dispersion of nanogels (sample N2, 3.90 g) was diluted with H_2O (148.5 g). The pH of the suspension was adjusted to 8.8 using aq. HCl 1.0 M. The reaction mixture was charged in a 250 ml reactor apparatus as previously described and it was purged with nitrogen for 30 min. Next, styrene (16.6 ml), which had been previously purged with nitrogen for 30 min, was injected into the reactor using a degassed syringe. The system was heated up to 75°C. The reaction was started upon injection of an aqueous KPS solution (1.0 ml, 11.3 mg/ml) and it was run overnight.

References

(1) S. C. Glotzer and M. J. Solomon, *Nat. Mater.*, 2007, **6**, 557–562

(2) A. Walther and A. H. E. Müller, *Chem. Rev.*, 2013, **113**, 5194–5261

(3) L. Gou and C. J. Murphy, *Nano Lett.*, 2003, **3**, 231–234

(4) A. Kuijk, A. Van Blaaderen and A. Imhof, *J. Am. Chem. Soc.*, 2011, **133**, 2346–2349

(5) C. C. Ho, A. Keller, J. A. Odell and R. H. Ottewill, *Colloid Polym. Sci.*, 1993, **271**, 469–

479

(6) Z. Li and X. Peng, *J. Am. Chem. Soc.*, 2011, **133**, 6578–6586

(7) D. V. Talapin, J. H. Nelson, E. V. Shevchenko, S. Aloni, B. Sadtler and A. P. Alivisatos, *Nano Lett.*, 2007, **7**, 2951–2959

(8) B. W. Longbottom, L. A. Rochford, R. Beanland and S. A. F. Bon, *Langmuir*, 2015, **31**, 9017–9025

(9) A. R. Morgan, A. B. Dawson, H. S. McKenzie, T. S. Skelhon, R. Beanland, H. P. W. Franks and S. A. F. Bon, *Mater. Horizons*, 2014, **1**, 65–68

(10) M. Okubo, K. Kanaida and T. Matsumoto, *Colloid Polym. Sci.*, 1987, **265**, 876–881

(11) S. C. Glotzer, *Science (80-.).*, 2004, **306**, 419–420

(12) A. Van Blaaderen, *Nature*, 2006, **439**, 545–546

(13) Z. Zhang, A. S. Keys, T. Chen and S. C. Glotzer, *Langmuir*, 2005, **21**, 11547–11551

(14) S. Sacanna, W. T. M. Irvine, P. M. Chaikin and D. J. Pine, *Nature*, 2010, **464**, 575–578

(15) Y. Wang, Y. Wang, X. Zheng, G. R. Yi, S. Sacanna, D. J. Pine and M. Weck, *J. Am. Chem. Soc.*, 2014, **136**, 6866–6869

(16) Z. Nie, D. Fava, E. Kumacheva, S. Zou, G. C. Walker and M. Rubinstein, *Nat. Mater.*, 2007, **6**, 609–614

(17) Q. Chen, J. K. Whitmer, S. Jiang, S. C. Bae, E. Luijten and S. Granick, *Science (80-.).*, 2011, **331**, 199–202

(18) Q. Chen, S. C. Bae and S. Granick, *Nature*, 2011, **469**, 381–384

(19) A. H. Gröschel, A. Walther, T. I. Löbling, F. H. Schacher, H. Schmalz and A. H. E. Müller, *Nature*, 2013, **503**, 247–251

(20) H. R. Sheu, M. S. El-Aasser and J. W. Vanderhoff, *J. Polym. Sci. Part A Polym. Chem.*, 1990, **28**, 629–651

(21) T. S. Skelhon, Y. Chen and S. A. F. Bon, *Soft Matter*, 2014, **10**, 7730–7735

(22) D. J. Kraft, W. S. Vlug, C. M. Van Kats, A. Van Blaaderen, A. Imhof and W. K. Kegel, *J. Am. Chem. Soc.*, 2009, **131**, 1182–1186

(23) A. H. Gröschel, A. Walther, T. I. Löbling, J. Schmelz, A. Hanisch, H. Schmalz and A. H. E. Müller, *J. Am. Chem. Soc.*, 2012, **134**, 13850–13860

(24) J. Zhang, B. A. Grzybowski and S. Granick, *Langmuir*, 2017, **33**, 6964–6977

(25) A. B. Pawar and I. Kretzschmar, *Macromol. Rapid Commun.*, 2010, **31**, 150–168

(26) J. Du and R. K. O'Reilly, *Chem. Soc. Rev.*, 2011, **40**, 2402–2416

(27) M. Pan, L. Yang, B. Guan, M. Lu, G. Zhong and L. Zhu, *Soft Matter*, 2011, **7**, 11187–11193

(28) Y. Xia, Y. Yin, Y. Lu and J. McLellan, *Adv. Funct. Mater.*, 2003, **13**, 907–918

(29) V. N. Manoharan, M. T. Elsesser and D. J. Pine, *Science (80-.).*, 2003, **301**, 483–487

(30) Y. S. Cho, G. R. Yi, J. M. Lim, S. H. Kim, V. N. Manoharan, D. J. Pine and S. M. Yang, *J. Am. Chem. Soc.*, 2005, **127**, 15968–15975

(31) S. Harley, D. W. Thompson and B. Vincent, *Colloids and Surfaces*, 1992, **62**, 163–176

(32) Z. Nie, W. Li, M. Seo, S. Xu and E. Kumacheva, *J. Am. Chem. Soc.*, 2006, **128**, 9408–9412

(33) D. C. Pregibon, M. Toner and P. S. Doyle, *Science (80-.).*, 2007, **315**, 1393–1396

(34) T. Kaufmann, M. T. Gokmen, C. Wendeln, M. Schneiders, S. Rinnen, H. F. Arlinghaus, S. A. F. Bon, F. E. Du Prez and B. J. Ravoo, *Adv. Mater.*, 2011, **23**, 79–83

(35) J. P. Rolland, B. W. Maynor, L. E. Euliss, A. E. Exner, G. M. Denison and J. M. DeSimone, *J. Am. Chem. Soc.*, 2005, **127**, 10096–10100

(36) C. Bae, J. Moon, H. Shin, J. Kim and M. M. Sung, *J. Am. Chem. Soc.*, 2007, **129**, 14232–14239

(37) S. Jiang, M. J. Schultz, Q. Chen, J. S. Moore and S. Granick, *Langmuir*, 2008, **24**, 10073–10077

(38) T. M. Ruhland, H. S. McKenzie, T. S. Skelhon, S. A. F. Bon, A. Walther and A. H. E. Müller, *Polymer (Guildf).*, 2015, **79**, 299–308

(39) S. Jiang, A. Van Dyk, A. Maurice, J. Bohling, D. Fasano and S. Brownell, *Chem. Soc. Rev.*, 2017, **46**, 3792–3807

(40) J. Krstina, C. L. Moad, G. Moad, E. Rizzardo, C. T. Berge and M. Fryd, *Macromol. Symp.*, 1996, **111**, 13–23

(41) J. Krstina, G. Moad, E. Rizzardo, C. L. Winzor, C. T. Berge and M. Fryd, *Macromolecules*, 1995, **28**, 5381–5385

(42) A. Lotierzo, R. M. Schofield and S. A. F. Bon, *ACS Macro Lett.*, 2017, **6**, 1438–1443

(43) N. G. Engelis, A. Anastasaki, G. Nurumbetov, N. P. Truong, V. Nikolaou, A. Shegiwal, M. R. Whittaker, T. P. Davis and D. M. Haddleton, *Nat. Chem.*, 2017, **9**, 171–178

(44) J. P. A. Heuts and N. M. B. Smeets, *Polym. Chem.*, 2011, **2**, 2407–2407

(45) A. A. Gridnev and S. D. Ittel, *Chem. Rev.*, 2001, **101**, 3611–3659

(46) D. M. Haddleton, E. Depaquis, E. J. Kelly, D. Kukulj, S. R. Morsley, S. A. F. Bon, M. D. Eason and A. G. Steward, *Polym. Sci. Part A Polym. Chem.*, 2001, **39**, 2378–2384

(47) D. R. Morsley, PhD Thesis, University of Warwick, 1999

(48) S. A. F. Bon, D. R. Morsley, J. Waterson, D. M. Haddleton, M. R. Lees and T. Horne, *Macromol. Symp.*, 2001, **165**, 29–42

(49) D. M. Haddleton, D. R. Morsley, J. P. O'Donnell and S. N. Richards, *J. Polym. Sci. Part A Polym. Chem.*, 1999, **37**, 3549–3557

(50) N. M. B. Smeets, U. S. Meda, J. P. A. Heuts, J. T. F. Keurentjes, A. M. van Herk and J. Meuldijk, *Macromol. Symp.*, 2007, **259**, 406–415

(51) A. Guinier and G. Fournet, *Small angle scattering of X-rays*, Wiley, New York, 1955

(52) I. . M. Kolthoff and I. . K. Miller, *J. Am. Chem. Soc.*, 1951, **73**, 3055–3059

(53) R. M. Fitch, *Polymer Colloids: A Comprehensive introduction*, Academic Press, London, 1997

(54) L. A. Fielding, J. Tonnar and S. P. Armes, *Langmuir*, 2011, **27**, 11129–11144

(55) P. J. Colver, C. A. L. Colard and S. A. F. Bon, *J. Am. Chem. Soc.*, 2008, **130**, 16850–16851

(56) R. F. A. Teixeira, H. S. McKenzie, A. A. Boyd and S. A. F. Bon, *Macromolecules*, 2011, **44**, 7415–7422

(57) L. Delafresnaye, P.-Y. Dugas, P.-E. Dufils, I. Chaduc, J. Vinas, M. Lansalot and E. Bourgeat-Lami, *Polym. Chem.*, 2017, **8**, 6217–6232

(58) S. C. Thickett and P. B. Zetterlund, *ACS Macro Lett.*, 2013, **2**, 630–634

(59) E. Limousin, N. Ballard and J. M. Asua, *Polym. Chem.*, 2019, **10**, 1823–1831

(60) B. T. T. Pham, C. H. Such and B. S. Hawkett, *Polym. Chem.*, 2015, **6**, 426–435

(61) A. Walther, M. Hoffmann and A. H. E. Müller, *Angew. Chemie - Int. Ed.*, 2008, **47**, 711–714

(62) A. Lotierzo and S. A. F. Bon, *Polym. Chem.*, 2017, **8**, 5100–5111

(63) N. Sheibat-Othman and E. Bourgeat-Lami, *Langmuir*, 2009, **25**, 10121–10133

(64) S. Fortuna, C. A. L. Colard, A. Troisi and S. A. F. Bon, *Langmuir*, 2009, **25**, 12399–12403

(65) H. P. Gregor and M. Frederick, *J. Polym. Sci.*, 1957, **23**, 451–465

(66) A. Katchalsky and P. Spitnik, *J. Polym. Sci.*, 1947, **2**, 432–446

(67) S. Kawaguchi, A. Yekta and M. A. Winnik, *J. Colloid Interface Sci.*, 1995, **176**, 362–369

(68) J. Yuan, W. Zhao, M. Pan and L. Zhu, *Macromol. Rapid Commun.*, 2016, **37**, 1282–1287

(69) C. Picard, P. Garrigue, M. C. Tatry, V. Lapeyre, S. Ravaine, V. Schmitt and V. Ravaine, *Langmuir*, 2017, **33**, 7968–7981

(70) R. Aveyard, B. P. Binks, J. H. Clint, P. D. I. Fletcher, T. S. Horozov, B. Neumann, V. N. Paunov, J. Annesley, S. W. Botchway, D. Nees, A. W. Parker, A. D. Ward and A. N. Burgess, *Phys. Rev. Lett.*, 2002, **88**, 246102–246105

(71) C. C. Lin and W. Y. Chiu, *J. Appl. Polym. Sci.*, 1979, **23**, 2049–2063

(72) R. G. Gilbert, *Emulsion polymerization, a mechanistic approach.*, Academic Press Inc., San Diego, 1995

(73) G. Moad and D. H. Solomon, *The chemistry of free radical polymerization*, Elsevier Science Inc., Oxford, UK, 2nd editio., 1995

(74) J. Hu, R. Qiao, M. R. Whittaker, J. F. Quinn and T. P. Davis, *Aust. J. Chem.*, 2017, **70**, 1161–1170

(75) L. Zhang and Y. Chen, *Polymer (Guildf).*, 2006, **47**, 5259–5266

(76) J. Ferreira, J. Syrett, M. Whittaker, D. Haddleton, T. P. Davis and C. Boyer, *Polym. Chem.*, 2011, **2**, 1671–1677

(77) D. Scalarone, M. Lazzari, V. Castelvetro and O. Chiantore, *Chem. Mater.*, 2007, **19**, 6107–6113

(78) T. Krasia and H. Schlaad, in *Metal-Containing and Metallosupramolecular Polymers and Materials*, 2006, pp. 157–167

(79) A. Bakac, M. E. Brynildson and J. H. Espenson, *Inorg. Chem.*, 1986, **25**, 4108–4114

(80) A. Bakac and J. H. Espenson, *J. Am. Chem. Soc.*, 1984, **106**, 5197–5202

(81) Girardot, R., Viguier, G., Ounsy, M. & Pérez, J. (2018), Foxtrot, https://www.synchrotron-soleil.fr/en/beamlines/swing

(82) F. Zhang, J. Ilavsky, G. G. Long, J. P. G. Quintana, A. J. Allen and P. R. Jemian, *Metall. Mater. Trans. A Phys. Metall. Mater. Sci.*, 2010, **41**, 1151–1158

(83) Alina G. et al. (2018), SasView, https://www.sasview.org/

(84) J. B. Hayter and J. Penfold, *Mol. Phys.*, 1981, **42**, 109–118

(85) J. P. Hansen and J. B. Hayter, *Mol. Phys.*, 1982, **46**, 651–656

5

Effect of salt addition to nanogel stabilized emulsion polymerizations

In this chapter the effect of background electrolyte addition (NaCl) to the nanogel stabilized emulsion polymerizations described in Chapter 4 was thoroughly investigated. As reported in previous literature studies on surfactant and surfactant-free emulsion polymerizations, the increase in ionic strength of the dispersing medium in these polymerizations led to the formation of latexes of increased particle diameter. Along with an increase in size, these polymer colloids were characterized by an increase in number of nanogels adsorbed on the polymer surface, as a function of the salt concentration in water. In particular, at the highest tested ionic strength, *ca.* 25 mM, polymeric particles surrounded by a dense layer of adsorbed stabilizing nanogels were formed. Kinetic studies carried out at varying NaCl concentrations confirmed that particle formation in the reaction followed a combination of a coagulative nucleation mechanism, characterized by a clustering process of Janus precursors to form bigger aggregates, and droplet nucleation. Preliminary film formation studies indicated the potential of this technique for the production of coherent polymer films which included a substructure of functional nanogels.

5.1 Introduction

As described in Chapter 1, one of the most common ways of synthetizing waterborne polymer colloids is *via* emulsion polymerization. In a standard emulsion polymerization process, a water-insoluble monomer, a surface-active agent and an initiator are added to water. Upon radical formation, for instance by thermal decomposition of the initiator, a dispersion of polymer particles is obtained. The name emulsion polymerization erroneously suggests the polymerization of droplets in oil-in-water emulsions, but actually commonly consists of the polymerization of micelles swollen in monomer.[1] Surfactant-free systems were also developed in the 1970s in a way to avoid tedious purification processes or detrimental side-effects resulted from the presence of surface-active agents in specific applications.[2] Even in this case, nucleation of monomer droplets in water is an unlikely event and particle formation takes place in the continuous phase *via* homogeneous nucleation (see Section 1.2.2).[1]

Other common ingredients of emulsion polymerization reactions are salts. They can act as pH regulators, redox couples to catalyze the initiator decomposition, buffers or anti-freezing agents, or can be added to obtain latexes of the desired size and dispersity. The latter can be particularly useful to obtain suspensions with specific viscosity properties.[3] The addition of electrolytes has a significant impact on emulsion polymerization reactions from a mechanistic standpoint. Their role in standard and surfactant-free emulsion polymerization was of some interest a few decades ago.[2–9] Differences were observed depending on the electrolyte type and concentration, as well as the presence of surfactants. Overall, previous research seemed to agree that the progressively increase in ionic strength in the continuous phase results in bigger polymer particles. This was attributed mostly to the formation of fewer particles in the particle formation step (Stage I of emulsion polymerization)[10] due to an increase in coagulative nucleation events;[2,4,6] fusion of primary particles in order to decrease their surface energy. It is clear that the increase in the obtained latex size is until a certain ionic strength, after which complete coagulation of the system is observed.[5] Mathematical treatment of the rate of coagulation of newly formed oligomers in Stage I clearly showed that the size of the first stable colloid formed is highly dependent on the ionic strength, as this affects directly the surface charge density and the electrostatic surface potential.[4] Interestingly, an estimate of the time

required for this controlled coagulation to happen was found to be in the timescale of few minutes (< 20 min) in the case of a 24h long reaction.[4,11] Additionally, an increase in electrolyte concentration seemed to shorten the duration of Stage I (particle formation) and decrease the polymerization rate during Stage II (particle growth).[3,5] In case of reactions carried out in the presence of soap, electrolyte addition was reported to influence the micelle size, the critical micelle concentration, micelle and, hence, latex particle charge density, concentration of monomer within the micelles and solubility of the monomer in the water phase.[5] It was also found that other than the increase in ionic strength, counterion specific interactions can be present.[3,4] For instance, the decrease in the initial rate of polymerization was more marked when $CaCl_2$ instead of KCl was added to sodium dodecylbenzenesulfonate-stabilized emulsion polymerizations.[3] This was attributed to the formation of a complex/salt with the surfactant, which would consequently decrease the concentration of emulsifier available in the system, although it is more likely to be related to the Schulze-Hardy rule; the valency of the ion of opposite charge to the colloid has a major impact on its colloidal stability.[12]

Whilst old literature mostly focused on the regulation of particle size and dispersity, more recent work indicated that, especially in the presence of seed particles, electrolytes could be used to produce nanocomposite materials. For instance Thickett and Zetterlund showed that the variation of ionic strength in emulsion polymerizations of styrene conducted in the presence of graphene oxide (GO) nano-sheets could lead to the formation of inorganic-organic hybrid particles.[13] As explained in Chapter 2, this behavior was attributed to the instability of GO at higher ionic strengths with the consequent enhanced likelihood of heterocoagulation with growing oligomers in the water phase. The inspiration for this work also came from other research, not strictly related to salt addition to emulsion polymerization reactions. These studies suggested that "complex" colloids could be synthetized by colloidal instability of smaller *stabilizers*, or seeds, coupled with good interaction with a *stabilized* phase. For instance, Vincent et al. showed the reversible adsorption of small positively charged latex particle onto much larger negatively charged poly(styrene) spheres.[14,15] Interestingly, both sets of latexes had a layer of poly(vinyl alcohol) adsorbed on their surface in a way that at different background electrolyte concentration the spacing in between the smaller colloids on top of the bigger

particles could be varied. In previous work from Bon et al. Laponite clay disks were rendered unstable by suspension of the clay in NaCl aq. solutions and, as a result, they behaved as Pickering stabilizers for oil-in-water miniemulsions.[16,17] Analogously, in Chapter 2 it was shown that destabilization of SiO_2 by pH lowering in methyl methacrylate Pickering emulsion polymerization led to the formation of polymer latexes surrounded by a shell of silica particles. Many other examples are present in the literature reporting the formation of oil-in-water emulsions by destabilizing inorganic particles or microgels.[18–22]

In all the examples above, the sol destabilization is resulted from a compression of the diffusive double layer with consequent reduction of electrical repulsion between seed particles. In Chapter 4 this concept was pushed forward when discussing the use of core-crosslinked poly(methyl methacrylate-*co*-methacrylic acid)-*block*-poly(*n*-butyl methacrylate) copolymer micelles, or *nanogels*, as stabilizing agents in styrene emulsion polymerizations. Fine tuning of the system *instability* was achieved by variation of the pH at which the polymerizations were conducted and provided control on the variation of the number of nanogels on the latex surface (see Figure 4.9). In this way latex particles carrying from a single to multiple carboxylic acid functional protrusions could be synthetized. The same should theoretically be possible by background electrolyte addition prior to polymerization, while still operating at the same pH. In this regard, Chapter 5 contains a compelling study on the progressive addition of NaCl to the surfactant-free emulsion polymerization of styrene in the presence of poly(methyl methacrylate-*co*-methacrylic acid)-*block*-poly(*n*-butyl methacrylate) core crosslinked micelles, synthetized as described in Chapter 4.

5.2 Results and discussion

5.2.1 Influence of salt addition on nanogel stability

Before discussing the role that a background electrolyte plays in an emulsion polymerization conducted in the presence of seed particles, it is convenient to describe the effect of salts to colloidal stability. Taking a step back, charged colloidal particles are known to rely on the repulsion of the electrostatic fields surrounding them to stay stable. A schematic representation of the electrical potential distribution

is shown in Figure 5.1, whereas its numerical distribution around spherical particles is given by Equation 5.1:[12]

$$\psi = \psi_0 \frac{R_s}{r} \exp[-\kappa(r - R_s)] \tag{5.1}$$

where ψ_0 is the surface potential, R_s is the radius of the sphere, r is the distance of any point in the double layer from the centre of the particle. The parameter κ in Equation 5.1 is a cluster of constants also known as the Debye-Hückel parameter:

$$\kappa = \left(\frac{1000 e^2 N_A}{\varepsilon k_B T} 2I \right)^{1/2} = \left(\frac{1000 e^2 N_A}{\varepsilon k_B T} \sum_i z_i^2 M_i \right)^{1/2} \tag{5.2}$$

where e is the elementary charge (C), N_A is the Avogadro number, k_B is the Boltzmann constant (m^2 kg s^{-2} K^{-1}), T is the absolute temperature (K), I is the ionic strength (M), z_i is the charge of the i ion, M_i is its molar concentration (M) and ε is the specific permittivity of the solvent (C^2 N^{-1} m^{-2}). κ is in m^{-1}. The reciprocal of κ, κ^{-1}, has units of length. In a way, the physical meaning of κ^{-1} is that of the thickness of the diffuse double layer.

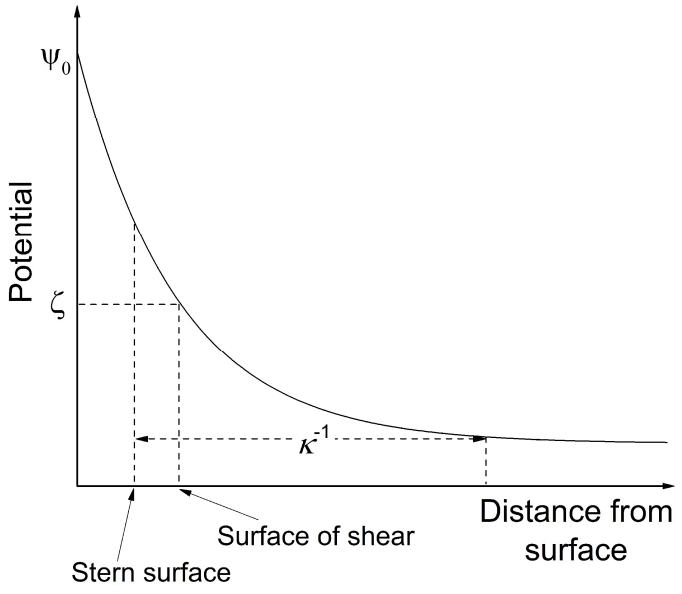

Figure 5.1 Schematic representation of the potential surrounding a charged surface. Some double-layer potentials of interest are here shown.

A measure of colloidal stability in electrostatically stabilized particles is the so-called ζ-potential, which is the potential at the surface of shear (Figure 5.1). The surface of shear is defined for a charged particle migrating in an electrical field as the boundary in between a layer of immobilized fluid surrounding the particle, which moves at the same speed as the particle, and the mobile fluid.[12] As depicted in Figure 5.1, the surface of shear occurs well within the diffuse double layer and in dilute electrolyte conditions can be assumed to coincide with the particle surface. ζ for diluted solutions of electrolytes, for which the diffuse double layer is well extended, is calculated from Equation 5.3:

(5.3) $$\zeta = \frac{q}{4\pi\varepsilon R_s} - \frac{q}{4\pi\varepsilon\left(R_s + k^{-1}\right)}$$

where q is the surface charge.

It is clear from Equations 5.2 and 5.3 that the addition of background electrolytes to a colloidal dispersion will result in a compression of the double layer, with a consecutive lowering of ζ (in absolute units).

Going back to the nanogel particles, the ζ -potential was measured at varying concentrations of NaCl in water (Figure 5.2A), which corresponded to different κ^{-1} values (Table 5.1).

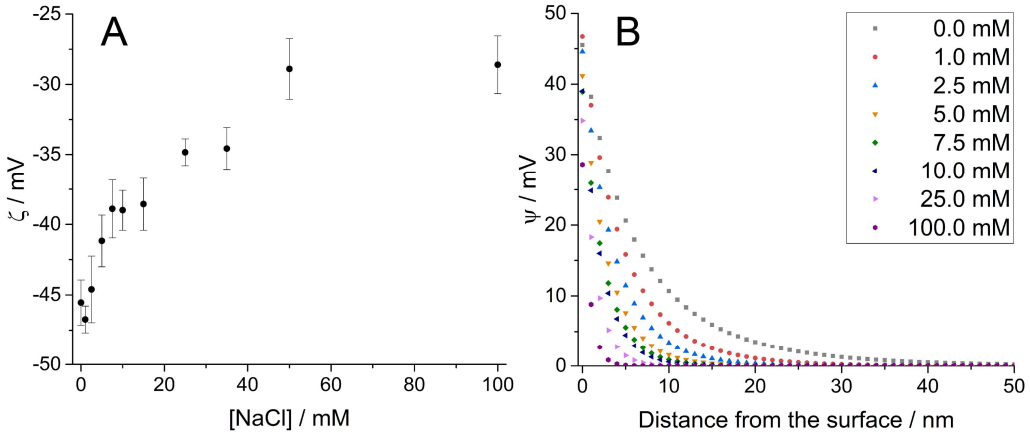

Figure 5.2 a) ζ-potential of N1 nanogels measured at different [NaCl] at 25°C in water. b) Electrical potential distribution around a spherical particle (R_s = 9 nm) at 25°C in water and in the presence of varying concentrations of NaCl. For the calculation of ψ the k^{-1} values reported in Table 5.1 were adopted and ζ was assumed equal to ψ_0. Note that ψ is here conveniently reported positive.

The addition of NaCl to nanogel dispersions resulted in a considerable suppression of ζ, which reached a plateau value of -29 mV at around [NaCl] = 50 mM (Figure 5.2A). A representation of the suppression of the overall potential distribution surrounding the particle at different salt concentrations was calculated using Equation 5.1 and is displayed in Figure 5.2B. This shows that in absence of added electrolyte, $\psi \rightarrow 0$ at *ca.* 50 nm. Despite the double layer compression, the nanogels were surprisingly stable over the whole range of [NaCl] tested, as also confirmed by dynamic light scattering (DLS) (Figure A5.1). This is interesting as the formation of patchy particles as showed in Chapter 4 was favored in a pH range where particle clustering started to occur (see Figure 4.11), which is considerably different from what observed for ionic strength increase.

Table 5.1 κ^{-1} at 25°C and 75°C calculated using Equation 5.2. κ^{-1} values are corrected for the ionic strength of the system at the two different conditions.

[NaCl]/ mM	κ^{-1} (25°C)[a] / nm	κ^{-1} (75°C)[b]/ nm
0.0	7.30	8.68
1.0	5.81	6.36
2.5	4.67	4.89
5.0	3.70	3.77
7.5	3.16	3.18
10.0	2.80	2.80
15.0	2.35	2.33
25.0	1.86	1.83
35.0	1.58	1.56
50.0	1.33	1.31
100.0	0.95	0.93

[a] (ζ measurement conditions) 25°C, 1.0 wt% nanogel aq. suspension, pH 8.8. *I* before NaCl addition ~ 1.73 mM.
[b] (Reaction conditions) 75°C, 0.3 wt% nanogel aq. suspension, pH 8.8, [KPS] = 0.25 mM. *I* before NaCl addition ~ 1.16 mM.

5.2.2 Emulsion polymerizations at different [NaCl]

The poly(methyl methacrylate-*co*-methacrylic acid)-*block*-poly(*n*-butyl methacrylate) polymeric nanogels were added to standard batch emulsion polymerizations of styrene as sole stabilizers of the system, using an analogous process as described in Chapter 4. The amount of nanogels was kept constant across

all the experiments at 2.85 wt% wrt to monomer, defined as weight ratio of nanogel/monomer x 100. This concentration was found to be the one leading to highly stable latexes in experiments conducted at basic pH and where no additional salts were added to the system (see Figure 4.8). Moreover, the pH was kept at a value of about 8.8 in all the reactions in order to have complete dissociation of the acid groups in the nanogel corona.[23,24] In the given experimental conditions, the system base ionic strength, before NaCl addition, was *ca.* 1.16 mM. In the latter case, it has been shown that Janus particles are formed, characterized by a single nanogel protrusion on the polystyrene surface (see Figure 5.4A). This was explained to be the result of the high stability provided by the fully ionized methacrylic acid (MAA) moieties on the nanogel surface (degree of ionization of PMAA, α, *ca*. 1).[23,24] The effect of NaCl addition on the emulsion polymerizations was tested by a series of reactions in NaCl aq. solutions of concentrations ranging from 0.0 to 25.0 mM (Table 5.2).

Table 5.2. Size, dispersity and coagulum formed in the nanogel-stabilized emulsion polymerizations of styrene conducted in the presence of a background electrolyte (NaCl).

[NaCl] / mM	DLS		CHDF[a]		Coagulum %[b]
	d_H / nm	PdI / -	D / nm	σ / nm	
0.0	91	0.016	89	10	-
1.0	93	0.021	89	12	-
2.5	107	0.050	97	25	-
5.0	158	0.086	138	49	-
7.5	262	0.080	269	96	1.7
10.0	505	0.184	462	146	2.0
15.0	642	0.186	599	146	22.0
25.0	963	0.243	-	-	42.6

Note: Polymerizations carried out overnight at 75°C, pH 8.8 and adopting N1 nanogels as stabilizers (N1/styrene= 2.85 wt%). KPS/styrene = 0.07 wt%, solid content = 9.0 wt%.

[a] Capillary hydrodynamic fractionation (CHDF) analysis; *D* is the weight average diameter and *σ* its standard deviation.

[b] Calculated as the solid content of the freeze-dried latex over the one obtained at [NaCl] = 0.0 mM.

All the synthetized latexes were stable over the course of few months after their synthesis. Even in the case of settling over a long storage time, the particles could easily be redispersed upon hand shaking of the latexes. In the reactions

performed at the two highest [NaCl] a substantial amount of coagulum was formed during the reaction, which was removed by filtration before performing further analysis. It is likely that when the double layer is highly suppressed (κ^{-1} < 2.0 nm in these two experiments), additional steric stabilization is required to avoid particle clustering. A similar behavior was observed when performing the reaction at pH 4.5, as described in Chapter 4, which was also at the edge of colloidal stability of the system. Whilst the formation of coagulum was not particularly problematic in laboratory scale experiments (~ 200 g), this must be tackled when thinking of industrial applications of the technique.

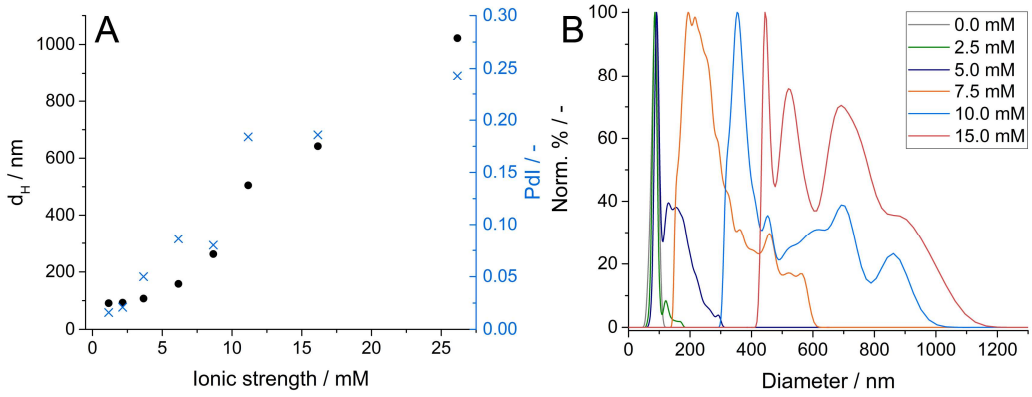

Figure 5.3 a) Variation of the particle hydrodynamic diameter (d_H) and dispersity (PdI) with the system total ionic strength (added NaCl + base ionic strength) of the nanogel-stabilized styrene emulsion polymerizations. b) Capillary hydrodynamic fractionation (CHDF) fractograms displaying the normalized weight size distribution of the latexes produced at different [NaCl].

DLS analysis of the latexes showed that the salt addition had a dramatic effect on the hydrodynamic diameter (d_H) and dispersity (PdI) of the obtained particles (Figure 5.3A and Table 5.2). This confirmed what previously observed in the literature; overall the addition of a background electrolyte to emulsion polymerizations produces bigger latex particles.[2–9] However, the extent of the addition on the latex hydrodynamic radius was more pronounced then what previously observed.[2,3,5] In fact, d_H varied from about 90 nm in absence of added electrolytes to almost 1000 nm when the reaction was carried out in 25.0 mM [NaCl]. The addition of salt seemed to have no effect on the final particle size for small additions of NaCl, *i.e.* 1.0 mM, after which a gradual increase of d_H with [NaCl] was observed up to about [NaCl] = 7.5 mM. At larger salt concentrations, a marked raise

in size was observed, which then increased in the range 10.0 – 25.0 mM [NaCl], along with the dispersity of the latexes (Figure 5.3A and Table 5.2).

Given the dispersity of the samples obtained, capillary hydrodynamic fractionation (CHDF) was used to obtain a more statistical representation of the particle size distribution. CHDF is a particle separation technique based on the following principle. When colloidal particles of different sizes are dispersed in a medium and travel across an open capillary on narrow dimension, typically 4-10 μm in diameter, they are separated and emerge in order of decreasing diameter.[25–27] The fractionation is the result of different travel velocities in the capillary caused by the formation of a parabolic flow.[28] After separation, the particles are analyzed by a turbidity detector. CHDF overcomes the limitations of dynamic light scattering measurements of hiding or underestimating the presence of lower-sized colloids in polydisperse mixtures.[10] CHDF fractograms of the nanogel stabilized latexes are shown in Figure 5.3B whereas the latexes weight average diameters (D) and standard deviations (σ) are reported in Table 5.2.

In Chapter 4 it was discussed that when the emulsion polymerizations were conducted at progressively lower pH, hence decreasing the degree of ionization of MAA in the nanogels, the patch density on the poly(styrene) latex surface could be tailored.[29] Scanning electron microscopy (SEM) analysis on the latexes obtained showed that the same could be achieved by background electrolyte addition (Figure 5.4). Alongside with the formation of Janus particles, as pure phase formed at 0.0 mM NaCl (Figure 5.4A), at 2.5 mM NaCl larger particles (*ca.* 130-190 nm) with more nanogels on their surface started to appear (Figure 5.4B). These patchy particles progressively increased in number and size moving from 2.5 to 7.5 mM NaCl. In the latter case, all the observed particles appeared to have multiple patches on their surface (Figure 5.4B). This came with a noticeable raise in dispersity. It was also apparent the presence of two distinct populations; one of bigger sizes, higher patch density and broader distribution and the other characterized by smaller particles and fewer patches on their surface. The addition of 10.0 mM of background electrolyte produced particles of much bigger sizes and with noticeable denser nanogel coverage on their surface (Figure 5.4C). In the series of samples from 10.0 to 25.0 mM, the nanogels became more densely packed on the polystyrene surface. In particular, at

25.0 mM [NaCl] just one particle population of considerable dispersity was formed, characterized by a very dense layer of nanogels on their surface.

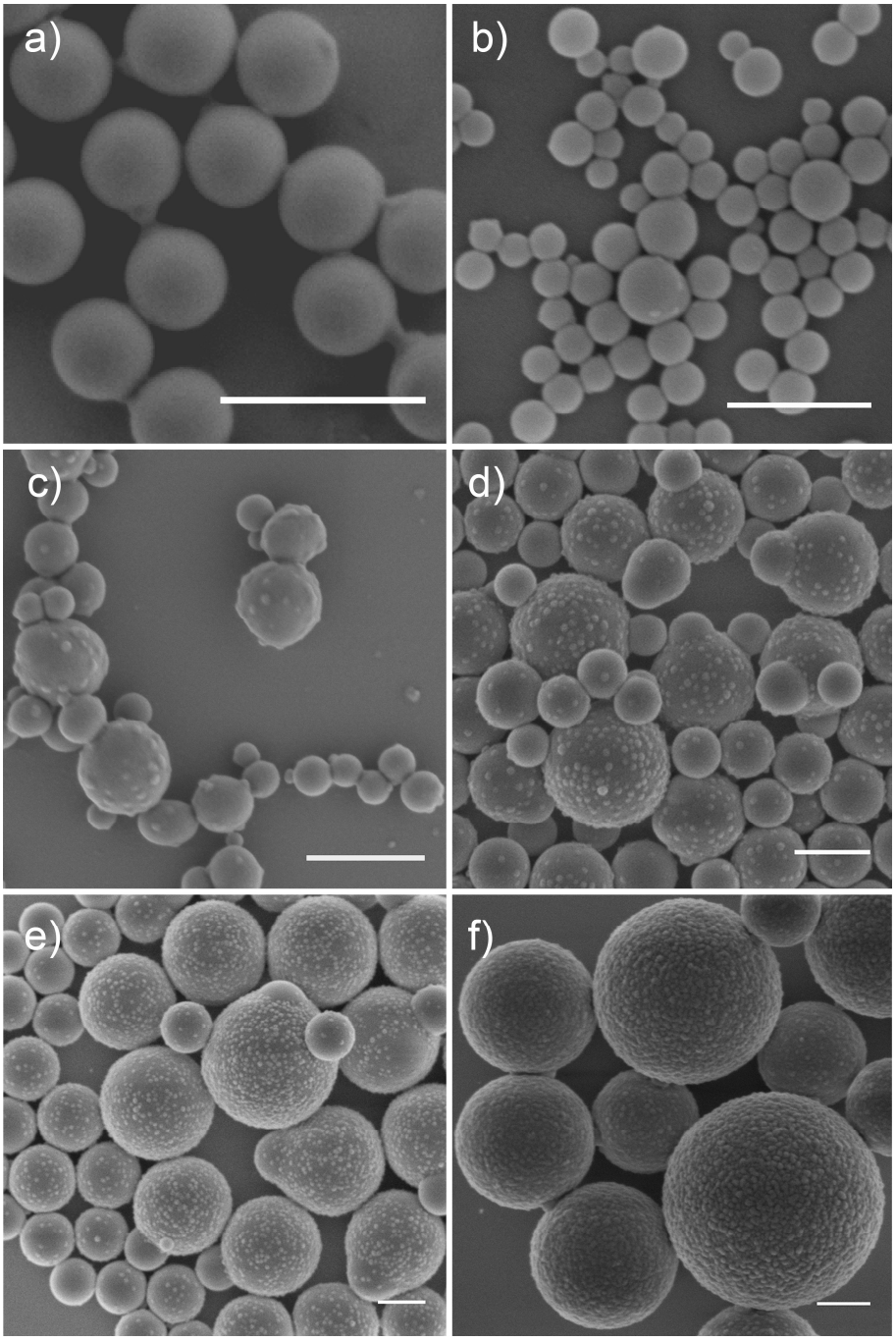

Figure 5.4 Emulsion polymerizations of styrene performed at pH 8.8 and in the presence of carboxylic acid functionalized nanogels as stabilizers. The reactions were conducted in the presence of a) 0.0 mM, b) 2.5 mM, c) 5.0 mM, d) 7.5 mM, e) 10.0 mM, f) 25.0 mM aq. NaCl as background electrolyte. Scale bars: 300 nm.

SEM analysis confirmed not only the trend observed by DLS and CHDF analysis, but also that patch density on the poly(styrene) surface can be varied by both pH adjustment and electrolyte addition. The similar effect of pH and ionic strength was to be expected as they both result in a compression of the electrical double layer surrounding the nanogels. However, if the lowering of pH seemed to have more control over the formation of less polydisperse, smaller (d < 200 nm) latexes with on average maximum 18 nanogels on their surface, destabilization *via* background electrolyte addition appeared to favor the formation of bigger (up to 1.5 μm), more polydisperse and densely covered latexes.

After these initial observations a series of questions still remained unanswered regarding the patchy and armoured particles formation mechanism and the origin of the apparent bimodality of the particle size distribution for 5.0 mM ≤ [NaCl] ≤ 15.0 mM. Additionally, in this range of salt concentrations a portion of the more densely covered latexes were not perfectly spherical. The frequency of the presence of such latexes decreased by moving from 2.5 mM to 25.0 mM. In particular in the latter all the latexes were spherical. In order to come to a better understanding of the process, some kinetic experiments were carried out on the reactions at 0.0, 7.5, 10.0 and 25.0 mM [NaCl]. Monomer conversion (X) *vs.* reaction time and d_H *vs.* X for these reactions are displayed in Figure 5.5. In order to discuss the data presented, the equation to calculate the rate of polymerization (R_p) in an emulsion polymerization reaction is represented:

$$R_p = \frac{dX}{dt}\frac{mol_M}{V_{H_2O}} = \frac{N_p}{V_{H_2O}}\frac{k_p C_{p,M}\bar{n}}{N_A} \tag{5.4}$$

where mol_M is the initial moles of monomer, V_{H_2O} is the total volume of water, k_p is the propagation rate coefficient of the monomer, $C_{p,M}$ is the concentration of the monomer within the latex particles, $\bar{n}$ is the average number of radicals per particle and N_A is the Avogadro number.

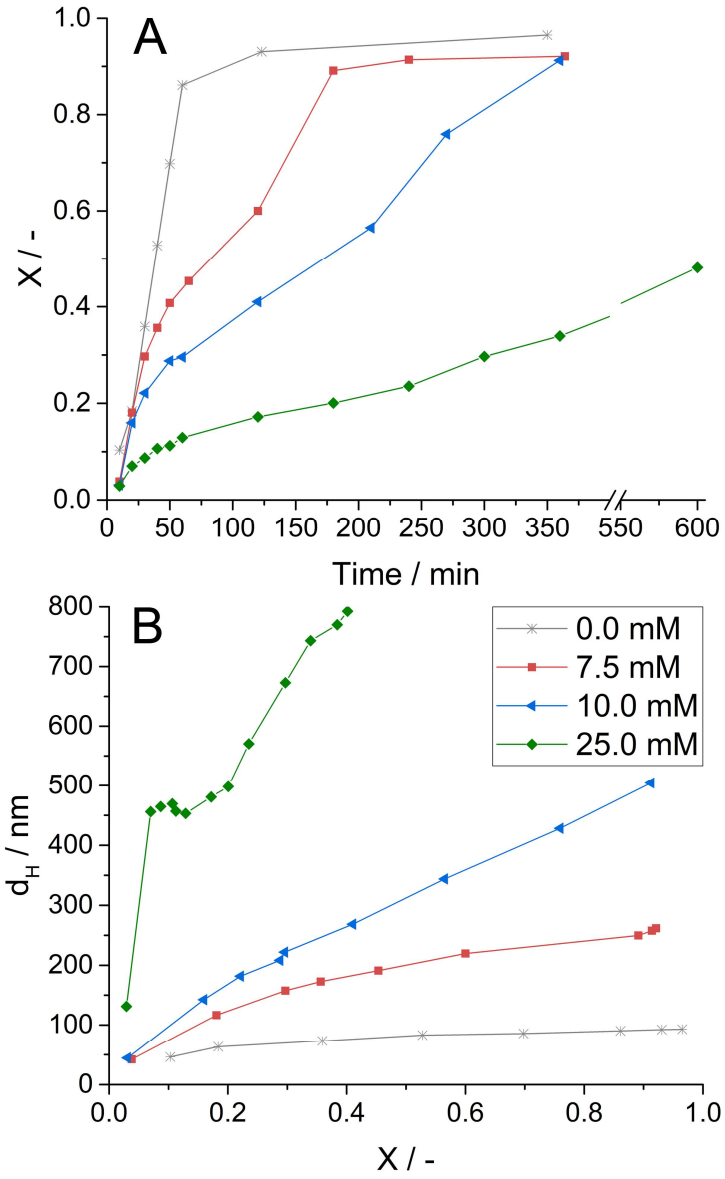

Figure 5.5 a) Evolution of monomer conversion (X) with time and b) hydrodynamic diameter (d_H) with X for the emulsion polymerizations conducted at 0.0, 7.5, 10.0 and 25.0 mM [NaCl].

The reactions with [NaCl] = 0.0 – 10.0 mM started at similar rate of polymerization, that is proportional to dX/dt. The reason for this is that N_p is initially the same in all the reactions and equal to the number of nanogels introduced. In Chapter 4 it was hypothesized that in the early stages of the reaction styrene polymerizes within the nanogels and phase-separates on the side forming a small Janus-like structure (see Figure 4.10). When no background electrolyte was added,

the nanogel high, unscreened charge can keep these growing Janus particles colloidally stable. In this case, R_p stayed relatively constant throughout the reaction, which reached *ca.* 90% conversion within the first hour. Instead, in the case of [NaCl] = 7.5 and 10.0 mM, at about 15/20% conversion, R_p decreased noticeably. The suppression of the rate of reaction upon salt addition in emulsion polymerization was described in the literature to be linked to an increase in coagulative nucleation events, which form a lower number of particles.[2,4,6] The same mechanism would explain how bigger particles bearing multiple nanogels on their surface are formed (Figure 5.4). Here it is similarly expected that upon growth of a soft polystyrene lobe off a nanogel particle, the partial screened charge (κ^{-1} *ca.* 9 and 3 nm respectively for [NaCl] = 0.0 mM and [NaCl] = 7.5-10.0 mM) it is not capable of granting colloidal stability and the nanogels cluster to decrease their surface energy. Samples taken during the reaction carried out at [NaCl] = 7.5 mM and analyzed *via* SEM confirmed that indeed this is the case (Figure 5.6). 24 min after the beginning of the reaction the system consisted of a mixture of unreacted nanogels, Janus nanogel-poly(styrene) precursors and a series of particles characterized by varying nanogel coverage and size. This also showed that the sample is of broad distribution from the very beginning of the reaction, which is not unexpected as clustering of Janus particles typically yields a broad mixture of products.[30–32] In this process, in the first stages of the reaction the latex particles can be formed by clusters of Janus precursors or nanogel clusters. This progressively decreases the concentration of available nanogels and results in a decreased nanogel coverage for particles formed in later stages of the reaction.

As the reaction conducted at [NaCl] = 7.5 mM progressed, at 120 min a portion of the more densely covered particles appeared deformed (Figure 5.6C). Interestingly, the extent of the deformation increased in the last stages of the reaction (Figures 5.6D and 5.4D). It is still not entirely clear what is the cause of such deformation and why the effect phased out at higher [NaCl]. The first possible explanation is that newly formed growing particles which loose colloidal stability can coalesce with bigger, more densely covered latexes. Alternatively, the effect could be explained as phase separation from a partially crosslinked latex. The nanogels could act as crosslinking points between the polymer chains making the shell of the latex partially crosslinked. As more poly(styrene) is formed, this would phase separate on the side of the latex as its radial growth is partially constrained.[30] In the case of the

reactions carried out at higher [NaCl], the higher nanogel coverage on the surface would create a more densely crosslinked shell, which would hinder the phase separation.

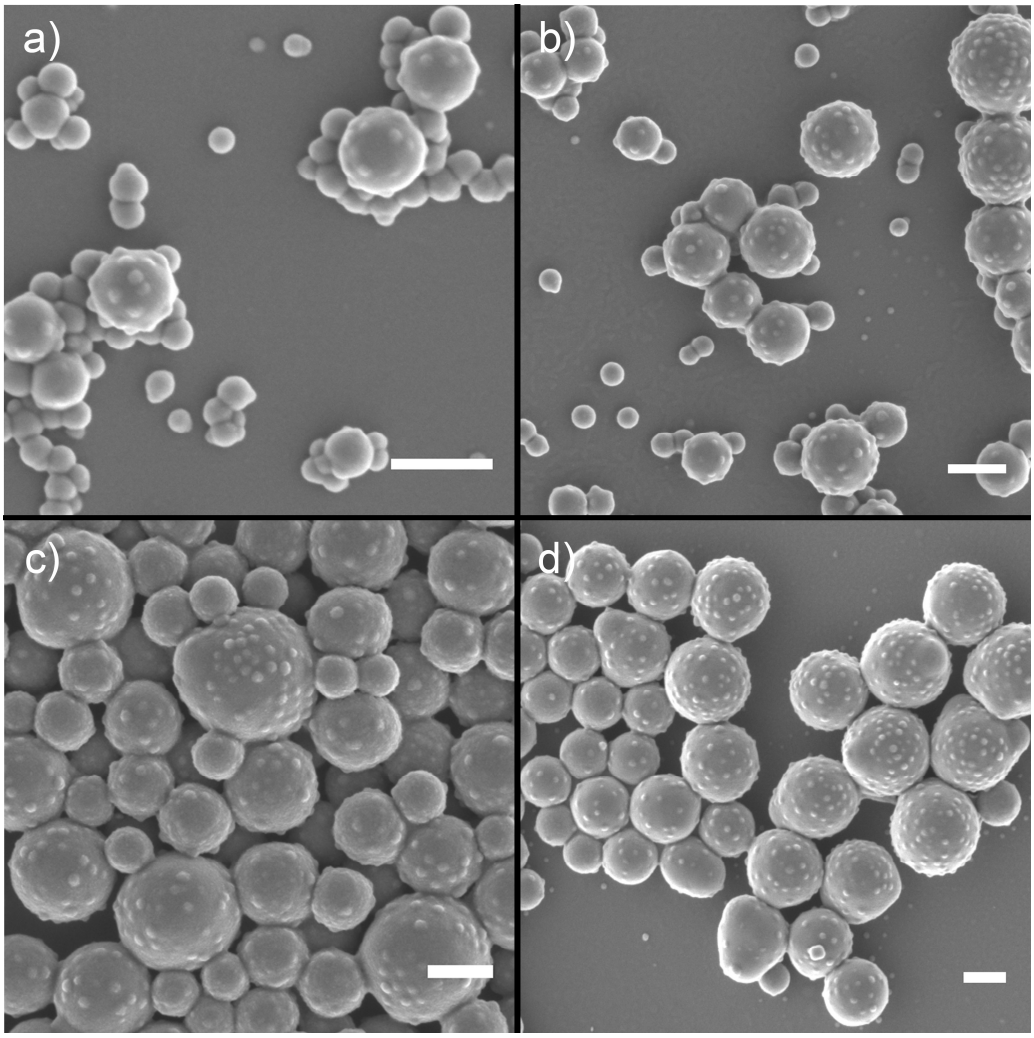

Figure 5.6 SEM analysis of the samples taken at a) 24 min (X = 0.14), b) 40 min (X = 0.33), c) 120 min (X = 0.67) and d) 150 min (X = 0.89) during an emulsion polymerization of styrene conducted in the presence of nanogels and [NaCl] = 7.5 mM. Scale bars: 200 nm.

The reaction carried out at 25.0 mM NaCl continued the trend observed in the previous experiments whilst including some additional interesting features. As shown in Figure 5.5B, clusters of about 450 nm in diameter were formed rapidly in the first stages of the reaction, at $X < 0.1$. Note that the data points reported in Figure 5.5B are average values. A more careful look at the DLS volume distribution of

samples taken at this stage of the reaction clearly displays the rapid formation of such objects (Figure 5.7). Interestingly, the clusters were not detected at time 0, after the system was heated up, in presence of monomer, but before initiator addition. Here it is argued that these clusters are monomer droplets highly covered in nanogels which heterocoagulated on their surface. Evidence for this statement will be presented in the next few pages. This provides further insight into the particle formation step and infers that the adopted nanogel can act as stabilizers only once they become (lightly) amphiphilic. Hence, Janus-like structures are formed first and then they can act as stabilizers. Additionally, once the clusters are formed, they do not appear to grow for about 50 min, after which a more steady growth with conversion is observed (Figure 5.5B).

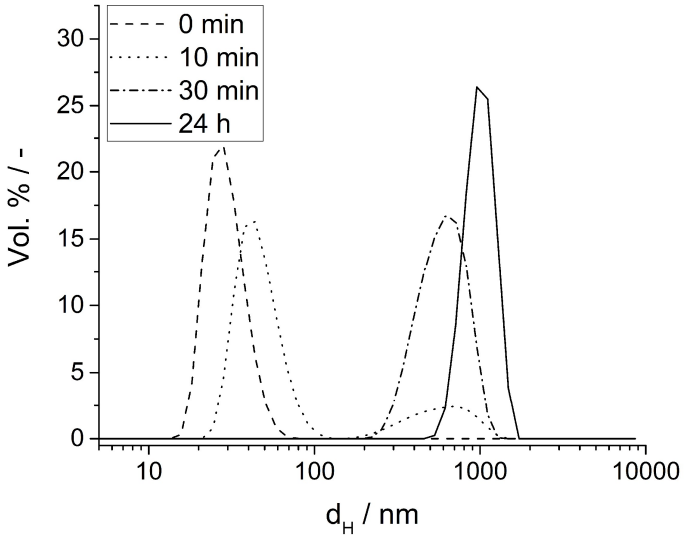

Figure 5.7 Particle size distribution at different stages of the emulsion polymerization of styrene carried out in presence of 25.0 mM [NaCl]. The time 0 sample was recorded before initiator injection.

For [NaCl] = 25.0 mM, as previously discussed, the formation of a significant lower number of particles came with a drastic lowering of R_p; X was *ca.* 50% after 10h. Using equation 5.4, R_p was found to be 1.7×10^{-2} mol s^{-1} dm^{-3} for [NaCl] = 0.0 mM and 2.7×10^{-3}, 1.9×10^{-3} and 4.8×10^{-4} mol s^{-1} dm^{-3} respectively for [NaCl] = 7.5, 10.0 and 25.0 mM after clustering. This drop in R_p is only partially explained in terms of reduction of N_p, as it is counteracted by a much greater average number of radical per particles ($\bar{n}$) that typically occurs in large latex particles.[33] In fact, while small latex particles

tend to obey the so-called zero-one kinetic, where $\bar{n}$ = 0.5, large particles follow a pseudo-bulk mechanism where $\bar{n}$ can reach much greater values.[33]

5.2.3 Preliminary film formation studies

The reaction conducted at [NaCl] = 25.0 mM led to the formation of what essentially appeared to be core-shell particles where a polystyrene core was surrounded by a dense shell of nanogels (Figure 5.4E). Two reactions were carried out using a mixture of styrene (Sty) and *n*-butyl acrylate (BA) in a way of synthetizing film forming latexes, which upon drying would form a film with a honeycomb substructure of stabilizing particles. As explained in Chapter 2, these films have been of particular interest in the scientific community for their potential of combining the properties of the two different phases used (usually polymeric and inorganic/cellulosic materials).[34–37] Two reactions were performed by using the same reaction conditions as the experiment conducted at the highest salt content, but where a Sty/BA monomer mixture was adopted; Sty/BA = 1.45:1 and 0.43:1 w:w. The estimated glass transition temperatures (T_g) according to the Fox equation[38] was 16 and -24°C respectively. SEM analysis of the latexes formed in the presence of increasing amounts of BA revealed an apparent lower nanogel coverage on the latex surface with respect to the reactions carried out with pure styrene (Figure 5.8). At Sty/BA = 0.43:1 w:w the latexes appeared almost not covered in nanogels and a large amount of smaller latex particles were present. These could potentially be the nanogels which did not adhere to the latex particles and were instead left unreacted in the system. A more plausible explanation is that secondary nucleation occurred, which is not unlikely in butyl acrylate emulsion polymerization.[39,40] The reason for the not visible nanogels on the latex surface could rather be related to the softer nature of BA-rich particles, where the nanogels are more embedded within the surface. Nevertheless, the reaction at the highest BA content presented a large amount of coagulum (*ca.* 80.0 %) and for this reason was not characterized further.

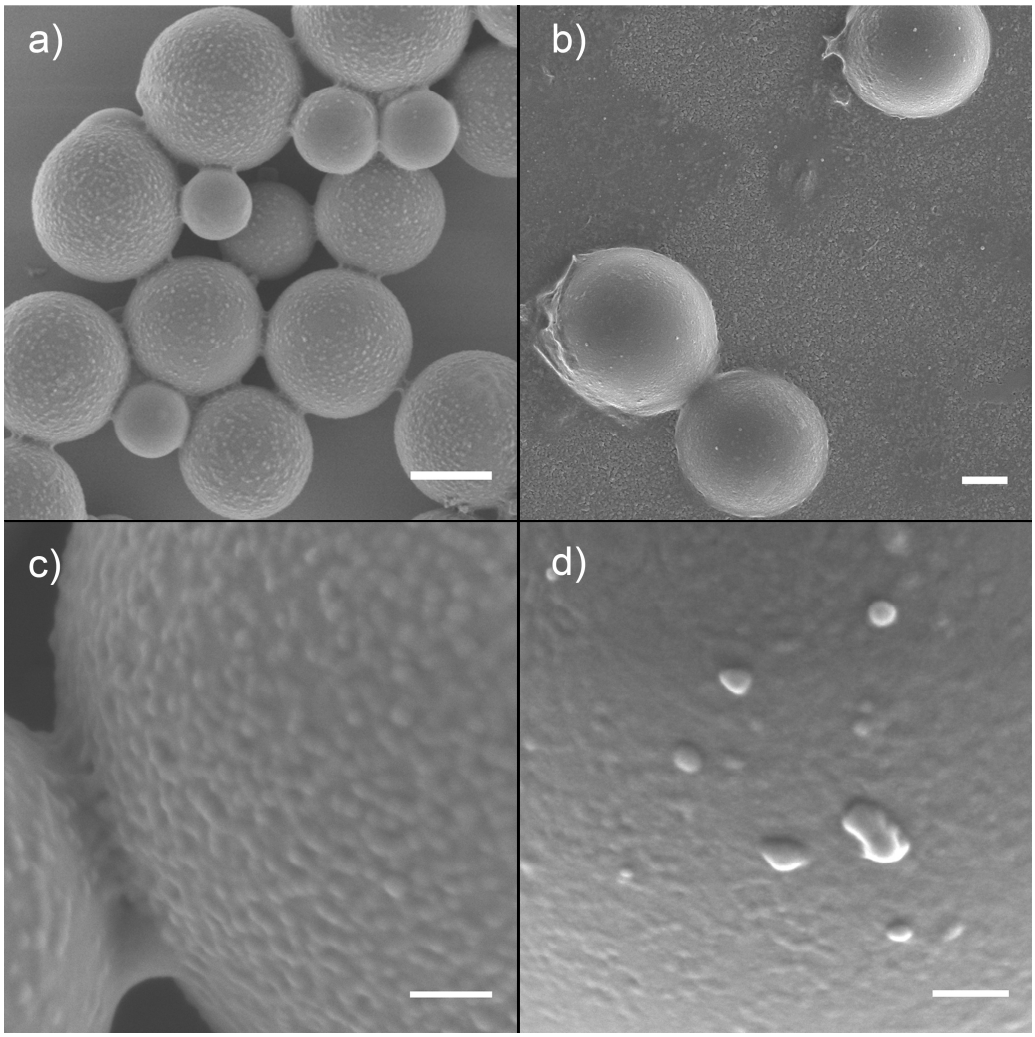

Figure 5.8 SEM images of the latexes synthetized at [NaCl] = 25.0 mM and styrene/butyl acrylate weight ratios of (a,c) 1.45:1 and (b,d) 0.43:1 w/w. Scale bars: (a,b) 500 nm and (c,d) 100 nm.

Some preliminary film formation studies were carried out on the latex with Sty/BA 1:45:1 w:w. Films with a good degree of transparency were obtained when casting latex suspensions on glass slides and drying them at 50-70°C (Figure 5.9). When the same was attempted at lower temperature (40°C) the films presented substantially higher opacity suggesting incomplete coalescence of the latex particles, and the presence of air voids in the film (Figure A5.2).[41] This was somewhat surprising as the expected T_g for this polymer was around 16°C (Table 5.3). Instead, when the T_g was measured *via* dynamic mechanical analysis (DMA) and differential scanning calorimetry (DSC) much higher values were obtained. The reason for the

increase in the observed T_g could be due to the presence of the nanogels. In Chapter 4 it was described that one of the features of these stabilizers is that they contain residual macromonomer and crosslinker double bonds (see Figure A4.2). These may act as crosslinking points in the polymer shell, as previously suggested in the discussion, and hence result in a higher T_g.[42]

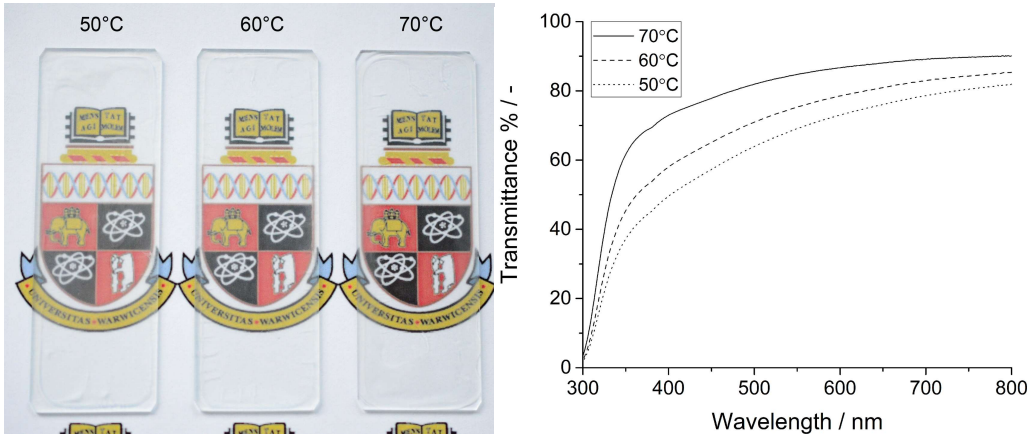

Figure 5.9 (Left) Polymer films obtained from casting a latex suspension on glass slides and drying at 50-70°C. (Right) UV-Vis spectra of the films.

Table 5.3 Glass transition temperature (T_g) of the latexes synthetized at [NaCl] = 25.0 mM and at Sty/BA = 1.45:1 w:w.

T_g (Fox) /[a] °C	T_g (DMA) /[b] °C	T_g (DSC) / °C
16	41	35

[a] Based on the homopolymers T_g; poly(styrene)[38] = 100°C and poly(*n*-butyl acrylate)[43] = -55°C.
[b] Measured on a polymer film 1.1 mm thick.

5.2.4 Additional studies

Further evidence that droplet nucleation could be an important mechanistic pathway for particle formation in the reactions at the highest [NaCl] came from a series of experiments conducted in suspension/miniemulsion polymerization conditions. As explained in Chapter 1, in these types of heterogeneous polymerizations particle nucleation occurs mostly, or completely, through droplet nucleation.[10,44] A (mini)emulsion is usually made by pre-homogenization of a monomer/water mixture which can be formed by a high shear homogenization step.

This forms monomer droplets which are then polymerized.[45,46] A series of miniemulsion/suspension styrene polymerizations were carried out by varying the nanogel concentration, [NaCl], solid content and type of initiator adopted. The description of all these reactions goes beyond the scope of this chapter. However, two examples are shown in Figure 5.10 for the polymerizations conducted at [NaCl] = 25.0 and 50.0 mM, at the same nanogel-to-styrene ratio as the experiments performed in this chapter and in the presence of an oil soluble initiator (AIBN). Very similar latexes in terms of particle size distribution and nanogel coverage were obtained with respect to when emulsion polymerization conditions were adopted. This reinforced the hypothesis of a possible strong influence of droplet nucleation on particle formation. Surprisingly, in all the miniemulsion/suspension polymerizations tested some smaller latexes with lower patch density were also formed. This is particularly surprising as these particles were expected to form by monomer diffusion from the water phase to a growing Janus primary particle. However, when operating in miniemulsion/suspension polymerization conditions a hydrophobe was present in all the reactions in a way to suppress the monomer concentration in the water phase.[47]

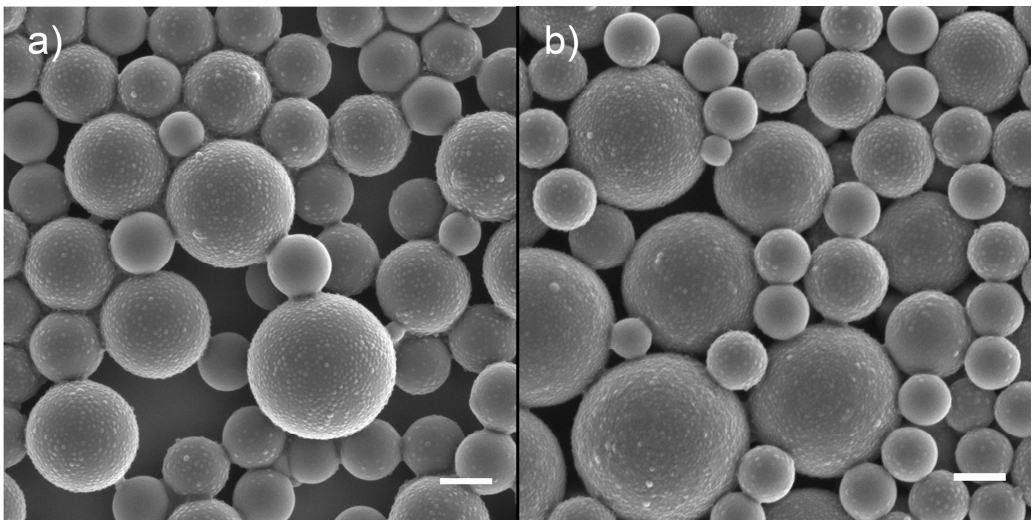

Figure 5.10 Miniemulsion/suspension polymerizations of styrene (5 wt% of stearyl methacrylate as hydrophobe) carried out at [NaCl] = a) 25.0 and b) 50.0 mM. Scale bars: 300 nm.

Another indication of droplet nucleation came from experiments conducted at [NaCl] = 25.0 mM performed in different vessels, and using varying agitation devices (*i.e.* stirrer bars or oval stirrers, and/or stirring rate). A particularly

interesting series of experiments is presented in Table 5.4, where the same reaction was repeated at different scales and/or in different vessels. Note that in these experiments a similar stirrer rate was adopted, although the resulting agitation in the vessel changed depending on the scale used. In particular, smaller scale experiments resulted in a much higher agitation, and hence smaller droplets formed, than the larger scale ones. From Table 5.4 it can be seen that in the former case much smaller latexes were obtained, reinforcing the hypothesis of the significant effect of droplets, and their size, on particle formation. Note that the influence of stirring on emulsion polymerizations stabilized by surfactants has previously been investigated.[48–50] It was mainly found that at higher stirring rates: a) the number of micelles was lowered as more droplet surface area covered in surfactant was available and b) more coalescence was observed. In emulsifier-free systems it was observed that higher agitation speeds led to higher particle coagulation and overall to latexes of larger diameters.[51] In these previous examples particle formation was mainly carried out in the water phase (within micelles or *via* homogenous nucleation). The reason for the opposite trend observed in this work could be explained by nucleation of droplets of decreasing sizes at higher agitation speeds.

Table 5.4 Emulsion polymerization of styrene conducted in the presence of nanogels and at [NaCl] = 25.0 mM; effect on the scale of the reaction.

Vessel	Mass / g	d_H / nm
10 ml Vial[a]	5.3	400
20 ml Vial[a]	11.2	440
50 ml RBF[b]	24.6	560
50 ml RBF[b]	48.2	847
250 ml RBF[b]	175.5	963

[a] A stirrer bar was used.
[b] Round bottom flask. An oval magnetic stirrer was used.

Finally, in Chapter 4 it was described that one feature of the nanogels adopted in this work is their ease of dispersibility after freeze drying (see Figure 4.5). Interestingly, when the latexes synthetized in this chapter (pure styrene series, Table 5.2) were freeze dried and redispersed in lightly basic water, they showed a similar behaviour (Figure A5.3). The ease of dispersibility was proportional to the degree of coverage of the latexes, with almost all the powder being redispersed in water at the

two highest tested [NaCl]. The cycle was not repeated multiple time in this case, so it did not confirm an inherent free-thaw stability. However, it suggested that a) indeed these nanogel covered latexes may have nanogel-like surface properties and b) the design of latexes bearing charged Pickering-type stabilizers may result in freeze-thaw stable materials.

5.3 Conclusion and outlook

This chapter detailed studies on the effect that a background electrolyte, in particular NaCl, plays on a nanogel stabilized emulsion polymerization process, as described in Chapter 4. It was observed that overall it is possible to fabricate a range of latexes characterized by varied size distribution and patch density by simply tailoring the salt concentration in the dispersing medium. This resembles what observed for pH adjustment in Chapter 4 and generally confirmed, as also seen in Chapter 2, that the controlled destabilization of the Pickering-type stabilizer resulted in a higher tendency of assembling into supracolloidal aggregates. This behavior was explained as a way for the system to reduce their surface energy, similarly to what is for instance observed with coagulative nucleation of primary radical in emulsion polymerization.[1]

Generally, the results contained in this chapter confirmed what previously observed in the literature; the addition of background electrolytes to an emulsion polymerization reaction produces larger particles. The entity of this effect was however more pronounced in the experiments detailed in this chapter. The reason for the observed behavior is possibly the result of a change in the particle formation mechanism between the reaction carried out at the lower and higher salt concentration range. At low salt content, patchy particles are likely formed by coagulative nucleation of Janus-like precursors into bigger clusters, whereas at higher [NaCl] droplet nucleation is believed to play a significant role, hence deviating from the trend observed in the literature. Some evidence for the occurrence of droplet nucleation was provided, although further investigations need to be carried out in order to assess the real mechanism of this process.

From a synthetic viewpoint, the reaction yields latexes of large dispersity especially at the highest salt concentration adopted. This is not necessarily perceived

as a negative feature of the reaction, however the large amount of coagulum produced (*ca.* 40 % based on total theoretical solid mass) needs to be tackled. It is still under investigation if the coagulation was dependent on the agitation intensity, and hence could be reduced by optimizing the stirring profile. The monomer composition also seemed to play an important role on this point. Already in the case of the latex tested for film formation studies (Sty/BA = 1.45:1 w:w), the amount of coagulum formed was considerably lower (*ca.* 21 %) at the same salt content, [NaCl] = 25.0 mM. In particular the protocols here developed for the synthesis of these softer latexes showed potential for the fabrication of structured latexes which are surrounded by a (compact) layer of colloidal stabilizers. Such materials can find application into polymeric films where an intricate substructure of stabilizing agent is present. This not only solves the problem of surfactant migration in polymer films, but it also has the advantage of combining the properties of the two different phases involved. Preliminary studies indicated that indeed it was possible to cast films formed by the latexes synthetized in this work. Future work in this regard will focus on the characterization of their mechanical and thermal properties, as well as the development of materials which can film form at lower temperatures.

5.4 Experimental

5.4.1 Materials

Styrene (≥ 99%) and *n*-butyl acrylate (≥ 99%) were purchased from Sigma Aldrich and filtered through activated basic aluminum oxide prior to use to remove the inhibitors. 2,2'-azobis(2-methylpropionitrile) (AIBN) was purchased from Sigma Aldrich and recrystallized from methanol before use. Potassium persulfate (KPS) (≥ 99.0%), sodium chloride (≥ 99.5%), sodium benzoate (≥ 99.0%), stearyl methacrylate (mixture of stearyl and cetyl methacrylates) were purchased from Sigma Aldrich and used as received.

5.4.2 Equipment & methods

Average hydrodynamic diameters and distributions were measured by dynamic light scattering (DLS) on a Malvern Zetasizer Nano ZS operating at 25°C

and at a detection angle of 173°. ζ-potential measurements on latexes were carried out at 1.0 wt% polymer in aq. [NaCl] at pH 8.8 using disposable folded cuvettes (Malvern). Scanning electron microscopy (SEM) images were collected on a ZEISS Gemini SEM. Samples were diluted in deionized water and casted on a silicon wafer fragment, which had been adhered to an aluminum stab using conductive copper tape. The samples prepared in this way were carbon or chromium coated before imaging. Film formation studies were carried out by casting 2.0 ± 0.1 ml of latex suspension on a glass slide. The film was left to dry in an oven at varied temperatures overnight. Dynamic mechanical analysis was performed on a PerkinElmer DMA 8000. DMA analysis was carried out on a 9.8×7.5×1.1 mm polymer film which was formed by casting multiple layers of the Sty/BA = 1.45:1 w:w latex suspension on a poly(propylene) pan, allowing each layer to dry overnight at 70°C. The final thickness was 1.1 mm. The sample for DMA analysis was heated at 5°C/min from -50°C to 150°C under N_2 at 1.00 Hz frequency and with a static force of 2.00 N. Differential scanning calorimetry (DSC) analysis was carried out on the same specimen on a Mettler-Toledo DSC1. The sample was heated and cooled twice at 10°C/min from 0°C to 120°C under N_2. UV-Vis spectra were recorded on an Agilent technologies Cary 60 UV-Vis. Spectra were recorded on the polymer films casted on glass slides positioned at a 90° angle with respect to the incident beam.

5.4.3 Nanogels stabilized emulsion polymerizations

In a typical emulsion polymerization experiment an aqueous dispersion of nanogels (3.50 g, 13.0 wt% aq. suspension) was diluted with aq. NaCl (154.5 g). The pH of the suspension was adjusted to 8.8 using aq. HCl 1.0 M. The reaction mixture was charged in a sealed 250 ml round bottom flask equipped with an oval stirrer bar and it was purged with nitrogen for 30 min. Next, styrene (15.95 g, *ca.* 17.5 ml), which had been previously purged with nitrogen for 30 min, was injected into the reactor using a degassed syringe. The system was heated up to 75°C. The reaction was started upon injection of an aqueous KPS solution (1.5 ml, 6.9 mg/ml) and was allowed to fully react overnight. When the kinetic of the reaction was monitored, samples (typically 1 g) were withdrawn throughout the polymerization to check monomer conversion *via* gravimetry. Kinetic experiments were monitored for 6-10 hours but the reactions were left to react overnight (total reaction time = 20-24h).

5.4.4 Nanogels stabilized miniemulsion/suspension polymerizations

In a typical miniemulsion/suspension polymerization experiment an aqueous dispersion of nanogels (1.75 g, 13.0 wt% aq. suspension) was diluted with aq. NaCl (31.50 g). The pH of the suspension was adjusted to 8.8 using aq. HCl 1.0 M. The reaction mixture was charged in a 60 ml jar equipped with a stirrer bar. Next, a monomer/initiator mixture containing styrene (7.60 g), stearyl methacrylate (0.40 g) and AIBN (10.0 mg) was added to the jar. The reaction mixture was first pre-emulsified using a homogenizer (Ultra-Turrax) and then sonicated using an ultrasound tip under vigorous stirring at 70% amplitude for 10 minutes (10 sec on, 10 sec off). The jar was immersed in an ice bath during the sonication to prevent the temperature from rising. The resulting emulsion was poured in a 100 ml round bottom flask equipped with stirrer bar, it was sealed and then purged with N_2 for 30 min. The polymerization was carried out at 75°C overnight (20 - 22h).

5.4.5 Capillary hydrodynamic fractionation (CHDF)

Particle size distributions were measured by capillary hydrodynamic fractionation (CHDF) using a CHDF 2000 (Matec Applied Sciences) instrument equipped with a Waters 486 UV detector (λ = 200 nm). A proprietary surfactant mixture (GR500) in DI water was used as eluent. The eluent was composed of a polyoxyethylene-based non-ionic surfactant (1.0 g/L), sodium dodecyl sulfate (29 mg/L) and sodium azide (0.5 mg/L). The eluent was filtered through a 0.2 μm filter before use. The flow rate was set at 1.3 ml/min and the column operated at 30°C and 4000 psi. Latex samples (*ca.* 9 wt% in water) were diluted 1:8.3 times in the eluent mixture prior to injection. The injection of the latex in the instrument was followed by the one of sodium benzoate, used as a flowrate marker (0.2 wt% in eluent).

References

(1) R. M. Fitch, *Polymer Colloids: A Comprehensive introduction*, Academic Press, London, 1997.

(2) J. W. Goodwin, J. Hearn, C. C. Ho and R. H. Ottewill, *Br. Polym. J.*, 1973, **5**, 347–362.

(3) D. C. Blackley and A. R. D. Sebastian, *Br. Polym. J.*, 1989, **21**, 313–326.

(4) J. W. Goodwin, R. H. Ottewill, R. Pelton, G. Vianello and D. E. Yates, *Br. Polym. J.*,

1978, **10**, 173–180.

(5) A. S. Dunn and Z. F. M. Said, *Polymer (Guildf).*, 1982, **23**, 1172–1176.

(6) M. E. Dobrowolska and G. J. M. Koper, *Soft Matter*, 2014, **10**, 1151–1154.

(7) J. L. Mateo and I. Cohen, *J. Polym. Sci. Part A*, 1964, **2**, 711–730.

(8) W. M. Thomas, E. H. Gleason and G. Mino, *J. Polym. Sci.*, 1957, **24**, 43–56.

(9) T. Guha and S. R. Palit, *J. Polym. Sci. Part A Gen. Pap.*, 1963, **1**, 877–893.

(10) P. A. Lovell and M. S. El-Aasser, *Emulsion Polymerization and Emulsion Polymers*, J. Wiley, 1997.

(11) R. Pelton, PhD Thesis, University of Bristol, 1976.

(12) P. C. Hiemenz and R. Rajagopalan, *Principles of Colloid and Surface Chemistry*, Taylor and Francis Group, 1997.

(13) S. C. Thickett and P. B. Zetterlund, *ACS Macro Lett.*, 2013, **2**, 630–634.

(14) B. Vincent, C. A. Young and T. F. Tadros, *Faraday Discuss. Chem. Soc.*, 1978, **65**, 296.

(15) S. Harley, D. W. Thompson and B. Vincent, *Colloids and Surfaces*, 1992, **62**, 163–176.

(16) S. A. F. Bon and P. J. Colver, *Langmuir*, 2007, **23**, 8316–8322.

(17) S. Cauvin, P. J. Colver and S. A. F. Bon, *Macromolecules*, 2005, **38**, 7887–7889.

(18) L. A. Fielding and S. P. Armes, *J. Mater. Chem.*, 2012, **22**, 11235–11244.

(19) T. G. Anjali and M. G. Basavaraj, *Langmuir*, 2018, **34**, 13312–13321.

(20) W. Wang, A. H. Milani, Z. Cui, M. Zhu and B. R. Saunders, *Langmuir*, 2017, **33**, 8192–8200.

(21) M. Destribats, M. Wolfs, F. Pinaud, V. Lapeyre, E. Sellier, V. Schmitt and V. Ravaine, *Langmuir*, 2013, **29**, 12367–12374.

(22) T. Sharma and J. S. Sangwai, *Ind. Eng. Chem. Res.*, 2015, **54**, 5842–5852.

(23) S. Kawaguchi, A. Yekta and M. A. Winnik, *J. Colloid Interface Sci.*, 1995, **176**, 362–369.

(24) A. Katchalsky and P. Spitnik, *J. Polym. Sci.*, 1947, **2**, 432–446.

(25) C. M. Miller, J. Venkatesan, C. A. Silebi, E. D. Sudol and M. S. El-Aasser, *J. Colloid Interface Sci.*, 1994, **162**, 11–18.

(26) C. A. Silebi and J. G. Dosramos, *J. Colloid Interface Sci.*, 1989, **130**, 14–24.

(27) J. G. DosRamos and C. A. Silebi, *J. Colloid Interface Sci.*, 1990, **135**, 165–177.

(28) R. B. Bird, W. E. Stewart and E. N. Lightfoot, *Transport Phenomena*, John Wiley & Sons, Inc, New York, 2nd editio., 2007.

(29) A. Lotierzo, B. W. Longbottom, W. H. Lee and S. A. F. Bon, *ACS Nano*, 2019, **13**, 399–407.

(30) H. R. Sheu, M. S. El-Aasser and J. W. Vanderhoff, *J. Polym. Sci. Part A Polym. Chem.*, 1990, **28**, 629–651.

(31) T. S. Skelhon, Y. Chen and S. A. F. Bon, *Soft Matter*, 2014, **10**, 7730–7735.

(32) D. J. Kraft, W. S. Vlug, C. M. Van Kats, A. Van Blaaderen, A. Imhof and W. K. Kegel, *J. Am. Chem. Soc.*, 2009, **131**, 1182–1186.

(33) R. G. Gilbert, *Emulsion polymerization, a mechanistic approach.*, Academic Press Inc., San Diego, 1995.

(34) T. Wang, P. J. Colver, S. A. F. Bon and J. L. Keddie, *Soft Matter*, 2009, **5**, 3842–3849.

(35) J. L. Keddie, E. Bourgeat-Lami, F. Dalmas, K. L. Elidottir, S. J. Hinder, I. Martín-Fabiani, M. Lansalot, M. L. Koh and I. Jurewicz, *ACS Appl. Nano Mater.*, 2018, **1**, 3956–3968.

(36) X. Zhou, H. Shao and H. Liu, *Colloid Polym. Sci.*, 2013, **291**, 1181–1190.

(37) E. Limousin, N. Ballard and J. M. Asua, *Polym. Chem.*, 2019, **10**, 1823–1831.

(38) P. C. Hiemenz and T. P. Lodge, *Polymer Chemistry*, Taylor and Francis Group, 2nd ed., 2007.

(39) S. Sajjadi, *RSC Adv.*, 2015, **5**, 58549–58560.

(40) S. Sajjadi and B. W. Brooks, *J. Polym. Sci. Part A Polym. Chem.*, 2000, **38**, 528–545.

(41) P. A. Steward, J. Hearn and M. C. Wilkinson, *Adv. Colloid Interface Sci.*, 2000, **86**, 195–267.

(42) E. Giebel, J. Getze, T. Röcker and A. Greiner, *Macromol. Mater. Eng.*, 2013, **298**, 439–446.

(43) W. A. Lee, *J. Polym. Sci. Part A-2 Polym. Phys.*, 1970, **8**, 555–570.

(44) B. Brooks, *Chem. Eng. Technol.*, 2010, **33**, 1737–1744.

(45) K. Landfester, *Annu. Rev. Mater. Res.*, 2006, **36**, 231–279.

(46) K. Landfester, in *Topics in Current Chemistry*, 2003, vol. 227, pp. 75–123.

(47) J. M. Asua, *Prog. Polym. Sci.*, 2002, **27**, 1283–1346.

(48) P. A. Weerts, J. L. M. Van der Loos and A. L. German, *Makromol. Chem.*, 1991, **192**, 1993–2008.

(49) M. Nomura, M. Harada, W. Eguchi and S. Nagata, *J. Appl. Polym. Sci.*, 1972, **16**, 835–847.

(50) M. Banerjee and R. S. Konar, *Polymer (Guildf).*, 1986, **27**, 147–157.

(51) Z. Song and G. W. Poehlein, *J. Polym. Sci. Part A Polym. Chem.*, 1990, **28**, 2359–2392.

6

Conclusions and Outlook

The aim of the thesis was to develop strategies for the synthesis of polymer colloids of different morphologies, as well as polymeric stabilizing agents, while maintaining good control over particle shape, size and dispersity. The synthetic protocols analyzed and developed involved the use of solid particles as stabilizers in (seeded) emulsion polymerizations, with a particular focus on the role that they play during the reaction. In particular, the materials synthetized in Chapters 2, 4 and 5 consisted of a polymer particle surrounded by a number of (in)organic stabilizing colloids, whereas Chapters 3 and 4 contained details on the synthesis of the polymeric stabilizers.

Chapter 2 contained a through kinetic and mechanistic investigation on Pickering emulsion polymerization using SiO_2 nanospheres as stabilizers. Styrene and methyl methacrylate were adopted as model monomers to come to a better understanding of the overall mechanism of the process. SiO_2 was found not to adsorb spontaneously to fully swollen poly(methyl methacrylate) latex particles, implying that it is the polymerization itself to drive the stabilizers towards the interface. Polymerizations followed by reaction calorimetry confirmed the key role of SiO_2 on particle formation, with a greater number of particles nucleated at larger stabilizer concentrations. Comparison of the kinetics with literature data, where molecular

surfactants were adopted instead, revealed striking kinetic similarities in terms of number of radical per particles and linear increase of $\bar{n}$ in stage II.

Future work: a more conclusive way of determining whether kinetically the process is greatly influenced by the presence of a shell of inorganic material would be to run reactions in the same experimental conditions but by using molecular surfactants instead. In the two sets of experiments care must be taken in having an overall similar number of nucleated particles, which, at the same monomer concentration, would also be of similar size. In these conditions, analysis of the latex molecular weight distribution by SEC could provide further insight on restrained radical entry within the particles caused by the stabilizer shell. In fact, in conditions of equal radical flux (same temperature, initiator concentration, monomer concentration and number of particles) a decrease in the frequency of radical entry within the particles would lead to higher molecular weights. In this regard, a protocol has already been developed to solubilize the polymer chains in THF from a dried polymer/SiO_2 sample taken at a given time during the reaction.

Furthermore, it would be interesting be able to synthetize latexes with multi-layer morphology, where for instance a further polymeric shell is grown around the silica shell. The properties of multiple materials can be combined in this way. An example could be the synthesis of a poly(butyl acrylate) (PBA) latex surrounded by a shell of SiO_2 nanoparticles and poly(methyl methacrylate) PMMA to be used as an additive in polymer blends, such as poly(vinyl chloride) (PVC). Core-shell PBA-PMMA latexes are already adopted in the fabrication of impact shock PVC given the chemical compatibility of PMMA and PVC.[1] It would be interesting to see what role the SiO_2 shell plays in impact resistance properties.

Chapter 3 investigated the use of ω-unsaturated methacrylate macromonomers in dispersion polymerization systems, with the final goal of synthetizing sulfur-free polymer dispersions of various morphologies. Particularly, it was of interest to make crosslinked di-block copolymer micelles to be used in Pickering emulsion polymerization processes. In dispersion polymerization when using ω-end unsaturated methacrylate macromonomers as macro-CTA, one must face with the dramatically lower C_T with respect to conventional organo-sulfur RAFT

agents.[2] All the dispersion polymerizations conducted under conventional dispersion polymerization conditions (*i.e.* adopting a lyophilic macro-RAFT agent) resulted in poor control on chain growth and/or the particle morphology obtained. These issues were solved by operating in seeded dispersion polymerization conditions by adopting a thermo-responsive diblock copolymer macro-RAFT agent, already phase-separated from solution. In this case dynamic rearrangement of the particles from spheres, to worms and then to large spherical objects/vesicles was observed.

Future work: the synthetic protocol of these reactions is drastically complicated by the low C_T values of these macromonomers. A way to simplify the protocol comes from the synthesis of polymeric nanogels in Chapter 4. An initial diblock copolymer latex can be synthetized in large amounts and without the need of purification steps in catalytic chain-transfer emulsion polymerization conditions. Crucial from this point of view is that one of the two blocks can be made lyophilic by for instance cooling or pH adjustment. If the right block lengths are targeted, this would result in a dispersion of polymer micelles which can easily be chain extended in emulsion/dispersion polymerization conditions to yield sulfur free spheres, worms or vesicles. In this way the only difference with a process mediated by a conventional organo-sulfur CTA would be the step were the initial self-assembly is induced not by polymerization but by a change in lyophilicity of one of the two blocks. In addition, this should come with a drop in molecular weight dispersity as usually more narrowly defined polymers can be obtained when methacrylate macromonomers block copolymers are synthetized in emulsion polymerization conditions.[3–5]

Chapter 4 described the synthesis of polymeric crosslinked diblock copolymer micelles, or *nanogels*, by catalytic chain transfer emulsion polymerization and RAFT, as detailed in the previous paragraph. The nanogels were adopted in standard styrene emulsion polymerizations as sole stabilizers, in the same way as SiO_2 nanospheres were used in Chapter 2. Nanogel additions in either aqueous dispersion or dry powder form allowed to control the final latex particle size and its dispersity, in the same way as molecular surfactants. Most importantly, given the crosslinked nature of the nanogels, the stabilizer unimers did not spread around the growing latex during the course of the reaction. In this way, in the reactions conducted at high pH, Janus particles were obtained. Instead, when the pH of the

dispersing phase was adjusted to lower values, the decreasing surface charge in the nanogel corona led to latexes with a higher nanogel density on their surface. Hence, the synthetic protocols presented in this work led to functional Janus and patchy particles were the stabilizer functionality is overexpressed only where the patch is located.

Future work: The synthetic pathways commonly adopted for the synthesis of Janus and patchy colloids usually consist of many steps, which require intermediate purification and/or yield particles in low amounts.[6] The products are typically rather well-defined, especially when template-based,[7] microfluidics[8] or lithography[9] techniques are adopted. However, such techniques with the current technology are not applicable in the order of 50-300 nm, which is instead the target of the process presented in this chapter. The synthetic protocol here described can yield particles in large amounts, without the need of purification steps and using only industrially-friendly emulsion polymerization protocols. Such colloids can hence find application in all the fields where Janus or patchy colloids are required. One obvious example is the coating industry which actively seeks ways of improve the films properties by using particles of different morphologies, which are however difficult to synthetize.[10]

Additionally, the use of reactive (macro)molecular surfactants in emulsion polymerization has been studied for a long time[11–13] for their potential of reducing surfactant migration in polymeric films, which often deteriorates the final coating properties.[10,14] Analogously, the latexes synthetized in this work can be adopted in soap-free formulations to achieve the same purpose.

Lastly, the nanogels can be synthetized with the required functionality to yield patchy latexes with a number of patches expressing the desired chemical properties. For instance, using similar protocols methacrylate monomers carrying poly(ethylene glycol), urea, amino, epoxide, sulfate, vinyl, hydroxy, hydrolysable inorganic precursors (*i.e.* 3-(trimethoxysilyl) propyl groups), metal-complexing aceto-acetoxy groups[15] can be adopted to incorporate into the nanogel synthesis.

Finally, in **Chapter 5** the effect of background electrolyte (NaCl) addition to the nanogel stabilized emulsion polymerization reactions described in Chapter 4 was investigated as a way to destabilize the nanogel suspension. The raise in ionic

strength in the continuous phase had a dramatic effect in the latex particle size and dispersity, with an increase in patch density at higher [NaCl]. In particular, at the highest tested ionic strength, polymeric particles surrounded by a dense layer of adsorbed stabilizing nanogels were formed. Kinetic studies suggested that particle formation, depending on [NaCl], may follow a combination of coagulative nucleation and droplet nucleation. Preliminary film formation studies resulted in the formation of coherent films, which included a substructure of functional nanogels.

Future work: The latexes synthetized at [NaCl] = 25.0 mM appeared to consist of a polymeric core surrounded by a dense shell of nanogels. In order to fully characterize these materials, it would be of interest to find a way of measuring the thickness of the shell. Small angle neutron scattering analysis is a useful tool to analyse core shell latexes, though it requires careful contrast matching if the scattering signal for the core or shell only is of interest.[16] To this end the same core-shell latexes have been synthetized using d_8-styrene as a monomer in a way to be able to core contrast match the latexes produced with the solvent (D_2O) in (ultra-)small-angle neutron scattering experiments.

References

(1) M. R. Moghbeli and S. Tolue, *J. Appl. Polym. Sci.*, 2009, **113**, 2590–2597

(2) D. J. Keddie, *Chem. Soc. Rev.*, 2014, **43**, 496–505

(3) J. Krstina, C. L. Moad, G. Moad, E. Rizzardo, C. T. Berge and M. Fryd, *Macromol. Symp.*, 1996, **111**, 13–23

(4) J. Krstina, G. Moad, E. Rizzardo, C. L. Winzor, C. T. Berge and M. Fryd, *Macromolecules*, 1995, **28**, 5381–5385

(5) N. G. Engelis, A. Anastasaki, G. Nurumbetov, N. P. Truong, V. Nikolaou, A. Shegiwal, M. R. Whittaker, T. P. Davis and D. M. Haddleton, *Nat. Chem.*, 2017, **9**, 171–178

(6) J. Du and R. K. O'Reilly, *Chem. Soc. Rev.*, 2011, **40**, 2402–2416

(7) V. N. Manoharan, M. T. Elsesser and D. J. Pine, *Science (80-.).*, 2003, **301**, 483–487

(8) Z. Nie, W. Li, M. Seo, S. Xu and E. Kumacheva, *J. Am. Chem. Soc.*, 2006, **128**, 9408–9412

(9) D. C. Pregibon, M. Toner and P. S. Doyle, *Science (80-.).*, 2007, **315**, 1393–1396

(10) S. Jiang, A. Van Dyk, A. Maurice, J. Bohling, D. Fasano and S. Brownell, *Chem. Soc. Rev.*, 2017, **46**, 3792–3807

(11) H. A. S. Schoonbrood and J. M. Asua, *Macromolecules*, 1997, **30**, 6034–6041

(12) J. F. Morizur, D. J. Irvine, J. J. Rawlins and L. J. Mathias, *Macromolecules*, 2007, **40**, 8938–8946

(13) O. Soula, R. Petiaud, M. F. Llauro and A. Guyot, *Macromolecules*, 1999, **32**, 6938–6943

(14) D. Scalarone, M. Lazzari, V. Castelvetro and O. Chiantore, *Chem. Mater.*, 2007, **19**, 6107–6113

(15) T. Krasia and H. Schlaad, in *Metal-Containing and Metallosupramolecular Polymers and Materials*, 2006, pp. 157–167

(16) M. . Wai, R. . Gelman, M. . Fatica, R. . Hoerl and G. . Wignall, *Polymer (Guildf).*, 1987, **28**, 918–922

A

Appendix

A.1 Calculation of E_k and ΔG

This section contains details on the calculations performed for the crude determination of the kinetic energy (E_k) of an oil droplet in a stirred reactor, as well as its comparison with the energy required to remove a solid particle from a soft interface (ΔG). In a standard emulsion polymerization, as described in Chapter 2, monomer and water are loaded in a sealed glass reactor, equipped with an anchor stirrer of diameter D (Figure A.1).

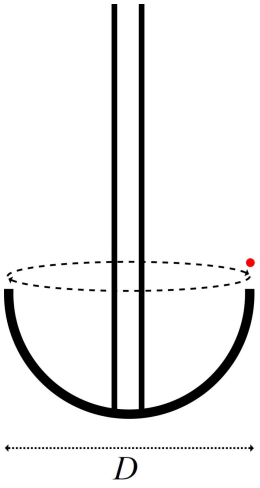

Figure A.1 Representation of an oil droplet (in red) moving at a radial distance with respect of an impeller stirrer of diameter D.

Upon rotation of the stirrer at a given velocity, Ω, a coarse suspension of emulsion droplets in water is formed. Next, it is considered a methyl methacrylate (MMA) droplet of mass *m*, positioned at a radial distance with respect to the center of the impeller. The velocity, v_k, of the droplet and its kinetic energy E_k are equal to:

(A.1) $$v_k = \pi D \Omega$$

(A.2) $$E_k = \frac{1}{2} m v_k^2$$

For D = 5 cm and Ω = 250 rpm, v_k = 0.654 m/s. This results in $E_k = 1.05\times10^{-16}$ Nm for a 100 μm droplet and $E_k = 1.05\times10^{-19}$ Nm for a 100 nm droplet. When comparing E_k with the energy required to displace a silica nanoparticle from the MMA-water interphase, ΔG, the values displayed in Table A.1 are obtained.

Table A.1 Values of ΔG at different adsorption angles θ_w of silica nanospheres on MMA droplets. Comparison of ΔG with the thermal energy and E_k.

θ_w / °	ΔG / mN*m	$\Delta G/k_bT$	$E_k/\Delta G$	
			100 μm droplet	100 nm droplet
10	1.36×10^{-21}	3.61×10^{-1}	7.75×10^{4}	7.75×10^{1}
20	2.14×10^{-20}	5.69×10^{0}	4.92×10^{3}	4.92×10^{0}
30	1.06×10^{-19}	2.81×10^{1}	9.97×10^{2}	9.97×10^{1}
40	3.22×10^{-19}	8.56×10^{1}	3.27×10^{2}	3.27×10^{1}
50	7.52×10^{-19}	2.00×10^{2}	1.40×10^{2}	1.40×10^{-1}
60	1.47×10^{-18}	3.91×10^{2}	7.16×10^{1}	7.16×10^{-2}
70	2.55×10^{-18}	6.77×10^{2}	4.13×10^{1}	4.13×10^{-2}
80	4.02×10^{-18}	1.07×10^{3}	2.62×10^{1}	2.62×10^{-2}
90	5.89×10^{-18}	1.56×10^{3}	1.79×10^{1}	1.79×10^{-2}

A.2 Derivation of Equation 2.6

The parameter *f* described in Chapter 2 is defined as the ratio between the total surface area of free silica in water and nanocomposite particles, which are polymer latexes surrounded by silica spheres. Before starting to derive *f*, an expression for the number of SiO_2 particles free in water at a given time *t*, N_{SiO_2}, will be obtained. During the discussion care will be taken in differentiating the latex nanocomposite particles and the polymer phase *only* of the nanocomposite particles.

An expression for N_{SiO_2}, was derived starting from some previous work by Bon et al.[1] In their work, N_{SiO_2} was defined as the difference of initial SiO_2 particles present, $N_{SiO_2,0}$, and the number of SiO_2 spheres adsorbed at the polymer latex surface, $N_{SiO_2,L}$:

$$N_{SiO_2} = N_{SiO_2,0} - N_{SiO_2,L} \tag{A.3}$$

with:

$$N_{SiO_2,0} = \frac{6m_{SiO_2,0}}{\pi\rho_{SiO_2} d_{SiO_2}^{\ 3}} \tag{A.4}$$

where m_{SiO_2} is the initial mass of silica, ρ_{SiO_2} is its density, d_{SiO_2} is the average silica diameter measured *via* TEM (*ca.* 24 nm).[1]

Next, it is observed that the total surface area occupied by the SiO_2 adsorbed at the polymer latex surface should be equal to the total surface area of the polymer particles (considering the polymer phase only of the nanocomposite latexes). This is true if a SiO_2 monolayer is adsorbed at the latex surface:

$$SA_{pol,i} N_{pol} = N_{SiO_2,L} A_{SiO_2,i,L} \tag{A.5}$$

where $SA_{pol,i}$ is the surface area of one polymer particle, N_{pol} is the total number of the polymer particles and $A_{SiO_2,i,L}$ is the area occupied by a SiO_2 sphere on a polymer latex particle. N_{pol} and N_p, defined in Chapter 2 as the number of latex nanocomposite particles, are equal but they are calculated from the size and density of respectively the polymer phase only of the nanocomposite particles and the whole particle.

Expressions for $SA_{pol,i}$, N_{pol} and $A_{SiO_2,i,L}$ can be calculated from:

(A.6) $$SA_{pol,i} = \pi d_{pol}^{\ 2}$$

(A.7) $$N_{pol} = \frac{6 m_{M,0} X}{\pi \rho_p d_{pol}^{\ 3}}$$

(A.8) $$A_{SiO_2,i,L} = \frac{\pi d_{SiO_2}^{\ 2}}{4P}$$

where d_{pol} is the diameter of the polymer phase only of the nanocomposite latexes, $m_{M,0}$ is the initial monomer mass, ρ_p is the polymer density, d_H is the latex nanocomposite hydrodynamic diameter and P is a packing parameter for the silica on the nanocomposite latex particles.[2] The polymer latexes for simplicity are assumed to be not swollen in monomer at any time of the reaction. Although this assumption is clearly not correct, d_H values were measured by DLS under very diluted conditions. At this concentration it can be reasonably assumed that the rather water-soluble methyl methacrylate will mostly diffuse out of the particles and move to water phase.

Substituting Equations A.6-A.8 into Equation A.5:

(A.9) $$N_{SiO_2,L} = \frac{SA_{pol,i} N_{pol}}{A_{SiO_2,i,L}} = \frac{24 P m_{M,0} X}{\pi \rho_p d_{pol} d_{SiO_2}^{\ 2}}$$

The combination of Equation A.9 and A.3 gives the desired expression for the number of SiO_2 particles in the water phase at a time t:

(A.10) $$N_{SiO_2} = \frac{6 m_{SiO_2,0}}{\pi \rho_{SiO_2} d_{SiO_2}^{\ 3}} - \frac{24 P m_{M,0} X}{\pi \rho_p d_{pol} d_{SiO_2}^{\ 2}} = \frac{6}{\pi d_{SiO_2}^{\ 2}} \left(\frac{m_{SiO_2,0}}{\rho_{SiO_2} d_{SiO_2}} - \frac{4 P m_{M,0} X}{\rho_p d_{pol}} \right)$$

Going back to the derivation of f, this parameter is defined as the ratio between the total surface area of free silica in water, SA_{SiO_2}, and the total surface area of nanocomposite particles, SA_L:

(A.11) $$f = \frac{SA_{SiO_2}}{SA_L} = \frac{SA_{SiO_2}}{\pi d_H^{\ 2} N_{pol}}$$

From Equation A.11, SA_{SiO_2} can be written as the product of the surface area of a single silica nanoparticle, $SA_{SiO_2,i}$, and the number of silica particles in the water phase, N_{SiO_2}. N_{pol} was substituted using Equation A.7:

(A.12) $$f = \frac{SA_{SiO_2,i} N_{SiO_2}}{\pi d_H^{\,2} \left(\frac{6 m_{M,0} X}{\pi \rho_p d_{pol}^{\,3}} \right)}$$

Next, Equation A.12 is combined with Equation A.10 and $SA_{SiO_2,i}$ is expressed as a function of d_{SiO_2}:

(A.13) $$f = \frac{\pi d_{SiO_2}^{\,2} \frac{6}{\pi d_{SiO_2}^{\,2}} \left(\frac{m_{SiO_2,0}}{\rho_{SiO_2} d_{SiO_2}} - \frac{4 P m_{M,0} X}{\rho_p d_{pol}} \right)}{\pi d_H^{\,2} \left(\frac{6 m_{M,0} X}{\pi \rho_p d_{pol}^{\,3}} \right)}$$

Finally, d_{pol} is expressed as $(d_H - 2d_{SiO_2})$ as the latex nanocomposite particles are assumed to be covered by a monolayer of silica spheres, half embedded in the polymer phase:

(A.14) $$f = \frac{6 \left(\frac{m_{SiO_2,0}}{\rho_{SiO_2} d_{SiO_2}} - \frac{4 P m_{M,0} X}{\rho_p (d_H - 2 d_{SiO_2})} \right)}{\pi d_H^{\,2} \left(\frac{6 m_{M,0} X}{\pi \rho_p (d_H - 2 d_{SiO_2})^3} \right)}$$

which can be mathematically rearranged to:

(A.15) $$f = \frac{m_{SiO_2,0} \rho_p \left(d_H - 2 d_{SiO_2} \right)^3}{m_{M,0} X \rho_{SiO_2} d_{SiO_2} d_H^{\,2}} - \frac{4 P \left(d_H - 2 d_{SiO_2} \right)^2}{d_H^{\,2}}$$

Finally, a correction parameter β is added to take into account the use of hydrodynamic diameters instead of actual nanocomposite latex sizes. This leads to Equation A.16 which is equivalent to Equation 2.6 of Chapter 2:

(A.16) $$f = \frac{m_{SiO_2,0} \rho_p \left(d_H \beta - 2 d_{SiO_2} \right)^3}{m_{M,0} X \rho_{SiO_2} d_{SiO_2} d_H^{\,2} \beta^2} - \frac{4 P \left(d_H \beta - 2 d_{SiO_2} \right)^2}{d_H^{\,2} \beta^2}$$

A.3 Additional Tables

Table A2.1 Reaction temperature, T_r, and propagation rate coefficient, k_p, for methyl methacrylate polymerizations at 5% (1) and 20% (2) monomer conversion.

SiO_2/M	$T_{r,1}$ / °C	$T_{r,2}$ / °C	ΔT / °C	$k_{p,1} \times 10^{-2}$ / $M^{-1}\ s^{-1}$	$k_{p,2} \times 10^{-2}$ / $M^{-1}\ s^{-1}$
2.00	334.92	335.89	0.97	8.53	8.73
1.50	334.91	335.72	0.81	8.53	8.70
1.00	334.73	335.51	0.78	8.50	8.66
0.75	334.78	335.53	0.75	8.51	8.66
0.50	334.88	335.58	0.70	8.53	8.67
0.10	334.75	335.36	0.61	8.50	8.62
0.00	334.70	335.26	0.56	8.49	8.60

Table A3.1 Evolution of molecular weight and dispersity during the HPMA semi-batch chain-extension of a $PGMA_{50}$ macromonomer in aqueous dispersion polymerization (Run 2).

Time h	$M_w \times 10^{-4}$ g/mol	$M_n \times 10^{-4}$ g/mol	$M_p \times 10^{-4}$ g/mol	$Đ_M$ -	X_i [a] -	X [b] -	DP_{HPMA} [c] -
0.0	4.59	2.03	3.12	2.26	0.00	0.00	0
1.0	9.33	2.20	3.07	4.23	0.72	0.12	18
2.0	19.25	3.31	3.37	5.81	0.89	0.30	45
4.0	27.37	4.41	31.34	6.20	0.94	0.63	94
6.5	37.96	6.02	35.62	6.31	0.93	0.93	139

[a] Instantaneous monomer conversion (X_i). DMF was used as internal standard.

[b] Cumulative monomer conversion (X).

[c] *DP* of HPMA block in $PGMA_{50}PHPMA_z$; Estimated from X_i, assuming only CTA chain-extension.

Table A3.2 Evolution of molecular weight and dispersity during the HPMA semi-batch chain-extension of a $PGMA_{27}$ macromonomer in aqueous dispersion polymerization (Run 3).

Time h	$M_w \times 10^{-4}$ g/mol	$M_n \times 10^{-4}$ g/mol	$M_p \times 10^{-4}$ g/mol	$Đ_M$ -	X_i [a] -	X [b] -	DP_{HPMA} [c] -
0.0	1.95	0.93	1.89	2.10	0.00	0.00	0
1.0	5.09	1.34	2.13	3.81	0.86	0.14	13
2.0	12.94	1.84	2.23	7.02	0.88	0.26	24
4.0	16.38	2.49	14.12	6.59	0.94	0.62	56
6.5	19.08	3.26	15.35	5.85	0.98	0.98	90

[a] Instantaneous monomer conversion (X_i). DMF was used as internal standard.

[b] Cumulative monomer conversion (X).

[c] *DP* of HPMA block in $PGMA_{27}PHPMA_z$; Estimated from X_i, assuming only CTA chain-extension.

Table A3.3 Evolution of molecular weight and dispersity during the HPMA semi-batch chain-extension of a $PGMA_{32}$ macromonomer in aqueous dispersion polymerization (Run 4).

Time h	$M_w \times 10^{-4}$ g/mol	$M_n \times 10^{-4}$ g/mol	$M_p \times 10^{-4}$ g/mol	$Đ_M$ -	X_i [a] -	X [b] -	DP_{HPMA} [c] -
0.0	2.19	1.20	2.02	1.82	0.00	0.00	0
1.0	2.24	1.17	2.63	2.25	0.59	0.07	7
2.0	2.61	1.38	4.34	3.14	0.89	0.22	22
4.0	3.55	2.09	5.79	2.78	0.96	0.48	48
5.0	4.40	2.38	6.60	2.78	0.97	0.60	60
6.0	4.98	2.64	6.85	2.59	0.97	0.73	73
8.5	5.73	3.06	7.63	2.49	0.99	0.99	100

[a] Instantaneous monomer conversion (X_i). DMF was used as internal standard.

[b] Cumulative monomer conversion (X).

[c] *DP* of HPMA block in $PGMA_{32}PHPMA_z$; Estimated from X_i, assuming only CTA chain-extension.

Table A4.1 Parameters used for the fitting of small-angle X-ray scattering (SAXS) of aqueous suspensions of the nanogels N1 and N2 at 1.0 wt% in deionized water. Both a sphere and a core-shell sphere form factor were tested for the fitting.

	N1		N2	
	Sphere	Core-shell	Sphere	Core-shell
Scale	1.56	0.82	1.09	0.48
Background	2.13×10^{-3}	2.00×10^{-3}	6.38×10^{-3}	5.00×10^{-3}
Sld core /[a] 10^{-6}Å^{-2}	10.27	9.85	10.27	9.85
Sld shell / 10^{-6}Å^{-2}	/	10.70	/	10.70
Sld solvent / 10^{-6}Å^{-2}	9.47	9.47	9.47	9.47
Radius core / Å	**88.62**	**36.71**	**116.03**	**29.67**
Thickness shell / Å	**/**	**42.62**	**/**	**84.50**
Volume fraction / -	0.01	0.01	0.01	0.01
Charge / e	10.25	8.97	10.70	11.50
Temperature / K	298.15	298.15	298.15	298.15
Salt concentration / M	0.00	0.00	0.00	0.00
Dielectric constant / -	80.40	80.40	80.40	80.40
Distribution of radius (log) / -	0.21	0.19	0.24	0.34
Distribution of thickness (log) / -	/	0.40	/	0.29
Chi^2/N_{pts} /[b] -	1.46	3.84	2.27	1.74
Total diameter (d_{SAXS}) / nm	**17.72**	**15.87**	**23.21**	**22.83**

[a] Scattering length density (Sld).

[b] Chi-square normalized by the number of data points. A lower value represents a better fit.

Table A4.2 Experimental details on the emulsion polymerization of styrene (Sty) using N1 nanogels as stabilizer. Solid content (*SC*), initial (pH_0) and final (pH_f) pH, hydrodynamic diameter (d_H) and polydispersity index (*PdI*) from DLS measurements.

Run	N1 /[a] g	H_2O / g	Sty / g	KPS /[b] mg	Final SC	N1/Sty[c] wt%	pH_0	pH_f	d_H / nm	PdI
1	40.00	81.0	12.0	7.8	0.13	38.90	/	8.7	235	0.160
2	12.00	81.0	9.2	6.0	0.10	15.22	/	8.8	115	0.160
3	8.00	121.0	12.8	8.3	0.10	7.29	/	8.6	108	0.060
4	3.00	131.0	13.3	8.6	0.09	2.85	/	8.8	102	0.020
5	1.05	121.0	12.1	7.9	0.09	1.01	/	8.3	106	0.008
6	0.40	131.0	13.0	8.5	0.09	0.36	/	6.7	127	0.009
9	3.00	121.0	12.3	8.0	0.09	2.85	5.5	5.2	141	0.028
12	3.00	121.0	12.3	8.0	0.09	2.85	5.0	5.0	169	0.091
13	3.00	121.0	12.3	8.0	0.09	2.85	4.5	4.2	270	0.209
14	0.13	121.0	12.5	19.7	0.09	0.12	8.8	3.4	164	0.031

[a] Mass of N1 suspension in water (solid content 11.7 wt%).

[b] KPS/Sty: 0.07 wt%.

[c] Defined as the weight ratio of nanogels N1/styrene×100.

Table A4.3 Experimental details on the emulsion polymerization of styrene N2 nanogels as stabilizer.

Run	N2 /[a] g	H_2O / g	Sty / g	KPS /[b] mg	Final SC	N2/Sty[c] wt%	pH_0	pH_f	d_H / nm	PdI
15	3.90	148.5	15.1	22.7	0.09	2.93	8.8	8.2	100	0.035
19	3.90	148.5	15.1	22.7	0.09	2.93	6.5	6.7	103	0.072
20	3.90	148.5	15.1	22.7	0.09	2.93	5.5	5.6	89	0.028
21	3.90	148.5	15.1	22.7	0.09	2.93	5.1	/	2572	1.000
22	3.90	148.5	15.1	22.7	0.09	2.93	4.5	/	44890	0.868
24	1.40	150.8	15.1	22.7	0.09	1.05	8.8	7.6	120	0.013
25	0.43	151.6	15.1	22.7	0.09	0.32	8.7	5.4	156	0.019
26	0.14	151.9	15.1	22.7	0.09	0.11	8.8	3.4	184	0.008
27	3.90	148.7	15.1	22.7	0.09	2.93	8.8	8.7	100	0.018
28	6.40	146.3	15.1	22.7	0.09	4.81	8.9	8.9	100	0.073
29[d]	0.00	152.0	15.1	22.7	0.09	0.00	8.1	7.9	292	0.025
30[d]	0.17	151.9	15.1	22.7	0.09	0.13	8.4	8.1	208	0.035
31	8.40	53.5	6.2	9.6	0.10	15.51	8.8	8.8	162	0.235
32	14.00	48.6	6.2	9.6	0.11	25.55	8.7	8.8	131	0.192
33	19.80	43.4	6.3	9.6	0.12	35.80	8.8	8.7	137	0.171
34	23.00	37.9	6.4	9.6	0.13	41.13	8.8	8.6	128	0.160

[a] Mass of N2 suspension in water (solid content 11.4 wt%).

[b] KPS/Sty: 0.15 wt%.

[c] Defined as the weight ratio of nanogels N2/styrene×100.

[d] An aqueous solution of 1.82×10^{-3} M sodium hydrogen carbonate ($NaHCO_3$) was adopted instead of deionized water.

A.4 Additional Figures

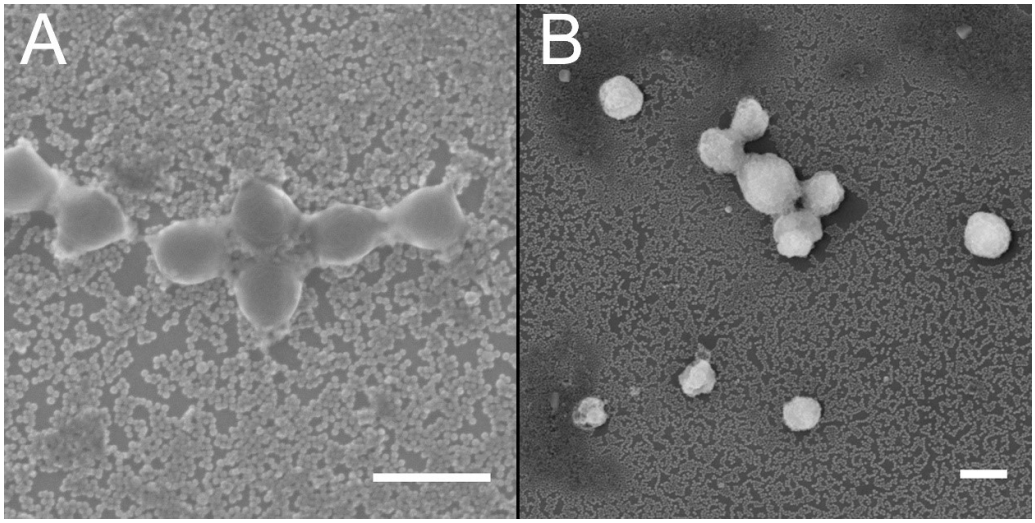

Figure A2.1 SEM pictures of a) 280 nm PMMA latex particles swollen with MMA in the presence of colloidal SiO_2 and b) of a 350 nm PMMA latex swollen with MMA and in the presence of colloidal SiO_2 after the application of ultrasounds. Scale bars: 500 nm.

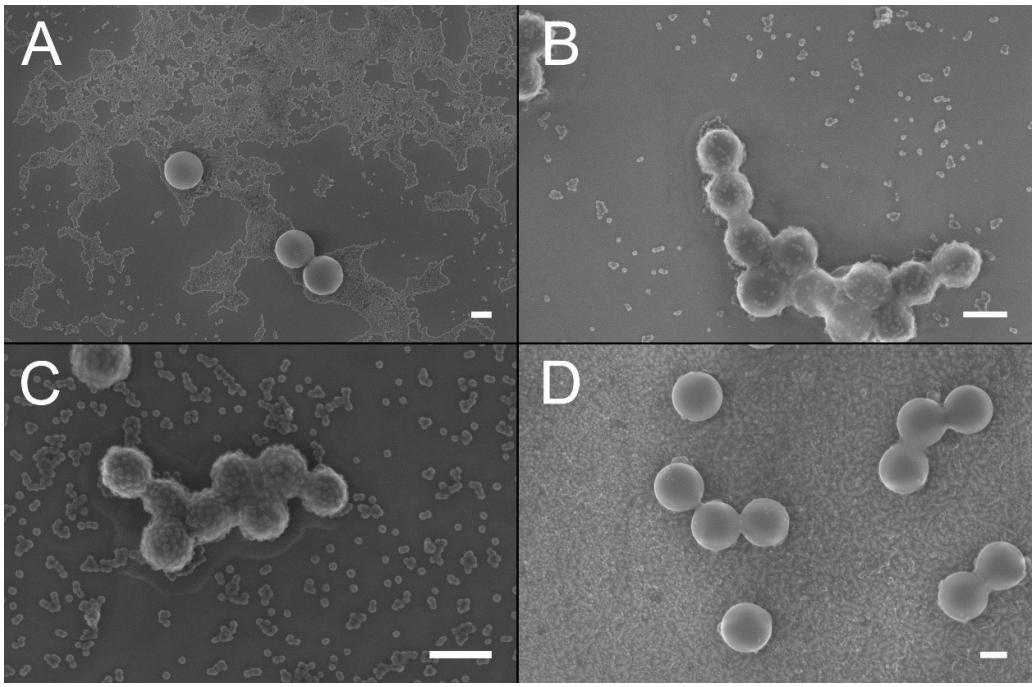

Figure A2.2 SEM images of the latex particles resulting from the Pickering emulsion polymerization of styrene a) in the absence of comonomer, in the presence of b) 1.0

wt% (with respect to styrene) and c) 3.0 wt% of di(ethylene glycol) ethyl ether acrylate or d) 1.0 wt% of methacrylic acid. Scale bars: 300 nm.

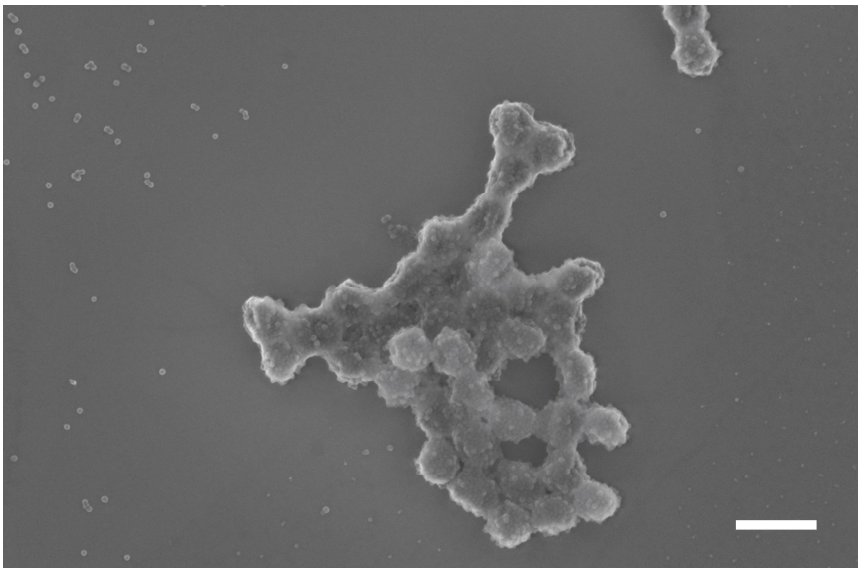

Figure A2.3 Pickering emulsion polymerization of MMA in the presence of colloidal SiO_2 for SiO_2 = 0.50 w/w. Scale bar: 500 nm.

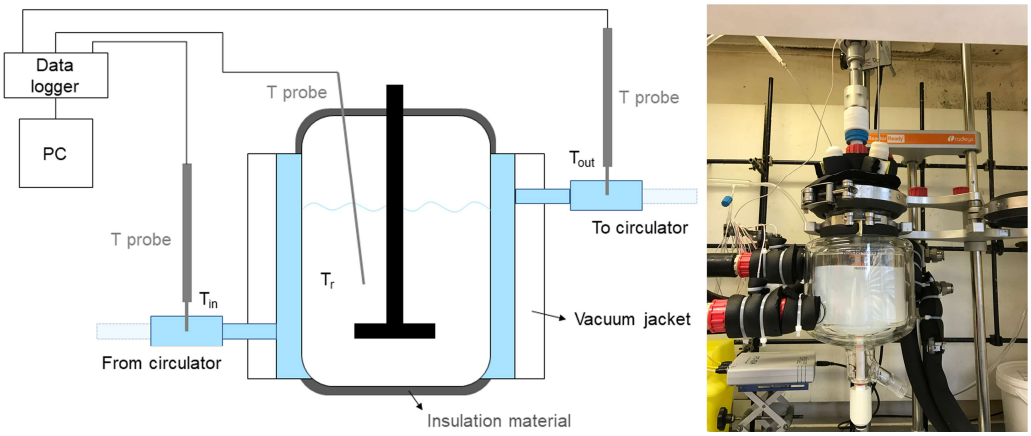

Figure A2.4 (Left) Schematic representation and (Right) picture of the home-made calorimetry reactor adopted in the MMA emulsion polymerizations.

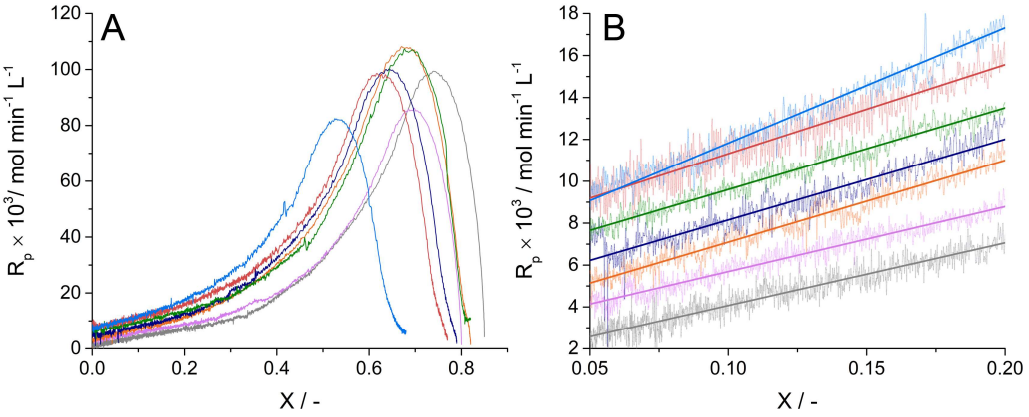

Figure A2.5 Variation in the polymerization rate (R_p) for the Pickering emulsion polymerization of MMA in the presence of nanosilica; a) values until *ca.* 80% conversion and b) values between 5 and 20% conversion superimposed with a linear fit of the data. SiO_2/M = 0.00 (grey), 0.10 (pink), 0.50 (orange), 0.75 (dark blue), 1.00 (green), 1.50 (red), 2.00 (light blue) w/w.

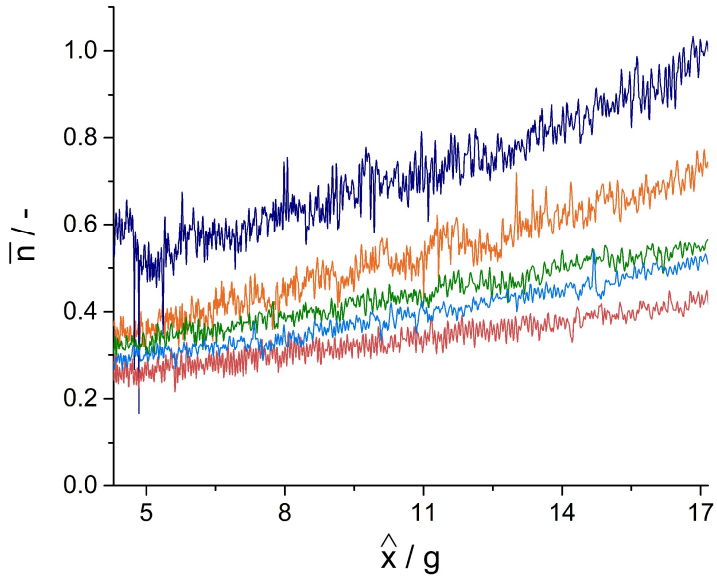

Figure A2.6 Variation in the average number of radicals per particle ($\bar{n}$) between 5 and 20% conversion for the Pickering emulsion polymerization of MMA in the presence of nanosilica. Conversion is here expressed as grams of monomer converted to polymer ($\hat{x}$). SiO_2/M = 0.50 (orange), 0.75 (dark blue), 1.00 (green), 1.50 (red), 2.00 (light blue) w/w.

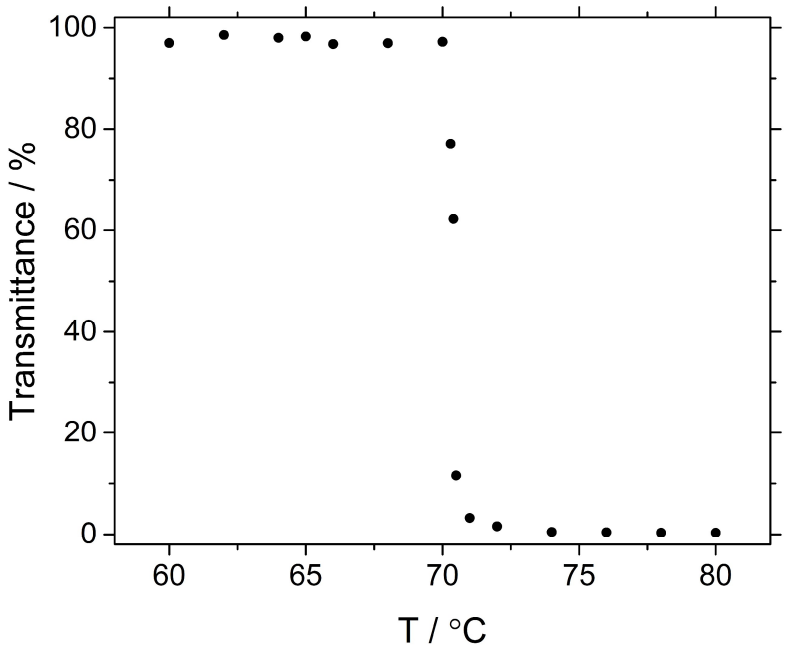

Figure A3.1 Transmittance % between 60 and 80°C of a 6.4 wt% $PGMA_{32}$-$PPEGMEMA_{10}$ solution in water from UV-Vis measurements.

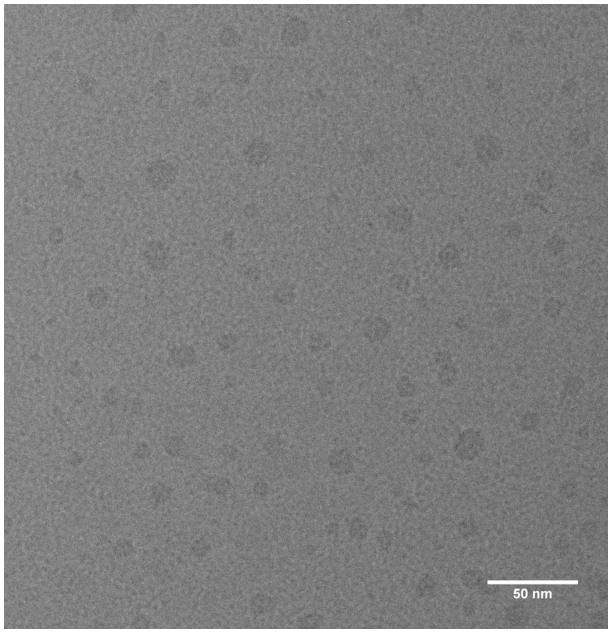

Figure A4.1 Cryogenic transmission electron microscopy (cryo-TEM) image of a 1.0 wt% aqueous suspension of N1 before crosslinking. Scale bar: 50 nm.

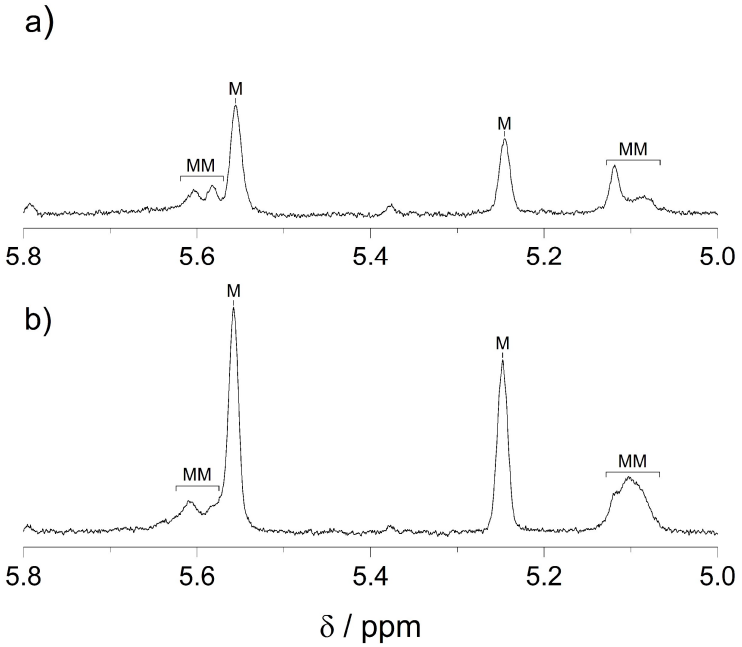

Figure A4.2 ^{1}H-NMR spectra of the vinyl region for N1 (a) and N2 (b) showing residual macromonomer (MM) and crosslinker (M) vinyl groups. Spectra recorded in D_2O at 1 wt% nanogels.

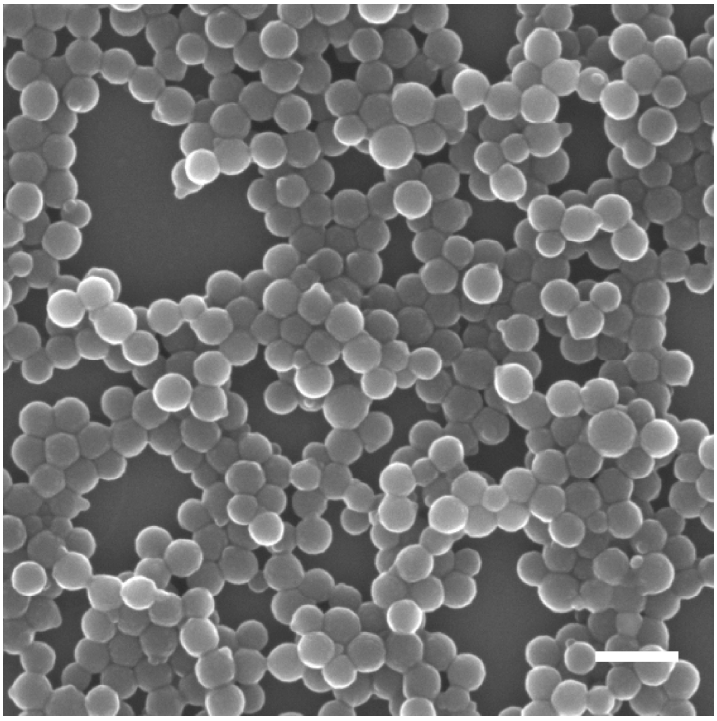

Figure A4.3 SEM image of the emulsion polymerization of styrene conducted at pH 8.8 and 2.9 wt% of N2 wrt monomer (Run 27, Table A4.3). No more than one nanogel can be seen on the surface on the polystyrene latex particles. Scale bar: 200 nm

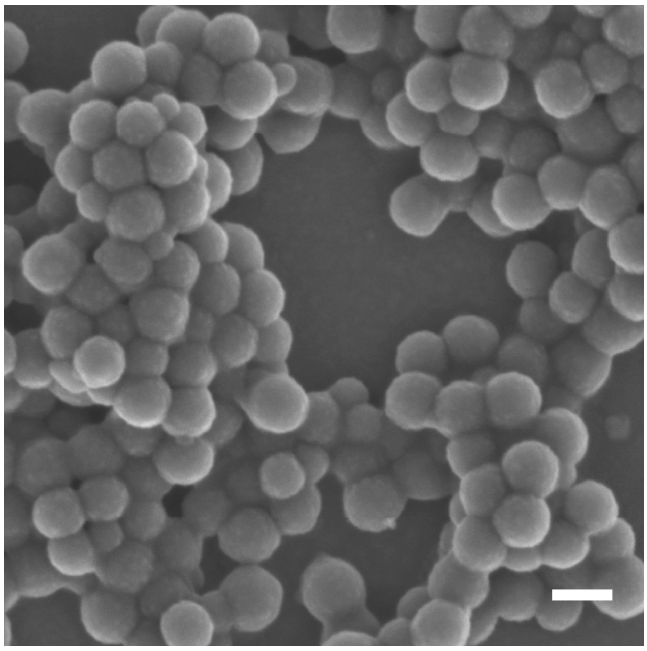

Figure A4.4 Emulsion polymerization of styrene conducted at pH 8.8 using uncrosslinked N2 polymer micelles (2.9 wt% wrt monomer) showing mostly spherical particles. Scale bar: 100 nm.

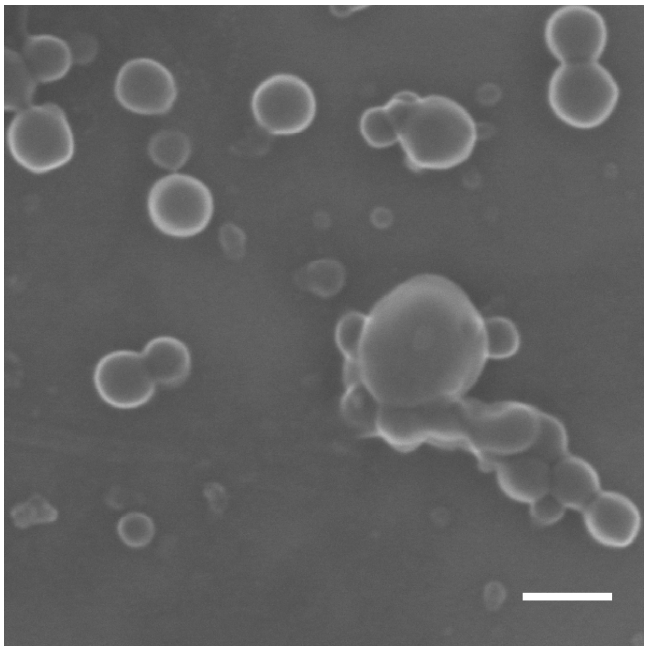

Figure A4.5 SEM image of the emulsion polymerization of styrene conducted at pH 8.8 and at 15.2 wt% of N1 wrt monomer (Run 2, Table A4.2). More patches can be occasionally seen on top of the polystyrene sphere, although control on particle size and dispersity is lost. Scale bar: 100 nm.

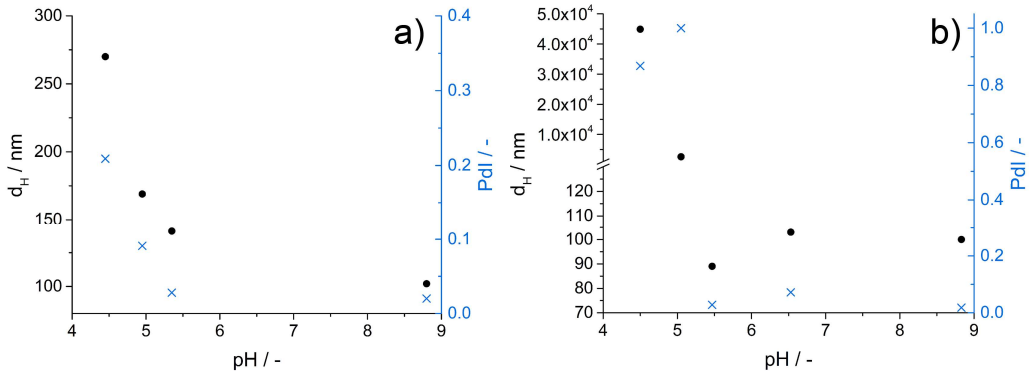

Figure A4.6 Effect of initial nanogel dispersion pH on the latex particle hydrodynamic diameter and distribution in the emulsion polymerization of styrene in the presence of N1 (a) and N2 (b) nanogels. In the case of N2, the polymerizations at pH 4.5 and 5.0 coagulated overnight.

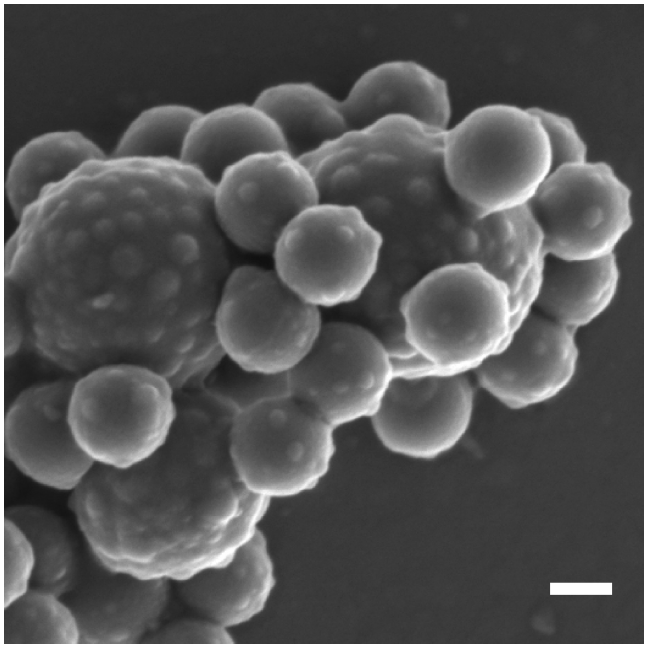

Figure A4.7 SEM image showing the formation of bigger patchy particle in the polymerization of styrene using N1 nanogels as stabilisers at 2.8 wt% wrt monomer and where the pH of the nanogel dispersion was adjusted to pH 4.5 prior to polymerization (Run 13, Table A4.2). Scale bar: 100 nm

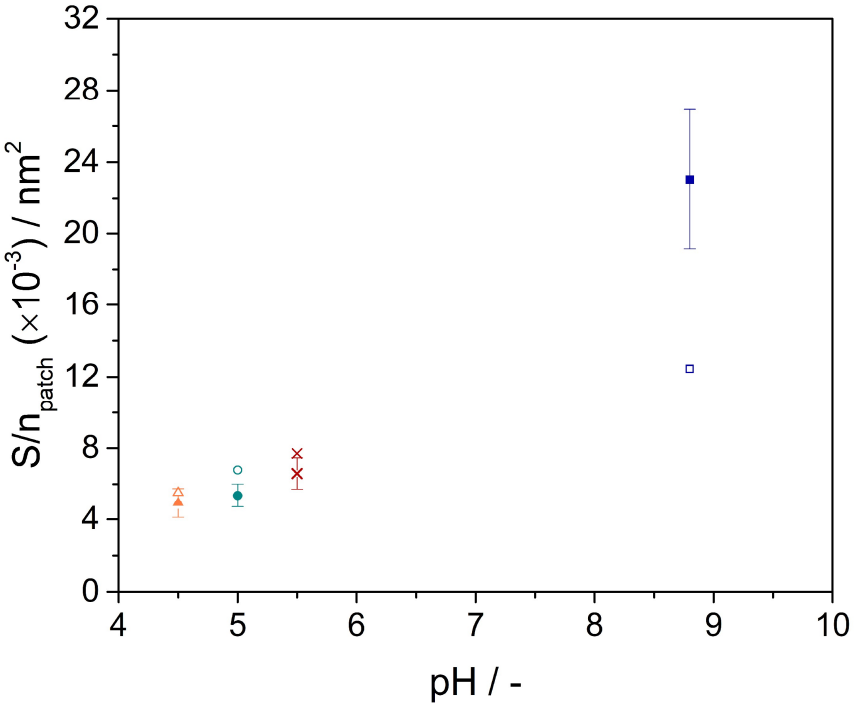

Figure A4.8 Comparison between experimental (filled symbols, from SEM image analysis) and calculated (empty symbols, from Table 4.2) values of S/n_{patch} as a function of pH.

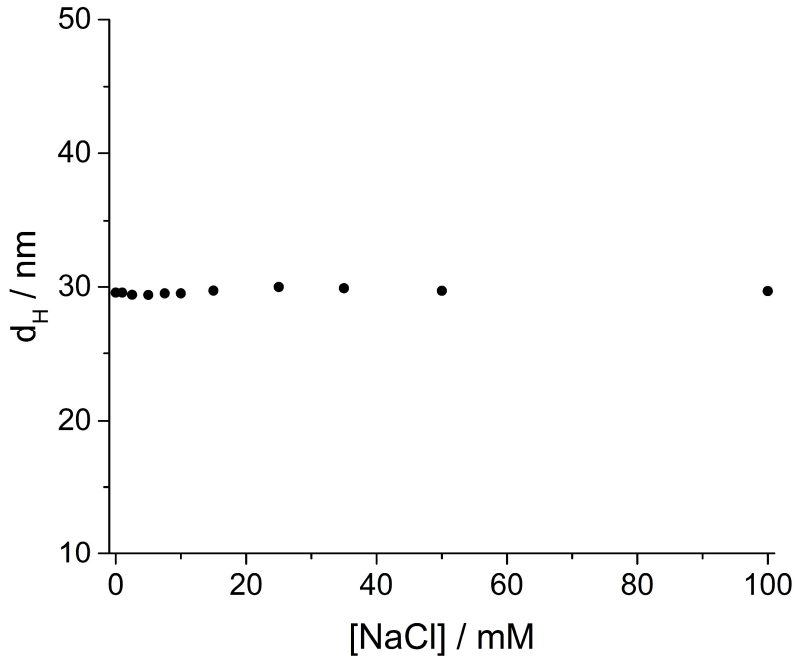

Figure A5.1 Hydrodynamic diameter (d_H) of 1.0 wt% of N1 nanogels in water at pH 8.8 and in presence of varying [NaCl].

Figure A5.4 Film formation of the Sty/BA = 1.45:1 w:w latex made in presence of [NaCl] = 25.0 mM and dried at 40°C.

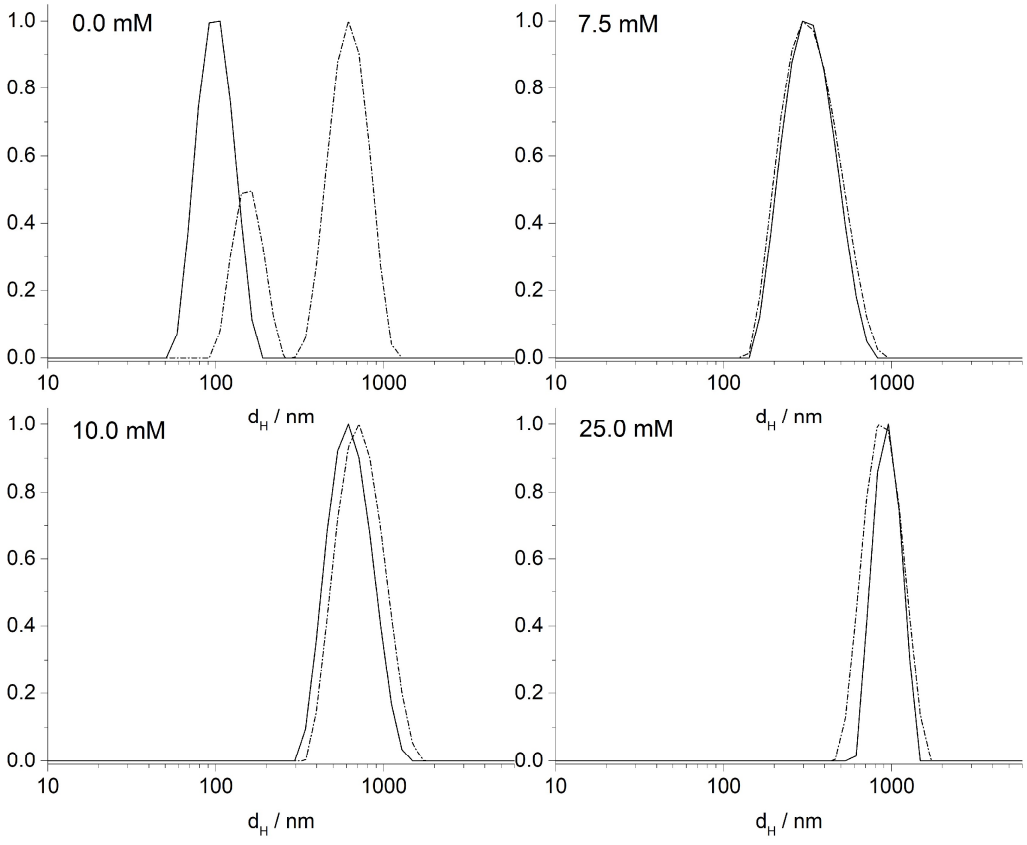

Figure A5.3 Normalized intensity-based distribution by DLS of poly(styrene) latexes formed in the presence of nanogels as stabilizers and at different salt concentrations. The solid lines represent the size distribution before freeze drying of the latexes, whereas the dotted lines show the distribution after freeze drying and redispersion of the dry powder in water.

References

(1) C. A. L. Colard, R. F. A. Teixeira and S. A. F. Bon, *Langmuir*, 2010, **26**, 7915–7921

(2) S. Fortuna, C. A. L. Colard, A. Troisi and S. A. F. Bon, *Langmuir*, 2009, **25**, 12399–12403